Technische Universität Braunschweig

Variational Formulations and Functional Approximation Algorithms in Stochastic Plasticity of Materials

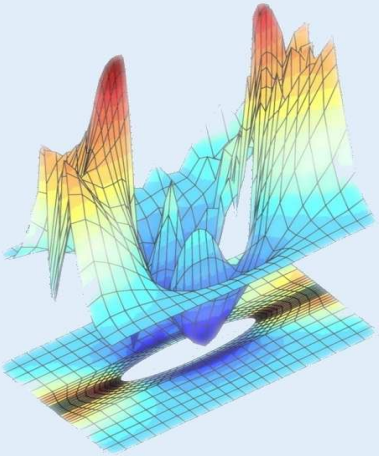

Dissertation

Bojana Rosić

University of Kragujevac

Variational Formulations and Functional Approximation Algorithms in Stochastic Plasticity of Materials

Von der
Carl-Friedrich-Gauß-Fakultät
Technische Universität Carolo-Wilhelmina zu Braunschweig
und
der Fakultät für Ingenieurwissenschaften
Universität Kragujevac
zur Erlangung des Grades
Doktor-Ingenieurin (Dr.-Ing.)
genehmigte Dissertation

von

Bojana Rosić
geboren am 16. August 1982
in Kragujevac, Serbien

Eingereicht am:	20. Juni 2012
Mündliche Prüfung am:	16. November 2012
1. Referent:	Prof. Hermann G. Matthies, Ph.D.
2. Referent:	Prof. Dr. Miroslav Živković
3. Referent:	Prof. Dr. Adnan Ibrahimbegović

2013

To my family. “You are the only reason I am. You are all my reasons.Thank you”

Abstract

A class of abstract stochastic variational inequalities of the second kind described by uncertain parameters is considered within the framework of infinitesimal and large displacement elastoplasticity theory. Particularly the focus is set on the rate-independent evolutionary problem with general hardening whose material characteristics are assumed to have positively-definite distributions. By exhibiting the structure of the evolutionary equations in a convex setting the mathematical formulation is carried over to the computationally more suitable mixed variational description for which the existence and uniqueness of the solution is studied. Time discretised as usual with backward Euler, the inequality is reduced to a minimisation problem for a convex functional on discrete tensor product subspaces whose unique minimiser is obtained via a stochastic closest point projection algorithm based on "white noise analysis". To this end a description in the language of non-dissipative and dissipative operators is used, both employing the stochastic Galerkin method in its fully intrusive or non-intrusive variant. The former method represents the direct, purely algebraic way of computing the response in each iteration of Newton-like methods. As the solution is given in a form of polynomial chaos expansion, i.e. an explicit functional relationship between the independent random variables, the subsequent evaluations of its functionals (the mean, variance, or probabilities of exceedence) are shown to be very cheap, but with limited accuracy. Due to this reason, the intrusive method is contrasted to the less efficient but more accurate non-intrusive variant which evaluates the residuum in each iteration via high-dimensional integration rules based on random or deterministic sampling - Monte Carlo and related techniques. In addition to these, the problem is also solved with the help of the stochastic collocation method via sparse grid techniques. Finally, the methods are validated on a series of test examples in plain strain conditions whose reference solution is computed via direct integration methods.

Rezime

U okviru teorije malih i velikih plastičnih deformacija razmatrana je klasa apstraktnih stohastičkih varijacionih nejednakosti opisanih slučajnim promenljivim. Poseban fokus je stavljen na asocijativni evolucioni problem sa generalnim ojačanjem čije materijalne karakteristike imaju distribuciju određenu zakonom maksimalne entropije. Proučavajući strukturu evolucionih jednačina uz pomoć konveksne teorije analizirani su uslovi za postojanje i jedinstvenost rešenja uz dodatnu matematičku reformulaciju problema u numerički prikladan mešoviti varijacioni opis. Dobijena nejednakost se nakon implicitne diskretizacije svodi na minimizaciju konveksnog funkcionala definisanog u tenzorskom prostoru. Rešenje tako postavljenog problema se može dobiti novouvedenom stohastičkom metodom projekcije najbliže tačke uz pomoć teorije analize belog šuma. Pomenuta metoda se sastoji od dva koraka: elastičnog i plastičnog, čiji su algoritmi bazirani na stohastičkoj Galerkinovoj metodi. Uz pomoć funkcionalne analize Galerkinov metod je formulisan na dva načina: direktan (intruzivan) i posredan (neintruzivan). Intruzivni metod predstavlja direktan, algebarski način dobijanja rešenja u svakoj iteraciji Njutnove metode. Zahvaljujući polinomnoj formi rešenja sve predstojeće evaluacije njegovih funkcionala, kao što su srednja vrednost, varijansa itd. postaju računski jako efikasne, ali ograničene tačnosti. U cilju unapređenja tačnosti Galekinova methoda je implementirana i u svojoj manje efikasnoj, neintruzivnoj varijanti, koja računa rezidual u svakoj Njutnovoj iteraciji numeričkom (determinističkom ili stohastičkom) integracijom. Obe varijante Galerkinovih metoda su upoređene sa metodom stohastičke kolokacije zasnovane na pravilu “sparse grid”-a. Konačno, sve predstavljene metode su verifikovane na seriji test primera u ravanskom stanju deformacije i za referentno rešenje dobijeno uz pomoć direktne integracije.

Zusammenfassung

Im Rahmen der Elastoplastizitätstheorie infinitesimaler und starker Verschiebungen wird eine Klasse von abstrakten, stochastischen Variationsungleichungen betrachtet, welche durch unsichere Parameter beschrieben werden. Im Speziellen wird das raten-unabhängige Evolutionsproblem mit allgemeiner Verfestigung betrachtet, dessen Materialeigenschaften-Verteilung als durch die Maximum-Entropie Methode gegeben angenommen wird. Durch die Darstellung der Struktur der Evolutionsgleichungen in einem konvexen Rahmen wird die Existenz und Eindeutigkeit der Lösung betrachtet und die mathematische Formulierung in eine berechnungstechnisch besser passende gemischt-variationale Beschreibung überführt. Innerhalb eines Euler-rückwarts Zeitschrittes reduziert sich die Ungleichung auf ein Minimierungsproblem für ein konvexes Energiefunktional auf diskreten Tensorproduktunterräumen, dessen eindeutige Lösung mithilfe eines stochastischen nächstgelegenen-Punkt-Projektionsalgorithmus basierend auf der "white noise" Analyse bestimmt wird. Hierzu wird eine Beschreibung basierend auf nicht-dissipativen und dissipativen Operatoren benutzt und die sogenannte intrusive stochastische Galerkinmethode in den Berechnungsprozess eingeführt. Diese Methode stellt einen direkten algebraischen Weg zur Berechnung der Lösung in jeder Iteration von Newton-ähnlichen Verfahren dar. Da die Lösung in der Form einer polynomiellen Chaos-Entwicklung gegeben ist, also einer expliziten Beschreibung des funktionalen Zusammenhangs der unabhängigen Zufallsvariablen, sind die nachfolgenden Auswertungen von Funktionalen dieser Lösung (Mittelwert, Varianz, Überschreitungswahrscheinlichkeit) berechnungstechnisch sehr günstig. Zusätzlich wird die Methode mit der nicht-intrusiven Variante verglichen, einem pseudo-Galerkin Verfahren, welches das Residuum in jeder Iteration mit Methoden zur hochdimensionalen Integration basierend auf zufälligen oder deterministischen Abtastverfahren auswertet. Abschließend wird die Methode mit einer Reihe von Testbeispielen mit einfachen Spannungsbedingungen validiert, deren Referenzlösungen über direkte Integrationsverfahren berechnet werden.

Acknowledgments

"No man is an island entire of itself." To my parents, sisters and nephew who encouraged me so much in life and helped to become the person I am today. Thank you for being an inspiration to achieve this goal, for all the love, support and understanding, but the most for teaching me how to approach the life with humanity. The greatest gratitude I owe to you, mother, and to you, father, for unselfish sacrifice and devoting yourselves to build a better road for my sisters and me. The smallest gratitude I can express is to dedicate this work to you.

The results reported in this thesis have been part of my research work at the Institute of Scientific Computing, Technische Universität Braunschweig, Germany and the Faculty of Engineering, University of Kragujevac. The thesis would not be possible without the financial, academic and technical support of Technische Universität Braunschweig, DAAD (Deutscher Akademischer Austauschdienst) Foundation, and DFG (Deutsche Forschungsgemeinschaft) whose help is greatly acknowledged.

Foremost I am sincerely and heartily grateful to my advisers, Professor Dr. Hermann G. Matthies and Professor Dr. Miroslav Živković, who unselfishly helped me to enroll the dual-degree studies between two universities. I very much appreciate everything Professor Matthies has done in the course of the supervision of this thesis, especially for his understanding, constant support, and all the mathematical knowledge I learned from him. Professor Živković provided me a safe space to explore new ideas and was a great support over the last few years for which I am grateful. Additionaly, I want to thank all of committee members—Professor Dr. Adnan Ibrahimbegović, Professor Dr. Dirk Lorenz and Professor Dr. Radovan Slavković—for taking their time to read and comment my thesis.

My appreciation likewise extends to my small but great scientific family (in chronological order): Dipl.-Inf. Dominik Jürgens, Dr. Alicia Ortega-Jürgens, Dipl.-Inf. Martin Krosche, Dr. Alexander Litvinenko, Dr. Dishi Liu, Dr. Rainer Niekamp, Dr. Oliver Pajonk, Dr. Joachim Rang, Dr. Elmar Zander and our secretary, M. A. Cosima Meyer. Thank you for making my research time on Institute of Scientific Computing enjoyable, but most of all for many valuable discussions and friendship. In this regard, I would especially like to thank Cosima Meyer who kindly helped me with the dissertation proofreading. Next to the group in Braunschweig, I was very pleased and honored to work with Dr. Anna Kučerová and Dr. Jan Sýkora at Czech Technical

University in Prague, whom I thank for the lovely cooperation and hopefully lifelong friendship.

I would also like to thank all participants of the graduate college MGK SFB 880 „Grundlagen des Hochauftriebs künftiger Verkehrsflugzeuge“ and colleagues in the SFB 880 project team for many useful discussions and interdisciplinary exchange. Likewise, I thank my colleagues at the Department of Applied Mechanics, Faculty of Engineering in Kragujevac.

Finally, there are a number of people who have become my friends over last few years. To Ilknur Yoldaş, for her hospitality, enthusiasm but mostly for all the fun we had during our German adventure. To Oliver Pajonk, for his friendship, sense of humor and the most valuable drinking beer lessons. To Martin Krosche, for always being friendly and supportive, but the most for endless “radio Mileva” talks. To Alicia Ortega-Jürgens, for being such a nice friend; and to family Škara for pleasant and lovely substitute of family surrounding. Ivana, Nada and Vladimir brought the wonderful Šumadija sense into my life in the moments when nostalgia was more than powerful. Thank you.

“Nijedan čovek nije ostrvo - sam po sebi celina.” Mojoj porodici kao večitoj inspiraciji svih mojih puteva i namera. Hvala vam što ste izvajali slobodu moga duha, za svu ljubav koju mi pružate, za beskonačnu podršku i razumevanje čak kada ni samu sebe nisam razumela. Hvala ti majko, i tebi oče na nesebičnoj žrtvi da čak i u najtežim vremenima podarite sestrama i meni ono najbolje i najhumanije u vama. Ovaj rad pripada vama.

Bojana Rosić
Braunschweig, June 2013

Contents

Chapter 1

Introduction

In order to enhance the quality and reliability of industrial design an important goal of engineering sciences is to understand and analyze the non-reversible behaviour of a structure under the influence of external excitations. Therefore, in last few decades a significant development of elastoplasticity theory has been made in terms of its mathematical formulation and numerical computation. With time the theory has grown into two separate branches: the classical and the finite strain theory. The classical theory is used to describe the irreversible phenomena based on the small strain assumption [215, 89, 224, 41, 160]. The theory consists of the complete study of the existence, uniqueness, and stability of the solution together with the various computational approaches for its numerical computation [92]. Even though existing algorithms are fully securing the desired accuracy, the practical application of infinitesimal models is limited to few real situations due to the small strain assumption. Consequently, the classical approach has been altered to a more complex and yet not completely understood finite strain theory. In contrast to the infinitesimal, the finite strain theory [101, 24, 54, 161, 40] deals with several issues such as the existence of the non-unique stress and strain measures, the problem of finding the physically acceptable decomposition of the total deformation into elastic and plastic parts, as well as non-objective material time derivatives of the spatial variables. In order to overcome these issues several different specifications of the rate equations have been considered over time and studied in many papers and books, such as [10, 24, 69, 159, 101, 161, 128]. Accordingly, the finite strain theory is considered to be controversial even though the computational analysis offers the numerical algorithms capable to solve the highly complex problems.

Regardless of their great practical application in every day life, the classical and finite strain models still cannot describe many phenomena. Properly calibrated elastoplastic models are successfully used to capture the most important aspects of material

behaviour arising in problems such as metal forming, the design of steel, etc. However, these models cope with the inability to describe materials undergoing significant changes in the micro-structure, such as soil, rock, concrete, powder, and bone tissue. In addition, the deterministic analysis fails to accurately predict the system response under poorly known excitations, for example seismic phenomena, wind, snow, etc. Nevertheless, up to the present time their study has been done in a quite deterministic way by "averaging" the existing experimental data and neglecting the influence of the obviously present uncertainty on the system response.

In order to improve the quality of the prediction this paper substitutes the deterministic approach with a more realistic stochastic counterpart which takes all present uncertainties into consideration.

1.1 Related work

The first attempt to describe elastoplastic equations in stochastic manner was published by Anders and Hori [8]. They considered the three-dimensional isotropic softening of a non-homogeneous elasoplastic body in small deformation conditions and for a quasi-static state described by random material properties. Assuming the elastic modulus to be the only uncertain variable, authors proposed a stochastic finite element method based on the Karhunen-Loève expansion along with the polynomial chaos expansion combined with the bounding body theory [167, 211]. The method searches for the joint distribution functions of variables of consideration by approximating the yield function via the perturbation expansion. However, the number of terms taken in the expansion in [8] is considerably small, mostly limited on one or two terms. This is a great disadvantage as it affects the accuracy of the method and may only handle random variables with embarrassingly small variances. In addition, another disadvantage may be subscribed to the complexity of numerical approximation, which does not allow more than one random parameter (in this particular case the Young modulus) to be considered.

Besides the bounding body media approach, another probabilistic finite element method for elastoplastic materials in 3-D case has been proposed. Namely, Ning, Wilson and Jiashou [170] developed a direct partial differential approach, which relies on the incremental theory of plasticity and the modified initial stress method introduced by Zhuo [170]. The method incorporates advantages of variational and constant stiffness approaches, and at the same time enables simultaneous iterative computations of the gradients and mean values of displacement and stresses.

Briefly, Ning and co-workers observed a random 3-D problem described by the Mohr-Coulomb yield criterion with uncertain elastic modulus, Poisson ratio, and strength parameters including the coefficient of internal friction and cohesive force. In order to describe the probabilistic elastoplastic behaviour, they rewrote the equilibrium equation in a set of sub-incremental and iterative equations. Following this, authors achieved the forward and back substitution of the global stiffness matrix within each iteration by adjoint vector methods. Although the probabilistic differentiation method has been derived for the case of more than one random parameter, the disadvantages still exist as all uncertain inputs are considered to be random variables, not random fields. In latter case the method efficiency can be jeporised due to presence of large number of random variables. In addition, the method cannot be used for input with large variances due to poor accuracy of the Taylor expansion used in calculation of reliablity index.

Even though the previously mentioned methods try to illuminate the elastoplastic behaviour, they fail to deliver full or enough accurate prediction of the structural behaviour under the influence of uncertainty. For a more realistic description, Jeremić and co-workers [208, 209, 105] derived the Fokker-Planck (FP) equations for the probability density function (PDF) of the random state variable, i.e. stress. The Fokker-Planck equation can be derived by taking linear/nonlinear constitutive equations and describing the variation of the state variable in time by the Kubo stochastic Liouville [120] equation. In this way one obtains the evolutionary probability density of the state variable which further may be translated to the linear and deterministic FP differential equation. According to [208, 209, 105] the PDF method does not suffer from the closure problem associated with the regular perturbation approach, neither does it require repetitive use of the computationally expensive Monte Carlo method [133, 32]. However, the method is, mathematically speaking, very complex and up to now can be used only for one-dimensional problems.

The quantification of uncertainty in finite deformation problems using the spectral stochastic finite element method (SSFEM) [78, 150] first appeared in the work of Acharjee and Zabras [3, 5, 4]. They considered the influence of the uncertainty in the initial configuration and the heterogeneity of the material on the deformation of a specimen via a spectral stochastic approach similar to the one presented in this work. In order to overcome difficulties arising from the employment of polynomial chaos algebra, they developed the collocation strategy with the help of a rigorous continuum sensitivity method (CSM). Though this method provides an attractive alternative to intrusive techniques, it does suffer from the curse of dimensionality. Furthermore, in its present form the method is not suitable for problems involving high dimensional uncertainties.

Another version of spectral approach can be found in [11]. The method considers the stochastic boundary value problems whose mathematical formulation involves inequality constraints. However, the paper lacks the important study of the existence and uniqueness of the solution as well as the full derivation of the problem. In a numerical way the problem is solved using the sparse grid approach where the stochastic convex domain of admissible stresses is described in a set of collocating points. In addition, the only uncertainty considered in the numerical examples is the one describing the hardening of material.

In order to provide more realistic description of elastoplastic models, as well as more efficient algorithms than previously mentioned, this thesis promotes the original idea of a functional approximation of random variables/fields used to describe the material characteristics of elastoplastic systems.

1.2 Purpose of the study

In reality one possess only incomplete knowledge on the material characteristics and external excitations imposed on a system. Therefore, the main purpose of this dissertation is to develop an understanding and provide the quantification of the uncertainty arising in problems described by irreversible phenomena. Following this the two primary aims of this study are:

1. to investigate the presence of uncertainty in elastoplastic systems on both the material and structural level, and to ascertain the proper mathematical formulation accurately representing random media, and

2. to develop the most suitable numerical algorithms for the integration of random evolutionary equations.

Once the model is constructed and the numerical algorithms are developed, the sensitivity analysis can be done to determine the behaviour of heterogeneous materials.

1.3 Scope and focus of research

The aim of the present study is to develop a mathematical formulation and numerical approximation of small deformation [215, 92] and large displacement elastoplastic

behaviour [101] in a stochastic setting, going from linear elasticity via perfect plasticity to plasticity with linear hardening. By exhibiting the structure of the evolutionary equations in a convex setting [92, 65, 188], the study is carried over to the variational inequality formulation for the stochastic problem. This will hopefully show the mathematical similarity between the deterministic and the new formulation, and thus help to explain the abstract variational inequality and its stochastic interpretation.

In engineering practice there are many phenomena which may be described by a deterministic variational inequality of a particular order, such as the obstacle and contact problem. Due to the necessity to solve these problems a powerful mathematical tool has been developed, see e.g. [112, 81, 62, 92]. However, many of known phenomena are of an uncertain nature, and thus an attempt is made to extend the theory to a more general case described by a stochastic variational inequality (SVI) [88, 87, 86]. The main goal of this thesis is to extend the mentioned class of random variational inequalities (RVI) described by a random monotone operator on a random subset of a Hilbert space [88, 87, 86] to a mixed SVI for the elastoplastic problem, and to provide the study of the uniqueness and the existence of the solution for such posed problem. Another goal is to offer the appropriate numerical tool for solving the mixed SVI by transforming the variational inequality to the equivalent convex minimisation problem. This goal will be achieved with the help of a novel approach - a stochastic closest point projection algorithm based on "white noise analysis" [194, 155, 193, 195].

For the sake of simplicity, the associative irreversible behaviour described by the Prandtl-Reuss flow rule and the von Mises function with linear elastic and mixed hardening is taken as a study example. The perfectly plastic material behaviour is not considered mathematically as it cannot be described within Sobolev spaces (see [148, 147]) regarding their ability to form shear narrow bands of very high displacement gradients. Once the model is adopted, the material parameters describing the constitutive relation and the evolution path are assumed to be uncertain and further modeled by a random variable, random field, or stochastic process [6, 46, 59], depending on their properties. Such posed problem is then numerically treated using stochastic Galerkin method, similar to the one in the classical finite element methods [151, 107, 108, 150, 73, 67, 155, 193, 194].

In order to separate the random part of the problem from the deterministic (spatial) one, the input random fields are approximated by the Karhunen-Loève expansion [78, 107, 110, 150], followed by polynomial chaos expansion à la Wiener [150, 238, 246] in each FEM integration point. Such an approach further allows an explicit functional relationship between the independent random variables and the solution, making the subsequent evaluations of functionals (the mean, covariance, or

probabilities of exceedence) very cheap [107]. In general two possible versions of stochastic Galerkin method are introduced: the non-intrusive, which uses the classical finite element method in a black-box fashion, and the intrusive, which requires the full knowledge of the model. Besides the Galerkin projection, several other versions of general non-intrusive methods such as stochastic collocation [17, 144, 172] are also discussed.

The intrusive Galerkin method directly computes a solution via linear and nonlinear operations of polynomial chaos algebra [56, 140, 150]. The method takes the ansatz of the response solution in a form of polynomial chaos expansion, which further allows the theory of functional analysis to be employed. As it does not rely on sampling, the method is shown to be very robust and efficient. However, the same procedure may be applied in another way by calculating the residuum via high-dimensional integration methods. These are known as non-intrusive Galerkin techniques [150, 11], as they are based on random sampling—Monte Carlo and related techniques—or deterministic sampling such as collocation methods.

By highlighting the dependence of the random solution on the uncertain parameters, the influence of individual uncertain characteristics on the structure response is investigated by testing several numerical problems in plain strain or plane stress conditions.

1.4 Significance of the study

As it is becoming increasingly difficult to ignore the presence of uncertainty in the description of materials, the main significance of this paper is to improve the existing mathematical models of elastoplastic phenomena by including the uncertanties into the problem. In recent years there has been an increasing interest in stochastic linear problems (see e.g. [107, 157, 244]), taking the form of linear elastic equations, while only few studies are considering more complex nonlinear phenomena. To allow further generalisation, this thesis offers a study of an elasto-plastic system, or, mathematically speaking, a variational inequality described by a random constitutive tensor. Such a model can be used as the surrogate for the description of rocks or soils, concrete, and many biological materials such as bone tissue. In these situations the stochastic models are more informative than the deterministic ones. They produce the full distribution of possible outcomes, give the confidence levels that a certain outcome will happen, provide correlations between the events, and so on. In this manner the description of real situations, such as the development of a tumor in

bone tissue, the breaking risk of a concrete dam, the confidence of materials in civil structures under the influence of known or uncertain excitations (seismic phenomena, wind, and snow), can be provided.

In addition to reasons previously mentioned, the stochastic elastoplastic formulation may also become very important in the process of the identification of material properties such as yield stress, hardening, etc. Namely, once a set of noisy and incomplete measurement data is provided one may alter (update) the a priori assumed probability model to a more realistic one with the help of Bayesian probabilistic models [122, 180, 192, 191]. The process of updating requires the computation of the system response when the input parameters are uncertain, which is the topic of this work. For example a constitutive tensor can be identified by measuring the deformation of a specimen under an applied force. On the other side, theoretically a constitutive tensor can be modelled with the help of the maximum entropy approach [222, 52] as one possess certain information about material characteristics a priori. Such model further can be updated (see [192, 191]) using the measurement and the stochastic elastoplastic formulation as presented in this work.

1.5 Expected results

One of the main objectives of this study is to propose several solution strategies for the propagation of uncertainties in an elastoplastic model. Uncertainty propagation with the help of direct integration techniques such as Monte Carlo methods requires a huge computational effort. To overcome this issue, the thesis investigates and develops more efficient methods for the computation of the unique solution of the stochastic convex optimisation problem. These methods employ the stochastic Galerkin projection in its fully intrusive or non-intrusive variant. The intrusive methods are essentially algebraic and require only one program-run, which makes them very efficient computationally. However, the algebraic operations require certain truncations which further may cause poor accuracy if the order of corresponding polynomials is not sufficiently high. Additionaly, the increase of the polynomial order is not an easy task since the memory requirements and the dimensions of the problem fastly grow. In order to overcome these problems a non-intrusive variant of the stochastic Galerkin method is pursued. The method integrates the residual with the help of one of several possible numerical techniques such as random sampling, full or sparse grid quadrature. The advantage of non-intrusive methods is the possibility to use FEM in a black-box manner. Such an approach delivers better accuracy in smaller stochastic dimensions at the expense of computational cost. Similar is valid for the stochastic

collocation method with the only difference that one does not need any improved communication with the deterministic software such as the call of the residual or stiffness functions.

1.6 Thesis outline

The thesis is organised as follows: Chapter 2 gives an overview on the mathematical theory of deterministic plasticity with the focus on the description of infinitesimal behaviour. Most of this chapter is a presentation of the existing work published in [195]. To give a better mathematical understanding the abstract mixed variational formulation of the infinitesimal problem is introduced and further extended to the large displacement case.

Chapter 3 offers the mathematical description of the stochastic elastoplastic behaviour described by uncertain parameters. The chapter starts with the description of uncertainties appearing in the elastoplastic problem and their modelling with the help of a fully or reduced parametric approach. Such modelled parameters are then introduced into the generalised formulation of the irreversible behaviour previously described in Chapter 2. Once the description of basic constitutive relations is provided, the abstract and mixed stochastic variational formulations of the problem are introduced. For computational purposes the problem is reduced to the minimization of the quadratic convex functional for which the numerical algorithms are proposed.

Chapter 4 outlines the process of the discretisation of the considered problem. As the input properties and the structure response are time, spatially and stochastically dependent, this chapter offers possible numerical strategies for the approximation of time intervals, geometrical domain, and probability space. In this light Chapter 4 is a preparation for Chapter 5, which further considers various numerical approaches used to solve the discretised problem. The main focus of Chapter 5 is set on the direct stochastic Galerkin method and its non-intrusive alternative as novel procedures, while the numerical methods already existing in literature are only shortly reviewed. Following this, the stochastic variant of the closest point projection algorithm [215] is introduced and analysed.

In order to enrich and clarify the structure of Chapter 5, Chapter 6 provides more details about functional approximations and polynomial chaos algebra. The chapter contributes the basic polynomial chaos operations of linear and nonlinear type for both scalar and tensor valued random variables together with the various numerical

approaches for their computation.

Furthermore, Chapter 7 outlines the structure of the library PLASTON (PLAsticity - STOchastic aNalysis), and provides a concise description of main routines and library modules by offering the most important user information. After this, some applications of numerical methods are presented in Chapter 8 on several test examples in plain strain conditions.

Chapter 2

Deterministic theory of plasticity

Everything, including that which happens in our brains, depends on these and only on these: A set of fixed, deterministic laws. A purely random set of accidents.

M. Minsky

In order to introduce the mathematical formulation of the stochastic elastoplastic behaviour a short overview of its origin, i.e. the deterministic theory, is presented. The description is based on the general loading behaviour and fundamental notions such as continuity and smoothness conditions, decomposition of the deformation into elastic and plastic parts, the associated flow rule, the loading criterion, and the isotropy. According to these the chapter studies the associative plasticity models described by a rate-independent response with the plastic flow occurring instantaneously upon activation, and enforcing the stresses to stay in the elastic domain bounded by an yield surface [92, 101, 115, 215]. The presence of viscosity and its influence on the plastic flow rate have been neglected since the viscoplastic solids exhibit permanent deformations but continue to undergo a creep flow as a function of time under the influence of the applied load, for more detail see [55, 93, 160, 215, 135, 234, 42].

2.1 General formulation

Let the material body $\mathcal{G}$ smoothly move through the Euclidean space $\mathbb{R}^3$ in the time interval $\mathcal{T} = [0, T] \subset \mathbb{R}_+$ such that in each moment it occupies a certain spatial

domain. The body represents a three-dimensional manifold with piecewise smooth Lipschitz continuous boundary $\Gamma = \partial\mathcal{G}$, on which are imposed boundary conditions in Dirichlet and Neumann form on $\Gamma_D \subseteq \partial\mathcal{G}$ and $\Gamma_N \subset \partial\mathcal{G}$ respectively, such that $\Gamma_D \cap \Gamma_N = \varnothing$ and $\partial\mathcal{G} = \bar{\Gamma}_N \cup \bar{\Gamma}_D$. The body is imagined as being an assemblage of material particles X moving in time to the new position $x = \varphi(X,t) : \mathcal{G}_0 \times \mathcal{T} \to \mathbb{R}^3$, where the twice piecewise continuously differentiable function $\varphi(X,\cdot)$ describes the path of the material point $X \in \mathcal{G}$ in $\mathbb{R}^3$. For any fixed time t the mapping $\varphi(\cdot,t)$ represents the new configuration $\mathcal{G}_t$, i.e. deformation [215, 30, 115, 24]. According to this two possible configurations are explored—the initial (material) $\mathcal{G}_0$ (at $t_0 = 0$) and the current (spatial) $\mathcal{G}_t$ (at arbitrary time t).

The body motion obeys several conservation laws [249, 229], i.e. the conservation of mass, linear and angular momentum, and the first and second law of thermodynamics. Under the assumption of quasi-static deformations, the linear momentum takes the form of the equilibrium equations given here in *spatial description* (with respect to the current configuration):

$$-\operatorname{div}\boldsymbol{\sigma} = \boldsymbol{f} \quad \text{a.e. in } \mathcal{G}_t \times \mathcal{T}, \tag{2.1}$$

where $\boldsymbol{\sigma} \in \operatorname{Sym}(\mathbb{R}^d)$ denotes the stress tensor and $\boldsymbol{f} \in \mathbb{R}^d$ describes volume forces. The continuity of forces on Γ_N implies:

$$\boldsymbol{\sigma}\cdot\boldsymbol{n} = \boldsymbol{\sigma}_N \quad \text{a.e. in } \Gamma_N \times \mathcal{T}, \tag{2.2}$$

where $\boldsymbol{n} \in \mathbb{R}^d$ is the exterior unit normal at $x \in \Gamma_N$, and $\boldsymbol{\sigma}_N \in \mathbb{R}^d$ is a prescribed surface tension. In addition, one may constrain the displacement $\boldsymbol{u} \in \mathbb{R}^d$ on Γ_D as:

$$\boldsymbol{u} = \boldsymbol{u}_0 \quad \text{a.e. in } \Gamma_D \times \mathcal{T}, \tag{2.3}$$

where $\boldsymbol{u}_0$ is the prescribed boundary displacement, here for the sake of simplicity assumed to be $\boldsymbol{u}_0 = \boldsymbol{0}$ (i.e. homogenous Dirichlet boundary conditions).

The spatial description in the form as previously given can be physically interpreted due to the presence of Cauchy stresses $\boldsymbol{\sigma}$. However, its practical implementation is limited since the coordinates $\boldsymbol{x}$ are not generally known before the problem is solved (e.g. finite strain case). Thus, very often Eqs. (2.1) to (2.3) are rewritten with respect to the initial configuration X (*material formulation*) as shown in [215, 101, 55].

The thermodynamic laws describe the state of the system in a local form with respect to the deformation gradient $\boldsymbol{F} = \nabla\varphi \in \mathrm{GL}_+(d)$, the local entropy $s \in \mathbb{R}$ and a set of additional internal variables $\boldsymbol{\eta} \in \mathcal{Q}$ belonging to the vector space or possibly manifold. Note that the deformation gradient $\boldsymbol{F}(x)$ belongs to the general linear

group (i.e. the smooth (differentiable) manifold locally similar to a linear space[1])

$$\boldsymbol{F}(x) \in \mathrm{GL}_+(d) = \{\boldsymbol{F} = \nabla\varphi(x) \in \mathbb{R}^{d\times d} \mid \det \boldsymbol{F} > 0\}, \tag{2.4}$$

and only exists under the smoothness assumption on the mapping $\varphi : \mathcal{G}_0 \to \mathcal{G}_t$ for all $x \in \mathcal{G}$. With respect to this, the thermodynamic state can be described in terms of the Helmholtz free energy [249]

$$\psi(\boldsymbol{F}, T, \boldsymbol{\eta}) = \inf_s \left(U(\boldsymbol{F}, s, \boldsymbol{\eta}) - sT\right), \tag{2.5}$$

and the evolution law:

$$\dot{\boldsymbol{\eta}} = \dot{\boldsymbol{\eta}}(\boldsymbol{F}, \boldsymbol{\eta}) \tag{2.6}$$

which takes into account historical effects due to the evolution of internal variables with time. The Helmholtz free energy in Eq. (2.5) is obtained via the Legendre transformation of the internal energy U and represents the function of the deformation gradient $\boldsymbol{F}$, the internal variables $\boldsymbol{\eta}$, and the temperature T. However, in this work one is only interested in isothermal conditions for which the temperature dependence is excluded.

When the irreversible process occurs, the system energy dissipates over time according to the reduced local Clausius-Duhem inequality [92, 90]:

$$\left(\frac{\partial\psi}{\partial\boldsymbol{F}} - \boldsymbol{P}\right) : \dot{\boldsymbol{F}} + \frac{\partial\psi}{\partial\boldsymbol{\eta}} : \dot{\boldsymbol{\eta}} \leq 0, \tag{2.7}$$

where $\dot{\boldsymbol{F}}$ is arbitrarily chosen such that the relations for the first Piola-Kirchhoff stress $\boldsymbol{P} = \partial\psi/\partial\boldsymbol{F}$ and the conjugate force $\boldsymbol{\chi} = -\partial\psi/\partial\boldsymbol{\eta}$ hold. In this notation the inequality Eq. (2.7) obtains the following form:

$$\boldsymbol{\chi} : \dot{\boldsymbol{\eta}} \geq 0 \tag{2.8}$$

further used to closely describe the associative, rate-independent, and isothermal irreversible processes in small and finite strain case. Namely, those two cases are different with respect to the measure of displacement $\boldsymbol{u} = x - X$ and strain (measure of deformation). In small strain case one has $\|\nabla_M \boldsymbol{u}\| \to \|\nabla_M \boldsymbol{u} \approx \nabla_S \boldsymbol{u} := \boldsymbol{u} \otimes \nabla_S\| << 1$, i.e. the overlapping of the current $\mathcal{G}_t$ and initial $\mathcal{G}_0$ configurations as a direct consequence. Here, ∇_M denotes the derivative with respect to the material coordinates, and ∇_S with respect to spatial ones. On the other side, in finite strain case the statement $\nabla_M \boldsymbol{u} \approx \nabla_S \boldsymbol{u}$ does not hold, and thus the description of the body is not unique [101, 24, 30, 55].

[1] This means that manifold can be described by a collection of charts, which lie within a linear space.

2.2 Small deformation plasticity

When the displacements are small compared to the initial size of body, one may neglect the difference between the initial and current configuration. This further means that the strain is uniquely defined as a symmetric part of the displacement gradient:

$$\boldsymbol{\varepsilon} = \nabla_S \boldsymbol{u} := \frac{1}{2}\left[\nabla \boldsymbol{u} + \nabla \boldsymbol{u}^T\right] \quad \text{a.e. in } \mathcal{G}, \tag{2.9}$$

and belongs to a space of symmetric tensors $\mathrm{Sym}\,(\mathbb{R}^d) = \{\boldsymbol{\epsilon} \in \mathbb{R}^{d\times d} : \boldsymbol{\epsilon} = \boldsymbol{\epsilon}^T\}$. The use of linearised strain as a measure of deformation is justified by the invariability condition under the rigid body displacements $\mathcal{U}_r := \{\boldsymbol{u} : \mathcal{G} \to \mathbb{R} \,|\, \boldsymbol{u} = \boldsymbol{a} + \boldsymbol{b}\boldsymbol{x},\ \boldsymbol{c} \in \mathbb{R}^d,\ \boldsymbol{b} \in \mathbb{R}^{d\times d} : \boldsymbol{b} = -\boldsymbol{b}^T\}$ such that $\boldsymbol{\varepsilon}(\boldsymbol{u}) = \boldsymbol{0}$ iff $\boldsymbol{u} \in \mathcal{U}_r$. Besides, the strain tensor is constrained by six so-called compatibility conditions [57, 169] and describes the change in volume via the sum of diagonal elements, as well as the change of the angles via off-diagonal elements (shear strains). Following this, from Eq. (2.5)–Eq. (2.8) one may deduce the Helmholtz free energy $\psi = \psi(\boldsymbol{\varepsilon}, \boldsymbol{\eta})$, evolution law $\dot{\boldsymbol{\eta}} = \dot{\boldsymbol{\eta}}(\boldsymbol{\varepsilon}, \boldsymbol{\eta})$, stress $\boldsymbol{\sigma} = \partial\psi/\partial\dot{\boldsymbol{\varepsilon}}$, and conjugate forces $\boldsymbol{\chi} = -\partial\psi/\partial\boldsymbol{\eta}$ as functions of the total strain $\boldsymbol{\varepsilon}$ and the vector of internal variables $\boldsymbol{\eta}$. These quantities describe the standard media [89, 91] for which the internal variables quantify the hardening/softening of material (i.e. the increase/decrease of its elastic limit σ_y). To these one may add the decoupling of the strain into elastic and plastic response via the additive decomposition:

$$\boldsymbol{\varepsilon} = \boldsymbol{\varepsilon}_e(\boldsymbol{\sigma}) + \boldsymbol{\varepsilon}_p(\boldsymbol{\eta}), \tag{2.10}$$

where the elastic strain $\boldsymbol{\varepsilon}_e$ defines the measure of the deformation when the distorted body returns to its original shape and size after the force is removed, and the plastic strain $\boldsymbol{\varepsilon}_p$ describes the irreversible behaviour, i.e. plays a role of an internal variable — the "memory" of the material.

In order to simplify the notation one may collect the set of "plastic-like" variables to *a generalized plastic strain* $\boldsymbol{E}_p := (\boldsymbol{\varepsilon}_p, \boldsymbol{\eta})$ and its conjugate stresses to a *generalised stress* $\boldsymbol{\Sigma} = (\boldsymbol{\sigma}, \boldsymbol{\chi})$. In this notation, following Eq. (2.10), one may rewrite the total Helmholtz energy as a sum

$$\psi = \psi_e(\boldsymbol{\varepsilon}_e) + \psi_{irr}(\boldsymbol{E}_p) \tag{2.11}$$

of reversible $\psi_e = \frac{1}{2}\langle \boldsymbol{\varepsilon}_e, A\boldsymbol{\varepsilon}_e\rangle$ and irreversible $\psi_{irr} = \frac{1}{2}\langle \boldsymbol{E}_p, H\boldsymbol{E}_p\rangle$ energy, both for simplicity taken as the quadratic functions of corresponding strains. Here, A and H denote the elastic and hardening operators, respectively, and $\langle\cdot,\cdot\rangle$ the corresponding

duality pairing. Similar to these the dissipation inequality in Eq. (2.8) transforms to:

$$\langle \boldsymbol{\Sigma}, \dot{\boldsymbol{E}}_p \rangle := \boldsymbol{\sigma} : \dot{\boldsymbol{\varepsilon}}_p + \langle \boldsymbol{\chi}, \dot{\boldsymbol{\eta}} \rangle \geq 0, \tag{2.12}$$

where the second term $\langle \boldsymbol{\chi}, \dot{\boldsymbol{\eta}} \rangle$ represents the dissipation due to the evolution of the internal variable $\boldsymbol{\eta}$.

Table 2.1: Plasticity described at material point

Model	Variable	Law valid a.e.
General hardening plasticity	Additive decomposition	$\boldsymbol{\varepsilon} = \boldsymbol{\varepsilon}_e + \boldsymbol{\varepsilon}_p$
		$\psi = \psi_e + \psi_{irr}$
	Generalised strain	$\boldsymbol{E}_p := (\boldsymbol{\varepsilon}_p, \boldsymbol{\eta})$
	Generalised stress	$\boldsymbol{\Sigma} = (\boldsymbol{\sigma}, \boldsymbol{\chi})$
	Reversible energy	$\psi_e = \frac{1}{2}\langle \boldsymbol{\varepsilon}_e, A\boldsymbol{\varepsilon}_e \rangle$
	Irreversible energy	$\psi_{irr} = \frac{1}{2}\langle \boldsymbol{E}_p, H\boldsymbol{E}_p \rangle$
	Hooke's law	$\boldsymbol{\sigma} = A\boldsymbol{\varepsilon}_e$
	Hardening law	$\boldsymbol{\chi} = H\boldsymbol{\eta}$
Elasticity	Strain	$\boldsymbol{\varepsilon} = \boldsymbol{\varepsilon}_e, \boldsymbol{\varepsilon}_p = 0, \boldsymbol{\eta} = 0$
	Energy	$\psi = \psi_e, \psi_{irr} = 0$
Perfect plasticity	Strain	$\boldsymbol{\varepsilon} = \boldsymbol{\varepsilon}_e + \boldsymbol{\varepsilon}_p, \boldsymbol{\eta} = 0$
	Energy	$\psi = \frac{1}{2}\langle \boldsymbol{\varepsilon} - \boldsymbol{\varepsilon}_p, A(\boldsymbol{\varepsilon} - \boldsymbol{\varepsilon}_p) \rangle$
Mixed hardening plasticity	Conjugate force	$\boldsymbol{\chi} = (\boldsymbol{\varsigma}, \zeta)$
	Internal variable	$\boldsymbol{\eta} = (\boldsymbol{\varepsilon}_p, \nu)$
	Kinematic law	$\boldsymbol{\varsigma} = -\boldsymbol{H}_{kin} : \boldsymbol{\varepsilon}_p$
	Isotropic law	$\zeta = -H_{iso}\nu$
	Hardening law	$\boldsymbol{\chi} = \boldsymbol{H} : \boldsymbol{\eta}, \boldsymbol{H}$
		$\boldsymbol{H} = \mathrm{diag}[\boldsymbol{H}_{kin}, H_{iso}]$

Depending on the properties of the general internal variable $\boldsymbol{E}_p$ one may separate elastic from plastic material behaviour. If $\boldsymbol{E}_p = \boldsymbol{0}$ the behaviour is purely *elastic (reversible)*, further described by a quadratic function $\psi_e := \psi(\boldsymbol{\varepsilon}_e)$, i.e. the Hooke's constitutive relation $\boldsymbol{\sigma} = A\boldsymbol{\varepsilon}_e = \boldsymbol{A} : \boldsymbol{\varepsilon}_e$. Here, $\boldsymbol{A} \in \mathcal{L}(\mathrm{Sym}(\mathbb{R}^d))$ denotes the fourth order symmetric, bounded, measurable, and pointwise-stable constitutive tensor; and A corresponding linear operator. For an isotropic homogenous material $\boldsymbol{A}$ takes the form of linear function $\boldsymbol{A} = K\boldsymbol{1} \otimes \boldsymbol{1} + 2G[\boldsymbol{I} - \frac{1}{3}\boldsymbol{1} \otimes \boldsymbol{1}]$ in terms of two material parameters[2], the bulk K and shear G moduli.

[2] $\boldsymbol{I}$ represents the fourth-order and $\boldsymbol{1}$ the second-order symmetric identity tensor

In case the internal variables $\boldsymbol{E}_p$ are present the material behaviour is plastic. In this work the focus is set only on two "simple" possible cases of such behaviour: perfect and mixed hardening plasticity (see Table 2.1). The perfect material undergoes irreversible changes of shape or size of the body without any further increase of stresses and loads, while the hardening material experiences the change of the domain of admissible stresses by its size (isotropic hardening) or position (kinematic hardening). For more details the reader is referred to [215, 92, 101, 55].

2.2.1 Associative plastic flow rule

The evolution of the plastic strain according to the *associative flow rule* is described by elastic domain $\mathcal{K}$—a closed convex set containing the origin ($\boldsymbol{\Sigma} = \mathbf{0} \in \mathcal{K}$)—which the stress cannot leave. In this sense, the dissipation in Eq. (2.12) becomes maximal [136] and for $\mathbf{0} \in \mathcal{K}$ the law is clearly satisfied.

Table 2.2: Plastic flow rule formulations

Dual	
Normal cone	$N_{\mathcal{K}}(\boldsymbol{\Sigma}) = \{\Xi \in \mathcal{E} \mid \langle \Xi, \boldsymbol{T} - \boldsymbol{\Sigma} \rangle \leq 0\} \subseteq \mathcal{E}$
Indicator of $\mathcal{K}$	$\Psi_{\mathcal{K}}(\boldsymbol{\Sigma}) = 0$, if $\boldsymbol{\Sigma} \in \mathcal{K}$, otherwise $\Psi_{\mathcal{K}}(\boldsymbol{\Sigma}) = \infty$
Flow rule	$\dot{\boldsymbol{E}}_p \in N_{\mathcal{K}}(\boldsymbol{\Sigma}) = \partial \Psi_{\mathcal{K}}(\boldsymbol{\Sigma}) \Leftrightarrow \langle \dot{\boldsymbol{E}}_p, \boldsymbol{\Sigma} - \boldsymbol{T} \rangle \leq 0$
Primal	
Conjugate dual	$\Psi^*_{\mathcal{K}}(\Xi) = \{\boldsymbol{T} \in \mathcal{Y} \mid \sup(\langle \Xi, \boldsymbol{T} \rangle - \Psi_{\mathcal{K}}(\boldsymbol{T}))\}$
Dissipation	$j(\dot{\boldsymbol{E}}_p) = \Psi^*_{\mathcal{K}}(\dot{\boldsymbol{E}}_p) = \{\boldsymbol{T} \in \mathcal{K} \mid \sup \langle \dot{\boldsymbol{E}}_p, \boldsymbol{T} \rangle\}$
Convex domain $\mathcal{K}$	$\mathcal{K} = \partial \Psi^*_{\mathcal{K}}(0) = \partial j(0)$
Barrier cone of $\mathcal{K}$	$\mathcal{K}^{\infty} := \{\Xi \mid \langle \Xi, \boldsymbol{T} \rangle < \infty \quad \forall \boldsymbol{T} \in \mathcal{K}\}$
Flow rule	$\boldsymbol{\Sigma} \in \partial \Psi^*_{\mathcal{K}}(\dot{\boldsymbol{E}}_p)$
Yield function	
Gauge function	$g_{\mathcal{K}}(\boldsymbol{\Sigma}) = \inf\{\lambda > 0 \mid \forall \Xi : \langle \Xi, \boldsymbol{\Sigma} \rangle \leq \lambda \Psi^*_{\mathcal{K}}(\Xi)\}$
Yield function	$\phi_{\mathcal{K}}(\boldsymbol{\Sigma}) := g_{\mathcal{K}}(\boldsymbol{\Sigma}) - 1$,
Convex domain	$\mathcal{K} = \{\boldsymbol{\Sigma} \mid \phi_{\mathcal{K}}(\boldsymbol{\Sigma}) \leq 0\}$
Flow rule	$\exists \lambda \geq 0 : \dot{\boldsymbol{E}}_p \in \lambda \partial \phi_{\mathcal{K}}(\boldsymbol{\Sigma}) \ \wedge \ \lambda \phi_{\mathcal{K}}(\boldsymbol{\Sigma}) = 0$

With the help of the definition of the elastic domain the flow rule can be described in two equivalent forms: dual and primal. The first is given in terms of indicator function $\Psi_{\mathcal{K}}(\boldsymbol{\Sigma})$ of $\mathcal{K}$, whose sub-differential represents the normal cone $N_{\mathcal{K}}(\boldsymbol{\Sigma})$

at point $\boldsymbol{\Sigma}$ on $\mathcal{K}$, see Table 2.2 and [92, 195, 168]. On the other side, the primal law introduces the convex and lower semi-continuous support function $\Psi^*_{\mathcal{K}}(\Xi)$ of $\mathcal{K}$, obtained by the Legendre-Fenchel transform of the indicator function. This function is identified with the dissipation $j(\dot{\boldsymbol{E}}_p)$, i.e. a non-negative (as $0 \in \mathcal{K}$), convex, lower-semicontinuous, and positively homogenous ($\forall \lambda > 0 : j(\lambda \Xi) = \lambda j(\Xi)$) function satisfying $j(0) = 0$. The effective domain of j is the so-called barrier cone $\mathcal{K}^\infty$ of $\mathcal{K}$, a closed convex cone. For such support functions one has $\mathcal{K} = \partial \Psi^*_{\mathcal{K}}(0) = \partial j(0)$, $\boldsymbol{\Sigma} \in \partial j(\dot{\boldsymbol{E}}_p) \Leftrightarrow \boldsymbol{\Sigma} \in \partial j(0)$ (as for any positively homogenous convex function), and $\langle \Xi, \boldsymbol{\Sigma} \rangle = j(\Xi)$. Following this, the primal formulation of the flow law (see Table 2.2) is equivalent to the dual form by stating that $\partial j^* = \partial \Psi_{\mathcal{K}}$ is a cone. For a detailed derivation please see the technical report by Rosić et al. [195].

As for the characterization of the elastic domain, the most common one is still missing, namely in terms of a yield function. For that the notion of a Minkowski [187] or gauge functional $g_{\mathcal{K}}(\boldsymbol{\Sigma})$ of a convex set $\mathcal{K}$ is needed. The functional defines the "canonical" yield function $\phi_{\mathcal{K}}(\boldsymbol{\Sigma})$ which further gives the definition of the flow rule as in Table 2.2. In case of a smooth function $\phi_{\mathcal{K}}(\boldsymbol{\Sigma})$ the sub-differential $\partial \phi_{\mathcal{K}}(\boldsymbol{\Sigma})$ is replaced by gradient $\nabla \phi_{\mathcal{K}}(\boldsymbol{\Sigma})$, and the flow rule obtains the form of the familiar relation of classical elastoplasticity: $\exists \lambda \geq 0 : \dot{\boldsymbol{E}}_p = \lambda \nabla \phi_{\mathcal{K}}(\boldsymbol{\Sigma}) \wedge \lambda \phi_{\mathcal{K}}(\boldsymbol{\Sigma}) = 0$, $\mathcal{K} = \{\boldsymbol{\Sigma} \mid \phi_{\mathcal{K}}(\boldsymbol{\Sigma}) \leq 0\}$. Note that over the years a large number of yield functions (criteria) have been developed mostly for materials used in engineering. For this the reader is referred to [55, 45, 236, 158] for further details.

2.2.2 Time discretisation of the flow rule

Let us divide the time interval $[0, T]$ into steps $\Delta t_n = t_n - t_{n-1}$ with time points denoted by $t_n, n = 0, 1, \cdots$. The goal is to approximate the state of the material such that the relations in Table 2.2 are satisfied at the end of the time increment given the state of the material at t_{n-1}. The state is described by values of the total strain $\boldsymbol{E}_n := (\boldsymbol{\varepsilon}_n, 0)$, its increment $\Delta \boldsymbol{E}_n$, and the plastic strain $\boldsymbol{E}_{p,n}$ (which then defines the stress $\boldsymbol{\Sigma}_n = A : (\boldsymbol{E}_n - \boldsymbol{E}_{p,n})$). To simplify the notation for all quantities to follow an index "n" is used to denote the quantity at time t_n.

In order to approximate the rate $\dot{\boldsymbol{E}}_p$ one may use the difference quotient $\Delta \boldsymbol{E}_{p,n} = (\boldsymbol{E}_{p,n} - \boldsymbol{E}_{p,n-1})/\Delta t_n$, which in an Euler backward fashion has to be in the normal cone $N_{\mathcal{K}}(\boldsymbol{\Sigma}_n)$ at the end of the increment t_n (see Table 2.2). This is a special case of Moreau's sweeping process [162]:

$$\frac{1}{\Delta t_n}(\Delta \boldsymbol{E}_{p,n}) \in N_{\mathcal{K}}(\boldsymbol{\Sigma}_n) = \partial \Psi_{\mathcal{K}}(\boldsymbol{\Sigma}_n). \tag{2.13}$$

As $N_{\mathcal{K}}$ is a cone it also holds that $\Delta \boldsymbol{E}_{p,n} \in N_{\mathcal{K}}(\boldsymbol{\Sigma}_n)$—one utilises the rate independence here—and hence the previous equation may be rewritten as a discrete normality rule:

$$\langle \Delta \boldsymbol{E}_{p,n}, \boldsymbol{T} - \boldsymbol{\Sigma}_n \rangle \leq 0, \quad \forall \boldsymbol{T} \in \mathcal{K}. \tag{2.14}$$

2.2.3 The closest point return algorithm

Both because this is the prototype for the actual computation and as this procedure is used in the abstract proofs, the well-known return mapping algorithm [215, 101, 195, 168] is described here starting with the dual rule in Table 2.2. As $\Delta \boldsymbol{E}_{p,n} = \boldsymbol{E}_{p,n} - \boldsymbol{E}_{p,n-1} = \boldsymbol{E}_n - \boldsymbol{E}_{e,n} - \boldsymbol{E}_{n-1} + \boldsymbol{E}_{e,n-1} = \Delta \boldsymbol{E}_n + \boldsymbol{E}_{e,n-1} - \boldsymbol{E}_{e,n} = A^{-1}(\boldsymbol{\Sigma}^{trial} - \boldsymbol{\Sigma}_n)$ with $\boldsymbol{\Sigma}^{trial} := A(\Delta \boldsymbol{E}_n + \boldsymbol{E}_{e,n-1})$, one obtains from $\langle \dot{\boldsymbol{E}}_p, \boldsymbol{\Sigma} - \boldsymbol{T} \rangle \leq 0$ the variational inequality

$$\langle \triangle \boldsymbol{E}_{pn}, \boldsymbol{T} - \boldsymbol{\Sigma}_n \rangle \leq 0, \quad \forall \boldsymbol{T} \in \mathcal{K} \tag{2.15}$$

and the equivalent minimisation functional

$$\langle \boldsymbol{\Sigma}_n, A^{-1}(\boldsymbol{T} - \boldsymbol{\Sigma}_n) \rangle \geq \langle A^{-1} \boldsymbol{\Sigma}^{trial}, \boldsymbol{T} - \boldsymbol{\Sigma}_n \rangle, \quad \forall \boldsymbol{T} \in \mathcal{K} \tag{2.16}$$

as a special case of a general variational inequality described in Section 2.3. This further leads to a constrained minimisation problem

$$\begin{aligned} \boldsymbol{\Sigma}_n &= \arg\min_{\boldsymbol{\Sigma} \in \mathcal{K}} \Phi(\boldsymbol{\Sigma}) \\ &= \arg\min_{\boldsymbol{\Sigma} \in \mathcal{K}} \{ \frac{1}{2} \langle A^{-1}(\boldsymbol{\Sigma}^{trial} - \boldsymbol{\Sigma}), \boldsymbol{\Sigma}^{trial} - \boldsymbol{\Sigma} \rangle \} \end{aligned} \tag{2.17}$$

in its familiar "closest-point-return" form. This means that $\boldsymbol{\Sigma}_n$ is the projection of $\boldsymbol{\Sigma}^{trial}$ onto the closed convex set $\mathcal{K}$ in the metric given by $\boldsymbol{A}^{-1}$, i.e. the norm $\langle \boldsymbol{\Sigma} : \boldsymbol{A}^{-1} : \boldsymbol{\Sigma} \rangle^{1/2}$. Observe that $\boldsymbol{\Sigma}^{trial}$ is the stress which would result if the increments were purely elastic.

2.3 Minimisation principle

After the preceding well-known description at a material point, the present and next section will cover some abstract results regarding the theory outlined in the previous

sections. As already discussed, the elastoplastic problem in each time step converts to the standard convex optimization problem described by a quadratic convex objective function Φ. In addition, if the minimisation is performed over a convex region then the existence and uniqueness of the globally optimal minimum directly follow [195, 224, 239].

Let $\Phi(z)$ be a strictly convex, continuous, Gâteaux differentiable, and coercive functional on a Hilbert space $\mathcal{Z}$, i.e. $\Phi(z) \to \infty$ as $\|z\| \to \infty$. In particular one may look at a continuous (or bounded $a(z_1, z_2) \leq c\|z_1\|\|z_2\|$), symmetric and $\mathcal{Z}$-elliptic ($a(z, z) \geq c\|z\|^2$) bilinear form $a : \mathcal{Z} \times \mathcal{Z} \to \mathbb{R}$ and an element $y \in \mathcal{Z}^*$. These are used to define the functional:

$$\Phi(z) = \frac{1}{2}a(z, z) - \langle y, z\rangle. \tag{2.18}$$

As a and y are continuous and Gâteaux-differentiable, and as a is $\mathcal{Z}$-elliptic, Φ has all the properties stated above. To handle the dissipation one has to allow for a second convex functional j on $\mathcal{Z}$, which may not be Gâteaux differentiable everywhere. This functional is supposed to be the support functional of a closed convex set $\mathcal{K} \subset \mathcal{Z}^*$ containing the origin. One then has (see [92, 195]):

Proposition 2.3.1. *With the notation and assumptions just described the problem to minimise*

$$\min_{z\in\mathcal{Z}} (\Phi(z) + j(z)) \tag{2.19}$$

has a unique solution:

$$w = \arg\min_{z\in\mathcal{Z}} (\Phi(z) + j(z)), \tag{2.20}$$

characterised by $0 \in \partial(\Phi(w) + j(w))$*, i.e.*

$$-\delta\Phi(w) \in \partial j(w), \tag{2.21}$$

where $\delta\Phi(w) = a(w, \cdot) - y$ *is the Gâteaux derivative of* Φ*. The last relation may also be written as:*

$$\forall z \in \mathcal{Z} : a(w, z - w) + j(z) - j(w) \geq \langle y, z - w\rangle, \tag{2.22}$$

i.e. an elliptic variational inequality of the second kind.

Proof. See [81]. □

For brevity's sake let us denote $w^* = -\delta\Phi(w)$. Then Eq. (2.21) becomes

$$w^* \in \partial j(w), \tag{2.23}$$

which is equivalent to

$$w \in \partial j^*(w^*) = \partial \Psi_{\mathcal{K}}(w^*), \tag{2.24}$$

or

$$\langle w, z^* - w^* \rangle \leq 0, \quad \forall z^* \in \mathcal{K}. \tag{2.25}$$

Following this one may write:

Theorem 2.3.2. *With the notation and assumptions as before, the problem:*

$$\min_{z \in \mathcal{Z}} \left(\Phi(z) + j(z) \right) \tag{2.26}$$

has a unique solution $w \in \mathcal{Z}$*,*

$$w = \arg\min_{z \in \mathcal{Z}} \left(\Phi(z) + j(z) \right) \tag{2.27}$$

characterised by

$$\exists w^* \in \mathcal{K},\ \forall z \in \mathcal{Z} :\ a(w, z) + \langle w^*, z \rangle = \langle y, z \rangle \tag{2.28}$$

and

$$\forall z^* \in \mathcal{K} :\ \langle w, z^* - w^* \rangle \leq 0. \tag{2.29}$$

Proof. Follows from Proposition 2.3.1 and Eq. (2.23)-Eq. (2.25). □

The bilinear form a defines a linear, continuous, self-adjoint, and coercive ($\langle Az, z \rangle \geq c_2 \|z\|^2$) operator $A : \mathcal{Z} \to \mathcal{Z}^*$ via

$$\forall v, z \in \mathcal{Z} :\ a(z, v) = \langle Az, v \rangle. \tag{2.30}$$

Due to the properties just stated, A has an inverse $A^{-1} : \mathcal{Z}^* \to \mathcal{Z}$ with the same attributes. This allows us to define a bilinear, continuous, symmetric, and coercive form a^* on $\mathcal{Z}^*$:

$$a^*(z_1^*, z_2^*) = \langle z_1^*, A^{-1} z_2^* \rangle, \tag{2.31}$$

or, in other words, if $u \in \mathcal{Z}$ solves:

$$\forall z \in \mathcal{Z} : \; a(u, z) = \langle z_2^*, z \rangle, \tag{2.32}$$

then

$$a^*(z_1^*, z_2^*) = \langle z_1^*, u \rangle. \tag{2.33}$$

If the bilinear form a can be identified in our application with the Helmholtz free energy, then a^* is the complementary energy.

We need the following result, now for variational inequalities of the first kind:

Proposition 2.3.3. *Let $\mathcal{V}$ be a Hilbert space, $\varphi : \mathcal{Z} \to \mathbb{R}$ a strictly convex Gâteaux-differentiable, coercive functional, and $\mathcal{K} \subset \mathcal{V}$ a non-empty, closed, convex set containing the origin. Then the minimisation problem:*

$$\min_{v \in \mathcal{K}} \varphi(v) \tag{2.34}$$

has a unique solution $u \in \mathcal{V}$,

$$u = \arg\min_{v \in \mathcal{K}} \varphi(v), \tag{2.35}$$

characterised by

$$\forall v \in \mathcal{K} : \quad \langle \delta\varphi(u), v - u \rangle \geq 0, \tag{2.36}$$

where $\delta\varphi$ is the Gâteaux-derivative of φ.

Proof. See [81]. □

Let $\mathcal{V} = \mathcal{Z}^*$, and $\varphi(z^*) = \frac{1}{2} a^*(y - z^*, y - z^*)$ with Gâteaux derivative:

$$\delta\varphi(z^*) = a^*(z^*, \cdot) - a^*(y, \cdot) = a^*(z^* - y, \cdot). \tag{2.37}$$

From Eq. (2.28) in Theorem 2.3.2 one may see that w solves :

$$\forall z \in \mathcal{Z} : \quad a(w, z) = \langle y - w^*, z \rangle, \tag{2.38}$$

and hence with Eq. (2.32)

$$\varphi(w^*) = \frac{1}{2} a^*(y - w^*, y - w^*) = \frac{1}{2} \langle y - w^*, w \rangle, \tag{2.39}$$

and

$$\delta\varphi(w^*) = a^*(w^* - y, \cdot) = -w \tag{2.40}$$

Eq. (2.36) reads

$$\forall z^* \in \mathcal{K}: \quad -\langle w, z^* - w^* \rangle \geq 0. \tag{2.41}$$

These results can be collected in:

Theorem 2.3.4. *With the notation and assumptions as before, the problem in Theorem 2.3.2 is equivalent to:*

$$w^* = \underset{z^* \in \mathcal{K}}{\arg\min} \ \frac{1}{2} a^*(y - z^*, y - z^*) \tag{2.42}$$

(w^* is in $\mathcal{K}$ the closest point to y in the a^* metric), characterised by:

$$\exists w \in \mathcal{Z}, \forall z \in \mathcal{Z}: \quad a(w, z) = \langle y - w^*, z \rangle \tag{2.43}$$

and

$$\forall z^* \in \mathcal{K}: \quad \langle w, z^* - w^* \rangle \leq 0. \tag{2.44}$$

Proof. Follows from Proposition 2.3.3 and Eq. (2.37)-Eq. (2.41). □

Hence, computing w^* as the closest point in Eq. (2.42), the pair (w, w^*) satisfies Theorem 2.3.2.

2.3.1 Functional spaces

The boundary value problem described by the equilibrium equation given in Section 2.1 will be recast in a weak form, also known as a variational formulation. This requires the definition of the functional spaces [92, 195] that are relevant to the problem considered in this work, namely plasticity with linear kinematic and isotropic hardening. The solution spaces are assumed to be the elements of the space of admissible functions. However, in a perfect plasticity case further described spaces are not applicable any more. In such a situation one introduces the space of functions of bounded deformation, as proposed in [147, 63]. For reasons of simplicity those spaces are not considered in this work.

Let $\mathcal{V}$ be a Hilbert space—with its dual $\mathcal{V}^*$—to which corresponds the space of the Bochner-Lebesgue p-integrable functions:

$$L_p(\mathcal{T},\mathcal{V}) = \{v : \mathcal{T} \to \mathcal{V} \mid \|v\|_{L_p} = \left(\int_0^T \|v(t)\|_{\mathcal{V}}^p \,\mathrm{d}t\right)^{\frac{1}{p}} < \infty,\ 1 \le p < \infty\} \tag{2.45}$$

with the usual extension to $\|v\|_{L_\infty} = \operatorname{ess\,sup}_{t\in\mathcal{T}} \|v(t)\|_{\mathcal{V}}$ for $p = \infty$. Going a step further one introduces the Sobolev space:

$$H^m(\mathcal{T},\mathcal{V}) = \{v \in L_2(\mathcal{G}) :\ \mathrm{D}^\alpha v \in L_2(\mathcal{G}),\ \alpha \le m\} \tag{2.46}$$

and for $u, v \in L_2(\mathcal{G})$ defines the duality pairing as:

$$\langle u, v\rangle_{L_2(\mathcal{G})} = \int_{\mathcal{G}} u(x)v(x)\,\mathrm{d}x, \tag{2.47}$$

such that for $u, v \in H^m(\mathcal{G})$

$$\langle u, v\rangle_{H^m(\mathcal{G})} = \sum_{|\alpha|\le m} \langle \mathrm{D}^\alpha u, \mathrm{D}^\alpha v\rangle \tag{2.48}$$

holds. In the previous notation $\alpha = (\alpha_1, ..., \alpha_d)$, $|\alpha| = \alpha_1 + ... + \alpha_d$, and the derivatives $D^\alpha v = \partial^{\alpha_1}...\partial^{\alpha_d} v$ are taken in a weak sense.

With the help of these definitions one may describe the space of admissible displacements as a Hilbert space $\mathcal{U}$ of one times differentiable functions including specified boundary conditions, see Table 2.3. This space is mapped to a strain space $\mathcal{E}$ via injective linear operator $\nabla_S \in \mathcal{L}(\mathcal{U},\mathcal{E})$ with the closed range, which for some constant $C_d > 0$ and all $u \in \mathcal{U}$ satisfies the following inequality $\|\nabla_S u\|_{\mathcal{E}} \ge C_d \|u\|_{\mathcal{U}}$. By additive decomposition the space of plastic strain $\mathcal{E}_p$ becomes the subspace of $\mathcal{E}$, i.e. the space of functions with zero trace. Similarly, the space of the internal variables $\mathcal{Q}$ is defined [195].

Besides previously described spaces, one may introduce the space of their functionals — dual spaces (also called stress or spaces of dynamic variables), see Table 2.3 and [92, 123]. To this set belongs the space of stresses $\mathcal{R} = \mathcal{E}^*$ determined by constitutive law $\boldsymbol{\sigma} = A\nabla_S \boldsymbol{u}$, which further gives $\boldsymbol{f} = \nabla_S^* \boldsymbol{\sigma} \in \mathcal{F} = \mathcal{U}^*$. Thus, the space of forces $\mathcal{F}$ is determined by operator $\nabla_S^* \in \mathcal{L}(\mathcal{E}^*, \mathcal{U}^*)$ dual to ∇_S. Similar is valid for the space of the conjugate thermodynamic forces $\mathcal{C}$. In order to simplify the notation, the definitions of the generalised strain space $\mathcal{P}$ and generalised stress space $\mathcal{Y}$ are

given as shown in Table 2.3. For a later formulation one may also introduce the so-called *primal* $\boldsymbol{w} := (\boldsymbol{u}, \boldsymbol{E}_p) \in \mathcal{Z}$ and *dual* $\boldsymbol{w}^* := (\boldsymbol{f}, \boldsymbol{\Sigma}) \in \mathcal{Z}^*$ variable given in corresponding "strain" $\mathcal{Z}$ and "stress" space $\mathcal{Z}^*$.

Table 2.3: The defintion of spaces for kinematic and dynamic variables together with the corresponding inner products

Variable	Space
Displacement $\boldsymbol{u}$ Force $\boldsymbol{f}$	$\mathcal{U} := \{\boldsymbol{u} \in H^1(\mathcal{G}) \mid \boldsymbol{u} = \boldsymbol{0} \text{ on } \Gamma_D\}$ $\mathcal{F} := \mathcal{U}^*$ $\langle \boldsymbol{f}, \boldsymbol{u} \rangle_{\mathcal{F}\times\mathcal{U}} := \int_{\mathcal{G}} \boldsymbol{f} \cdot \boldsymbol{u} \, \mathrm{d}x + \int_{\Gamma_N} \boldsymbol{g} \cdot \boldsymbol{u} \, \mathrm{d}s$
Strain $\boldsymbol{\varepsilon}$ Plastic strain $\boldsymbol{\varepsilon}_p$ Stress $\boldsymbol{\sigma}$	$\mathcal{E} := \{\boldsymbol{\varepsilon} \mid \boldsymbol{\varepsilon} \in L_2(\mathcal{G}, \mathrm{Sym}\,(\mathbb{R}^d)\}$ $\mathcal{E}_p := \{\boldsymbol{\varepsilon}_p \in \mathcal{E} : \ \mathrm{tr}\, \boldsymbol{\varepsilon}_p = 0 \ \text{ a.e. in } \mathcal{G}\}$ $\mathcal{R} := \mathcal{E}^* = \{\boldsymbol{\sigma} \colon \boldsymbol{\sigma} \in L_2(\mathcal{G}, \mathrm{Sym}(\mathbb{R}^d)\}$ $\langle \boldsymbol{\sigma}, \boldsymbol{\varepsilon} \rangle_{\mathcal{R}\times\mathcal{E}} := \int_{\mathcal{G}} \boldsymbol{\sigma} : \boldsymbol{\varepsilon} \, \mathrm{d}x$
Internal variables $\boldsymbol{\eta}$ Conjugate force $\boldsymbol{\chi}$	$\mathcal{Q} := \{\boldsymbol{\eta} \mid \boldsymbol{\eta} = (\boldsymbol{\varepsilon}_p, \nu) \in L_2(\mathcal{G}, \mathrm{Sym}(\mathbb{R}^d \times \mathbb{R})\}$ $\mathcal{C} := \{\boldsymbol{\chi} \mid \boldsymbol{\chi} = (\boldsymbol{\varsigma}, \zeta) \in L_2(\mathcal{G}, \mathrm{Sym}(\mathbb{R}^d) \times \mathbb{R}\}$ $\langle \boldsymbol{\chi}, \boldsymbol{\eta} \rangle_{\mathcal{C}\times\mathcal{Q}} := \int_{\mathcal{G}} \boldsymbol{\varsigma} : \boldsymbol{\varepsilon}_p \, \mathrm{d}x + \int_{\mathcal{G}} \zeta \cdot \nu \, \mathrm{d}x$
Gen. pl. def. $\boldsymbol{E}_p$ Gen. stress $\boldsymbol{\Sigma}$	$\mathcal{P} = \mathcal{E}_p \times \mathcal{Q}$ $\boldsymbol{\Sigma} \in \mathcal{Y} := \mathcal{R} \times \mathcal{C}$ $\langle \boldsymbol{\Sigma}, \boldsymbol{E}_p \rangle_{\mathcal{Y}\times\mathcal{P}} := \langle \boldsymbol{\sigma}, \boldsymbol{\varepsilon}_p \rangle_{\mathcal{R}\times\mathcal{E}} + \langle \boldsymbol{\chi}, \boldsymbol{\eta} \rangle_{\mathcal{C}\times\mathcal{Q}}$
Primal $\boldsymbol{w} := (\boldsymbol{u}, \boldsymbol{E}_p)$ Dual $\boldsymbol{w}^* := (\boldsymbol{f}, \boldsymbol{\Sigma})$	$\mathcal{Z} := \mathcal{U} \times \mathcal{P}$ $\mathcal{Z}^* := \mathcal{F} \times \mathcal{Y}$ $\langle \boldsymbol{w}^*, \boldsymbol{w} \rangle_{\mathcal{W}^*\times\mathcal{W}} := \langle \boldsymbol{f}, \boldsymbol{u} \rangle_{\mathcal{F}\times\mathcal{U}} + \langle \boldsymbol{\Sigma}, \boldsymbol{E}_p \rangle_{\mathcal{Y}\times\mathcal{P}}$

2.3.2 Variational formulation

As the variational form taken by elastoplastic problems includes variational inequalities and hence the corresponding minimization problems, this section collects some general results on this topic, mostly coming from the works of Stampacchia [131, 112], Glowinski [81], Duvaut and Lions [62], etc. In these papers one may find the description of the variational inequalities arising in problems such as stationary elasticity, perfect plasticity, and the contact problem.

Linear elasticity

Following the definitions for functional spaces in Section 2.3.1, one is able to introduce the linear functional:

$$l(\boldsymbol{v}) := \int_{\mathcal{G}} \boldsymbol{f}(x,t) \cdot \boldsymbol{v}(x)\, \mathrm{d}x + \int_{\Gamma_N} \boldsymbol{g}(x) \cdot \boldsymbol{v}(x)\, \mathrm{d}s, \tag{2.49}$$

together with the operator $A : \mathcal{E} \to \mathcal{R}$:

$$\langle A\boldsymbol{\varepsilon}, \boldsymbol{\epsilon} \rangle_{\mathcal{R}\times\mathcal{E}} = \int_{\mathcal{G}} [\boldsymbol{A} : \boldsymbol{\varepsilon}(x)] : \boldsymbol{\epsilon}(x)\, \mathrm{d}x, \quad \forall \boldsymbol{\epsilon} \in \mathcal{E} \tag{2.50}$$

such that the linear Hooke's law takes the form $\langle A\boldsymbol{\varepsilon}, \boldsymbol{\epsilon} \rangle = \langle \boldsymbol{\sigma}, \boldsymbol{\epsilon} \rangle$, $\forall \boldsymbol{\epsilon} \in \mathcal{E}$, i.e. $\boldsymbol{\sigma} = A\boldsymbol{\varepsilon} := \boldsymbol{A} : \boldsymbol{\varepsilon}$. By virtue of previous assumptions, the bilinear form

$$a(\boldsymbol{u}, \boldsymbol{v}) = \int_{\mathcal{G}} A\boldsymbol{\varepsilon}(\boldsymbol{u}) : \boldsymbol{\varepsilon}(\boldsymbol{v})\, \mathrm{d}x, \tag{2.51}$$

introduces an inner product $\|\boldsymbol{u}\|_A = a(\boldsymbol{u}, \boldsymbol{u})^{1/2}$ in the space $\mathcal{U}$, called the *energy inner product* [92, 202]. The energy norm is equivalent to the standard norm $\|\boldsymbol{u}\|_1$ of the space $H^1(\mathcal{G})$, i.e. $C_1\|\boldsymbol{u}\|_1 \leq \|\boldsymbol{u}\|_A \leq C_2\|\boldsymbol{u}\|_1$ (C_1 and C_2 are constants). Note that in the following text the usual Euclidean norm in $L_2(\mathcal{G})$ is denoted as $\|\boldsymbol{u}\| = (\boldsymbol{u}, \boldsymbol{u})^{1/2}$.

In this notation the weak form of equilibrium Eq. (2.1) can be further stated as follows:

Problem 2.3.5. ***Primal formulation of Elasticity problem PE****. For a given loading $\boldsymbol{f} \in \mathcal{F}$ find the solution $\boldsymbol{u} \in \mathcal{U}$ such that*

$$a(\boldsymbol{v}, \boldsymbol{u}) := \langle A\boldsymbol{\varepsilon}(\boldsymbol{u}), \boldsymbol{\varepsilon}(\boldsymbol{v}) \rangle = \ell(\boldsymbol{v}), \quad \forall \boldsymbol{v} \in \mathcal{U}, \tag{2.52}$$

i.e.

$$A\boldsymbol{u} = \ell \quad \text{in } \mathcal{U}^*, \tag{2.53}$$

is satisfied.

In terms of the Lax Milgram theorem [124] the conditions of boundness and $\mathcal{U}$-ellipticity of the bilinear form a directly imply the well-possedness of the problem in the sense of Hadamard, and therefore Problem 2.3.5 admits the unique solution. For

more details see [92].

The primal formulation in Problem 2.3.5 is not the only possible description of elastic behaviour. If one adopts the displacement $\boldsymbol{u} \in \mathcal{U}$ and stress $\boldsymbol{\sigma} \in \mathcal{R}$ as variables of consideration, the description in Problem 2.3.5 changes to the so-called *mixed formulation*, where the solution space is not any more the space $\mathcal{U}$ alone, but the Cartesian product of spaces $\mathcal{U}$ and $\mathcal{R}$. According to this, the mixed formulation requires the introduction of a new—dual— operator $A^* := A^{-1}$ and the energy norm $\|\boldsymbol{\sigma}\|^2_{A^*} = \langle A^*\boldsymbol{\sigma}, \boldsymbol{\sigma}\rangle := \langle \boldsymbol{\sigma}, \boldsymbol{\sigma}\rangle_{A^*}$ via the continuous, symmetric, and coercive bilinear form:

$$a^*(\boldsymbol{\sigma}, \boldsymbol{\tau}) = \langle A^*\boldsymbol{\sigma}, \boldsymbol{\tau}\rangle = \int_{\mathcal{G}} A^{-1}\boldsymbol{\sigma} : \boldsymbol{\tau} \, \mathrm{d}x. \tag{2.54}$$

If a is identified in our application with the Helmholtz free energy ψ_e, then a^* is identified with the complementary energy ψ_e^* via the Legendre-Frenchel transformation:

$$\psi_e^*(\boldsymbol{\sigma}) = \sup_{\boldsymbol{\varepsilon}\in\mathcal{E}}\{\langle \boldsymbol{\sigma}, \boldsymbol{\varepsilon}\rangle_{\mathcal{R}\times\mathcal{E}} - \psi_e(\boldsymbol{\varepsilon})\} = \frac{1}{2}\int_{\mathcal{G}} \boldsymbol{\sigma} : (\boldsymbol{A}^{-1} : \boldsymbol{\sigma}) \, \mathrm{d}x = \frac{1}{2}a^*(\boldsymbol{\sigma}, \boldsymbol{\sigma}). \tag{2.55}$$

In addition to a^* the mixed description requires the definition of the continuous bilinear form b as follows:

$$b(\boldsymbol{\tau}, \boldsymbol{v}) := \langle B\boldsymbol{\tau}, \boldsymbol{v}\rangle = \langle B^*\boldsymbol{v}, \boldsymbol{\tau}\rangle = \int_{\mathcal{G}} \boldsymbol{\varepsilon}(\boldsymbol{v}) : \boldsymbol{\tau} \, \mathrm{d}x, \tag{2.56}$$

further leading to:

Problem 2.3.6. ***Mixed formulation of Elasticity problem ME****. For a given loading $\boldsymbol{f} \in \mathcal{F}$ and the space of admissible stresses $\mathcal{R}$ find the solution $\boldsymbol{u} \in \mathcal{U}$ such that*

$$\begin{aligned} a^*(\boldsymbol{\sigma}, \boldsymbol{\tau}) - b(\boldsymbol{\tau}, \boldsymbol{u}) &= \boldsymbol{0}, \quad \forall \boldsymbol{\tau} \in \mathcal{R} \\ b(\boldsymbol{\sigma}, \boldsymbol{v}) &= \ell(\boldsymbol{v}) \quad \forall \boldsymbol{v} \in \mathcal{U} \end{aligned} \tag{2.57}$$

hold. In terms of operators previous equations become

$$\begin{aligned} A^*\boldsymbol{\sigma} - B^*\boldsymbol{u} &= 0 \\ B\boldsymbol{\sigma} &= \ell. \end{aligned} \tag{2.58}$$

The uniqueness of the solution can be proven in a similar manner as for the case of the primal problem, for more information see [92, 202].

From the optimisation point of view the primal and mixed problems may be reformulated to a minimisation of the certain cost functional $\Phi(\boldsymbol{v})$, assuming that the bilinear form a is symmetric. In other words, the primal Problem 2.3.5 transforms to the minimisation of:

$$\Phi(\boldsymbol{v}) = \frac{1}{2}a(\boldsymbol{v},\boldsymbol{v}) - \langle \ell, \boldsymbol{v}\rangle, \tag{2.59}$$

a strictly convex, continuous, Gâteaux differentiable, and coercive functional on a Hilbert space $\mathcal{U}$, i.e. $\Phi(\boldsymbol{v}) \to \infty$ as $\|\boldsymbol{v}\| \to \infty$. As a and ℓ are continuous and Gâteaux-differentiable, and as a is $\mathcal{U}$-elliptic, Φ has all desired properties and thus the primal formulation in Problem 2.3.5 may be rewritten as a convex unconstrained minimisation problem

$$\boldsymbol{w} = \arg\min_{\boldsymbol{v}\in\mathcal{U}}(\Phi(\boldsymbol{v})). \tag{2.60}$$

The minimum satisfies $\delta(\Phi(\boldsymbol{w})) = 0$, where $\delta\Phi(\boldsymbol{w}) = a(\boldsymbol{w},\cdot) - \ell$ denotes the Gâteaux derivative of Φ.

Similarly, the dual minimisation Problem 2.3.6 (see [229] chapter I) reads:

$$\boldsymbol{\sigma} = \arg\min_{\boldsymbol{\sigma}\in S}(\Phi^*(\boldsymbol{\sigma})) = \arg\min_{\boldsymbol{\sigma}\in S}[\frac{1}{2}a^*(\boldsymbol{\sigma},\boldsymbol{\sigma}) - \int_{\Gamma_D}\boldsymbol{\sigma}(x)\boldsymbol{n}(x)\boldsymbol{u}_0(x)\,\mathrm{d}\Gamma], \tag{2.61}$$

where the *statically admissible set* $S = \{\boldsymbol{\sigma} \in \mathcal{R}_d : \boldsymbol{\sigma}\cdot\boldsymbol{n} = \boldsymbol{t}_N\}$ requires the definition of the Hilbert space $\mathcal{R}_d = \{\boldsymbol{\sigma} \in \mathcal{R} : -\mathrm{div}\boldsymbol{\sigma} = \boldsymbol{f}\}$ with the norm $(\boldsymbol{\sigma},\boldsymbol{\tau})_{\mathcal{R}_d} = (\boldsymbol{\sigma},\boldsymbol{\tau})_{\mathcal{R}} + (\mathrm{div}\,\boldsymbol{\sigma}, \mathrm{div}\,\boldsymbol{\tau})_{L_2}$.

Elastoplasticity

After integrating both the flow rule in its primal form (see Table 2.2) and the equilibrium Eq. (2.1) previously multiplied by test function $v - \dot{u}$ over the computational domain $\mathcal{G}$, one may arrive to the primal formulation of the elastoplastic behaviour, i.e. a variational inequality of the second kind [92, 240, 229, 97]:

$$a(w(t), z - \dot{w}(t)) + j(z) - j(\dot{w}(t)) \geq \langle f, z - \dot{w}(t)\rangle, \quad \forall z \in \mathcal{K}. \tag{2.62}$$

Here, j denotes the dissipation functional, $\langle f, z - \dot{w}(t)\rangle$ the linear continuous functional, and $a(z,w) = \langle Az, w\rangle$ the bilinear form with $A : \mathcal{Z} \to \mathcal{Z}^*$ being a linear, continuous, self-adjoint, and coercive (i.e. $\langle Az, z\rangle \geq c_2\|z\|^2$) operator. The inequality is posed on a convex non-empty domain $\mathcal{K}$ to which the test functions z belong. To allow for the dissipation functional, one may pose the problem on a primal space $\mathcal{Z} := \mathcal{U} \times \mathcal{P}$ (a space of primal solution w, see Table 2.3), and thus generalise for-

mulation to the *abstract* one:

Theorem 2.3.7. ***Problem ABS-P.*** *Given a function $f \in H^1(\mathcal{T}, \mathcal{Z}^*)$ with $f(0) = 0$, there exists a unique function $w \in H^1(\mathcal{T}, \mathcal{Z}^*)$ with $w(0) = 0$ and $\dot{w}(t) \in \mathcal{K}^\infty$, which solves the following problem a.e. in $t \in \mathcal{T}$:*

$$\forall z \in \mathcal{Z}: \quad a(w(t), z - \dot{w}(t)) + j(z) - j(\dot{w}(t)) \geq \langle f(t), z - \dot{w}(t) \rangle. \tag{2.63}$$

If in addition $f_1, f_2 \in H^1(\mathcal{T}, \mathcal{Z}^*)$ with $f_1(0) = f_2(0)$ are two different loadings, and $w_1, w_2 \in H^1(\mathcal{T}, \mathcal{Z}^*)$ are the corresponding solutions, then

$$\|w_1 - w_2\|_{L_\infty} \leq c \|\dot{f}_1 - \dot{f}_2\|_{L_1}. \tag{2.64}$$

Proof. The existence, stability and uniqueness of the solution $w \in H^1(\mathcal{T}, \mathcal{Z}^*)$ with $w(0) = 0$ and $\dot{w}(t) \in \mathcal{K}^\infty$ are studied in [92] for a given $f \in H^1(\mathcal{T}, \mathcal{Z}^*)$ with $f(0) = 0$. □

The primal problem is not uniformly concave/convex, therefore generalized Newton methods (radial return) often exhibit bad global convergence properties. In order to overcome this difficulty one reformulates Theorem 2.3.7 by introducing the function $w^* \in H^1(\mathcal{T}, \mathcal{Z}^*)$ coming from the definition of the sub-differential:

$$\partial j(\dot{w}) := \{w^* \in \mathcal{Z}^* : \; j(z) \geq j(\dot{w}(t)) + \langle w^*(t), z - \dot{w}(t) \rangle, \quad \forall z \in \mathcal{Z}\}. \tag{2.65}$$

This together with the positive homogeneity of j allows to write $j(\dot{w}) = \langle w^*, \dot{w} \rangle$ and $j(z) \geq \langle w^*, z \rangle$, which substituted to Eq. (2.62) gives an equality

$$a(w(t), z) + \langle w^*(t), z \rangle = \langle f, z \rangle, \quad \forall z \in \mathcal{Z} \tag{2.66}$$

followed by an inequality:

$$w^* \in \partial j(\dot{w}), \text{ a.e. } t \in \mathcal{T}. \tag{2.67}$$

Going back to convex analysis [65] one has that $w^*(t) \in \partial j(\dot{w}(t))$, and thus $\dot{w}(t) \in \partial j^*(w^*)(t)$ for all $t \in \mathcal{T}$. With this in mind one may rewrite Eq. (2.67) to:

$$\forall z^* \in \mathcal{K}: \quad \langle \dot{w}(t), z^* - w^*(t) \rangle \leq 0 \quad \forall t \in \mathcal{T}, \tag{2.68}$$

and subsequently pose a mixed formulation of the abstract plasticity problem, which will be used further:

Theorem 2.3.8. ***Problem ABS-M****. With the notation and assumptions above there are unique functions,* $w \in H^1(\mathcal{T}, \mathcal{Z}^*)$ *and* $w^* \in H^1(\mathcal{T}, \mathcal{Z}^*)$ *with* $w(0) = 0$ *and* $w^*(0) = 0$*, which solve the following problem a.e.* $t \in \mathcal{T}$*:*

$$\forall z \in \mathcal{Z} : \; a(w(t), z) + \langle w^*(t), z\rangle = \langle f(t), z\rangle \tag{2.69}$$

and

$$\forall z^* \in \mathcal{K} : \; \langle \dot{w}(t), z^* - w^*(t)\rangle \leq 0. \tag{2.70}$$

If, in addition, $f_1, f_2 \in H^1(\mathcal{T}, \mathcal{Z})$ *with* $f_1(0) = f_2(0) = 0$ *are two different loadings, and* $w_1, w_2 \in H^1(\mathcal{T}, \mathcal{Z})$ *and* $w_1^*, w_2^* \in H^1(\mathcal{T}, \mathcal{Z}^*)$ *are the corresponding solutions, then*

$$\|w_1 - w_2\|_{L_\infty} \leq c\|\dot{f}_1 - \dot{f}_2\|_{L_1} \tag{2.71}$$

and

$$\|w_1^* - w_2^*\|_{L_\infty} \leq c^*(\|\dot{f}_1 - \dot{f}_2\|_{L_1} + \|f_1 - f_2\|_{L_\infty}) \leq c^{**}\|\dot{f}_1 - \dot{f}_2\|_{L_1}. \tag{2.72}$$

Proof. The existence and uniqueness may be proven in a similar manner as for the primal abstract problem, for further details see [195]. □

2.4 Large deformation elastoplasticity

The theory of infinitesimal plasticity is very simple and clear, however not very applicable in practice. In real situations such as metal forming the assumption of linear deformation is not appropriate due to existence of non-negligible local rotations. This further results in non-unique stress and strain measures, as well as non-objective material time derivatives of the spatial variables.

In early works the finite deformation theory was based on the assumption of hypoelasticity, i.e. the additive decomposition of the rate of deformation into elastic and plastic parts, where the elastic part is described by the hypoelastic rate equation [15]. However, experiments have shown that the hypoelastic formulation is not so adequate due to the inconsistency with elastic response in some specific situations observed in [53, 54]. This constatation has been proven in the work of Simo and Pister [218] for the Jaumann, Green-Naghdi and Truesdell formulations. Therefore, the hypoelastic formulation is replaced by the hyperelastic one [217] which decomposes the deformation gradient in a multiplicative way. Such an approach is found to be mathematically more complex than the first mentioned. To reduce the complex-

ity scientists investigated different numerical approaches to the problem [184]. This tendency is recently replaced by a theory of the evolution processes given in terms of the second law of thermodynamics with respect to the current configuration [216] or the intermediate one [130].

Due to the previously mentioned reasons, the theory of finite deformation plasticity is very much controversial and still study of research, see [1, 69, 159]. Hence, in this work only the large displacement analysis is considered.

2.4.1 Description of kinematics

In contrast to infinitesimal, the finite deformation theory is not uniquely described as the current and initial configuration are not overlapping. In other words, the displacement field is not infinitesimal, and one may distinguish the initial $\mathcal{G}_0$ from the current (deformed) configuration $\mathcal{G}_T$. Accordingly, there are at least two possible descriptions of the material behaviour depending on the choice of the reference configuration. The description with respect to the initial configuration is called *material or Lagrangian*, while the *spatial (Euler) description* is the one given with respect to the current configuration.

In order to relate the mentioned configurations, one introduces the deformation gradient, see Section 2.1, which splitts by a multiplicative decomposition [143]

$$\boldsymbol{F} = \boldsymbol{F}^e \boldsymbol{F}^p \tag{2.73}$$

to the plastic $\boldsymbol{F}^p$ and elastic $\boldsymbol{F}^e$ gradients, locally defining an intermediate configuration. In the following discussion the material will be assumed to be plastically isochoric for which $\boldsymbol{F}^p$ belongs to a special linear group:

$$\boldsymbol{F}^p \in SL(d) = \{\boldsymbol{F}^p \mid \det \boldsymbol{F}^p = 1\}, \tag{2.74}$$

such that the hydrostatic pressure can be evaluated directly from the determinant of $\boldsymbol{F}^e$ [30]. In a more general case, when the isochoric condition is not assumed, the deformation gradient belongs to a general linear group, i.e. $\boldsymbol{F}^p \in GL_+(d)$.

Even though the deformation tensor relates the initial with the current configuration, this quantity has no physical meaning. The physical description of the deformation, i.e. the change in time with stretching and the change of angle between two elemental vectors of the body, is only possible in terms of *right* $\boldsymbol{C} = \boldsymbol{F}^T \boldsymbol{F} = \boldsymbol{C}^e \boldsymbol{C}^p$ and *left*

$\boldsymbol{b} = \boldsymbol{F}\boldsymbol{F}^T = \boldsymbol{b}^e\boldsymbol{b}^p$ Cauchy Green deformation tensors [30, 101]. Once these tensors are introduced, the further mathematical description of the elastoplastic behaviour can be given in terms of the Green-Lagrangian finite strain tensor $\boldsymbol{E} = \frac{1}{2}(\boldsymbol{C} - \boldsymbol{I})$ or the Eulerian-Almansi finite strain tensor [3] $\boldsymbol{e} = \varphi_*(\boldsymbol{E}) = \boldsymbol{F}^{-T}\boldsymbol{E}\boldsymbol{F}^{-1}$. Besides these, other deformation measures [10] can be equivalently used for the material description.

Table 2.4: Stress measures

Stress	Relation	Stress	Relation
I Piola-Kirchhoff	$\boldsymbol{P} = J\boldsymbol{\sigma}\boldsymbol{F}^{-1}$	Cauchy	$\boldsymbol{\sigma} = J^{-1}\boldsymbol{\tau}$
(Non-sym.)	$= \boldsymbol{\tau}\boldsymbol{F}^{-T}$	(Sym.)	$= J^{-1}\boldsymbol{P}\boldsymbol{F}^T$
	$= \boldsymbol{F}\boldsymbol{S}$		$= J^{-1}\boldsymbol{F}\boldsymbol{S}\boldsymbol{F}^T$
II Piola-Kirchhoff	$\boldsymbol{S} = J\boldsymbol{F}^{-1}\boldsymbol{\sigma}\boldsymbol{F}^{-T}$	Kirchhoff	$\boldsymbol{\tau} = J\boldsymbol{\sigma}$
(Sym.)	$= \boldsymbol{F}^{-1}\boldsymbol{\tau}\boldsymbol{F}^{-T}$	(Sym.)	$= \boldsymbol{P}\boldsymbol{F}^T$
	$= \boldsymbol{F}^{-1}\boldsymbol{P}$		$= \boldsymbol{F}\boldsymbol{S}\boldsymbol{F}^T$

Similarly to strain, the definition of stress also depends on the chosen reference configuration, see Table 2.4. Namely, one may differ a second Piola-Kirchhoff stress $\boldsymbol{S}$ which relates forces and areas in the initial configuration from the first Piola-Kirchhoff stress $\boldsymbol{P}$ representing the force in the current configuration exerted per unit area in the initial configuration. Note that the stresses expressed with respect to the current configuration, such as the Cauchy $\boldsymbol{\sigma}$ and Kirchhoff $\boldsymbol{\tau}$ stresses, are the only ones having the real physical meaning.

The stresses are conjugated to the strain tensors [30, 101] by the energy law:

$$\frac{1}{2}\boldsymbol{S} : \dot{\boldsymbol{C}} = \boldsymbol{P} : \dot{\boldsymbol{F}} = \boldsymbol{\tau} : \boldsymbol{d}, \tag{2.75}$$

from which follows the connection between the second Piola-Kirchhoff stress $\boldsymbol{S}$ and the right Cauchy Green tensor $\boldsymbol{C}$, the first Piola-Kirchhoff stress $\boldsymbol{P}$ and the change of the deformation $\dot{\boldsymbol{F}}$, as well as the Kirchhoff stress $\boldsymbol{\tau}$ and the rate of deformation $\boldsymbol{d} = \varphi_*(\dot{\boldsymbol{E}}) = \boldsymbol{F}^{-T}\dot{\boldsymbol{E}}\boldsymbol{F}^{-1}$, i.e. $\boldsymbol{d} = (\boldsymbol{l} + \boldsymbol{l}^T)/2$ where symmetry is kept in $\boldsymbol{l} = \dot{\boldsymbol{F}}\boldsymbol{F}^{-1}$ known as a velocity gradient.

[3] obtained by a push forward operation φ_* applied on the Green-Lagrangian tensor

2.4.2 Evolution equations

The irreversible and work-dissipating elastoplastic processes are usually described with the help of the energy function and evolution equations for internal variables. In contrast to the small strain theory the local equations are not necessarily formulated in objective rate forms [142, 24, 101] due to the existence of non-negligible rotations. In order to avoid incorrect results, the choice of rates as well as the evolution equations has to be made such that the objectivity and the second law of thermodynamics are fulfilled. Another problem of large strain plasticity is a violation of the classical convexity properties due to the assumption of finite strains and their multiplicative split. Therefore, one has to introduce more general notions of poly- and quasi-convexity in the description of the considered energy potential [40, 161].

The goal of the multiplicative decomposition of the deformation gradient is to make the separation of the elastic $\boldsymbol{F}^e$ from the plastic deformation gradient $\boldsymbol{F}^p$ such that the elastic properties depend only on $\boldsymbol{F}^e$. This further means that the free energy can be expressed as:

$$\psi = \psi(\boldsymbol{F}^e, \boldsymbol{\eta}), \tag{2.76}$$

where $\boldsymbol{\eta} \in \mathbb{R}^m$ denotes the vector of internal variables which records changes in $\boldsymbol{F}^p$ and may influence the elastic properties. Moreover, the energy satisfies the material objectivity requirements: $\psi(Q\boldsymbol{F}^e, \boldsymbol{\eta}) = \psi(\boldsymbol{F}^e, \boldsymbol{\eta}) \quad \forall Q \in SO(d) \Leftrightarrow \psi(\boldsymbol{F}^e, \boldsymbol{\eta}) = \psi({\boldsymbol{F}^e}^T \boldsymbol{F}^e, \boldsymbol{\eta})$; and defines the first Piola-Kirchhoff $\boldsymbol{P}$ stress and conjugate force $\boldsymbol{\chi}$ [101, 40] as:

$$\boldsymbol{P} = \frac{\partial \psi}{\partial \boldsymbol{F}}, \quad \boldsymbol{\chi} = -\frac{\partial \psi}{\partial \boldsymbol{\Xi}_p}, \tag{2.77}$$

respectively. Here, $\boldsymbol{\Xi}_p = (\Pi := {\boldsymbol{F}^p}^{-1}, \boldsymbol{\eta})$ represents the *generalised plastic* strain closely determining the components of the conjugate force $\boldsymbol{\chi} := (\boldsymbol{\varsigma}, \zeta)$ such that $\boldsymbol{\varsigma} = -\partial\psi/\partial\Pi$ and $\zeta = -\partial\psi/\partial\boldsymbol{\eta}$. Variable $\boldsymbol{\varsigma}$ denotes the so-called back-stress, here used in an invariant form[4] $\tilde{\boldsymbol{\varsigma}} = \Pi^T \boldsymbol{\varsigma}$ with Π being a linear operator from the cotangent bundle of the intermediate configuration into itself [101].

Collecting the conjugate forces into the *generalised stress*: $\boldsymbol{\Sigma} := (\tilde{\boldsymbol{\varsigma}}, \zeta)$ one may introduce the convex non-empty set of admissible stresses $\mathcal{K}$ (contains $\mathbf{0}$) whose indicator function $\Psi_{\mathcal{K}}(\boldsymbol{\Sigma}) = 0$ when $\boldsymbol{\Sigma} \in \mathcal{K}$, otherwise $\Psi_{\mathcal{K}}(\boldsymbol{\Sigma}) = \infty$. This allows us to carry the same mathematical description of the flow rule as in Section 2.2.1

[4] Invariance under all plastic deformations

[40]. Namely, by introducing the sub-differential

$$\begin{aligned} \partial\Psi_{\mathcal{K}}(\boldsymbol{\varsigma},\zeta) &= \{\tilde{\boldsymbol{\Xi}}_p \in \mathbb{R}^{d\times d}\times\mathbb{R}^m : \quad \Psi_{\mathcal{K}}(\tilde{\boldsymbol{\varsigma}}+\boldsymbol{T},\zeta+\tau) \geq \\ \Psi_{\mathcal{K}}(\tilde{\boldsymbol{\varsigma}},\zeta) &+ \tilde{\Pi}:\boldsymbol{T}+\tilde{\boldsymbol{\eta}}\cdot\tau, \quad \forall(\boldsymbol{T},\tau)\in\mathbb{R}^{(d\times d)}\times\mathbb{R}^m\} \end{aligned} \tag{2.78}$$

one may distinguish the primal rule:

$$\dot{\tilde{\boldsymbol{\Xi}}}_p := (\boldsymbol{F}^p\dot{\Pi},\dot{\boldsymbol{\eta}}) \in \partial\Psi_{\mathcal{K}}(\tilde{\boldsymbol{\varsigma}},\zeta), \tag{2.79}$$

from its dual:

$$(\tilde{\boldsymbol{\varsigma}},\zeta) \in \partial\Psi^*_{\mathcal{K}}(\tilde{\Pi},\boldsymbol{\eta}), \tag{2.80}$$

where $\Psi^*_{\mathcal{K}}$ denotes the conjugate dual of $\Psi_{\mathcal{K}}$, i.e. support function of $\mathcal{K}$ (see Section 2.2.1):

$$\Psi^*_{\mathcal{K}}(\tilde{\Pi},\boldsymbol{\eta}) = \sup\{\tilde{\boldsymbol{\varsigma}}:\tilde{\Pi}+\zeta\cdot\boldsymbol{\eta}\}. \tag{2.81}$$

Function $\Psi^*_{\mathcal{K}}$ is a homogenous function of degree 1 (i.e. $\Psi^*_{\mathcal{K}}(\alpha(\tilde{\Pi},\boldsymbol{\eta})) = \alpha\Psi^*_{\mathcal{K}}(\tilde{\Pi},\boldsymbol{\eta})$, for all $\alpha>0$) often identified with the dissipation rate, see Section 2.2.1.

Another formulation of the flow rule can be given in terms of the yield function $\phi_{\mathcal{K}}$ describing the convex domain[5] $\mathcal{K}=\{\boldsymbol{\Sigma}\in\mathbb{R}^{d\times d}\times\mathbb{R}^m : \phi_{\mathcal{K}}(\boldsymbol{\Sigma})\leq 0\}$. In a special case when $\phi_{\mathcal{K}}$ is smooth enough this formulation results in the very well known Kuhn-Tucker condition: $\dot{\tilde{\boldsymbol{\Xi}}}_p = \lambda\partial_\Sigma\phi_{\mathcal{K}}(\Sigma)$, $\lambda\geq 0, \phi_{\mathcal{K}}\leq 0$, $\lambda\phi_{\mathcal{K}}=0$, where λ represents the plastic multiplier.

The theory as given in this section relates to the case of general material behaviour described by a free convex energy function, see Eq. (2.76). However, one may specialize it to the case of linear elasticity, perfect plasticity, and mixed linear hardening plasticity as shown in Table 2.5. This model describes the isotropic elastic response in terms of the Saint-Venant Kirchhoff hyperleastic energy ψ_e given in a quadratic form. The direct consequence of this assumption is the linear relation A between the second Piola-Kirchhoff stress $\boldsymbol{S}$ and Green-Lagrange strain $\boldsymbol{E}$, which allows the model to inherit the favourable properties regarding the poly-convexity conditions. This further means that the strain energy remains the convex function with respect to any of the intrinsic deformation measures, such as the deformation gradient, its co-factor, and the determinant J. Note that the constitutive relationship in Table 2.5 is written with respect to the material description. However, its reformulation to the spatial representation can be easily done by applying the Lie derivative on the Kirchhoff stress as shown in [101].

[5] Note that $\phi(\Sigma)$ does not depend on the first Piola-Kirchhoff stress

Table 2.5: Large deformation plasticity

Theory	Variable	law
Linear elasticity	Energy	$\psi_e = \frac{1}{2}\boldsymbol{E} : A\boldsymbol{E}$
	Constitutive law	$\boldsymbol{S} = A\boldsymbol{E}$
Perfect plasticity	Internal variable	$\boldsymbol{G}_p := \boldsymbol{C}^{p\,-1} = (\boldsymbol{F}^{p\,T}\boldsymbol{F}^p)^{-1}$
	Energy	$\psi = \psi(\boldsymbol{C}, \boldsymbol{G}_p)$
	Yield function	$\phi_{\mathcal{K}} = \phi_{\mathcal{K}}(\boldsymbol{S}, \boldsymbol{C})$
	Plastic dissipation	$D_p := -\boldsymbol{S}\frac{1}{2}\boldsymbol{C}\frac{\partial \boldsymbol{G}_p}{\partial t}\boldsymbol{G}_p^{-1} > 0$
	Evolution equation	$\dot{\boldsymbol{G}}_p = -2\dot{\lambda}\boldsymbol{C}^{-1}\partial_{\boldsymbol{S}}\phi_{\mathcal{K}}\boldsymbol{G}_p$
Mixed hardening plasticity	Kinematic law	$\Xi = \text{const} \cdot \boldsymbol{G}_p$
	Yield function	$\phi_{\mathcal{K}}(\boldsymbol{C}, \boldsymbol{S}, \varsigma, \zeta) = 0$
	Plastic dissipation	$D_p := -\boldsymbol{S} \cdot \frac{1}{2}\boldsymbol{C}\frac{\partial \boldsymbol{G}_p}{\partial t}\boldsymbol{G}_p^{-1}$ $-\varsigma\frac{1}{2}\boldsymbol{C}\frac{\partial \Xi}{\partial t}\Xi^{-1} + \zeta\frac{\partial \nu}{\partial t} > 0,$
	Flow rule	$\dot{\boldsymbol{G}}_p = -2\dot{\lambda}\boldsymbol{C}^{-1}\partial_{\boldsymbol{S}}\phi_{\mathcal{K}}\boldsymbol{G}_p$
		$\dot{\Xi} = -2\dot{\lambda}\boldsymbol{C}^{-1}\partial_{\varsigma}\phi_{\mathcal{K}}\Xi$
		$\dot{\nu} = \dot{\lambda}\boldsymbol{C}^{-1}\partial_{\zeta}\phi_{\mathcal{K}}$

With respect to the previous assumptions the perfect plastic behaviour is described by elastic strain energy, which can be expressed as a function in terms of one argument, i.e. the deformation gradient $\boldsymbol{F}^e$, or two arguments: the right Cauchy-Green tensor $\boldsymbol{C}$ and the internal variable $\boldsymbol{C}_p^{-1}$, see Table 2.5. Once the energy is declared, one may determine the system dissipation properties from the second law of thermodynamics:

$$\left(\boldsymbol{S} - 2\frac{\partial \Psi}{\partial \boldsymbol{C}}\right)\frac{1}{2}\frac{\partial \boldsymbol{C}}{\partial t} - 2\frac{\partial \Psi}{\partial \boldsymbol{G}_p}\frac{1}{2}\frac{\partial \boldsymbol{G}_p}{\partial t} \geq 0. \tag{2.82}$$

The law specifies the dissipation functional D_p and the evolution equations, see Table 2.5, obtained via the maximum dissipation principle [128, 101, 136]. Note that this description uses the invariant form of the yield function $\phi_{\mathcal{K}}$ with the second Piola-Kirchhoff stress $\boldsymbol{S}$ and the right Cauchy Green deformation tensor $\boldsymbol{C}$ as arguments.

By further generalisation of the model, one arrives to the mixed hardening case (or generalised Prager-Ziegler rule) described by a scalar variable ν, the isotropic hardening, and a tensor variable Ξ, the kinematic hardening. According to [101] one may assume that Ξ is proportional to $\boldsymbol{C}^{p,-1}$, which means that they share the same principal directions (eigenvectors). Following this, the second principle of thermo-

dynamics reads:

$$\left(\boldsymbol{S} - 2\frac{\partial \Psi}{\partial \boldsymbol{C}}\right)\frac{1}{2}\frac{\partial \boldsymbol{C}}{\partial t} - 2\frac{\partial \Psi}{\partial \boldsymbol{G}_p}\frac{1}{2}\frac{\partial \boldsymbol{G}_p}{\partial t} - 2\frac{\partial \Psi}{\partial \boldsymbol{\Xi}}\frac{1}{2}\frac{\partial \Xi}{\partial t} - \frac{\partial \Psi}{\partial \nu}\frac{1}{2}\frac{\partial \nu}{\partial t} \geq 0 \qquad (2.83)$$

and further reduces to D_p, see Table 2.5. Similar to before, the evolution equations follow from the principle of maximal dissipation and under the smoothness assumption have the form given in Table 2.5 [101].

2.4.3 Variational formulation

The weak form of equilibrium equations in spatial description can be formally written in the same manner as in the case of small displacements, see Section 2.3.2. The reasons for this are the infinitesimal virtual displacements and the boundary conditions imposed on the deformed configuration. However, the spatial description of the equilibrium equations is not very suitable since the deformed configuration and corresponding coordinates are only known once the problem has been solved. Additionaly, the coordinates do not stay fixed, and the configuration keeps evolving. To avoid this issue, the equilibrium conditions are usually expressed with respect to the initial configuration fixed for a deformable body, i.e.

$$a^m(\boldsymbol{w}, \boldsymbol{\tau}) = -\langle \Upsilon(\boldsymbol{w}), \boldsymbol{\tau} \rangle_{\mathcal{G}_0} = \ell^m(\boldsymbol{w}), \quad \forall \boldsymbol{w} \in \mathcal{U}, \qquad (2.84)$$

where $\mathcal{U} = \{\boldsymbol{u} : \mathcal{B} \to \mathbb{R}^3 \mid \boldsymbol{u}_0(\boldsymbol{X}) = 0 \quad \forall \boldsymbol{X} \in \Gamma_D\}$ [215]. Here, all terms are determined via the spatial-material transformation of variables of consideration (see [101]). In this regard, the right hand side of Eq. (2.84) becomes:

$$\ell^m(\boldsymbol{w}) = \langle \boldsymbol{w}, \boldsymbol{F}_b \rangle_{\mathcal{G}_0} + \int_{\Gamma_N} \boldsymbol{w} \cdot \boldsymbol{T} \, \mathrm{d}\Gamma, \qquad (2.85)$$

where $\Upsilon := \varepsilon(\boldsymbol{w}(\varphi(\boldsymbol{X})) = 0.5(\boldsymbol{w} \otimes \boldsymbol{\nabla}_{\boldsymbol{S}} + \boldsymbol{\nabla}_{\boldsymbol{S}} \otimes \boldsymbol{w}) = 0.5(\nabla_M \boldsymbol{w} \boldsymbol{F}^{-1} + \boldsymbol{F}^{-T} \nabla_M \boldsymbol{w})$ denotes the Gâteaux derivative of the Green-Lagrange deformation $\boldsymbol{E}$ [101].

Note that Eq. (2.84) is expressed in terms of the second Piola-Kirchhoff tensor related to the Kirchhoff tensor $\boldsymbol{\tau}$ via $\boldsymbol{S} = \boldsymbol{F}^{-1}\boldsymbol{\tau}\boldsymbol{F}^{-T}$. However, the weak formulation can be recasted in terms of other stress measures, for more information please see [101, 215].

2.5 Summary

This chapter briefly summarizes the theory behind small and large deformation elastoplasticity simultaneously constructing the solid mathematical background necessary for better understanding of the following chapters. Special attention is given to the convex analysis and the theory of variational inequalities resulting in an abstract formulation of the elastoplastic problem in both the primal and mixed form. Additionally, the chapter offers reformulation of the mixed problem to the minimisation of a convex functional in a form as used in practical numerical algorithms. In finite case this is only valid under certain assumptions of poly- or quasi- convexity of the energy potential.

Chapter 3

Plasticity described by uncertain parameters

As far as the laws of mathematics refer to reality, they are not certain, and as far as they are certain, they do not refer to reality.

A. Einstein

Uncertainties in inelastic systems arise from a variety of sources including the geometry of the problem, material properties, boundary conditions, initial conditions, or excitations imposed on the system. As a result, depending on the source of the randomness, the system behaviour has an uncertain character. In the deterministic sense the parameters describing elastic (reversible)/inelastic (irreversible) behaviour are determined by indentation techniques and then considered as constants in the classical model [215]. However, in case of materials such as soil and bone this approach does not properly describe the output due to the existence of significant changes on the micro-structural level. In order to give a more reliable description of heterogeneous materials, this chapter introduces the material parameters as random fields and processes via the maximum entropy principle [222], and further reformulates the classical plasticity theory in a stochastic variational setting. Particularly the chapter focuses on the infinitesimal problem of generalised standard media [89, 91] described by a von Mises yield function, i.e. the stochastic variational inequality of a second kind.

3.1 Related work

Stochastic elastoplasticity is a relatively new research area which aims to quantify the influence of uncertainty appearing in material properties, geometry and possible external loadings on the elastoplastic system response. In the literature, so far, there are not many publications on this topic. Most of them consider linear problems described by elliptic partial differential equations, see e.g. [107, 244, 245, 220, 156]. On the other side, the nonlinear problems have been considered only recently in the last few years [174, 140, 109].

To the author's knowledge there are two main streams in modelling stochastic infinitesimal elastoplastic behaviour: the approximate plasticity theory by Anders and Hori [9, 8], and the moment equations method by Jermić and Sett [105, 209]. The pioneering work of Andres and Hori [9, 8] studies the fault formation rate-independent problem described by Young's modulus as uncertain parameter. The model is developed with the help of the bounding media analysis and the modulus taken in a form of a homogenous Gaussian random field. Such posed problem is then resolved by the numerical method that uses the perturbation expansion around the stochastic mean. However, the perturbation is characterized by an inability to accurately approximate the problems described by moderate or large variances in input material properties. Besides this, the method faces the so-called "closure" problem in which the higher order moments cannot be computed without prior knowledge of the lower order moments.

In order to find a more accurate representation, Jeremić et al. [105] and Sett et al. [209] recently developed new formulations for the general 1-D elastoplastic constitutive rate equation with random material properties and random strain rate. The approach is of the moment equations type, and directly provides the second order exact expression for the evolution of the probability density functions of the stress variable via the generic Eulerian–Lagrangian form of the Fokker–Planck–Kolmogorov equation (FPKE), see Kavvas [106]. In this way the closure problem is resolved on the expense of the complexity of the algorithm and slight overestimation of the response variance.

In contrast to the infinitesimal, the finite deformation theory is not yet completely understood in the deterministic sense. Namely, the convexity of the total potential energy functional is broken and thus the symmetry between the potential energy principle and complementary energy is lost [161, 40]. These problems lead to the complicated phenomena followed by high degrees of nonlinearity, which are very

difficult to handle especially in a stochastic setting. Therefore the stochastic description of the large deformation plasticity seems not to be an easy task; and the only work pursued so far in this direction can be found in [3, 4, 5]. These papers consider the simple plasticity problem described by a power plastic flow law with uncertain isotropic resistance or the fiber orientation of the hyperelastic material.

Even though previously mentioned studies provide some sort of stochastic elastoplastic models, most of them are affected by improper parametrisation. The models do not take into account the uncertainty of the material properties describing the constitutive equations. Even if they do, the principle of maximum distribution [222] is not followed. This may result in the non-convexity of the energy functionals due to the negative values of the system properties. Moreover, the models are based on weak approximations of the response surface causing the over- or under-estimation of the variance.

In order to resolve the previously mentioned problems the formulation given in this work starts with the classical description of the deterministic elastoplasticity (see Chapter 2) and extends it to the stochastic one with the help of the convex analysis and variational inequality theory. In this way, the total reformulation of the problem is avoided, and the abstract similarity between the deterministic and stochastic approaches is shown.

3.2 Motivation

Elastoplasticity has found an important place in the field of computational mechanics due to its large practical application. However, presently the variety of models that exist (e.g. [215, 101, 55]) relies on the assumption of the complete knowledge of the system, i.e. one assumes that the material characteristics, as well as the external loadings applied on the structure are entirely known. The question posed in this work is if one can really trust purely deterministic models as it has been done until now. Namely, uncertainty is widely present, starting from the mathematical model which cannot perfectly match the data up to poorly known external loadings. The uncertainty arises on both structural and parametric levels including the geometrical uncertainty, uncertainty in initial and boundary conditions, etc.

Due to the previously mentioned reasons, this thesis investigates the impact of the model parametric uncertainty on the system response, as well as the accuracy of the mathematical model describing the true physics. In order to achieve this, the

uncertainties in:

- history of loading $\boldsymbol{f}(t, x, \omega)$,
- constitutive tensor $\boldsymbol{A}(x, \omega)$, i.e. the corresponding material properties such as the bulk $K(x, \omega)$ and shear $G(x, \omega)$ moduli,
- and the domain of admissible stresses $\mathcal{K}(\omega)$ determined by random yield stress $\sigma_y(x, \omega)$, isotropic $H_{iso}(x, \omega)$ and kinematic $H_{kin}(x, \omega)$ hardening

are assumed. Moreover, the mentioned properties are modelled as random fields/processes according to the principle of maximal distribution [222]. Note that such description of parameters further can be improved by collecting the measurement data and solving an inverse problem in a Bayesian fashion [192, 180, 191, 154, 196, 122].

3.3 Modelling uncertainty

Let $(\Omega, \mathcal{F}, \mathbb{P})$ be the probability space with the total mass equal to unity, where Ω denotes the space of elementary events, $\mathcal{F} \subset 2^{\Omega}$ a σ-algebra of subsets of Ω, and $\mathbb{P}$ a probability measure [14, 28, 176]. In this space one may introduce the set of uncertain material parameters as described in the previous Section 3.2, and further model them as random fields and/or stochastic processes [6, 59] in two distinguishable ways: the fully-parametric and reduced-parametric approach. With the help of expert knowledge the first approach makes assumptions on the distributions of uncertain parameters and further includes them as such into the model. In general prior information on uncertain parameters is given in terms of second order statistics (the mean and the variance) and/or additional properties such as the definition of support, positive-definiteness, etc. In contrast to this, the reduced-parametric method focuses more on the analysis of parameters as part of some relation than individually on each of them. However, similarly to the full approach the method requires certain expert knowledge. The only difference is that this knowledge is not applied on each parameter individually but more on a part of specific group.

3.3.1 Random variable and maximum entropy principle

In $(\Omega, \mathcal{F}, \mathbb{P})$ the random variable (RV) $\kappa(\omega)$ is formally defined as a Borel measurable function with values in some vector space $\mathcal{V}$, i.e. as a mapping:

$$\kappa : (\Omega, \mathcal{F}) \to (\mathcal{V}, \mathcal{B}(\mathbb{R})) \tag{3.1}$$

shortly written as $\kappa : \Omega \to \mathcal{V}$. In many problems the space Ω is not concretely accessible so that the usual idea of a function (formula) looses much of its meaning. The representation of RVs, therefore, often differs from what is used for "normal" variables. Namely, the RV is described in terms of a single function

$$F_\kappa := \mathbb{P}(\omega : \ \kappa(\omega) \leq x) = \mathbb{P}(\kappa \leq x), \tag{3.2}$$

called a *probability distribution function* [6, 59]. The function F_κ is non-decreasing, non-negative, goes to unity as $x \to \infty$, approaches zero when $x \to -\infty$ and takes values in [0,1]. Furthermore, if F_κ is absolutely continuous its derivative— a non-negative real-valued Borel measurable function $f := \mathrm{d}F_\kappa / \mathrm{d}x$ $(f > 0)$ on $\mathbb{R}$— describes the density of the probability at each point in the sample space. This function is known as the probability density function (PDF) and may be used for the description of κ instead of F_κ.

Following previous definitions the unknown parameter κ can be modelled as a random variable $\kappa(\omega)$. This actually means that one has to assign to $\kappa(\omega)$ some probability distribution F_κ. However, that is not an easy task. The decision depends on the properties the quantity may have as well as on possible information about its second order characteristics collected by experiments. Once this information is available, the decision can be made with the help of the principle of the maximum entropy distribution [220], otherwise ad-hoc assumptions have to be introduced.

The principle of the maximum entropy distribution [182, 52, 104, 127, 220, 222] can be used to determine the unknown distribution of the material property if some data in a form of expected values or other statistical functionals are available. If nothing is known about the distribution except that it belongs to a certain class, then the distribution with the largest entropy has to be chosen.

The distribution can be found by solving the optimization problem

$$f_\kappa(x) = \arg\max_{f \in \mathcal{C}_f} W(f) \tag{3.3}$$

of maximizing the entropy

$$W(f) = \int_{-\infty}^{+\infty} f(x)\log(f(x))dx \tag{3.4}$$

determined by a probability density function $f(x)$ of the RV κ [210]. Here, $\mathcal{C}_f$ denotes the admissible set of all PDFs satisfying following constraints (i.e. available information):

- the mean value constraint

$$\mathbb{E}(g(\kappa)) = \int_{\Omega} g(\kappa(x,\omega))\mathbb{P}(\mathrm{d}\omega) = \mu, \tag{3.5}$$

  where $g : \kappa \mapsto g(\kappa)$ is known function of κ[1],

- and the support function constraint

$$\text{supp } f(x) = \chi, \tag{3.6}$$

  where χ may be bounded or not bounded.

The solution of the optimisation problem in Eq. (3.3) can be found by numerous methods proposed in the literature: the interior-reflective Newton method [51], Powell's dogleg method [44], etc. For more information the reader is addressed to [220, 222].

The random variables and their functions describe the properties independent of material position. For this reason, they cannot be used for modelling the heterogeneous properties such as bulk and shear moduli, or for the time dependent processes such as the external loading. To overcome this issue, one has to generalise the notion of the random variable to a *random field* (RF) [6, 59] by taking the vector space $\mathcal{V}$ in Eq. (3.1) as a space of continuous functions $\mathcal{C}(\mathcal{G}, \mathbb{R})$ on the geometrical domain $\mathcal{G}$. Note that if the domain $\mathcal{G}$ is interpreted as a time interval $\mathcal{T} = [-T, T]$ then the *random field* has a meaning of *stochastic process*. Loosely speaking, the random field may be seen as an indexed family of random variables $\{\kappa(x,\omega), (x \in \mathcal{G} \subset \mathbb{R}^d, \omega \in \Omega)\}$, or as a measurable mapping

$$\kappa : \mathcal{G} \times \Omega \to \mathcal{V} \tag{3.7}$$

on a common probability space $(\Omega, \mathcal{B}, \mathbb{P})$. This allows a RF to be considered as a

[1] As a function of RV κ, $g(\kappa)$ also represents the RV.

function of both elementary events $\omega \in \Omega$ and $x \in \mathbb{R}^d$ [198], or as a set of all finite dimensional distribution functions [59]:

$$F_\kappa(k_1, .., k_n; x_1, ..., x_n) = \mathbb{P}(\kappa(x_1) \leq k_1, .., \kappa(x_n) \leq k_n), \tag{3.8}$$

where $\{x_1, x_2, ..., x_n\} \in \mathcal{G}$ and $\{k_1, ..., k_n\} \in \mathbb{R}$.

In practice, however, the information in Eq. (3.8) is often not accessible. In the best case scenario only the second order statistics, such as the mean value $\bar{\kappa}(x)$ (see Eq. (3.5)) and the covariance $\text{cov}_\kappa(x_1, x_2)$, are known. The mean $\bar{\kappa}(x)$ is usually obtained by averaging the experimantal data, while the covariance is computed according to:

$$\text{cov}_\kappa(x_1, x_2) := \mathbb{E}(\widetilde{\kappa}_{x_1} \otimes \widetilde{\kappa}_{x_2}), \tag{3.9}$$

where $\widetilde{\kappa}(x) = \kappa(x) - \bar{\kappa}(x)$ ($\mathbb{E}(\widetilde{\kappa}(x)) = 0$) denotes the fluctuation of the field. According to the maximum entropy principle [222], the available information can assist in selecting the distribution of the field in a similar manner as for RV. Basically, there are several rules for choosing the distribution function:

- the distribution is normal if nothing is known about κ besides its mean and standard deviation,
- the uniform distribution on the interval $[a, b]$ is the maximum entropy distribution among all continuous distributions supported in the interval $[a, b]$,
- and the exponential distribution is the maximum entropy distribution among all continuous distributions supported in $[0, \infty)$ (positive-definite).

3.3.2 Fully-parametric approach

The parametric method approaches the problem of quantifying the uncertainty in the system by modelling each of the parameters one is uncertain about in a form of a random field/process, as further described. Let us take the constitutive tensor $\boldsymbol{A}$ as a corresponding example. By the parametric approach the distributions of maximally 21 independent parameters (random fields) are chosen according to the maximum entropy principle. This corresponds to a full material anisotropy. However, in a more simple situation such as isotropy, the number of parameters reduces on the expense of mutual dependency. The dependence complicates the problem of choosing distributions as the random fields have to fulfill certain restrictions on the probability distributions coming from the global properties of the constitutive tensor.

In general, for a quantity $\kappa(\omega)$ one may adopt one of two possible types of random fields (random variables): Gaussian or non-Gaussian. *Gaussian random fields* [2, 6, 25, 102] appear very natural regarding the properties of Gaussian random variables—independence and simple specification of their finite distributions via the second order information (the mean value and covariance). If covariance is not known one may adopt its theoretical substitute, see [2]. However, Gaussian random fields are not suitable for practical application as for example they are not positive-definite. Therefore, more general *non-Gaussian random fields* [83, 82] are introduced. They represent the nonlinear transformation ϕ of a standard Gaussian random field $\theta(x,\omega)$ with zero mean and unit variance [175]:

$$\kappa(x,\omega) = \phi(x,\theta(x,\omega)) = F_{\kappa}^{-1} \circ \mathrm{erf}(\theta(x,\omega)), \tag{3.10}$$

where F_κ denotes a non-Gaussian and erf a Gaussian distribution function. Its mean value

$$\mathbb{E}(\kappa(x,\omega)) = \int_{\mathcal{G}} \phi(x,\omega)\mathbb{P}_\theta(\mathrm{d}w), \tag{3.11}$$

and covariance

$$\mathrm{cov}_\kappa(x,y) = \int_{\mathcal{G}}\int_{\mathcal{G}} \phi(x,w_1)\phi(x,w_2)dF_{\theta(x),\theta(y)}(w_1,w_2) - \mu_\kappa(x)\mu_\kappa(y) \tag{3.12}$$

are given with respect to the second order statistics of Gaussian RF. In Eq. (3.11) $\mathbb{P}_\theta(\mathrm{d}w)$ denotes a standard Gaussian measure and $F_{\theta(x),\theta(y)}$ in Eq. (3.12) represents the joint probability density of two random variables $\theta(x)$ and $\theta(y)$.

Regarding the covariance, one may model the random field $\kappa(x,\omega)$ as *homogenous* or *heterogeneous*. Homogeneous random field is a field with constant mean and covariance $\mathrm{cov}(x,y) = c(x-y)$ as a function of the distance alone [46], or, more rigorously, the field all of which probability distributions in Eq. (3.8) remain the same under the translations. However, the latter definition is rarely employed in practice. Furthermore, the random field can be modelled as isotropic if the covariance function depends on the distance alone, or, more generally speaking, the probability distribution function is invariant under orthogonal transformations [46, 2].

Following the previous discussion, the elastoplastic behaviour in this work is modelled by taking all material properties (i.e. yield stress, hardening parameters, bulk and shear moduli) in a form of lognormal random fields. Such decision is made due to the positive-definite property of corresponding constitutive and hardening tensors. In this manner the convexity of the considered problem is ensured.

The lognormal random fields are restricted to a positive cone in a vector space; however, their logarithms $\theta(x,\omega) = \ln \kappa(x,\omega)$ are not and may have any value. Assuming $\theta(x,\omega)$ to have finite variance one may choose a Gaussian distribution for a maximum entropy of $\ln \kappa(x,\omega)$. With respect to this a generic field of some random elastoplastic parameter is adopted in the form of the modified lognormal distribution

$$\kappa(x,\omega) = \kappa_0(x) + \kappa_1(x)\exp(\mu + \sigma\theta(x,\omega)). \tag{3.13}$$

Here, κ_0 and κ_1 are given functions of coordinates, μ, σ are the mean value and standard deviation of the base Gaussian field, and $\theta(x,\omega)$ is the normally distributed random field with zero mean and unit variance.

3.3.3 Reduced-parametric approach

In the previous sections the so-called fully-parametric approach was considered. However, such modelling cannot represent the "model uncertainties" via nonlinear mapping $\kappa \mapsto A(\kappa)$. The reason is that the modelled matrix $\boldsymbol{A} := A(\kappa)$ belongs to a small subspace of all matrices satisfying the required properties (e.g. the subset of positive definite and symmetric matrices $\mathbb{R}^{n\times n}_{+}$) [221, 85, 220, 84]. In addition, the fully–parametric approaches require the large amount of information, i.e. the type of the probability distributions and at least second order statistics for each uncertain parameter. This makes the modelling process more complicated because the identification of possibly large number of parameters from the small amount of experimental data is practically not feasible. Hence, the total number of system parameters has to be reduced. One way of doing this is to take for a parameter the random matrix (tensor) $\boldsymbol{A}$ obtained from the optimisation problem in Eq. (3.3) under the constraints of some already given a priori (available) information. In this way the anisotropic heterogeneous media [221, 220, 85, 84] can be modelled with the help of the minimal number of parameters such as the mean and the parameters prescribing the fluctuations of the tensor, i.e. correlation lengths and coefficient of dispersion.

Modelling of constitutive tensors

Instead of modelling material parameters such as the bulk and shear moduli, one may try to model the constitutive tensor $\boldsymbol{A}$, hardening tensor $\boldsymbol{H}$, or Hill's tensor (in yield criterion) with the help of the mathematical theory of random matrices in high-dimension and information theory [210]. For simplicity reasons in the further text

only the elastic constitutive tensor $\boldsymbol{A}$ is considered. However, a similar procedure can be performed for other tensors as well.

The expert knowledge one posseses about the tensor $\boldsymbol{A}$ is as such: the tensor is symmetric, positive-definite second order random field with the mean value $\mathbb{E}(\boldsymbol{A}) = \bar{\boldsymbol{A}}$ and finite second order moment. Similar is valid for its inverse. This a priori information follows from the basic requirements of the well-possedness of the elastoplastic problem; and is just naturally imposed constraint used to model $\boldsymbol{A}$ with the help of the maximum entropy approach, see Section 3.3.1 and [221, 220]. Thus, let the constitutive tensor $\boldsymbol{A}(x)$ be a matrix-valued heterogeneous random field with values in a set $\mathbb{R}^{n\times n}_{+}$. In addition, let the mean value of $\boldsymbol{A}(x)$ be a matrix $\bar{\boldsymbol{A}}$—belonging to a set of real squared symmetric positive-definite matrices which may take into account possible material symmetries such as isotropic, orthogonal, transversal, etc.— and let the fluctuation part of the field $\tilde{\boldsymbol{A}} := \boldsymbol{A} - \bar{\boldsymbol{A}}$ be purely anisotropic [2]. Then, the random tensor $\boldsymbol{A}$ admits the decomposition

$$\boldsymbol{A}(x,\omega) = \boldsymbol{U}_A^T(x)\boldsymbol{T}(x,\omega)\boldsymbol{U}_A(x) \tag{3.14}$$

advocated in [221, 220, 85, 84]. Here, $\boldsymbol{T}(x,\omega)$ represents the source of uncertainty and $\boldsymbol{U}_A(x)$ the Cholesky factor of the mean matrix $\bar{\boldsymbol{A}}(x)$. This means that the fluctuations of the random field are fully controlled by $\boldsymbol{T}(x,\omega)$, while the mean is determined by $\boldsymbol{U}_A(x)$. Note that in this formulation the mean matrix is not random but deterministic and depends only on the spatial coordinate x—the heterogeneous field. Otherwise, if the matrix $\bar{\boldsymbol{A}}$ is irrelevant of the spatial coordinates then the field $\boldsymbol{A}$ is homogenous. In a more general case, when the field $\boldsymbol{A}$ admits possible anisotropic fluctuations around the mean (not just locally), the matrix $\boldsymbol{U}_A$ becomes random and has a more general form than upper triangular. However, this kind of model goes beyond the scope of this work. For more information please see [221, 220, 85, 84].

The stochastic germ $\boldsymbol{T}(x,\omega)$ of the random matrix $\boldsymbol{A}$ cannot be arbitrarily chosen. This matrix belongs to $\Im$, an ensemble of square real symmetric positive-definite random matrices with finite second order moment (i.e. $\mathbb{E}(\boldsymbol{T}(x,\omega)) = \boldsymbol{I}$, $\boldsymbol{I}$ is the unity matrix), and the probability distribution constructed with the help of the maximum entropy principle [222] (see Section 3.3.1). In other words, the field $\boldsymbol{T}(x,\omega)$ is given by a nonlinear transformation (see [221])

$$\boldsymbol{T}(x,\omega) = \phi(\Gamma(x,\omega)), \tag{3.15}$$

where the set $\Gamma(x,\omega) = \{\theta_{ij}(x,\omega), 1 \le i \le j \le n\}$ consists of n independent Gaussian random fields θ_{ij} with zero mean and unit variance. To this set one may as-

[2] Even for isotropic mean media the modelled heterogeneous random field $\boldsymbol{A}$ is locally anisotropic.

sociate the set of autocorrelation functions $\{r_{ij}(x),\ \text{s.t. } r_{ij}(0) = 1, 1 \leq i \leq j \leq n\}$ parametrised by correlation lengths $\{l_c^m\}_{m=1}^d$ [179], one for each dimension of the Euclidean space. For simplicity reasons the correlation lengths for different θ_{ij} are often taken to be identical. According to this, the random field $\boldsymbol{T}(x,\omega)$ fundamentally differs from the random matrices defined in an usual mathematical sense [221]. Namely, the field $\boldsymbol{T}(x,\omega)$ admits the Cholesky decomposition:

$$\boldsymbol{T}(x,\omega) = \boldsymbol{U}^T(x,\omega)\boldsymbol{U}(x,\omega) \tag{3.16}$$

resulting in the random upper triangular real square matrix $\boldsymbol{U}(x,\omega)$ with the elements:

$$\boldsymbol{U}_{ij} = \begin{cases} \frac{\delta_T}{\sqrt{n+1}}\theta_{ij} & \text{if } i < j \\ \frac{\delta_T}{\sqrt{n+1}}\sqrt{c_F F_\varphi^{-1}(\text{erf}(\theta_{ij}))} & \text{if } i = j. \end{cases} \tag{3.17}$$

Here, $\delta_T := (\mathbb{E}\{\|\boldsymbol{T}(x,\omega) - \mathbb{E}\{\boldsymbol{T}(x,\omega)\}\|^2)/\|\mathbb{E}\{\boldsymbol{T}(x,\omega)\}\|^2$ denotes the coefficient of the dispersion, erf standard cumulative distribution and F_φ^{-1} the reciprocal cumulative distribution function, i.e. a non-linear isoprobabilistic transformation that maps a Gaussian field θ_{ij} into a positive-distributed field (Gamma, lognormal etc.). The normalisation of such transformation is done by introducing the normalisation constant c_F. This constant equals 2 when F_φ represents the Gamma distribution $F_{\Gamma(\alpha_j,1)}$ with parameter

$$\alpha_j = 0.5[(n+1)/\delta_T^2 + 1 - j] \tag{3.18}$$

[221]. Similarly,

$$c_F = e^{-1/2}[(n+1)/\delta_T^2 + 1 - j] \tag{3.19}$$

when F_φ denotes a lognormal cumulative distribution.

Following the previous definitions of the random tensor $\boldsymbol{T}$ and the matrix $\boldsymbol{U}_A$, one may show that the heterogeneous and non-normalised random field $\boldsymbol{A}$ (see Eq. (3.14)) is the positive-definite and invertible matrix with bound $\mathbb{E}(\|\boldsymbol{A}^{-1}(x)\|^2) \leq c < \infty$ for all fixed $x \in \mathcal{G}$. In addition, the tensor $\boldsymbol{A}$ admits the finite fluctuation [221]:

$$\delta_A(x) = \left[\frac{\mathbb{E}\{\|\boldsymbol{A}(x) - \bar{\boldsymbol{A}}(x)\|^2\}}{\|\bar{\boldsymbol{A}}(x)\|^2}\right]^{1/2} = \frac{\delta_T}{\sqrt{n+1}}\left[1 + \frac{(\text{tr}(\bar{\boldsymbol{A}}))^2}{\text{tr}(\bar{\boldsymbol{A}})^2}\right]^{1/2}, \tag{3.20}$$

described by the coefficient of dispersion δ_T and the mean model. In this manner the tensor $\boldsymbol{A}$ meets all the requirements for the description of the elastoplastic material.

3.4 Stochastic plasticity – general formulation

Let $(\Omega, \mathcal{B}, \mathbb{P})$ be a probability space with Ω the set of elementary events ω, $\mathbb{P}$ the probability measure, and $\mathcal{B}$ an σ-algebra on the set Ω. The uncertain parameters introduced in Section 3.2 belong to this space, and are here generally denoted by $\kappa(x, \omega)$. The body represents the three-dimensional manifold with piecewise smooth Lipschitz continuous boundary $\Gamma = \partial\mathcal{G}$ on which are imposed boundary conditions in Dirichlet and Neumann form on $\Gamma_D \subseteq \partial\mathcal{G}$ and $\Gamma_N \subset \partial\mathcal{G}$ respectively, such that $\Gamma_D \cap \Gamma_N = \varnothing$ and $\partial\mathcal{G} = \bar{\Gamma}_N \cup \bar{\Gamma}_D$. The body is imagined to be an assemblage of material particles moving in the time interval $\mathcal{T} = [0, T] \subset \mathbb{R}_+$ assumed to pass simultaneously [215, 30, 115, 24]. Under the influence of the external loads the body $\mathcal{G}$ deforms, moves and changes its configuration. The motion is described by a sequence of mappings between the initial $\mathcal{G}_0$ and the current configuration $\mathcal{G}_t(\omega)$:

$$\boldsymbol{x}(\omega) = \varphi(\boldsymbol{X}, t, \omega) \ : \ \mathcal{G}_0 \times \mathcal{T} \times \Omega \to \mathbb{R}^3 \tag{3.21}$$

such that the continuous function $\varphi(X, \cdot, \omega)$ for fixed $\omega \in \Omega$ is twice-differentiable and describes the path of the particle X. Similarly for fixed X and ω the function $\varphi(X, \cdot, \omega)$ describes the new configuration $\mathcal{G}_t(\omega)$, and for fixed pair (X, t) it is measurable with respect to $\mathcal{B}$. From this follows that the randomness in $\boldsymbol{x}(\omega)$ at some arbitrary time $t \in \mathcal{T}$ determines the uncertain geometry of $\mathcal{G}_t$. In order to describe the motion the reference configuration can be chosen arbitrary, i.e any smooth image of the body including those configurations never occupied. However, to simplify the analysis the reference configuration is chosen to be time and ω-independent. Assuming that the initial geometry is known these requirements satisfies only the initial configuration, and thus the body motion is further described with respect to $\mathcal{G}_0$ (material description).

The body motion in Eq. (3.21) has a similar form as in the deterministic case (see Section 2.1). The only difference is ω as the "extra" parameter. This means that the six conservation laws [249, 229] in the stochastic description have the same form as in a classical formulation. However, the laws have to be satisfied not only almost everywhere in $\mathcal{G}$—as in Section 2.1—but also $\mathbb{P}$-almost surely. Besides this, the rest of the description is the same. Namely, the local thermodynamical state is identified with the set $(\boldsymbol{F}(\omega), s(\omega), \boldsymbol{\eta}(\omega))$, where $\boldsymbol{F}(\omega)$ is the random local deformation gradient, $s(\omega)$ the random local entropy, and $\boldsymbol{\eta}(\omega)$ the vector of random internal variables. In order to properly define these terms the weak differentiation operator ∇ is introduced. The operator maps a single tensor product $\varphi_1(x)\varphi_2(\omega)$ to $(\nabla\varphi_1(x), \varphi_2(\omega))$.

Following this, the deformation gradient becomes:

$$\boldsymbol{F}(x,\omega) = \nabla\varphi(x,\omega) := [\nabla\varphi_1(x)]\varphi_2(\omega), \tag{3.22}$$

where the split to $\varphi_1(x)$ and $\varphi_2(\omega)$ is described later in Chapter 4 Section 4.4. Once more, as in Section 2.1, the focus of the study is on the isothermal process described by a free random Helmholtz energy $\psi(\boldsymbol{F}(\omega), \boldsymbol{\eta}(\omega))$, the evolution law $\dot{\boldsymbol{\eta}}(\omega) = \dot{\boldsymbol{\eta}}(\boldsymbol{F}(\omega), \boldsymbol{\eta}(\omega))$ and the dissipation inequality:

$$\boldsymbol{\chi}(\omega) : \dot{\boldsymbol{\eta}}(\omega) \geq 0 \quad \forall\omega \in \Omega. \tag{3.23}$$

These laws are then combined with the principle of the conservation of the momentum, i.e. the equilibrium equation (see Section 2.1):

$$\text{div}\, \boldsymbol{\sigma}(x,\omega) + \boldsymbol{f}(x,t,\omega) = \boldsymbol{0}, \quad \forall \boldsymbol{x} \in \mathcal{G}_t, \forall t \in \mathcal{T}, \forall\omega \in \Omega \tag{3.24}$$

$$\boldsymbol{v}(x,\omega) = \boldsymbol{v}_0(x,\omega) = \boldsymbol{0}, \quad \text{on } \partial\Gamma_D, \forall\omega \in \Omega, \tag{3.25}$$

$$\hat{\boldsymbol{t}}(x,\omega) = \hat{\boldsymbol{t}}_0(x,\omega), \quad \text{on } \partial\Gamma_N, \forall\omega \in \Omega, \tag{3.26}$$

where the stress $\boldsymbol{\sigma}$, the force $\boldsymbol{f}$ and non-zero Neumann conditions are defined as random fields over the probability space Ω. In further analysis the initial conditions are taken to be homogeneous for reasons of simplicity. Note that this assumption does not globally affect the formulation.

3.5 Small deformation plasticity

Assuming the mapping between the space of displacements and strains to be linear one arrives to the small deformation theory determined by an additive decomposition of strain into elastic and plastic parts $\mathbb{P}$-almost surely. Formally, the problem is seen as a special case of general principles given in Section 3.4, where the displacements are assumed to be sufficiently small compared to the original dimensions of the body.

3.5.1 Functional spaces

In contrast to the deterministic description fully defined by functional spaces described in Section 2.3.1, the stochastic formulation requires the introduction of the

spaces of random variables with finite variance. Only with the help of these one may further define the spaces of the variables of consideration.

Spaces of RVs

The material properties describing the time evolution equations of elastoplastic material are considered to be random variables with respect to spatial position and time. Their description starts with the introduction of the linear space $L_p(\Omega, \mathcal{F}, \mathbb{P})$ of all random variables κ which belong to $(\Omega, \mathcal{F}, \mathbb{P})$ and have finite L_p-norm [176, 102], i.e.

$$L_p(\Omega, \mathcal{F}, \mathbb{P}) := L_p(\Omega) = \{\|\kappa\|_p = (\int_\Omega |\kappa(\omega)|^p \ \mathrm{d}\mathbb{P}(\omega))^{1/p} < \infty\} \tag{3.27}$$

with the usual extension to $\|\kappa\|_\infty = \operatorname{ess\,sup}\{|\kappa(\omega)| : \omega \in \Omega\}$ for $p = \infty$. Note that L_p norm with $1 \leq p \leq \infty$ has all the required properties of a norm, in contrast to the case when $0 < p < 1$ and the triangle inequality fails. For $p = 0$ the corresponding space $L_0(\Omega, \mathcal{F}, \mathbb{P})$ describes a space of all RVs equipped with the topology of convergence in probability, while the norm $\|\kappa\|_1 = \mathbb{E}(\kappa) < \infty$ describes the Banach space $L_1(\Omega, \mathcal{F}, \mathbb{P})$ of the integrable random variables. This space is important because the random variable κ has the mean only if it belongs to space $L_1(\Omega, \mathcal{F}, \mathbb{P})$. In further text one assumes RVs to be of the square integrable type, i.e. they span the vector space $L_2(\Omega, \mathcal{F}, \mathbb{P})$ described by an inner product:

$$\langle \kappa_1(\omega) | \kappa_2(\omega) \rangle = \mathbb{E}(\kappa_1(\omega)\kappa_2(\omega)). \tag{3.28}$$

Note that the inner product in Eq. (3.28) is equal to zero only if $\kappa(\omega)$ is equal to zero $\mathbb{P}$-almost surely. According to the Riesz–Fischer theorem [176, 102] such assumption completes the $L_2(\Omega, \mathcal{F}, \mathbb{P})$ space to a Hilbert space with the norm:

$$\|\kappa\|_2 := \|\kappa\|_{L_2} = \sqrt{\langle \kappa_1(\omega) | \kappa_2(\omega) \rangle}, \tag{3.29}$$

equal to the covariance $\langle \kappa_1, \kappa_2 \rangle = \operatorname{cov}(\kappa_1, \kappa_2)$ of two zero-mean RVs κ_1 and κ_2. In addition, one may show that the L_2-space is dense in L_1, i.e. $\|\kappa\|_1 \leq \|\kappa\|_2$. Moreover, by generalisation with the help of Lyapunov's inequality, one may show that the space L_q is dense in L_p for $0 \leq p \leq q \leq \infty$ such that:

$$\|\kappa\|_p \leq \|\kappa\|_q, \quad L_q \subseteq L_p, \quad 1/p + 1/q = 1 \tag{3.30}$$

holds.

However, in this thesis the author is mostly interested in spaces of Gaussian random variables $\boldsymbol{\theta}$ as a basis of other kinds of RVs. Assuming that $\boldsymbol{\theta}$ are standard one may define the inner product according to Eq. (3.28) as $\langle\theta_1|\theta_2\rangle = \mathbb{E}(\theta_1\theta_2)$. This product completes the closed subspace of $L_2(\Omega,\mathcal{B},\mathbb{P})$ of centered Gaussian random variables [102] to a Hilbert Gaussian space Θ. The normally distributed random variables $\boldsymbol{\theta} := \{\theta_1(\omega),...,\theta_k(\omega),...\}$ in Θ are orthonormal, i.e. uncorrelated, and hence they form a complete orthonormal system (CONS) for Θ. Moreover, Gaussian RVs possess moments of all orders, meaning that the product of Gaussian RVs belonging to Θ is again in $L_2(\Omega)$. Due to these favourable properties the Gaussian RVs are used as a stochastic CONS in the following discussion.

Definition of tensor product spaces

When working with uncertain variables such as displacement and stress, one has to formally introduce the linear space $\mathscr{V} = L_2(\Omega,\mathcal{B},\mathbb{P};\mathcal{V})$ with $\mathcal{V}$ being the deterministic Hilbert space of variable of consideration, see Section 2.3.1. The space is built such that for $v \in \mathscr{V}$ and $\omega \in \Omega$ one has

$$v(\cdot,\omega) \in \mathcal{V}, \tag{3.31}$$

and for $x \in \mathcal{G}$:

$$v(x,\cdot) \in L_2(\Omega,\mathcal{B},\mathbb{P}). \tag{3.32}$$

In other words, the variables live in a space obtained as a tensor product of the corresponding deterministic space $\mathcal{V}$ and the stochastic space (S). The choice of (S), and hence the stochastic regularity of the solution, depend on the stochastic regularity of the right hand side and parameters [107]. For the sake of simplicity, (S) is taken to be $L_2(\Omega)$ such that

$$\mathscr{V} \simeq \mathcal{V} \otimes (S) \tag{3.33}$$

is the Hilbert space induced by the inner product:

$$\langle\langle u|v\rangle\rangle = \mathbb{E}(\langle u|v\rangle_{\mathcal{V}}), \tag{3.34}$$

and duality pairing:

$$\langle\langle u,v\rangle\rangle = \mathbb{E}(\langle u,v\rangle_{\mathcal{V}}). \tag{3.35}$$

Here, $\mathbb{E}(\cdot) = \int_\Omega(\cdot)\mathbb{P}(\,\mathrm{d}\omega)$ is the mathematical expectation with respect to the probability measure $\mathbb{P}$.

Following previous definitions, one may construct Table 3.1 by substituting the de-

terministic generic space $\mathcal{V}$ in $\mathscr{V}$ with the proper space of definition as described in

Table 3.1: The definition of the stochastic spaces for kinematic and dynamic variables together with the corresponding inner products

Variable	Space	Duality pairing
$\boldsymbol{u}$	$\mathscr{U} := \mathcal{U} \otimes (S)$	
$\boldsymbol{f}$	$\mathscr{F} := \mathcal{U}^* \otimes (S)$	$\langle\!\langle \boldsymbol{f}, \boldsymbol{u} \rangle\!\rangle_{\mathscr{F}\times\mathscr{U}} := \mathbb{E}\left(\langle \boldsymbol{f}, \boldsymbol{u} \rangle_{\mathcal{F}\times\mathcal{U}}\right)$
$\boldsymbol{\varepsilon}$	$\mathscr{E} := \mathcal{E} \otimes (S)$	
$\boldsymbol{\sigma}$	$\mathscr{R} = \mathcal{R} \otimes (S)$	$\langle\!\langle \boldsymbol{\sigma}, \boldsymbol{\varepsilon} \rangle\!\rangle_{\mathscr{R}\times\mathscr{E}} := \mathbb{E}\left(\langle \boldsymbol{\varepsilon}, \boldsymbol{\sigma} \rangle_{\mathcal{R}\times\mathcal{E}}\right)$
$\boldsymbol{\eta}$	$\mathscr{Q} = \mathcal{Q} \otimes (S)$	
$\boldsymbol{\chi}$	$\mathscr{C} = \mathcal{C} \otimes (S)$	$\langle\!\langle \boldsymbol{\chi}, \boldsymbol{\eta} \rangle\!\rangle_{\mathscr{C}\times\mathscr{Q}} := \mathbb{E}(\langle \boldsymbol{\chi}, \boldsymbol{\eta} \rangle_{\mathcal{C}\times\mathcal{Q}})$
$\boldsymbol{E}_p$	$\mathscr{P} := \mathcal{P} \otimes (S)$	
$\boldsymbol{\Sigma}$	$\mathscr{Y} := \mathcal{Y} \otimes (S)$	$\langle\!\langle \boldsymbol{\Sigma}, \boldsymbol{E}_p \rangle\!\rangle_{\mathscr{Y}\times\mathscr{P}} := \mathbb{E}\left(\langle \boldsymbol{\Sigma}, \boldsymbol{E}_p \rangle_{\mathcal{Y}\times\mathcal{P}}\right)$
$\boldsymbol{w}$	$\mathscr{Z} = \mathscr{U} \times \mathscr{P}$	
$\boldsymbol{w}^*$	$\mathscr{Z}^* = \mathscr{F} \times \mathscr{Y}$	$\langle\!\langle \boldsymbol{w}^*, \boldsymbol{w} \rangle\!\rangle_{\mathscr{Z}^*\times\mathscr{Z}} := \mathbb{E}\left(\langle \boldsymbol{w}^*, \boldsymbol{w} \rangle_{\mathcal{Z}^*\times\mathcal{Z}}\right)$

Chapter 2 Section 2.3.1 for each variable of consideration. Here, $\mathscr{U}$ represents the space of displacements, $\mathscr{F}$ of forces, $\mathscr{E}$ of deformations, $\mathscr{R}$ of Cauchy stresses, $\mathscr{Q}$ of internal variables, and $\mathscr{C}$ of conjugate forces. In general, these spaces may be written in a short form as a space $\mathscr{P}$ of the generalised plastic deformation $\boldsymbol{E}_p := (\boldsymbol{\varepsilon}_p, \boldsymbol{\eta})$ and the space $\mathscr{Y}$ of the generalised stress $\boldsymbol{\Sigma} := (\boldsymbol{\sigma}, \boldsymbol{\chi})$. Furthermore, separating the primal $\boldsymbol{w} := (\boldsymbol{u}, \boldsymbol{E}_p)$ from the dual variable $\boldsymbol{w}^* := (\boldsymbol{f}, \boldsymbol{\Sigma})$, one may distinguish the primal space $\mathscr{Z} = \mathscr{U} \times \mathscr{P}$ from its dual $\mathscr{Z}^* = \mathscr{F} \times \mathscr{Y}$. This notation allows the description of the uncertain elastoplastic behaviour to be given in the similar framework as in Section 2.2, with the only difference that constitutive and evolution laws must hold almost surely $\forall \omega \in \Omega$. Another difference is that the presence of the uncertainty requires some simple extensions such as the definition of the linear mapping

$$\nabla_S : \quad \mathscr{U} \to \mathscr{E} \tag{3.36}$$

between the displacement $\mathscr{U}$ and the deformation $\mathscr{E}$ spaces. Namely, the differentiation is done in a weak sense such that for a single tensor product $u_1(x)u_2(\omega) \in \mathscr{U} := \mathcal{U} \otimes (S)$ one has:

$$\nabla_S : u_1(x)u_2(\omega) \to (\nabla_S u_1(x))u_2(\omega). \tag{3.37}$$

By linearity and continuity this can be extended to a linear bounded operator:

$$\boldsymbol{\nabla}_S = (\nabla_S \otimes I): \quad \mathscr{U} \otimes (S) \to \mathcal{E} \otimes (S), \tag{3.38}$$

used in the following description.

3.5.2 Material point description

The formulation in one material point is a straightforward generalisation of the formulation given in Section 2.2, as summed in Table 3.2. Similar to the deterministic

Table 3.2: Stochastic plasticity described at material point

Model	Variable	Law valid a.s.
Elasticity	Deformation	$\boldsymbol{\varepsilon}_x(\omega) = \boldsymbol{\varepsilon}_{ex}(\omega)$
	Energy	$\psi_{ex}(\boldsymbol{\varepsilon}_{ex}(\omega)) = \frac{1}{2}\mathbb{E}(\langle \boldsymbol{\varepsilon}_{ex}, A_x \boldsymbol{\varepsilon}_{ex} \rangle_x)$
	Hooke's law	$\boldsymbol{\sigma}_x(\omega) = -\nabla_{\boldsymbol{\varepsilon}} \psi_{ex}(\omega) = \boldsymbol{A}_x(\omega) : \boldsymbol{\varepsilon}_{ex}(\omega)$
Perfect plasticity	Deformation	$\boldsymbol{\varepsilon}_x(\omega) = \boldsymbol{\varepsilon}_{ex}(\omega) + \boldsymbol{\varepsilon}_{px}(\omega)$
	Energy	$\psi_x(\omega) = \psi_{ex}(\omega) + \psi_{irrx}(\omega)$
	Hooke's law	$\boldsymbol{\sigma}_x(\omega) = -\nabla_{\boldsymbol{\varepsilon}} \psi_x(\omega) = \boldsymbol{A}_x(\omega) : \boldsymbol{\varepsilon}_{ex}(\omega)$
	Flow rule	$\mathbb{E}(\langle \dot{\boldsymbol{\varepsilon}}_{px}, \boldsymbol{\tau} - \boldsymbol{\sigma} \rangle_x) \leq 0, \forall \boldsymbol{\tau}_x(\omega) \in \mathcal{K}_x(\omega)$
	Elastic domain	$\mathcal{K}_x(\omega)$
General hardening plasticity	Deformation	$\boldsymbol{E}_{px}(\omega) := (\boldsymbol{\varepsilon}_{px}(\omega), \boldsymbol{\eta}_x(\omega))$
		$\boldsymbol{\varepsilon}_x(\omega) = \boldsymbol{\varepsilon}_{ex}(\omega) + \boldsymbol{\varepsilon}_{px}(\omega)$
	Energy	$\psi_x(\omega) = \psi_{ex}(\omega) + \psi_{irrx}(\omega)$
		$\psi_{irr}(\omega) = \frac{1}{2}\mathbb{E}(\langle \boldsymbol{E}_{px}, \boldsymbol{H}_x \boldsymbol{E}_{px} \rangle_x)$
	Hooke's law	$\boldsymbol{\Sigma}_x(\omega) := (\boldsymbol{\sigma}_x(\omega), \boldsymbol{\chi}_x(\omega)) = -\nabla_{\boldsymbol{\varepsilon}} \psi_x(\omega)$
	Flow rule	$\mathbb{E}(\langle \dot{\boldsymbol{E}}_p, \boldsymbol{T} - \boldsymbol{\Sigma} \rangle_x) \leq 0$
Mixed hardening plasticity	Hardening	$\boldsymbol{H}(\omega) = \mathrm{diag}[\boldsymbol{H}_{kin}(\omega), H_{iso}(\omega)]$
	Conj. stress	$\boldsymbol{\chi}(\omega) = (\boldsymbol{\varsigma}(\omega), \zeta(\omega))$
	Conj. strain	$\boldsymbol{\eta}(\omega) = (\boldsymbol{\varepsilon}_p(\omega), \nu(\omega))$
	Hard. law	$\boldsymbol{\chi}(\omega) = \boldsymbol{H}(\omega) : \boldsymbol{\eta}(\omega)$
	Back stress	$\boldsymbol{\varsigma}(\omega) = \boldsymbol{H}_{kin}(\omega) : \boldsymbol{\varepsilon}_p(\omega)$
	Isotropic stress	$\zeta(\omega) = H_{iso}(\omega)\nu(\omega)$

formulation one may distinguish three different cases of material behaviour: linear

elasticity, perfect plasticity, and general hardening plasticity (further on specialised to a linear case). Throughout this work the focus is set on the general and linear hardening models whose special cases represent elasticity and perfect plasticity. The linear elasticity (reversible behaviour) in a material point x is specified by the random total deformation $\boldsymbol{\varepsilon}_x(\omega)$ equal to the elastic deformation $\boldsymbol{\varepsilon}_{ex}(\omega)$ $\mathbb{P}$-almost surely. As a consequence, the Helmholtz free energy $\psi_x(\omega)$ only consists of the elastic part $\psi_{ex}(\boldsymbol{\varepsilon}_{ex}(\omega))$ defined as a mathematical expectation of $\langle \boldsymbol{\varepsilon}, A\boldsymbol{\varepsilon} \rangle$ in a material point x. Taking the partial derivative of the energy in a weak sense one obtains Hooke's law for $\boldsymbol{\sigma}_x(\omega)$ (see Table 3.2) valid almost surely on Ω. In this definition the double dot product is interpreted in a weak sense. The same law is also valid in a perfect plasticity case. The only difference is that the random total deformation is additively decomposed almost surely to the random plastic $\boldsymbol{\varepsilon}_p(\omega)$ and elastic $\boldsymbol{\varepsilon}_e(\omega)$ part, and energy to its reversible $\psi_{ex}(\omega)$ and irreversible $\psi_{irrx}(\omega)$ part. The stochastic evolution of a plastic deformation $\dot{\boldsymbol{E}}_p$ (or $\dot{\boldsymbol{\varepsilon}}_{px}$) is described by a flow rule valid almost surely on the elastic domain $\mathscr{K}_x(\omega)$. This variable consists of a random plastic deformation $\boldsymbol{\varepsilon}_{px}(\omega)$ and the vector of the random internal variables $\boldsymbol{\eta}_x(\omega)$. The internal variables are energy conjugated to the random stress $\boldsymbol{\sigma}_x(\omega)$ and conjugate force $\boldsymbol{\chi}_x(\omega)$, which are gathered in a generalised random stress $\boldsymbol{\Sigma}_x = (\boldsymbol{\sigma}_x(\omega), \boldsymbol{\chi}_x(\omega))$ described by a random constitutive $\boldsymbol{A}_x$ tensor and random hardening $\boldsymbol{H}_x$. Taking the hardening to be linear, i.e. determined by the random isotropic $H_{iso}(\omega)$ and kinematic modulus $\boldsymbol{H}_{kin}(\omega)$, one may reduce the previous model to the mixed hardening case, see Table 3.2.

3.5.3 Associative plastic flow rule

Let be given the convex closed and nonempty subset $\mathscr{K}$ of $\mathscr{R}$ containing the origin 0 $\mathbb{P}$-almost surely. The indicator function of this set $\Psi_{\mathcal{K}}(\boldsymbol{\Sigma})$ is equal to 0 in $\mathbb{P}$-almost sure sense if the stress belongs to a set, otherwise takes the value at infinity. Furthermore, one may define a normal cone $N_{\mathcal{K}}(\boldsymbol{\Sigma})$ to $\mathscr{K}$ in a point $\boldsymbol{\Sigma}$ such that the stochastic flow rule in dual form can be written as given in Table 3.3, similarly to the dual rule in Table 2.2. Analogously, the primal flow rule is determined by a support function $\Psi^*_{\mathscr{K}}$ with the convex domain $\mathscr{K}$ as sub-differential. In practical computation the convex set $\mathscr{K}$ is expressed via the yield function $\phi_{\mathscr{K}}$, which under the smoothness assumption gives the classical formulation of the flow rule similar to the one in Table 2.2. Therefore, following the correspondence between Table 2.2 and Table 3.3, one may introduce the convex closed set

$$\mathscr{F} \times \mathscr{Y} \supset \mathscr{K} = \{(\boldsymbol{f}, \boldsymbol{\sigma}, \boldsymbol{\chi}) \mid (\boldsymbol{\sigma}, \boldsymbol{\chi}) \in \tilde{\mathscr{K}}\} \tag{3.39}$$

Table 3.3: Flow rule formulations

Primal	
Support function	$\Psi^*_{\mathscr{K}}(\Xi) = \sup\{\langle\!\langle \Xi, \boldsymbol{T}\rangle\!\rangle - \varphi(\boldsymbol{T}) \mid \boldsymbol{T} \in \mathscr{Y}\}$
Dissipation	$j(\dot{\boldsymbol{E}}_p) = \Psi^*_{\mathscr{K}}(\dot{\boldsymbol{E}}_p) = \{\sup \langle\!\langle \dot{\boldsymbol{E}}_p, \boldsymbol{T}\rangle\!\rangle \mid \boldsymbol{T} \in \mathscr{K}\}$
Flow rule	$\boldsymbol{\Sigma}(\omega) \in \partial\Psi^*_{\mathscr{K}}(\dot{\boldsymbol{E}}_p)$
Dual	
Cone	$N_{\mathcal{K}}(\boldsymbol{\Sigma}) = \{\Xi \in \mathcal{E} \mid \langle\!\langle \Xi, \boldsymbol{T} - \boldsymbol{\Sigma}\rangle\!\rangle \le 0\} \subseteq \mathcal{E}$
Indicator	$\Psi_{\mathscr{K}}(\boldsymbol{\Sigma}(\omega)) = 0$, if $\boldsymbol{\Sigma} \in \mathcal{K}$, else $\Psi_{\mathscr{K}}(\boldsymbol{\Sigma}(\omega)) = \infty$
Flow rule	$\boldsymbol{N}_{\mathscr{K}}(\boldsymbol{\Sigma}(\omega)) = \partial\Psi_{\mathscr{K}}(\boldsymbol{\Sigma}(\omega)) \Leftrightarrow \langle\!\langle \dot{\boldsymbol{E}}_p, \boldsymbol{\Sigma} - \boldsymbol{T}\rangle\!\rangle \le 0$
Yield function	
Yield function	$\phi_{\mathscr{K}}(\boldsymbol{\Sigma}(\omega)) := g_{\mathscr{K}}(\boldsymbol{\Sigma}(\omega)) - 1,$
Gauge	$g_{\mathscr{K}}(\boldsymbol{\Sigma}) = \inf\{\lambda > 0 \mid \forall \Xi :\ \langle\!\langle \Xi, \boldsymbol{\Sigma}\rangle\!\rangle \le \lambda\Psi^*_{\mathscr{K}}(\Xi)\}$
Convex domain	$\mathscr{K} = \{\Sigma \in \mathscr{R} :\ \phi(\omega, \Sigma(\omega)) \le 0\ \mathbb{P}\text{ a.s.}\}$
Flow rule	$\exists\lambda \ge 0 :\ \dot{\boldsymbol{E}}_p(\omega) \in \lambda(\omega)\partial\phi_{\mathscr{K}}(\boldsymbol{\Sigma}(\omega))$
	$\wedge\ \lambda\phi_{\mathcal{K}}(\boldsymbol{\Sigma}(\omega)) = 0$

with the barrier cone $\mathscr{K}^\infty = \{0\} \times \tilde{\mathscr{K}}^\infty$, where

$$\mathscr{Y} \supset \tilde{\mathscr{K}} = \{(\boldsymbol{\sigma}, \boldsymbol{\chi}) \in \mathscr{R} \times \mathscr{C} \mid \phi_{\mathscr{K}}(x, \omega, \boldsymbol{\sigma}_x, \boldsymbol{\chi}) \le 0, \forall x \text{ a.e. in } \mathcal{G}, \forall\omega \text{ a.s. in } \Omega\} \tag{3.40}$$

and $\tilde{\mathscr{K}}^\infty \subseteq \mathscr{P}$. Once $\mathscr{K}$ is defined, we are ready to extend the mathematical theory given in Chapter 2 to the more general case including the uncertainties of material parameters or the right hand side.

3.5.4 Variational formulation

As described in the previous chapter, the variational formulation of elastoplastic behaviour is part of the theory of variational inequalities. This theory was initiated by Kinderlehrer et al. in [112], Duvaut et al. in [62] and Glowinski in [81], who considered free boundary value problems in partial differential equations that can be modeled and analyzed as elliptic variational inequalities. However, these studies were oriented on the deterministic problems and not on the stochastic problems. Only very recently few studies tried to combine the monotone operator theory and convex analysis with the measure theory in order to prove the existence results for the stochastic elliptic variational inequalities. Namely, Gwinner in his papers [88, 87, 86]

proves the existence of the solution for the special class of nonlinear elliptic stochastic boundary value problems with unilateral Signorini boundary conditions. Under reasonable assumptions he shows that the solution lies in an appropriate Bochner - Lebesgue space of measurable functions. Furthermore, Ghosh et al. [80] investigate a class of stochastic second order nonlinear variational inequalities with bilateral constraints on the example of the stochastic game with the stopping times, while Forster et al. in [68] studies stochastic elliptic variational inequalities of the second kind described by a bilinear form with stochastic coefficients with the example of the obstacle problem and the Richardson equation.

Existing results in previously mentioned studies are further extended with the help of the theory of the deterministic variational inequalities to the description of the stochastic elastoplastic problem given by Eq. (3.24). The variational description is formulated on the Hilbert tensor product space $\mathscr{Z} := \mathcal{Z} \otimes (S)$ isomorphic to $L_2(\Omega, \mathbb{P}; \mathcal{Z})$, i.e. the space of $\mathcal{Z}$-valued RVs with finite variance. In this way the stochastic problem can have the same theoretical properties as the underlying deterministic one, which is highly desirable for any further numerical approximation. Moreover, the theory represents the abstract extension of Section 2.3.2, and thus can follow the same pattern as before.

Let $(\Omega, \mathcal{B}, \mathbb{P})$ be a probability space and $(\mathcal{U}, \langle \cdot, \cdot \rangle)$ a separable Hilbert space in which one considers for fixed ω the linear functional $\ell(\omega)(v) \in \mathcal{L}(\mathcal{U}, \mathbb{R}) = \mathcal{U}^*$. This function for each fixed $v \in \mathcal{V}$ represents the Borel measurable function on Ω [88, 87, 86]. In other words, the stochastic representative $\ell \in \mathcal{L}(\mathscr{U}, \mathbb{R}) = \mathscr{U}^*$ of the linear functional in Eq. (2.49) becomes:

$$\ell(v) := \langle\langle \ell(\omega), v \rangle\rangle = \mathbb{E}(\ell(\omega)) = \int_\Omega \ell(\omega)(v) \mathbb{P}(\, \mathrm{d}\omega), \tag{3.41}$$

where for fixed ω the functional $\ell(\omega)(v)$ has the same form as in the deterministic case (see Eq. (2.49)). In a similar manner one may define the stochastic bilinear form

$$a : \mathscr{Z} \times \mathscr{Z} \mapsto \mathbb{R} : \; a(z, w) := \langle\langle Az, w \rangle\rangle, \tag{3.42}$$

where $\langle\langle \cdot, \cdot \rangle\rangle$ is the duality pairing between $(\mathcal{Z} \otimes (S))^* = \mathcal{Z}^* \otimes (S)^*$ and $\mathcal{Z} \otimes (S)$. The bilinear form is associated with a linear, continuous, self-adjoint and coercive operator $A : \mathscr{Z} \mapsto \mathscr{Z}^*$. In addition, it is continuous for each ω in Ω, as well as measurable in $\mathcal{B}$. By a similar procedure one may define the dissipation rate:

$$j(\dot{w}) = \int_\Omega j(\omega)(\dot{w}) \mathbb{P}(\mathrm{d}\omega). \tag{3.43}$$

Let us remark that—loosely speaking—the stochastic weak form is just the expected value of its deterministic counterpart formulated on the tensor product space, whose solution is an element of this space. Note that the same notation is used as in the deterministic formulation in the hope that the meaning is already clear from the content.

Following previous definitions one may interpret stochastic linear and bilinear mappings as the parameter ω-dependent deterministic forms. This further leads to a stochastic description of the elastoplastic problem analogue to the one presented in Problem 2.3.7:

Problem 3.5.1. ***Problem SP-P****: given a function $\tilde{f} \in H^1(\mathcal{T}, \mathscr{F})$ with $\tilde{f}(0) = 0$, set $f = [\tilde{f}, 0] \in H^1(\mathcal{T}, \mathscr{F} \times \mathscr{Y})$. Then, there exists a unique function $w = (\boldsymbol{u}, \boldsymbol{E}_p) \in H^1(\mathcal{T}, \mathscr{Z})$ with $w(0) = 0$ and $\dot{w}(t) \in \mathscr{K}^\infty$ which solves a.s. in Ω, a.e. in $\mathcal{T}$:*

$$a(w(t), z - \dot{w}(t)) + j(z) - j(\dot{w}) \geq \langle\!\langle f, z - \dot{w}(t) \rangle\!\rangle \tag{3.44}$$

for all $z = (v, (\boldsymbol{\mu}, v)) \in \mathscr{Z}$. If in addition $\tilde{f}_1, \tilde{f}_2 \in H^1(\mathcal{T}, \mathscr{F})$ are two different loadings, and $w_1, w_2 \in H^1(\mathcal{T}, \mathscr{Z})$ are the corresponding solutions then:

$$\|w_1 - w_2\|_{L_\infty(\mathcal{T}, \mathscr{Z})} \leq c \|\dot{f}_1 - \dot{f}_2\|_{L_1(\mathcal{T}, \mathscr{F})} \tag{3.45}$$

determines the stability of the solution.

The existence and uniqueness of the solution are summarized in the following theorem, obtained by slightly rewriting Theorem 7.3. in [92]:

Theorem 3.5.2. *Let $\mathscr{Z}$ be a Hilbert space; $\mathscr{K} \subset \mathscr{Z}$ a nonempty, closed, convex cone; $a : \mathscr{Z} \times \mathscr{Z} \mapsto \mathbb{R}$ a bilinear form that is symmetric, bounded and $\mathscr{Z}$-elliptic; $\ell \in H^1(\mathcal{T}; \mathscr{Z}^*)$ with $\ell(0) = 0$ $\mathbb{P}$-almost sure, and $j : \mathscr{K} \mapsto \mathbb{R}$ non-negative, convex, positively homogeneous and Lipschitz continuous. Then there exists the unique solution w of Problem 3.5.1 satisfying $w \in H^1(\mathcal{T}, \mathscr{Z})$.*

Proof. The proof of the existence is derived from the time discretisation of the problem and the construction of the linear interpolant of the discrete solution. The interpolant approaches the abstract solution w for the limit case of the time step approaching zero. For a detailed derivation please see [92]. The proof of the uniqueness follows from the assumption of two different solutions w_1 and w_2, and $z = \dot{w}_2$

and $z = \dot{w}_1$ respectively, such that:

$$a(w_1, \dot{w}_2 - \dot{w}_1) + j(\dot{w}_1) - j(\dot{w}_2) \leq \langle\langle \ell, \dot{w}_2 - \dot{w}_1 \rangle\rangle \tag{3.46}$$

and

$$-a(w_1, \dot{w}_2 - \dot{w}_1) + j(\dot{w}_2) - j(\dot{w}_1) \leq -\langle\langle \ell, \dot{w}_2 - \dot{w}_1 \rangle\rangle \tag{3.47}$$

are satisfied. After summation one obtains:

$$a(w_2 - w_1, w_2 - w_1) \leq 0 \quad \mathbb{P}- \text{ a.s.} \tag{3.48}$$

which due to the $\mathscr{Z}$-ellipticity of a leads to $w_1 = w_2$ $\mathbb{P}$-almost surely. □

The mixed formulation of the stochastic plasticity problem with combined general hardening as an analogue to Problem 2.3.8 reads:

Theorem 3.5.3. ***Problem SM-P****: there are functions $w = (\boldsymbol{u}, \boldsymbol{\eta}) \in H^1(\mathcal{T}, \mathscr{Z})$ with $w(0) = 0$ and $w^* \in H^1(\mathcal{T}, \mathscr{Z}^*), w^*(0) = 0$ and $\dot{w} \in \mathscr{K}^\infty$ such that a.s. in Ω, a.e. in $\mathcal{T}$:*

$$a(w(t), z) + \langle\langle \dot{w}(t), z \rangle\rangle = \langle\langle f, z \rangle\rangle \tag{3.49}$$

for all $z = (v, (\boldsymbol{\mu}, \upsilon)) \in \mathscr{Z}$ and

$$\forall z^* \in \mathscr{K} \subset \mathcal{Z}^* : \quad \langle\langle \dot{w}, z^* - w^* \rangle\rangle \leq 0. \tag{3.50}$$

If in addition $\tilde{f}_1, \tilde{f}_2 \in H^1(\mathcal{T}, \mathscr{F})$ are two different loadings, and $w_1, w_2 \in H^1(\mathcal{T}, \mathscr{Z})$ and $w_1^*, w_2^* \in H^1(\mathcal{T}, \mathscr{Z}^*)$ the corresponding solutions, then:

$$\|w_1 - w_2\|_{L_\infty(\mathcal{T}, \mathscr{Z})} \leq c \|\dot{f}_1 - \dot{f}_2\|_{L_1(\mathcal{T}, \mathscr{F})} \tag{3.51}$$

and

$$\|w_1^* - w_2^*\|_{L_\infty(\mathcal{T}, \mathscr{Z}^*)} \leq c^* \|\dot{f}_1 - \dot{f}_2\|_{L_1(\mathcal{T}, \mathscr{F})}. \tag{3.52}$$

The existence and uniqueness of the solution are determined by similar assumptions as made in the abstract primal problem:

Theorem 3.5.4. *Under same assumptions as given in Theorem 3.5.2 the solution w^* of Problem 3.5.3 exists and it is unique.*

Proof. Follows from the proof of Theorem 3.5.2. □

In case that the $\mathscr{Z}$-elliptic bilinear form is given as

$$\begin{aligned} a(w_1, w_2) = \quad & \int_\Omega \int_{\mathcal{G}} (\boldsymbol{\varepsilon}(\boldsymbol{u}_1) - \boldsymbol{\varepsilon}_p^1 : A(\boldsymbol{\varepsilon}(\boldsymbol{u}_2) - \boldsymbol{\varepsilon}_p^2) \, \mathrm{d}x \, \mathbb{P}(\mathrm{d}\omega) \\ & + \int_\Omega \int_{\mathcal{G}} H_{iso} \nu^1 \nu^2 \, \mathrm{d}x \, \mathbb{P}(\mathrm{d}\omega) \\ & + \int_\Omega \int_{\mathcal{G}} \boldsymbol{H}_{kin} \boldsymbol{\varepsilon}_p^1 : \boldsymbol{\varepsilon}_p^2 \, \mathrm{d}x \, \mathbb{P}(\mathrm{d}\omega), \end{aligned} \tag{3.53}$$

the general hardening reduces to the case of the linear mixed hardening. As a special case, the linear mixed hardening admits the same theory as already presented, and thus is not repeated here.

3.6 Large deformation plasticity

The reasons for introducing uncertainty in the large deformation model are essentially the same as in case of small deformation plasticity. Hence, the assumptions given in Section 3.3 are further taken to be valid. The theory follows Section 3.4 and the deterministic formulation in Section 2.4.

Table 3.4: Stress and strain formulations

Name	Law
Gen. plas. deform.	$\boldsymbol{\Xi}_p(\omega) = (\Pi(\omega), \boldsymbol{\eta}(\omega)),\ \Pi(\omega) := \boldsymbol{F}^{p-1}(\omega)$
Energy	$\psi(\omega) = \psi(\boldsymbol{F}^e(\omega), \boldsymbol{\eta}(\omega)),$
I Piola-Kirchhoff	$\boldsymbol{P}(\omega) = \partial\psi/\partial\boldsymbol{F},$
Conjugate force	$\boldsymbol{\chi}(\omega) := (\boldsymbol{\varsigma}(\omega), \zeta(\omega)) = -\partial\psi/\partial\boldsymbol{\Xi}_{\boldsymbol{p}},$ $\boldsymbol{\varsigma}(\omega) = -\partial\psi/\partial\Pi$ and $\zeta(\omega) = -\partial\psi/\partial\boldsymbol{\eta}.$
Generalised stress	$\boldsymbol{\Sigma}(\omega) := (\tilde{\boldsymbol{\varsigma}}(\omega), \zeta(\omega)), \tilde{\boldsymbol{\varsigma}}(\omega) = \Pi^T(\omega)\boldsymbol{\varsigma}(\omega)$

Let X be a material particle and $\varphi(X, t, \omega)$ the mapping between the initial and the current configuration in the time interval $\mathcal{T}$ as introduced in Eq. (3.21). The function is assumed to be smooth enough such that the deformation gradient $\boldsymbol{F}$ exists and has a form as given in Eq. (3.22) with the differentiation operator understood in a weak sense. Once the deformation gradient is known, one may split it by multiplicative

decomposition to the random plastic $\boldsymbol{F}^p$ and elastic $\boldsymbol{F}^e$ part $\mathbb{P}$- almost surely:

$$\boldsymbol{F}(\omega) = \boldsymbol{F}^e(\omega)\boldsymbol{F}^p(\omega), \quad \mathbb{P}- \text{ a.s.} \tag{3.54}$$

This further allows the definitions of the strain as well as the stress measures in a similar manner as given in Section 2.4.1, see Table 3.4. The only difference is that now they represent random variables (fields).

Assuming the material objectivity in $\mathbb{P}$-almost sure sense, the system is described by random free energy $\psi(\boldsymbol{F}_e, \boldsymbol{\eta})$ with random elastic gradient $\boldsymbol{F}^e(\omega)$ and internal variables $\boldsymbol{\eta}(\omega)$ as arguments. These further determine the random generalised stress $\boldsymbol{\Sigma}(\omega)$ and conjugate forces $\boldsymbol{\chi}(\omega)$, see Table 3.4. The plastic state is specified by a random plastic deformation gradient $\boldsymbol{F}^p(\omega)$ and possibly by a vector-valued random internal variable $\boldsymbol{\eta}(\omega)$. These quanitities describe the random general plastic deformation $\boldsymbol{\Xi}_p(\omega) = (\Pi(\omega), \boldsymbol{\eta}(\omega))$, where $\Pi := \boldsymbol{F}^{p-1}$. The evolution of the plastic deformation is driven by a plastic flow rule, also known as normality rule, which similarly to a small deformation plasticity rule may be written in primal and dual forms. The law essentially has the same form as in Section 2.4.1 (only valid $\mathbb{P}$-almost surely). Hence, the final results are merely just recollected in Table 3.5. Namely, with the help of the yield function one may introduce the closed non-empty convex domain:

$$\mathscr{K} = \{(\boldsymbol{f}, \Sigma) \mid \Sigma \in \tilde{\mathscr{K}}\} \tag{3.55}$$

with the barrier cone $\mathscr{K}^\infty = \{0\} \times \tilde{\mathscr{K}}^\infty$, where

$$\tilde{\mathscr{K}} = \{\Sigma \mid \phi_{\mathscr{K}}(x, \omega, \Sigma) \leq 0, \text{ a.e. in } \mathcal{G}, \text{ a.s. in } \Omega\}. \tag{3.56}$$

From Eq. (2.78) follow the indicator function of the set $\mathscr{K}$:

$$\Psi_{\mathcal{K}}(\boldsymbol{\Sigma}) = \begin{cases} 0 & \boldsymbol{\Sigma} \in \mathcal{K} \text{ a.s.} \\ \infty, & \text{otherwise,} \end{cases} \tag{3.57}$$

and its sub-differential:

$$\begin{aligned} \partial\Psi_{\mathcal{K}}(\boldsymbol{\varsigma}, \zeta) = \{\tilde{\Xi}_p \in L_2(\Omega, \mathbb{R}^{d\times d} \times \mathbb{R}^m) : \ \Psi_{\mathcal{K}}(\tilde{\boldsymbol{\varsigma}} + \boldsymbol{T}, \zeta + \tau) \geq \\ \Psi_{\mathcal{K}}(\tilde{\boldsymbol{\varsigma}}, \zeta) + \langle\langle \tilde{\Pi}, \boldsymbol{T} \rangle\rangle + \langle\langle \tilde{\boldsymbol{\eta}}, \tau \rangle\rangle, \quad \forall (\boldsymbol{T}, \tau) \in L_2(\Omega, \mathbb{R}^{(d\times d)} \times \mathbb{R}^m)\}, \end{aligned} \tag{3.58}$$

which further leads to the primal formulation of the flow rule in Table 3.5. The dual of the indicator function is known as the dissipation

$$\Psi^*_{\mathcal{K}}(\tilde{\Pi}, \boldsymbol{\eta}) = \sup \{\langle\langle \tilde{\boldsymbol{\varsigma}}, \tilde{\Pi} \rangle\rangle + \langle\langle \zeta, \boldsymbol{\eta} \rangle\rangle\} \tag{3.59}$$

featuring the dual formulation of the flow rule in Table 3.5.

Table 3.5: Normality rule

Primal	$\dot{\tilde{\boldsymbol{\Xi}}}_p \in \partial\Psi(\tilde{\boldsymbol{\zeta}}, \zeta), \dot{\tilde{\boldsymbol{\Xi}}}_p := (\boldsymbol{F}^p\dot{\tilde{\Pi}}, \dot{\boldsymbol{\eta}})$	a.s.
Dual	$(\tilde{\boldsymbol{\zeta}}, \zeta) \in \partial\Psi^*_{\mathcal{K}}(\tilde{\Pi}, \boldsymbol{\eta})$	a.s.
Yield function	$\dot{\boldsymbol{\Xi}}_p = \lambda\partial_\Sigma\phi(\Sigma), \quad \lambda \geq 0, \phi \leq 0, \quad \lambda\phi = 0$	a.s.

Following previous statements, one may conclude that the geometrical nonlinear plasticity is very similar to the small deformation plasticity. These similarities are further used in the numerical computation of desired functionals.

3.6.1 Constitutive description

The elastic behaviour is assumed to be described by a linear Saint Venant law which takes into consideration the quadratic energy function $\psi_e = \frac{1}{2}\langle\langle \boldsymbol{E}, \boldsymbol{A}\boldsymbol{E}\rangle\rangle$, where $\boldsymbol{E}(\omega) = \frac{1}{2}(\boldsymbol{F}^T(\omega)\boldsymbol{F}(\omega) - \boldsymbol{I})$. As a consequence, the model has the same stress-strain relationship as in the small deformation case, i.e. $\langle\langle \Xi, \boldsymbol{A}\boldsymbol{E}\rangle\rangle = \langle\langle \Xi, \boldsymbol{S}\rangle\rangle$, $\forall \Xi \in \mathscr{E}$. Here, $\boldsymbol{S}$ denotes the random second Piola-Kirchhoff stress tensor, i.e. the derivative of energy ψ_e with respect to the Green-Lagrange strain tensor. For the source of randomness is taken the elastic constitutive tensor $\boldsymbol{A}$, assumed to have the same properties as in a case of small deformations. With such an assumption the stochastic model of large displacement plasticity inherits the poly-convexity conditions and can be considered in a similar manner as the infinitesimal one. Thus, in order to avoid any repeating the results are only collected in Table 3.6.

3.6.2 Variational formulation

Let $(\Omega, \mathcal{B}, \mathbb{P})$ be a probability space in which the linear functional (see Eq. (3.41))

$$\ell(\boldsymbol{v}) = \int_\Omega \int_{\mathcal{G}_t} \boldsymbol{v} \cdot \boldsymbol{f} \, \mathrm{d}x \, \mathbb{P}(\mathrm{d}\omega) + \int_\Omega \int_{\Gamma_N} \boldsymbol{v} \cdot \hat{\boldsymbol{\sigma}} \, \mathrm{d}\Gamma \, \mathbb{P}(\mathrm{d}\omega) \tag{3.60}$$

is defined with respect to the current configuration, where $\hat{\boldsymbol{\sigma}}$ represents the initial stress. The functional ℓ is continuous and measurable with respect to $\mathcal{B}$. Similarly,

Table 3.6: Stochastic large deformation plasticity

Theory	Variable	law a.s.
Linear elasticity	Energy	$\psi_e(\omega) = \frac{1}{2}\langle\langle \boldsymbol{E}(\omega), A(\omega)\boldsymbol{E}(\omega)\rangle\rangle$
	Constitutive law	$\boldsymbol{S}(\omega) = A(\omega)\boldsymbol{E}(\omega)$
Perfect plasticity	Internal variable	$\boldsymbol{G}_p(\omega) = \boldsymbol{C}^{p-1}(\omega)$
	Energy	$\psi(\omega) = \psi(\boldsymbol{C}(\omega), \boldsymbol{G}_p(\omega))$
	Yield function	$\phi_{\mathcal{K}}(\omega) = \phi_{\mathcal{K}}(\boldsymbol{S}(\omega), \boldsymbol{C}(\omega))$
	Plastic dissipation	$D_p := -\boldsymbol{S} \cdot \frac{1}{2}\boldsymbol{C}\frac{\partial \boldsymbol{G}_p}{\partial t}\boldsymbol{G}_p^{-1} > 0$
	Evolution equation	$\dot{\boldsymbol{G}}_p = -2\dot{\lambda}\boldsymbol{C}^{-1}\partial_{\boldsymbol{S}}\phi_{\mathcal{K}}\boldsymbol{G}_p$
Mixed hardening plasticity	Kinematic law	$\boldsymbol{\Xi}(\omega) = \text{const} \cdot \boldsymbol{G}_p(\omega)$
	Yield function	$\phi_{\mathcal{K}}(\omega)(\boldsymbol{C}, \boldsymbol{S}, \varsigma, \zeta) = 0$
	Plastic dissipation	$D_p := -\boldsymbol{S} \cdot \frac{1}{2}\boldsymbol{C}\frac{\partial \boldsymbol{G}_p}{\partial t}\boldsymbol{G}_p^{-1}$ $-\varsigma\frac{1}{2}\boldsymbol{C}\frac{\partial \Xi}{\partial t}\Xi^{-1} + \zeta\frac{\partial \nu}{\partial t} > 0$
	Flow rule	$\dot{\boldsymbol{G}}_p = -2\dot{\lambda}\boldsymbol{C}^{-1}\partial_{\boldsymbol{S}}\phi_{\mathcal{K}}\boldsymbol{G}_p$
		$\dot{\boldsymbol{\Xi}} = -2\dot{\lambda}\boldsymbol{C}^{-1}\partial_{\varsigma}\phi_{\mathcal{K}}\boldsymbol{\Xi}$
		$\dot{\nu} = \dot{\lambda}\boldsymbol{C}^{-1}\partial_{\zeta}\phi_{\mathcal{K}}$

let us define the bilinear form corresponding to Eq. (3.42) as:

$$a^s(\boldsymbol{u}, \boldsymbol{v}) := \langle\langle A\boldsymbol{\varepsilon}(\boldsymbol{u}), \boldsymbol{\varepsilon}(\boldsymbol{v})\rangle\rangle_{\mathcal{G}_t} := \int_\Omega \int_{\mathcal{G}_t} A\boldsymbol{\varepsilon}(\boldsymbol{u}) \cdot \boldsymbol{\varepsilon}(\boldsymbol{v}) \, \mathrm{d}x\mathbb{P}(\mathrm{d}\omega), \tag{3.61}$$

where the strain measure $\boldsymbol{\varepsilon}(\boldsymbol{v}) := \nabla_S \boldsymbol{v}$ is of the linear type due to the definition of the virtual test functions $\boldsymbol{v}$. Here, ∇_S is the symmetric differential operator given by Eq. (3.37) such that the bilinear form a^s admits the same properties as in the small deformation case, see Section 3.5.4. Namely, operator A is linear, continuous, coercive, and symmetric. Following this, the variational equilibrium equation becomes:

$$a^s(\boldsymbol{u}, \boldsymbol{v}) = -\ell(\boldsymbol{v}). \tag{3.62}$$

However, as previously mentioned, the current configuration is not suitable to be taken for the reference due to the unknown coordinates x. Instead, for the reference one chooses the initial— time and ω-independent—configuration. Following the same procedure as in Section 2.4.3 one may rewrite a^s to:

$$a^m(\boldsymbol{w}, \boldsymbol{S}) = \langle\langle \Upsilon(\boldsymbol{w}), \boldsymbol{S}\rangle\rangle_{\mathcal{G}_0} := \int_\Omega \int_{\mathcal{G}_t} \Upsilon(\boldsymbol{w}) \cdot \boldsymbol{S} \, \mathrm{d}\boldsymbol{X} \, \mathbb{P}(\mathrm{d}\omega), \tag{3.63}$$

where $\Upsilon = \frac{1}{2}(\boldsymbol{F}^T \nabla_M \boldsymbol{w} + \nabla_M \boldsymbol{w}^T \boldsymbol{F})$ $\mathbb{P}$-almost surely. In this description the second Piola-Kirchhoff stress is used, so that the linear functional obtains the form:

$$\ell^m(\boldsymbol{w}) = \langle\langle \boldsymbol{w}, \boldsymbol{F}_b \rangle\rangle_{\mathcal{G}_0} + \int_\Omega \int_{\Gamma_N} \boldsymbol{w} \cdot \boldsymbol{T} \, \mathrm{d}\Gamma \, \mathbb{P}(\mathrm{d}\omega), \tag{3.64}$$

where $\boldsymbol{F}_b$ is the volume force and $\boldsymbol{T}$ the initial stress in material description. Thus, the final form of equilibrium Eq. (3.62) reads:

$$a^m(\boldsymbol{w}, \boldsymbol{S}) = -\ell^m(\boldsymbol{w}). \tag{3.65}$$

3.7 Conclusion

The present chapter develops the stochastic model of an irreversible behaviour described by uncertain material parameters and right hand side. Formally speaking the model is an extension of the classical deterministic theory carried out with the help of mathematical tools such as convex analysis and variational inequality theory. Starting from the global description of the stochastic irreversible behaviour in Section 3.4, both the small (Section 3.5) and the finite deformation (Section 3.6) descriptions are fully derrived and presented. The latter case considers the large displacement theory as a natural generalisation of the infinitesimal one. For simplicity reasons, the infinitesimal theory is initially described in one material point (Section 3.5.2) and then extended to the whole domain by introducing tensorial spaces in Section 3.5.1. In this setting the existence and uniqueness of the solution for linear elliptic partial differential equations and second order stochastic variational inequalities (see Section 3.5.4) are shown. In addition, the transformation of variational inequality to the stochastic convex optimisation problem is provided. The convexity is guaranteed by choosing the positive definite distribution for material properties via the maximum entropy principle (see Section 3.3).

Particulary this chapter studies linear elasticity, perfect plasticity, and general hardening plasticity with emphasis on mixed linear hardening. These problems are written in two equivalent forms: the abstract primal and mixed formulation, from which the latter one is employed in computational algorithms, see Chapter 5.

Chapter 4

Discretisation

An approximate answer to the right problem is worth a good deal more than an exact answer to an approximate problem.

J. Tukey

The elastoplastic model presented in Chapter 3 requires the introduction of the tensorial product space $\mathcal{V} \otimes (S)$ in which both $\mathcal{V}$ and (S) are the infinite dimensional sub-spaces. In addition, the models are time-dependent as the evolutionary laws for the plastic-like variables are introduced. In such a setting the practical computation is not possible, and hence the suitable discretisation has to be introduced. Therefore, this chapter considers the mid-point algorithms for the time discretisation of the evolutionary equations, as well as the spatial discretisation of the problem via finite element methods. These lead to the system of equations with stochastic coefficients, the discretisation of which is considered in Chapter 5. To this end, the tractable representation of the random field in the countable number of the mutually independent random variables is introduced, as well as the stochastic version of the closest point projection algorithm formulated by a straightforward extension of the very well known radial return map algorithm [215, 92].

4.1 Related work

Elastoplasticity theory is a very broad research subject. There are many papers and publications which deal with the discretisation problems in time and spatial domain.

This section only briefly reviews some of the existing methods and computational approaches to this problem. For more detailed information the reader is addressed to [215, 92].

For the first time the implicit Euler time integration algorithm has been applied in the work of Wilkins [241] for the problem of the elastoplastic evolutionary equation. He considered the first order differential equation and constructed the algorithm which is the precursor of today's classical closest point projection algorithms. Later on, the implicit Euler has been extended to the general mid-point algorithms [177, 178, 215, 92], for which the corresponding stability analysis is studied in [214, 215, 92]. In contrast to the mentioned one-time step methods, Artioli et al. [12] have studied the double-step methods as their natural extension in the case of linear hardening plasticity. In addition, they proposed an exponential type of algorithm which appears to outperform the single and double step integration algorithms on the expense of efficiency [13]. However, these are not the only time integration schemes. Basically, for the time discretisation one may use any kind of general integration methods designed for ordinary differential equations such as, for example, the Runge-Kutta method [43, 35] or the BDF2 method [64]. The stability of the BDF2 method together with the practical application in J_2 plasticity has been studied in [181]. However, these methods are not often used in practice due to the complicated algorithmic scheme which is not so suitable for the numerical implementation.

In computational applications the spatial discretisation of the mentioned problems is mostly done with the help of finite element methods [21, 250] as the most appropriate for experimental verification. However, these methods are not the most suitable for the consideration of the error estimates or the accurate approximations of the stress tensor. For this reason, the spatial discretisation techniques are still the subject of research, especially in an adaptive manner [39]. Typical examples are: the finite difference method [43], the boundary finite element method [50, 31], the least square approach [29, 223, 206] and the wavelet based methods [166].

In addition to time and space discretisations, one also requires the discretisation of the random fields describing the elastoplastic differential equations. The random field discretisation [82, 235] can be performed in several ways depending on its representation. The most often used are series expansion methods reviewed in [153]. For example, the interpolation method interpolates the random field via the finite element shape functions in nodal positions [134], while the approximation of the field in the mid-point of the element is studied in [121]. Another possibility is to spatially average the random field over some sub-domain as in [235]. However, the most often used are the spectral representations described in [78, 107, 145], which are considered later in this work. The detailed discussion about their numerical computation

can be found in [108, 227, 190, 153], as well as in [7].

4.2 Time discretisation

The time discretisation of elastoplastic evolutionary equations presented in Chapter 3 is done with the help of the generalised family of mid-point methods. The mid-point methods are described by the parameter ϑ taking the values in the bounded interval $[1/2, 1]$ due to the stability properties of the algorithm. However, these are not the only possible time discretisation methods, but the most often used in practice. Instead, one may use any other kind of implicit Runge-Kutta methods, e.g. [35, 64].

4.2.1 Abstract problem

Let the time interval $[0, T]$ be divided into L_t equal time increments such that $t_n = n\Delta t, n = 1, \dots L_t$, where $\Delta t := T/L_t$ is the time step-size. Furthermore let the time approximation of some quantity q in time t_n be denoted as q_n, its backward difference as $\Delta q_n := q_n - q_{n-1}$, and the backward divided difference as $\delta q_n := \Delta q_n / L_t$. Using this notation the evolutionary variational inequality in Eq. (3.44) can be approximated by the following algorithm as a special case of Moreau's sweeping process [162, 92]:

Problem 4.2.1. ***Problem ABS-Prim-Time:*** *find* $\breve{w} := \{w_n\}_{n=0}^{L_t} \in \mathscr{Z}_h$ *with* $w_0 = 0$ *such that for all* $0 \leq n \leq L_t$ *and all* $z \in \mathscr{Z}$ *holds:*

$$\begin{aligned} a(w_{n-1+\vartheta}, z - \delta w_n) \quad &+ \quad j(z) - j(\delta w_n) \\ &\geq \quad \ell_{n-1+\vartheta}(z - \delta w_n), \quad \mathbb{P} - \textit{a.s.} \end{aligned} \tag{4.1}$$

By replacing $\delta w_n \approx \Delta w_n$ *previous equation transforms to*

$$\begin{aligned} \vartheta a(\Delta w_n, z - \Delta w_n) \quad &+ \quad j(z) - j(\Delta w_n) \\ &\geq \quad \ell_{n-1+\vartheta}(z - \Delta w_n) - a(w_{n-1}, z - \Delta w_n) \end{aligned} \tag{4.2}$$

required to hold $\mathbb{P}$*-a.s. for all* $z \in \mathscr{Z}$*. Furthermore, the solution* w_n *is unique and*

admits the stability condition:

$$\max_{0\leq n\leq L_t} \|w_n^1 - w_n^2\|_{\mathscr{Z}} \leq c\|\ell^1 - \ell^2\|_{L_\infty(\mathcal{T};\mathscr{Z}^*)}. \tag{4.3}$$

Uniqueness and existence of the solution in Problem 4.2.1 follow from the proof presented in Section 3.5.4 and [92]. Note that in Problem 4.2.1 the term $w_{n-1+\vartheta}$ is used as a shortcut for the term $\vartheta w_n + (1-\vartheta)w_{n-1}$, $\ell_{n-1+\vartheta}$ for $\ell(t_{n-1+\vartheta})$ and $t_{n-1+\vartheta}$ for $(n-1+\vartheta)\Delta t = \vartheta t_n + (1-\vartheta)t_{n-1}$.

Setting $\vartheta = 1$ for the implicit Euler discretisation and $y_n := \ell(t_n) - a(w_{n-1}, \cdot)$, one may see that Problem 4.2.1 can be easily transformed to a time-discrete version of Theorem 3.5.3:

Theorem 4.2.2. ***Problem ABS-Mix-time****: find solution $\Delta w_n \in \mathscr{K}^\infty \subset \mathscr{Z}$ such that exists $w_n^* \in \mathscr{K}$ in all t_n satisfying*

$$\forall z \in \mathscr{Z}_h : \; a(\Delta w_n, z) + \langle\langle w_n^*, z\rangle\rangle = \langle\langle y_n, z\rangle\rangle \quad \mathbb{P}- \text{ a.s.} \tag{4.4}$$

and

$$\forall z^* \in \mathscr{K} : \; \langle\langle \Delta w_n, z^* - w_n^*\rangle\rangle \leq 0 \quad \mathbb{P}- \text{ a.s.} \tag{4.5}$$

The approximate solutions $\{w_n\}$, $\{w_n^*\}$ converge as $\Delta t \to 0$ to the solutions $w(t)$ and $w^*(t)$ of the problem ABS-M in Theorem 3.5.3.

Proof. Everything except the convergence of w_n^* is already shown. This follows along analogous arguments as proof of the uniqueness in Problem 4.2.1 (see [92]). □

For computational purposes the minimisation Problem 2.3.4 has much greater importance than the abstract formulation given in Problem 3.5.3. Due to this the following problem is further studied:

Theorem 4.2.3. ***Problem ABS-D:*** *for all t_n find w_n^* by minimisation:*

$$w_n^* = \operatorname*{arg\,min}_{z^*\in\mathscr{K}} \frac{1}{2} a^*(y_n - z^*, y_n - z^*), \tag{4.6}$$

where $y_n = \ell(t_n) - a(w_{n-1}, \cdot)$ *and* w_n *is the closest point in* $\mathscr{K}$ *to* y_n *in the* a^**-metric. Computing* $\Delta w_n \in \mathscr{Z}$ *by*

$$\forall z \in \mathscr{Z} : \; a(\Delta w_n, z) = \langle\!\langle y_n - w_n^*, z \rangle\!\rangle \quad \mathbb{P} - a.s. \tag{4.7}$$

one has that $\Delta w_n \in \mathscr{K}^\infty$ *and*

$$\forall z^* \in \mathscr{K} : \; \langle \Delta w_n, z^* - w_n^* \rangle \leq 0 \quad \mathbb{P} - a.s. \tag{4.8}$$

Proof. One can make similar assumptions to Proposition 2.3.3 and Eq. (2.37)-Eq. (2.41) from which then follows the proof of theorem. □

However, the time discretisation introduces a certain numerical error into the model. Under the standard regularity conditions and fixed ω the error is of the following type:

$$\max_n \|u_n - w_n\|_a \leq c\Delta t \tag{4.9}$$

for $\vartheta \neq 1/2$ and

$$\max_n \|u_n - w_n\|_a \leq c\Delta t^2 \tag{4.10}$$

for $\vartheta = 1/2$, where $\|\cdot\|_a$ is a norm with respect to the bilinear form a [92]. Here, w_n represents the solution of Problem 4.2.1 and u_n the solution of the original Problem 3.5.1 in time t_n.

4.2.2 General hardening plasticity

Theorem 4.2.3 is the abstract formulation of the elastoplastic behaviour. However, let us rewrite it for the case of the general hardening plasticity. For this one may use the backward Euler time discretisation and the same identification of $\mathscr{Z}$, $\mathscr{Z}^*$ and variables as in Section 3.5.4. Then, following Theorem 4.2.3 one may define the bilinear form

$$\begin{aligned} a^g(\boldsymbol{w}, \boldsymbol{z}) &= a^p(\boldsymbol{\varepsilon}_p(\boldsymbol{u}), \boldsymbol{\varepsilon}_p(\boldsymbol{v})) + a^h(\boldsymbol{\eta}, \boldsymbol{\varrho}) \\ &= \langle\!\langle \boldsymbol{\varepsilon}(\boldsymbol{u}) - \boldsymbol{\varepsilon}_p(\boldsymbol{u}), A(\boldsymbol{\varepsilon}(\boldsymbol{v}) - \boldsymbol{\varepsilon}_p(\boldsymbol{v})) \rangle\!\rangle + \langle\!\langle \boldsymbol{\eta}, H\boldsymbol{\varrho} \rangle\!\rangle \end{aligned} \tag{4.11}$$

and its dual

$$a^{g*}(\boldsymbol{\Sigma}_1, \boldsymbol{\Sigma}_2) = a^{p*}(\boldsymbol{\sigma}_2, \boldsymbol{\sigma}_2) + \langle\!\langle \boldsymbol{\chi}_1, \boldsymbol{H}^{-1} : \boldsymbol{\chi}_2 \rangle\!\rangle, \tag{4.12}$$

where $a^{p*}(\boldsymbol{\sigma}, \boldsymbol{\tau}) = \boldsymbol{\sigma} : \boldsymbol{A}^{-1} : \boldsymbol{\tau}$. The inverse tensors $\boldsymbol{A}^{-1}$ and $\boldsymbol{H}^{-1}$ are part of the definition of the constitutive laws and are positive-definite, symmetric and bounded (see Section 3.5.2). Following this, one may introduce the analogue of the Theorem 4.2.3 as:

Corollary 4.2.4. ***General hardening.*** *Set* $\boldsymbol{S}_n = \boldsymbol{A} : \boldsymbol{E}_{pn}$, $\boldsymbol{y}_n = \boldsymbol{S}_n - a^g(\boldsymbol{E}_{p,n-1}, \cdot))$ *and compute* $\Delta \boldsymbol{E}_{pn} \in \mathscr{K}^\infty$, $\boldsymbol{E}_{pn} = \boldsymbol{E}_{p,n-1} + \Delta \boldsymbol{E}_{pn}$ *and* $\boldsymbol{\Sigma}_n \in \mathscr{K}$ *as the unique solution of*

$$\forall \boldsymbol{M} : a^g(\Delta \boldsymbol{E}_{pn}, \boldsymbol{M}) + \langle\!\langle \boldsymbol{\Sigma}_n, \boldsymbol{M} \rangle\!\rangle = \langle\!\langle \boldsymbol{y}_n, \boldsymbol{M} \rangle\!\rangle, \quad \mathbb{P} - a.s. \tag{4.13}$$

$$\forall \boldsymbol{T} \in \mathscr{K} : \langle\!\langle \Delta \boldsymbol{E}_{pn}, \boldsymbol{T} - \boldsymbol{\Sigma}_n \rangle\!\rangle \leq 0, \quad \mathbb{P} - a.s.. \tag{4.14}$$

Proof. Existence, uniqueness, and stability of the solution follow from Problem 4.2.1. □

In order to pose the corresponding minimisation problem one may recall the derivation given in Section 2.2.3 and propose the closest point projection algorithm:

Corollary 4.2.5. *Set* $\boldsymbol{\Sigma}^{trial} = \boldsymbol{y}_n = \boldsymbol{S}_n - a^g(\boldsymbol{E}_{p,n-1}, \cdot)$. *Compute the unique minimizer of:*

$$\boldsymbol{\Sigma}_n = \underset{\boldsymbol{\Sigma} \in \mathscr{K}}{\arg\min} \frac{1}{2} a^{g*}(\boldsymbol{\Sigma}^{trial} - \boldsymbol{\Sigma}, \boldsymbol{\Sigma}^{trial} - \boldsymbol{\Sigma}) \tag{4.15}$$

and $\Delta \boldsymbol{E}_{pn}$ *as the unique solution of*

$$\forall \boldsymbol{M} : \; a^g(\Delta \boldsymbol{E}_{pn}, \boldsymbol{M}) = \langle \boldsymbol{y}_n - \boldsymbol{\Sigma}_n, \boldsymbol{M} \rangle. \tag{4.16}$$

Then, $\Delta \boldsymbol{E}_{pn}$ *and* $\boldsymbol{\Sigma}_n$ *solve the problem in Corollary 4.2.4 and* $\Delta \boldsymbol{E}_{pn} \in \mathscr{K}^\infty$ *satisfies*

$$\forall \boldsymbol{T} \in \mathscr{K} : \quad \langle\!\langle \Delta \boldsymbol{E}_{pn}, \boldsymbol{T} - \boldsymbol{\Sigma} \rangle\!\rangle \leq 0. \tag{4.17}$$

Proof. Existence and uniqueness of the solution follow from Corollary 4.2.4. □

Furthermore, the general hardening plasticity can be specialized to the linear hardening and perfect plasticity case by assuming appropriate constitutive relations as

described in Chapter 3. For more information on these formulations the interested reader is addressed to [195].

Let us remark that Theorem 4.2.3 and Corollary 4.2.5 can lead to a completely dual formulation [92]. However, the computations are usually performed according to the mixed formulation in Corollary 4.2.4 on a global level, whereas upon discretisation at each Gauss-point the local computation is usually done according to the dual formulation.

4.2.3 Closest point projection

This section considers the problem of the minimisation of the functional representing the evolutionary path of the plastic strain for the case of general hardening (see Corollary 4.2.5). More special cases such as perfect plasticity and linear hardening can be easily derived by taking into account appropriate restrictions (see [191]).

The minimisation as given in Corollary 4.2.5 belongs to the class of the optimization problems with inequality constraints [137, 163] of the following form:

$$\begin{aligned} &\text{minimise} && \Phi_n(\omega) := \frac{1}{2}\langle\!\langle \boldsymbol{\Sigma}_n^{trial} - \boldsymbol{\Sigma}_n, A^{-1}(\boldsymbol{\Sigma}_n^{trial} - \boldsymbol{\Sigma}_n)\rangle\!\rangle, \\ &\text{subject to} && \boldsymbol{\Sigma}_n \in \mathscr{R}: \quad \phi_n(\boldsymbol{\Sigma}_n) \leq 0, \end{aligned} \tag{4.18}$$

where Φ_n is the convex functional in time n and $\phi_n(\boldsymbol{\sigma})$ is the convex mapping from $\mathscr{R}$ to $\mathscr{K}$ called the yield function. In deterministic theory [215, 137, 55] the optimization problem in Eq. (4.18) is generally solved by the so-called *closest point projection* or *radial return map* algorithm[1]. The algorithm consists of two steps: *reversible* (non-dissipative) and *irreversible* (dissipative), often called *elastic predictor* and *plastic corrector*. The non-dissipative step defines the trial state, while actual projection happens in the corrector step if certain conditions are fulfilled. More precisely, if the stress lies outside of the elastic domain. In such a case the dissipative step searches for the closest distance in the energy norm of a trial state to a convex set of elastic domain, and then projects the stress back to the yield surface.

Let us assume that the quantities: the total strain $\boldsymbol{E}_{n-1} = (\boldsymbol{\varepsilon}_{n-1}, \mathbf{0})$, the plastic strain $\boldsymbol{E}_{p,n-1} = (\boldsymbol{\varepsilon}_{p,n-1}, \boldsymbol{\eta}_{n-1})$, and the displacement increment $\Delta\boldsymbol{u}_{n-1}$ are given at time t_{n-1} (beginning of the step). Then, one may compute the stress $\boldsymbol{\Sigma}_{n-1}$ via

[1] the second name is more appropriate for perfect plastic behaviour

constitutive relationships (see Section 3.5.2). The goal is to update those fields in time t_n assuming that the time Δt_n and load $\Delta \boldsymbol{f}_n$ increments are known.

Non-dissipative step

In the proceeding numerical computation one first deals with the geometrical nonlinearities and solves the equilibrium equation Eq. (4.16) for the increment of the displacements. This is the global phase of the algorithm in which the configuration is updated. In second phase the configuration is fixed and the quantities are updated such that the stress admissibility condition is satisfied. Therefore, one first solves the equilibrium Eq. (4.16) rewritten in a form of residual:

$$\mathbf{Q}(\Delta \boldsymbol{E}_{p,n}, \boldsymbol{M}) := a^g(\Delta \boldsymbol{E}_{p,n}, \boldsymbol{M}) - \langle\!\langle \boldsymbol{y}_n - \boldsymbol{\Sigma}_n, \boldsymbol{M} \rangle\!\rangle = \mathbf{0} \tag{4.19}$$

which further represents a nonlinear equation with respect to the displacement increment. Namely, the plastic strain $\boldsymbol{E}_{p,n}(\omega)$ and the consistency parameter $\lambda_n(\omega)$ [2] are nonlinear functions in terms of $\boldsymbol{E}_n(\omega)$. As $\boldsymbol{E}_{p,n}(\omega)$ is regarded as a given fixed history variable, the only remaining independent variable is $\boldsymbol{u}_n$, i.e. $\Delta \boldsymbol{u}_n(\omega)$ as $\boldsymbol{u}_{n-1}(\omega)$ represents the convergent solution from the previous step. This means that the operator $\mathbf{Q}(\omega)$ is nonlinear in $\Delta \boldsymbol{u}_n(\omega)$, and hence the system in Eq. (4.19) has to be solved iteratively [21, 250]. However, this is only possible after spatial and stochastic discretisation have been performed.

By solving the equilibrium Eq. (4.19) one obtains the increment of the displacement $\Delta \boldsymbol{u}_n$, and hence the increment of the elastic deformation $\Delta \boldsymbol{E}_{en} := (\nabla_S(\Delta \boldsymbol{u}_n(\omega)), \mathbf{0})$ by freezing the plastic flow $\Delta \boldsymbol{E}_{pn} = \mathbf{0}$. As the increment of the total strain is purely elastic, one may employ Hooke's constitutive law to compute the increment of the forecasted (trial) Cauchy stress, i.e. $\boldsymbol{\Sigma}_n^{trial}(x_g, \omega) = \boldsymbol{\Sigma}_{n-1} + \boldsymbol{C}(x_g, \omega) : \Delta \boldsymbol{E}_{en}(x_g, \omega)$, where the generalised constitutive modulus $\boldsymbol{C}(x_g, \omega) = \text{diag}[\boldsymbol{A}(x_g, \omega), \boldsymbol{H}(x_g, \omega)]$ consists of $\boldsymbol{A}(x_g, \omega) = K(x_g, \omega)\mathbf{1} \otimes \mathbf{1} + 2G(x_g, \omega)\left(\boldsymbol{I} - \frac{1}{3}\mathbf{1} \otimes \mathbf{1}\right)$ and $\boldsymbol{H}(x_g, \omega) = \text{diag}\,[\boldsymbol{H}_{kin}(x_g, \omega), H_{iso}(x_g, \omega)]$. Note that the double-dot tensor multiplication : is applied on the random quantities, and thus admits slightly different properties than the usual double-dot multiplication (see Chapter 5 and Chapter 6).

Once the trial stress has been computed, one may check its admissibility with respect to the yield condition $\phi(\boldsymbol{\Sigma}_n^{trial}(x_g, \omega)) \leq 0$ at time t_n. If $\phi(\boldsymbol{\Sigma}_n^{trial}(x_g, \omega)) \leq 0$ $\mathbb{P}$-almost surely the step is non-dissipative and $(\cdot)_n = (\cdot)_{n-1}$. Otherwise, the stress is

[2] this parameter will be introduced later

non-admissible and one has to perform the dissipative step as further described. Note that in the following discussion the term x_g is not used for simplicity of notation.

Dissipative step

The solution of the minimisation problem is determined by a Kuhn-Tucker theorem [137]:

Theorem 4.2.6. *Let $\Phi_n(\omega)$ be a Gâteaux differentiable functional on $\mathscr{R}$ and ϕ_n a Gâteaux differentiable mapping from $\mathscr{R}$ into $\mathscr{K}$. Assume that Gâteaux differentials are linear in their increments. Suppose $\boldsymbol{\Sigma}_n$ minimises Φ_n subject to $\phi_n(\boldsymbol{\Sigma}) \leq 0$ a.s. and that $\boldsymbol{\Sigma}_n$ is a regular point of the inequality $\phi_n(\boldsymbol{\Sigma}_n) \leq 0$ a.s. Then there is a Lagrange multiplier $\lambda \in \mathscr{R}^*, \lambda \geq 0$ such that the Lagrangian:*

$$\mathcal{L}_n(\omega) = \Phi_n(\omega) + \langle\langle \phi_n, \lambda \rangle\rangle \tag{4.20}$$

is stationary at $\boldsymbol{\Sigma}_n$ almost surely; furthermore $\langle\langle \phi_n, \lambda \rangle\rangle = 0$ a.s.

Proof. The proof of previous theorem can be found in [137]. □

According to this, the solution of Eq. (4.18) is obtained from the optimality condition:

$$\partial_{\boldsymbol{\Sigma}} \mathcal{L}_n = 0 \text{ and } \partial_\lambda \mathcal{L}_n = 0 \quad \text{a.s.} \tag{4.21}$$

in which the second equation may be rewritten in a Kuhn-Tucker form:

$$\lambda \geq 0 \text{ and } \lambda \phi_n(\boldsymbol{\Sigma}_n) = 0 \text{ a.s.} \tag{4.22}$$

If Φ_n and ϕ_n are convex— the positive cone $\mathscr{K}$ is closed and has non-empty interior—and if the regularity condition is satisfied the saddle point condition is sufficient requirement for the existence and optimality of the solution [137]:

Theorem 4.2.7. *Assume that there exists $\lambda_s \in \mathscr{R}^*, \lambda_s \geq 0$, and an $\boldsymbol{\Sigma}_s \in \mathscr{R}$ such that the Lagrangian $\mathcal{L}(\boldsymbol{\Sigma}, \lambda) = \Phi(\boldsymbol{\Sigma}) + \langle\langle \phi(\boldsymbol{\Sigma}), \lambda \rangle\rangle$ has saddle point at $(\boldsymbol{\Sigma}_s, \lambda_s)$ i.e.*

$$\mathcal{L}(\boldsymbol{\Sigma}_s, \lambda) \leq \mathcal{L}(\boldsymbol{\Sigma}_s, \lambda_s) \leq \mathcal{L}(\boldsymbol{\Sigma}, \lambda_s), \tag{4.23}$$

for all $\boldsymbol{\Sigma} \in \mathscr{R}, \lambda \geq 0$*. Then* $\boldsymbol{\Sigma}_s$ *solves Eq. (4.18).*

Proof. The saddle-point condition with respect to λ [137] gives:

$$\langle\!\langle \phi(\boldsymbol{\Sigma}_s), \lambda \rangle\!\rangle \leq \langle\!\langle \phi(\boldsymbol{\Sigma}_s), \lambda_s \rangle\!\rangle \tag{4.24}$$

for all $\lambda \geq 0$ a.s. Thus, one may take some $\lambda_g \geq 0$ a.s. and pose

$$\langle\!\langle \phi(\boldsymbol{\Sigma}_s), \lambda_g + \lambda_s \rangle\!\rangle \leq \langle\!\langle \phi(\boldsymbol{\Sigma}_s), \lambda_s \rangle\!\rangle, \tag{4.25}$$

from which it follows:

$$\langle\!\langle \phi(\boldsymbol{\Sigma}_s), \lambda_g \rangle\!\rangle \leq 0. \tag{4.26}$$

Due to the convexity assumption one has that $\phi(\boldsymbol{\Sigma}_s) \leq 0$ with respect to which the saddle-point condition implies

$$\langle\!\langle \phi(\boldsymbol{\Sigma}_s), \lambda_s \rangle\!\rangle = 0, \quad \text{a.s.} \tag{4.27}$$

Assuming that $\boldsymbol{\Sigma}_g \in \mathscr{R}$ and $\phi(\boldsymbol{\Sigma}_g) \leq 0$, the saddle-point condition transforms to:

$$\Phi(\boldsymbol{\Sigma}_s) = \Phi(\boldsymbol{\Sigma}_s) + \langle\!\langle \phi(\boldsymbol{\Sigma}_s), \lambda_s \rangle\!\rangle \leq \Phi(\boldsymbol{\Sigma}_g) + \langle\!\langle \phi(\boldsymbol{\Sigma}_g), \lambda_s \rangle\!\rangle \leq \Phi(\boldsymbol{\Sigma}_g). \tag{4.28}$$

This further implies that λ_s minimises $\Phi(\boldsymbol{\Sigma})$ subject to $\phi(\boldsymbol{\Sigma}) \leq 0$. □

Following the previous theorem one may rewrite the standard optimality conditions Eq. (4.21) at one material point x_g to:

$$\begin{aligned} \boldsymbol{r}_s(\omega) := \boldsymbol{A}^{-1}(\boldsymbol{\Sigma}_n^{trial} - \boldsymbol{\Sigma}_n) + \lambda_n \partial_{\boldsymbol{\Sigma}} \phi(\boldsymbol{\Sigma}_n) &= 0 \quad \text{a.s.} \\ \phi_s(\omega) := \phi(\boldsymbol{\Sigma}_n) &= 0 \quad \text{a.s.} \end{aligned} \tag{4.29}$$

After simple mathematical derivation with the help of the constitutive relations given in Section 3.5.2, the first relation in Eq. (4.29) transforms to

$$\Delta \boldsymbol{E}_{p,n}(\omega) - \lambda_n \partial_{\boldsymbol{\Sigma}} \phi(\boldsymbol{\Sigma}_n(\omega)) = 0 \text{ a.s.} \tag{4.30}$$

This is exactly the expression used in the classical formulation of elastoplasticity theory.

Note that the system in Eq. (4.29) is in general nonlinear. Its linearisation can be performed with the help of the local Newton method, for example. However, due to the dependence on the ω-parameter this can be done only after the stochastic discretisation.

4.2.4 Large deformation analysis

The time integration of the J_2 flow theory in finite strains is basically the same as in the infinitesimal plasticity case. The problem reduces to a general form of the convex optimization problem in a similar pattern as given in Eq. (4.18). Its unique minimizer can be computed with the help of the closest point projection algorithms similar to those already presented in Section 4.2.3. The only difference lies in the stress and strain measures, i.e. the hyperelastic relationships, here only briefly summarized. For the complete mathematical derivation the reader is referred to [215, 101, 21].

The J_2 flow theory in finite deformations represents the natural extension of the small deformation plasticity. Namely, the theory is based on the assumption of the convex stored hyperelastic energy function for which the corresponding numerical algorithm becomes the classical radial return map. Moreover, in absence of the plastic flow the algorithm reduces to the finite elasticity case [215, 212, 217, 213].

Let us assume that the energy $\psi(\boldsymbol{C}, \boldsymbol{C}^p, \boldsymbol{\eta})$ is convex and admits the volumetric/deviatoric decomposition such that [215]:

$$\begin{aligned} \psi &= \psi_v(J^e) + \psi_d(\bar{\boldsymbol{b}}^e) + \psi_h(\boldsymbol{\eta}) \\ &= K(\frac{1}{2}((J^e)^2 - 1) - \ln J^e) + \frac{1}{2}G(\mathrm{tr}(\bar{\boldsymbol{b}}^e) - 3) + \psi_h(\boldsymbol{\eta}) \end{aligned} \tag{4.31}$$

holds, where $\bar{\boldsymbol{b}}^e = (J^e)^{-2/3}\boldsymbol{b}^e$, $J^e = \det(\boldsymbol{C}^e)$, and $\psi_h(\boldsymbol{\eta})$ is the stored internal plastic energy. To this complies the constitutive law (see Eq. (2.77)) given in terms of the Kirchhoff stress tensor:

$$\boldsymbol{\tau} = 2\boldsymbol{F}^e \frac{\partial \psi}{\partial \boldsymbol{C}^e}(\boldsymbol{F}^e)^T = J^e p\mathbf{1} + \boldsymbol{s}, \tag{4.32}$$

where $p = \frac{K}{2}((J^e)^2 - 1)/J^e$ denotes the pressure and $\boldsymbol{s}$ the deviatoric stress. For a complete formulation, one requires the defintion of a set of admissible stresses via the invariant form of the yield criterion, e.g.

$$\phi(\boldsymbol{\tau}, \boldsymbol{\chi}) = \|\mathrm{dev}\,(\boldsymbol{\tau} - \boldsymbol{\varsigma})\|_{J_2} - \sqrt{\frac{2}{3}}[\sigma_y + \zeta] \tag{4.33}$$

in a von-Mises sense. To these is added the associative plastic flow rule in material description:

$$\dot{\bar{\boldsymbol{C}}}^{p-1} = -\frac{2}{3}\lambda \mathrm{tr}(\boldsymbol{b}^e)\boldsymbol{F}^{-1}\boldsymbol{n}\boldsymbol{F}^{-T}, \quad \dot{\boldsymbol{\eta}} = -\lambda \partial_{\boldsymbol{\chi}}\phi(\boldsymbol{\tau}, \boldsymbol{\chi}), \tag{4.34}$$

or in spatial one [215, 101]:

$$L_v \boldsymbol{b}^e = -\frac{2}{3}\lambda \mathrm{tr}(\boldsymbol{b}^e)\boldsymbol{n} \tag{4.35}$$

$$L_v \bar{\boldsymbol{q}} = \lambda \frac{2}{3} H_{kin} \mathrm{tr}(\boldsymbol{b}^e)\boldsymbol{n}, \tag{4.36}$$

$$\dot{q} = -\frac{2}{3} H_{iso} \lambda. \tag{4.37}$$

Here, $\boldsymbol{n} = \boldsymbol{s}/\|\boldsymbol{s}\|$ is the normal, $\boldsymbol{s} = \mathrm{dev}(\boldsymbol{\tau} - \boldsymbol{\varsigma})$ is deviatoric stress, L_v denotes the Lie derivative of a function [101], $\bar{\boldsymbol{q}}$ is the back-stress, and q is the isotropic hardening. Note that the flow relations are similar to those in infinitesimal plasticity, and thus can be numerically integrated in a similar manner as before.

Following the previous notation, let at time t_{n-1} be given $\{\varphi_{n-1}, \bar{\boldsymbol{b}}^e_{n-1}, \boldsymbol{\eta}_n\}$, $\boldsymbol{F}_{n-1}$ (see Eq. (3.22)) and corresponding stresses $\boldsymbol{\tau}_{n-1}$ and $\boldsymbol{\chi}_{n-1}$. Then, one may compute the increment of the displacement by solving the equilibrium equation:

$$a^m(\boldsymbol{w}, \boldsymbol{S}_n) = -\ell^m_n(\boldsymbol{w}) \tag{4.38}$$

which can be rewritten in a form of a nonlinear residual dependent only on $\Delta \boldsymbol{u}_n$:

$$\boldsymbol{Q}(\Delta \boldsymbol{u}_n) := a^m(\boldsymbol{w}, \boldsymbol{S}_n) - \ell^m_n(\boldsymbol{w}) = 0. \tag{4.39}$$

By solving previous equation for the increment of displacement $\Delta \boldsymbol{u}_n$, one may update the deformation path according to:

$$\varphi_n = \varphi_{n-1} + \Delta \boldsymbol{u}_n(\varphi_n(\boldsymbol{X})), \tag{4.40}$$

and hence the deformation gradient from $\boldsymbol{F}_{n-1}$ to $\boldsymbol{F}_n = [1 + \nabla_s \Delta \boldsymbol{u}_n]\boldsymbol{F}_{n-1}$. Once these quantities are known, given loading increment $\Delta \boldsymbol{f}_n$ one may update the kinematic and dynamic quantities from time t_{n-1} to time t_n.

Basically, the update algorithm has the same predictor-corrector form as the one given in Section 4.2.3. The predictor assumes the step to be purely elastic, and then updates the state according to the yield criterion—the corrector step. Notice that in comparison to algorithm for small deformation case the only difference lies in the choice of stress and strain measures. The algorithm starts by freezing the plastic flow so that the intermediate configuration does not change and:

$$[\boldsymbol{C}^{p-1}_n]^{trial} := \boldsymbol{C}^{p-1}_{n-1}, \quad \boldsymbol{\eta}^{trial}_n = \boldsymbol{\eta}_{n-1} \tag{4.41}$$

hold. Introducing the operators of push-forward and pull-back, i.e. the relative deformation gradients

$$\boldsymbol{f}_n = \boldsymbol{F}_n \boldsymbol{F}_{n-1}^{-1}$$

and

$$\bar{\boldsymbol{f}}_n = (J_n/J_{n-1})^{-1/3} \boldsymbol{f}_n$$

Eq. (4.41) transforms to:

$$\bar{\boldsymbol{b}}_{e,n}^{trial} = \bar{\boldsymbol{f}}_n \bar{\boldsymbol{b}}_{n-1}^{e} \bar{\boldsymbol{f}}_n^T \tag{4.42}$$

given in spatial description. In this formulation the trial stress can be computed according to:

$$\begin{aligned} \boldsymbol{\tau}_n^{trial} &= p_n J_n \mathbf{1} + \boldsymbol{s}_n^{trial}, \text{where} \\ \boldsymbol{s}_n^{trial} &= G \text{dev}\, \bar{\boldsymbol{b}}_{e,n}^{trial}, \text{and} \\ p_n &= \psi_v'(J_n). \end{aligned} \tag{4.43}$$

Once the trial stress is evaluated, one may check the yield condition and, if necessary, proceed with the dissipative step. The dissipative step solves the Lagrangian in Eq. (4.20) for the multiplier $\Delta\lambda$ and updates the strain-like variables in material description according to:

$$\bar{\boldsymbol{C}}_n^{p-1} - \bar{\boldsymbol{C}}_{n-1}^{p-1} = -\frac{2}{3}\Delta\lambda [\boldsymbol{C}_n^{p-1} : \boldsymbol{C}_n] \boldsymbol{F}_n^{-1} \boldsymbol{n}_n \boldsymbol{F}_n^{-T}, \tag{4.44}$$

$$\boldsymbol{\eta}_n - \boldsymbol{\eta}_{n-1} = -\Delta\lambda \partial_{\boldsymbol{\chi}} \phi_n, \tag{4.45}$$

or in spatial description as given in [215, 101].

Note that the formulation considered here is only semi-discretised, because the finite element discretisation of Eq. (4.38) is not performed yet and ω-dependence is widely present.

4.3 Spatial discretisation

The solution of the elastoplastic problem belongs to the tensor product space $\mathscr{V} = \mathcal{V} \otimes (S)$, where $\mathcal{V}$ denotes the appropriate deterministic space (see Section 2.3.1) and (S) the stochastic space (see Section 3.5.1). The tensor representation allows the discretisation of each of the components separately. This section briefly reviews the finite element (FEM) discretisation [22] of the sub-space $\mathcal{V}$, i.e. the semi-discretisation

$\mathscr{V}_h := \mathcal{V}_h \otimes (S)$ of the tensor space $\mathscr{V}$ representing strains, stresses, or displacements. In the next chapter the discretisation of (S) will be considered, and hence the full discretisation of the problem.

The FEM discretisation of displacement $\mathcal{U}$ and plastic strain $\mathcal{E}$ (or stress $\mathcal{R}$) spaces is done with the help of piecewise affine and piecewise constant functions, respectively. Besides FEM, one may use any other available discretisation technique such as the finite difference approach [126], the least square method [223, 206], etc.

Let the domain $\mathcal{G}$ be discretised via partition $\mathcal{T}_h$ in a finite element way such that:

$$\mathcal{G} \approx \mathcal{G}_h = \bigcup_{\mathcal{G}_e \in \mathcal{T}_h} \mathcal{G}_e \tag{4.46}$$

represents the union of the closed subsets $\mathcal{G}_e$ with a non-empty interior and Lipschitz closed boundary. Then, by taking the finite number L_n of shape functions $N_j(x)$ as ansatz [49], i.e.

$$\mathcal{U}_h := \text{span}\,\{N_j(x)\}_{j=1}^{L_n} \in \mathcal{U}, \tag{4.47}$$

one may discretise the displacement as

$$u(x,\omega) \approx u_h(x,\omega) = \sum_{i=1}^{L_n} u_i(\omega) N_i(x) := \boldsymbol{N}(x)\boldsymbol{u}(\omega), \tag{4.48}$$

where $\boldsymbol{N} = [N_1(x), N_2(x), \dots N_{L_n}(x)]$ denotes the vector of shape functions and $\boldsymbol{u}(\omega) = [u_1(\omega), \dots u_{L_n}(\omega)]^T$ represents corresponding coefficients, i.e. random variables in (S). As functions in $\mathscr{U}_h := \mathcal{U}_h \otimes (S)$ are continuous, $\boldsymbol{\varepsilon}$ is well defined as an operator:

$$\boldsymbol{\varepsilon}(u_h)(y) = \nabla_S(\boldsymbol{N}(y)\boldsymbol{u}(\omega)) \tag{4.49}$$

in each FEM integration point y. This further determines the discretised space $\mathscr{E}_h$.

By taking the piecewise constant functions the space of general plastic deformation $\mathcal{E}_p$ and stress $\mathcal{R}$ are approximated as:

$$\boldsymbol{\varepsilon}_{ph} = \sum_{i=1}^{L_e} \boldsymbol{\varepsilon}_{pi} V_i, \quad \boldsymbol{\sigma}_h = \sum_{i=1}^{L_e} \boldsymbol{\sigma}_i V_i, \tag{4.50}$$

where V_i denotes the i-th indicator function over element j. The function takes the value 1 when $i = j$, otherwise $V_i = 0$. Similar is valid for internal variables $\boldsymbol{\eta}_h$, internal forces $\boldsymbol{\chi}_h$ and corresponding spaces $\mathcal{Q}_h$ and $\mathcal{C}_h$. In other words, the stress

space $\mathcal{R}$ is discretised by:

$$\mathcal{R}_h = \{\boldsymbol{\sigma}_h \in \mathcal{R} : \boldsymbol{\sigma}_{\mathcal{G}_e} = \text{const} \ \ \forall \mathcal{G}_e \in \mathcal{T}_h\} \subset \mathcal{R}. \tag{4.51}$$

Following previous definitions one may define the discretised spaces $\mathcal{P}_h := \mathcal{E}_{ph} \times \mathcal{Q}_h$ and $\mathcal{Y}_h := \mathcal{R}_h \times \mathcal{C}_h$, of the general plastic strain $\boldsymbol{E}_{ph}$ and the general stress $\boldsymbol{\Sigma}_h$, resepectively (see Section 3.5.1). In addition, let $\mathscr{Z} := \mathcal{Z} \otimes (S)$ be a tensor product space between Hilbert space $\mathcal{Z}$ and the space (S) of variables with finite variance (see Section 3.5.1). Its convex, closed, non-empty subset (cone) is denoted by $\mathscr{K}^\infty$. Let us assume that the same assumptions are valid as they are given in Theorem 3.5.2; then one may perform the finite element approximations $\mathscr{Z}_h = \mathcal{Z}_h \otimes (S)$ of the space $\mathscr{Z}$ (see Section 4.3) and $\mathscr{K}_h^\infty = \mathscr{Z}_h \cap \mathscr{K}^\infty$ of the convex subset $\mathscr{K}^\infty \subset \mathscr{Z}$.

With the help of previously made assumptions one may formulate the discretised version of Problem 4.2.1 on a subspace $\mathscr{Z}_h$ as:

Problem 4.3.1. ***Abstract problem ABS-Prim-FEM.*** *Find $w_{hn} : \mathcal{T} \to \mathscr{Z}_h$ with $w_{h0} = 0$ and $\Delta w_{hn} \in \mathscr{K}_h^\infty$ such that for all $t \in \mathcal{T}$ and all $z_h \in \mathscr{Z}_h$ the second order inequality:*

$$\begin{aligned} a(\Delta w_{h,n}, z_h - \Delta w_{h,n}) \quad &+ \quad j(z_h) - j(\Delta w_{h,n}) \\ &\geq \quad \ell_{h,n}(z_h - \Delta w_{h,n}) - a(w_{h,n-1}, z_h - \Delta w_{h,n}) \end{aligned} \tag{4.52}$$

is valid $\mathbb{P}$-almost surely.

The previous analysis is given with respect to the finite element approximation of considered spaces. However, the major difficulty in solving the primal Problem 4.3.1 is the non-differential term of the dissipation functional j, which may be solved by regularisation (j is approximated as a sum of differentiable terms), or by discretisation of the inequality via a set of integration points to a set of uncoupled inequities, i.e.

$$j(z) \approx j_h(z_h). \tag{4.53}$$

This further modifies the inequality in Eq. (4.52) by including j_h [92].

Existence and uniqueness of the solution are given under the same conditions as before, see Theorem 3.5.2. If one assumes that the functional $j(\cdot)$ is proper on $\mathscr{Z}_h$, then the discrete counterpart of the abstract problem has unique solution [81, 92]

which for fixed ω satisfies the Céa's type of inequality [49]

$$\max_n \|u_n - w_{h,n}\|_a \leq c\Delta t + c\left[n\sum_{j=1}^{L}\inf_{\boldsymbol{z}_j\in\mathscr{K}}\|\dot{w}_{j-1+\theta} - z_j\|_{\mathscr{Z}}\right]^{1/2}. \tag{4.54}$$

Here, Δt is the time step and $\|\cdot\|_a$ is norm with respect to the bilinear form a, $w_{h,n}$ denotes the discretised solution of Problem 4.3.1 and u_n the solution of original Problem 3.5.1 in time t_n. However, the error estimate as given in Eq. (4.54) is not complete as the problem is only semi-discretised and the general error estimate requires the discretisation of the stochastic space (S) as shown in Section 4.4.

Similarly to primal, one may discretise Problem 4.2.2 given in a mixed form by taking the subspaces $\mathscr{Z}_h \subset \mathscr{Z}$ and $\mathscr{Z}_h^* \subset \mathscr{Z}^*$, where $\mathscr{K}_h = \mathscr{Z}_h \cap \mathscr{K}$. The discretisation can be formulated in a variational:

Problem 4.3.2. ***Problem ABS-Mix-FEM:*** *find $\Delta w_{h,n} \in \mathscr{K}_h^\infty \subset \mathscr{Z}_h$ and $\exists w_{h,n}^* \in \mathscr{K}_h$ such that for all t_n*

$$\forall z \in \mathscr{Z}_h:\ a(\Delta w_{h,n}, z) + \langle\langle w_{h,n}^*, z\rangle\rangle = \langle\langle y_{h,n}, z\rangle\rangle \quad \mathbb{P}-\ a.s. \tag{4.55}$$

and

$$\forall z_h^* \in \mathscr{K}_h:\ \langle\langle \Delta w_{h,n}, z^* - w_{h,n}^*\rangle\rangle \leq 0 \quad \mathbb{P}-\ a.s. \tag{4.56}$$

or in a minimisation form as:

Corollary 4.3.3. ***Problem ABS-D:*** *find $w_{h,n}^*$ such that for all t_n holds:*

$$w_{h,n}^* = \arg\min_{z_h^*\in\mathscr{K}_h} \frac{1}{2}a^*(y_{h,n} - z_h^*, y_{h,n} - z_h^*) \tag{4.57}$$

with $y_{h,n} = \ell(t_n) - a(w_{h,n-1}, \cdot)$ and $w_{h,n}$ being the closest point in $\mathscr{K}_h$ to $y_{h,n}$ in the a^*-metric. Computing $\Delta w_{h,n} \in \mathscr{Z}_h$ by

$$\forall z \in \mathscr{Z}_h:\ a(\Delta w_{h,n}, z) = \langle\langle y_{h,n} - w_{h,n}^*, z_h\rangle\rangle \quad \mathbb{P}-a.s. \tag{4.58}$$

one has that $\Delta w_{h,n} \in \mathscr{K}_h^\infty$ satisfies

$$\forall z_h^* \in \mathscr{K}_h:\ \langle \Delta w_{h,n}, z^* - w_{h,n}^*\rangle \leq 0 \quad \mathbb{P}-a.s. \tag{4.59}$$

Specializing Corollary 4.3.3 to the general hardening case one obtains:

Corollary 4.3.4. *Set* $\boldsymbol{\Sigma}^{trial} = \boldsymbol{y}_{hn} = \boldsymbol{S}_{hn} - a^g(\boldsymbol{E}_{p,h,n-1}, \cdot)$. *Compute the unique minimizer of:*

$$\boldsymbol{\Sigma}_{hn} = \underset{\boldsymbol{\Sigma}_h \in \mathscr{K}_h}{\arg\min} \frac{1}{2} a^{g*}(\boldsymbol{\Sigma}_h^{trial} - \boldsymbol{\Sigma}_h, \boldsymbol{\Sigma}_h^{trial} - \boldsymbol{\Sigma}_h) =: \underset{\boldsymbol{\Sigma}_h \in \mathscr{K}_h}{\arg\min} \Phi_h \tag{4.60}$$

and $\Delta \boldsymbol{E}_{p,hn}$ *as unique solution of*

$$\mathbf{Q}(\Delta \boldsymbol{E}_{p,hn}, \boldsymbol{M}) := a^g(\Delta \boldsymbol{E}_{p,hn}, \boldsymbol{M}) - \langle\langle \boldsymbol{y}_{hn} - \boldsymbol{\Sigma}_{hn}, \boldsymbol{M} \rangle\rangle = \mathbf{0}. \tag{4.61}$$

Then, $\Delta \boldsymbol{E}_{p,hn}$ *and* $\boldsymbol{\Sigma}_{hn}$ *solve the problem in Problem 4.3.2 and* $\Delta \boldsymbol{E}_{p,hn} \in \mathscr{K}_h^\infty$ *satisfies*

$$\forall \boldsymbol{T} \in \mathscr{K}_h : \quad \langle\langle \Delta \boldsymbol{E}_{p,hn}, \boldsymbol{T} - \boldsymbol{\Sigma}_h \rangle\rangle \leq 0. \tag{4.62}$$

Proof. Existence and uniqueness of the solution can be found in [195]. □

Note that the discretised problems presented in this section are, however, only semi-dicretised since all formulations are ω-dependent. Due to this they can be only numerically treated when the discretisation of the stochastic space (S) is performed.

4.4 Stochastic discretisation

The discretisation of the stochastic space (S) of RVs with finite variance is done such that only a finite number of random variables is used in the problem description. The best way to satisfy this condition is to approximate random fields by series expansion methods, where the number of random variables tend to be small, but large enough to satisfy the accuracy and computational requirements for a certain type of problem. In a case of the weak sense stationary and homogeneous processes (random fields) the expansion is of the Fourier type [199], a special case of Karhunen-Loève expansion[3] [78, 76, 145, 107]. The expansion approximates random fields or stochastic processes as a sum of products of functions defined on the time or spatial domain and functions of random variables. Due to this property the KLE is often called the *tensor product* representation.

[3] valid in a general case of non-stationary and non-homogeneous processes or random fields

4.4.1 The Karhunen-Loève expansion

For its favourable properties a Karhunen-Loève expansion (KLE) (also known as a proper orthogonal decomposition) is chosen for the discretisation of the random field. The principal idea behind the KLE is that given an ensemble of data one can find a basis of a given dimension that spans the data optimally in L_2 sense. It was invented independently by Karhunen (1947), Loève (1948), and Kac and Siegert (1947) and widely described in many books and papers [33, 47, 75, 77, 78, 99, 197, 201, 227, 152]. Therefore, here only short description. For more information the reader is referred to [78, 108, 107].

Let be given the random field $\kappa(x,\omega)$ and its admissible covariance function $\mathrm{cov}_\kappa(x_1,x_2) := \mathbb{E}(\tilde{\kappa}_{x_1} \otimes \tilde{\kappa}_{x_2})$, where $\tilde{\kappa}_{x_1}$ and $\tilde{\kappa}_{x_2}$ represent the fluctuations of the random field (see Eq. (3.9) and the text following). The admissibility condition [26, 203] requires that the covariance is symmetric and positive-definite, i.e. $\sum_{k=1}^{n}\sum_{j=1}^{n} c_k \mathrm{cov}_\kappa(x_k,x_j)c_j \geq 0$ for all $x_k, x_j \in \mathbb{R}$ and $c_k, c_j \in \mathbb{C}$. With this in mind the random field $\kappa(x,\omega)$ admits the expansion:

$$\kappa(x,\omega) = \sum_{k=0}^{\infty} \sqrt{\lambda_k}\xi_k(\omega)\kappa_k(x) \tag{4.63}$$

in which the split into the spatial $\kappa_k(x)$ and stochastic $\xi_k(\omega)$ part has occurred. Taking $\lambda_0 = 1$, $\xi_0(\omega) = 1$ and $\kappa_0(x) = \bar{\kappa}(x)$ the previous formulation transforms to:

$$\kappa(x,\omega) = \bar{\kappa}(x) + \sum_{k=1}^{\infty} \sqrt{\lambda_k}\xi_k(\omega)\kappa_k(x), \tag{4.64}$$

where $\bar{\kappa}(x)$ is the mean value of the random field, $\xi_k(\omega)$ are the uncorrelated zero mean and unit variance random variables ($\mathbb{E}(\xi_m\xi_n) = \delta_{mn}$), and (λ_i, κ_i) is the pair of eigenvalues and eigenfunctions of the covariance kernel cov_κ, respectively.

For computational purposes the series in Eq. (4.64) is truncated to a finite number of terms M:

$$\hat{\kappa}(x,\omega) = \bar{\kappa}(x) + \sum_{k=1}^{M} \sqrt{\lambda_k}\xi_k(\omega)\kappa_k(x), \tag{4.65}$$

such that the approximation is the best one achieved in $L_2(\mathcal{G}\times\Omega) \cong L_2(\mathcal{G}) \otimes L_2(\Omega)$ norm. In other words, the truncated expansion in Eq. (4.65) converges to $\kappa(x,\omega)$ in

variance uniformly, i.e. in $L_\infty(\mathcal{G}) \otimes L_2(\Omega)$:

$$\sup \mathbb{E}((\kappa(x) - \hat{\kappa}(x))^2) = \sup_{x \in \mathcal{G}} \sum_{k=M+1}^{\infty} \lambda_k \kappa_k(x)^2 \to 0, \text{ as } M \to \infty. \tag{4.66}$$

The KLE computation is performed by solving the spatially FEM-discretised eigenvalue problem [107]:

$$\boldsymbol{W}\boldsymbol{\kappa}_k = \lambda_k \boldsymbol{M}\boldsymbol{\kappa}_k \tag{4.67}$$

with $\boldsymbol{\kappa}_k$ being the eigenfunctions, λ_k the corresponding eigenvalues, $\boldsymbol{W} = \boldsymbol{MCM}$ a symmetric positive semi-definite matrix, and $\boldsymbol{M}$ a Gram matrix with elements $\boldsymbol{M}_{ij} = \int_{\mathcal{G}} N_i(x_1) N_j(x_2) dx_1 dx_2$. Regarding properties of matrix $\boldsymbol{W}$, the solution of Eq. (4.67) can be obtained with the help of a Krylov subspace method [200, 95] with a sparse matrix approximation. This method comes very naturally as it does not require an assembled form of the dense matrices $\boldsymbol{W}$ and $\boldsymbol{M}$. On the other side, Krylov subspace methods are very suitable for the implementation as one may use open libraries such as LAPACK or ARPACK [125]. However, for the problem of huge dimensions one may use sparse hierarchical matrix techniques [110] as more suitable tools. They represent an efficient and fast discretisation of the random fields due to their log-linear computational cost of the matrix-vector products and log-linear storage requirement.

Finally, having the solution of the eigenproblem one may rewrite the Karhunen-Loéve expansion in Eq. (4.65) in a discretised form as:

$$\kappa(x, \omega) \approx \bar{\kappa}(x) + \sum_{k=1}^{M} \sqrt{\lambda_k} \boldsymbol{\kappa}_k \boldsymbol{N}(x) \xi_k(\omega), \tag{4.68}$$

where the first term $\bar{\kappa}(x)$ represents the mean value of the given random field in the finite element basis.

Note that the Karhunen-Loève expansion in Eq. (4.65) is straightforward in a case of the Gaussian random field (see Section 3.3.2) due to mutual independence of the uncorrelated random variables $\xi_k(\omega)$, which represent a linear combination of Gaussian random variables. On the other side, in a case of the non-Gaussian random field (i.e. the nonlinear transformation of Gaussian, see Section 3.3.2) the random variables $\xi_k(\omega)$ are uncorrelated and generally unknown. However, they can be computed via the following integration [78]:

$$\xi_k(\omega) = \frac{1}{\sqrt{\lambda_k}} \int_{\mathcal{G}} (\kappa(x, \omega) - \bar{\kappa}(x)) \kappa_k(x) \mathrm{d}x. \tag{4.69}$$

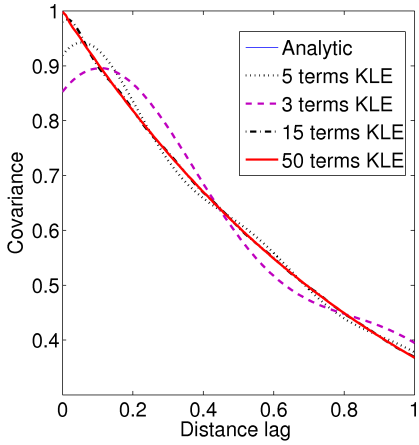

a) $l_c = 1$

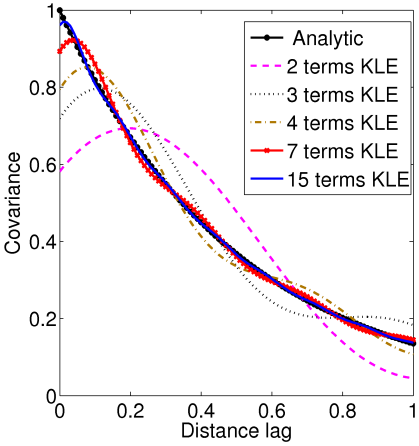

b) $l_c = 0.5$

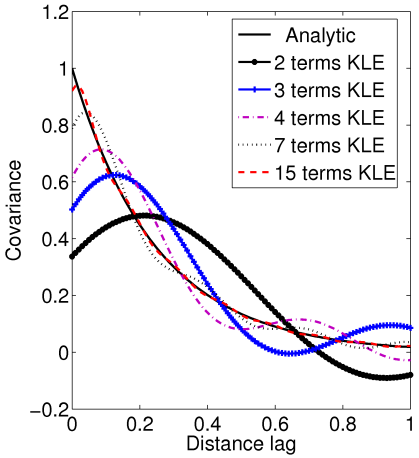

c) $l_c = 0.25$

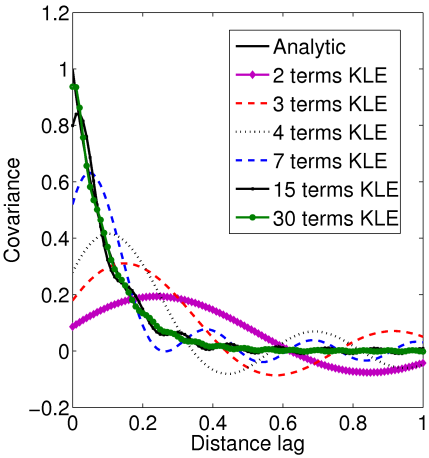

d) $l_c = 0.1$

Figure 4.1: Comparison of numerical and analytical covariance functions $exp(-r/l_c)$ for different values of correlation lengts l_c and different number M of KLE terms.

Example 4.4.1. *Let us take the zero mean first order process described by the non-smooth correlation function $exp(-r/l_c)$ with the correlation length l_c taking the values in interval $[1 \div 0.1]$ as shown in Fig. 4.1. The goal is to compare the analytical with the numerically computed covariance. As one may notice in Fig. 4.1, the simulation result agrees better with the analytical result if the ratio of the length of the process (in this case the unit measure) and the correlation length is smaller. A smaller ratio implies a highly correlated process. Such a process requires a smaller number of random variables to be taken into the expansion. Also, note that the non-smooth correlation function at zero lag leads to less good approximation result for that point.*

Example 4.4.2. *The fluctuation of the random field depends on the chosen value of the correlation lengths. This dependence is shown in Fig. 4.2, where the correlation length l_c of the centered Gaussian random field is varied. The Gaussian field is numerically simulated by 500 KLE terms (full approximation) and two types of covariance functions: the smooth and non-smooth correlation functions of the exponential type. The results show that the smooth correaltion function produces the smooth realisations of the Gaussian random field (see Fig. 4.2, a)-c)), as expected. The function is smooth for $r = 0$ in contrast to the square root function which is not differentiable in $r = 0$ (hence corresponding realisations are not smooth). One may also note that with decrease of the correlation lengths the fluctuation of the random field realisations increases. Going from a)-c) and from d)-f) in Fig. 4.2 one may notice that fluctuations become larger due to the smaller value of the correlation length.*

Example 4.4.3. *Let us take the random field as used in the numerical results in Chapter 8, and investigate the values of the KLE modes of the base Gaussian random field with respect to the mean value and the standard deviation, see Fig. 4.3. In addition, let us distinguish two cases: the non-smooth and the smooth corresponding correlation function. As shown in Fig. 4.3, the first KLE mode is the smoothest and takes the largest value. Going from the left to the right, the number of terms in the KLE grows, and thus the amplitude of the 20-est mode decreases, while fluctuations grow. Similar is valid for the realisations of the random field. Namely, the small number of the KLE terms does not accurately represent the considered random field, see Fig. 4.4. The approximation delivers different variance than the random field possess. On the other side, taking the large number of terms is not always necessary as sometimes the eigenvalues may decay quite fast enough.*

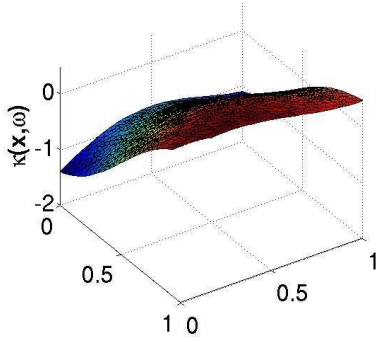

a) cov $= \exp(-r^2/1^2)$

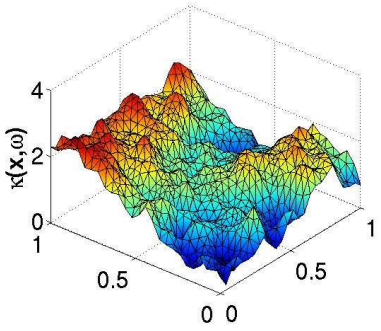

d) cov $= \exp(-r/1)$

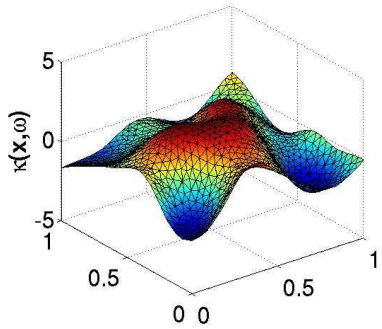

b) cov $= \exp(-r^2/0.25^2)$

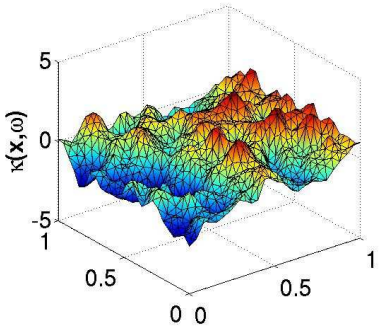

e) cov $= \exp(-r/0.25)$

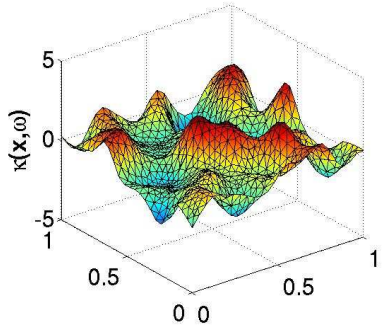

c) cov $= \exp(-r^2/0.125^2)$

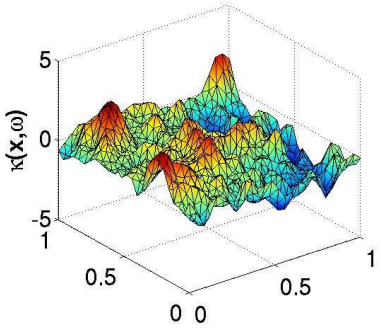

f) cov $= \exp(-r/0.125)$

Figure 4.2: Comparison of realisations for Gaussian cov $= exp(-r^2/l_c^2)$ and square-root cov $= exp(-r/l_c)$ covariance functions for different values of correlation lengths l_c

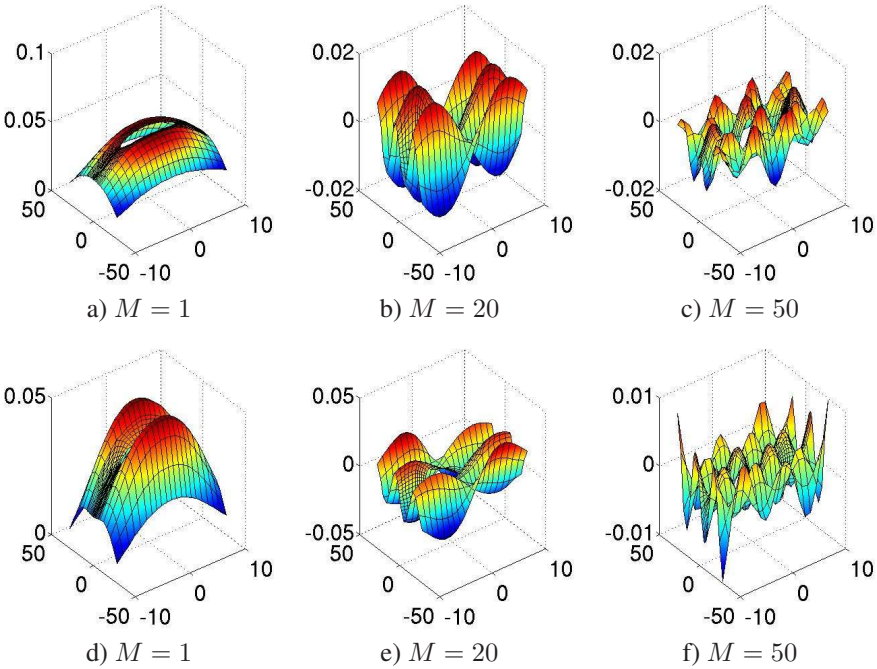

a) $M = 1$ b) $M = 20$ c) $M = 50$

d) $M = 1$ e) $M = 20$ f) $M = 50$

Figure 4.3: The shape of M-th KLE mode for smooth (a-c) and non-smooth (d-f) correlation function

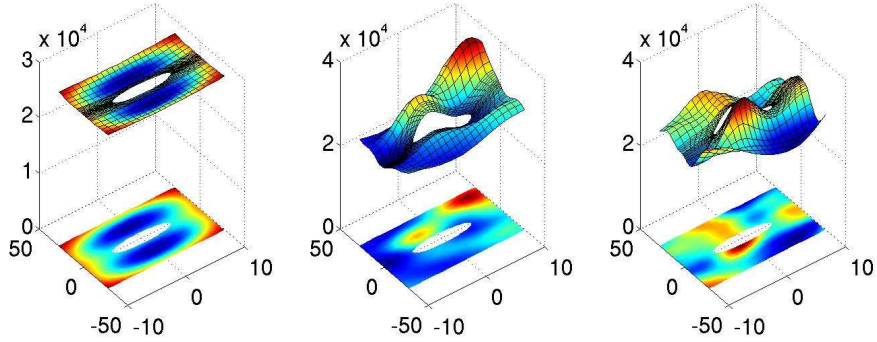

a) M=1 b) M=20 c) M=50

Figure 4.4: Realisations of lognormal random field with the number of terms M kept in KLE

4.4.2 The KLE/PC expansion

Since the probability density functions of uncorrelated random variables in the Karhunen-Loève expansion are unknown they are evaluated by integration, see Eq. (4.69). However, one may use the functional approximation instead. The basic idea is to represent the RV as a function of some other—more simple—type of random variables as explained in detail in Chapter 6. In other words, one may approximate the RV $\xi_k(\omega)$ by a convergent polynomial chaos expansion (PCE):

$$\xi_k(\omega) = \sum_{\alpha \in \mathcal{J}} \xi_k^{(\alpha)} H_\alpha(\boldsymbol{\theta}(\omega)), \tag{4.70}$$

where $\xi_k^{(\alpha)}$ are the coefficients and $H_\alpha(\boldsymbol{\theta}(\omega))$ the Hermite polynomials with uncorrelated and independent Gaussian RVs $\boldsymbol{\theta}(\omega)$ as arguments. Once the approximation of $\xi_k(\omega)$ is computed, one may substitute it back to Eq. (4.63) such that:

$$\kappa(x,\omega) = \sum_{k=0}^{M} \sum_{\alpha \in \mathcal{J}} \sqrt{\lambda_k} \xi_k^{(\alpha)} H_\alpha(\boldsymbol{\theta}(\omega)) \kappa_k(x) \tag{4.71}$$

holds. The series in Eq. (4.71)—further called the KLE/PC expansion—is a common way used to approximate the non-Gaussian random fields [152, 151, 107], see the numerical procedures described in Chapter 5.

For computational purposes one may neglect the terms in the PCE representing the small value of the product such as $\lambda_k(\xi_k^{(\alpha)})^2\alpha!$ as they contribute to the small change in variance. Following this, the truncated form of Eq. (4.71) becomes:

$$\kappa(x,\omega) \approx \sum_{k=0}^{M} \sum_{\alpha \in \mathcal{J}_{M,p}} \sqrt{\lambda_k} \xi_k^{(\alpha)} H_\alpha(\boldsymbol{\theta}(\omega)) \kappa_k(x), \tag{4.72}$$

where $\mathcal{J}_{M,p}$ is the multi-index set determined by M RVs and the polynomial order p. The error of this type of truncation is given in terms of the following estimator:

$$\|\kappa(x,\omega) - \kappa(x,\omega)_M\|_{L_2(\Omega)\otimes L_2(\mathcal{G})} = \sum_{k>M}^{\infty} \sum_{\alpha \in \mathcal{J} \setminus \mathcal{J}_M} \lambda_k (\xi_k^{(\alpha)})^2 \alpha!. \tag{4.73}$$

Note that in the most general case both expansions converge in $L_2(\Omega)$. Due to this the positive definiteness of the random field realistions for some fixed $\tilde{\omega}$ may be violated since polynomials are not bounded. That may cause numerical instability as

Hadamard's requirements of the well-posedness are not satisfied. To avoid this kind of problem the expansion in Eq. (4.73) for fixed $\tilde{\omega}$ has to be done by a point-wise transformation of the Gaussian random field [152, 149, 151].

4.5 Summary

The material models introduced in Chapter 3 are time, ω- and spatially dependent, and thus one has to discretise them. Time integration is studied with respect to the general mid-point integration schemes from which the simplest variant is chosen, i.e. the implicit Euler method. In regard to this, the time-discrete version of the abstract problem is analysed in Section 4.2.1, while the general hardening plasticity in Section 4.2.2. For computational purposes the time-discretization algorithm is considered in Section 4.2.3 in a form of the closest point projection for small deformation plasticity. This is further extended in Section 4.2.4 to the J_2 finite deformation plasticity. Besides the time discretisation, this chapter offers the brief overview of the spatial discretisation of the problem in Section 4.3. However, the time and spatial discretisations are not enough to numerically threat the problem. The reason for this are the input material characteristics described as uncertain. Therefore, their stochastic discretisation is studied in Section 4.4 in a usual computational manner with the help of the combination of the Karhunen-Loève and polynomial chaos expansions. This kind of discretisation allows the description of quantities in a form of polynomial chaos expansion in each local FEM integration point. Such representation is then suitable for the implementation of intrusive Galerkin methods as described further in Chapter 5.

Chapter 5

Numerical approaches

There are always two choices. Two paths to take. One is easy. And its only reward is that it's easy.

Unknown

The semi-discretised equations in Chapter 4 are ω-dependent, and thus cannot be numerically treated before the stochastic discretisation has been preformed. Therefore, one of the primary goals of this chapter is to discretise the stochastic space (S) and to propose several solution strategies. According to the type of the RV representation they use, the strategies are classified into: the direct integration (RV represented by sample), the direct Galerkin method (RV given by polynomial approximation), and the pseudo-Galerkin and collocation methods (RV represented by combination of polynomial approximation and samples). These methods are extended form of the corresponding counterparts used for solving linear stochastic problems, e.g. [107, 145, 244, 140, 157, 191].

A novelty in this work is the construction of the purely algebraic method for solving the stochastic variational inequality of the second kind. The method relies on the appropriate weak approximation of the convex elastic domain, which further allows the stochastic closest point projection (SCPP) method to be a purely deterministic procedure. The idea is to project the problem in a Galerkin manner—similar to the one in the classical finite element approach—onto the polynomial basis of the discretised space. The projection is done in a purely algebraic manner without any sampling. This is achieved with the help of the polynomial chaos algebra (see Chapter 6) and the construction of the probability estimates for the RV inequalities. Such introduced method is fully straightforward and intrusive, i.e. it is efficient and requires reformu-

lation of the finite element code.

Another way of solving the stochastic variational inequality in terms of projection is based on the approximation of the convex domain on the finite set of the integration points such that the density of the approximated stochastic space in (S) is fulfilled. In this manner one avoids possibly not enough sharp estimates used to functionally approximate the random inequalities in an intrusive approach. The points used in the approximation are part of the random or deterministic integration rules. As the integration is not full, this kind of approach leads to much cheaper estimates than the direct integration approach, also studied in this work.

The chapter is organized as follows: Section 5.1 briefly reviews the existing solution strategies with the special emphasis on the direct integration techniques, which are described in Section 5.3. The largest part of this chapter (Section 5.4.1 and Section 5.4.2) deals with the stochastic Galerkin and its pseudo-version. The study focuses on the small deformation plasticity case as the finite J_2 theory represents its natural extension. Finally, some of the adaptive techniques are advocated in Section 5.6.

5.1 Related work

In the last decade the numerical methods for solving stochastic partial differential equations (SPDE) corresponding to the description of linear elastic behaviour have developed quickly and on many fronts. To reduce the cost of direct integration techniques, Ghanem and Spanos [78] and later Matthies and Keese [145, 107] proposed to use the Karhunen-Loève expansion in combination with white noise analysis for the random field discretisation. This has inspired many scientists to follow the same path and construct various numerical approaches for solving the large stochastic parametrised linear systems of equations in intrusive (algebraic), or non-intrusive (numerical) way. For example, the intrusive approach has been studied in [140, 145, 73, 76, 17, 247], the setting of the non-intrusive Galerkin approach in [61, 109, 244, 16, 144, 5] and the interpolation in [114, 139].

In contrast to linear SPDEs, the nonlinear ones are still considered as a relatively young research area, especially in the field of elastoplasticity. Initially, Acharjee and Zabaras [4, 3] proposed the intrusive numerical algorithm for solving the large deformation stochastic hyperelastic problem. They studied the influence of the uncertain initial configuration, as well as the uncertain material parameters on the stress

response with the help of the polynomial chaos expansion. However, the method does not provide the intrusive solution strategy for the stochastic inequalities arising in the definition of the elastoplastic behaviour. Namely, the approximation of the convex elastic domain is done with the help of perturbation-like techniques or collocation. A similar study was recently provided by Arnst and Ghanem [11] for the contact and elastoplastic problem in a small deformation regime. Besides these, other kinds of approaches have been also investigated as already discussed in Chapter 1. For example, Anders and Hori [9] treated uncertainties with the help of the perturbation technique in combination with the Karhunen-Loève expansion of the global stiffness matrix. The method is characterised by an inability to accurately approximate the random fields described by moderate and large variances. A complex, but mathematically speaking "deterministic" version of the numerical method for solving one-dimensional stochastic elastoplastic problems can be found in [209, 105]. The approach is of the moment equations type and it is based on the Eulerian-Lagrangian form of the Fokker-Planck equations.

5.2 Representation of a random variable

Selection and assessment of the numerical methods for the uncertainty propagation through the elastoplastic model strongly depends on the random variable representation, which may take the form of:

- sampling
- distribution
- moments
- or the functional approximation [180].

The benefits and detriments of those techniques vary greatly depending on the particular application and available computational resources. For those who prefer a simple black-box FEM fashioned technique the best variant is the sampling method, i.e. the direct integration (see Section 5.3). Its purpose is to evaluate the RV at some —randomly or deterministically—chosen points $\omega_s \in \Omega$, and then to statistically process the data. However, in terms of practical (industrial) utilisation the method is not very comfortable to use due to its computational inefficiency.

Representing the random variables in terms of distribution or moments, one reformulates the elastoplastic model into a not necessarily simpler but equivalent conservation (e.g. Fokker-Planck) equations for probability (see [105, 209, 208]) or more complicated evolutionary integro-differential equations. These methods require huge computational effort and until now have been only used yet for some small test examples, not real applications.

In recent years an alternative representation has gained increasing momentum. The idea is to describe an RV κ as a function of other — known — RVs of some simple type. A typical example is given by polynomials of normalised Gaussian RVs. This is Wiener's polynomial chaos expansion (PCE) [238, 102], also called more recently "white noise analysis" [98, 96]. In some way this representation allows the idea of using the algebra of RVs as primitive objects, and hence aquires a distinctly functional analytic flavour [207]. In this chapter such approach is fully derived with the help of the knowledge presented in Chapter 6.

5.3 Direct integration methods

The goal of stochastic analysis is to calculate the response statistics, i.e. some functionals of the solution such as the mean value and variance of the displacement, the probability exceedence of the von Mises stress, etc. For a fixed $x \in \mathcal{G}$ these statistics may be written as the mathematical expectation of a functional of the solution $\Psi(x, \omega, u(x, \omega))$ [151] :

$$\Psi_u(x) := \mathbb{E}(\Psi(x, \omega, u(x, \omega))) = \int_\Omega \Psi(x, \omega, u(x, \omega))\mathbb{P}(d\omega) \tag{5.1}$$

in infinite dimensional space. However, in practical computation the integral in Eq. (5.1) is finite dimensional since the random fields $u(x, \omega)$ and $\Psi(x, \omega, u(x, \omega))$ are only approximated by a finite set $\boldsymbol{\theta} = \{\theta_i\}_{i=1}^M$ of independent RVs (see Section 4.4 and Chapter 6). The RV independence allows the integral in Eq. (5.1) to be transformed to

$$\Psi_u(x) = \int_{\Omega_1} \dots \int_{\Omega_M} \Psi(x, \omega, \boldsymbol{N}(x)\boldsymbol{u}(\omega))\, \mathrm{d}\mathbb{P}_1(\omega_1) \cdots \mathrm{d}\mathbb{P}_M(\omega_M) \tag{5.2}$$

according to Fubini's lemma, where the triple $(\Omega^{(M)}, \mathcal{B}^{(M)}, \mathbb{P}_M)$— with $\Omega^{(M)} = \Omega_1 \times \ldots \times \Omega_M \subset \mathbb{R}^M$ and $\Omega_j = \text{range}\ (\theta_j) = \theta_j(\Omega)$—defines the probability space. Here, $\mathbb{P}_i(\omega_i)$ denotes the probability distribution of θ_i and $\omega = (\omega_1, \dots, \omega_M) \in$

$\Omega^{(M)}$.

The integral in Eq. (5.2) in general cannot be evaluated exactly, but rather numerically via the finite sum:

$$\Psi_u(x) \approx \Psi_N = \sum_{j=1}^{N} w_j \Psi(x, \boldsymbol{\theta}^{(j)}, \boldsymbol{u}(\boldsymbol{\theta}^{(j)})) \tag{5.3}$$

in a set of points $\{\boldsymbol{\theta}^{(j)}\}_{j=1}^{N}$ described by weight functions $\{w_j\}_{j=1}^{N}$. This corresponds to the integration by the quadrature rule (the set of the deterministic points and corresponding weights) [94, 233, 70, 34, 114] or to the Monte Carlo method and its quasi-variants—the points are selected according to the underlying probability measure [204, 100, 72, 36, 32, 133, 132].

Algorithm 1: Schematic representation of direct integration algorithm

Direct Integration method

1: generate the sequence $\{\boldsymbol{\theta}_j|_{j=1,2,\ldots,N}\} \subset \Theta_M$
2: **for** $j = 1 \rightarrow N$ **do**
3: evaluate input RFs $\kappa = \{K, G, \sigma_y, \ldots\}$ at $\boldsymbol{\theta}^{(j)}$:
4: - base Gaussian field in KLE
5: $\gamma(x, \boldsymbol{\theta}^{(j)}) = \sum_{k=1}^{M} \sqrt{\lambda_k}\gamma_k(x)\theta^{(k)}$
6: - apply transformation
7: $\kappa(x, \boldsymbol{\theta}^{(j)}) = \kappa_0 + \kappa_1 \exp(\gamma(x, \boldsymbol{\theta}^{(j)}))$
8: run FEM code with property $\kappa(x, \boldsymbol{\theta}^{(j)})$ to obtain:
9: $\eta(x, \boldsymbol{\theta}^{(j)}) \in \{\boldsymbol{u}(x, \boldsymbol{\theta}^{(j)}), \boldsymbol{\sigma}(x, \boldsymbol{\theta}^{(j)}), \boldsymbol{\epsilon}(x, \boldsymbol{\theta}^{(j)}), \ldots\}$
10: **end for**
11: compute integral
12: $\Psi_N = \sum_{j=1}^{N} \Psi(x, \eta(\boldsymbol{\theta}^{(j)}))w_j$

The numerical integration as given in Eq. (5.3) has a very nice property. Namely, one may independently compute the integrand in each integration point by the finite element method procedure (or some other deterministic solver), see Algorithm 1, and then sum the corresponding results. As there is no interaction between the particular solutions, all terms in the sum may be computed in the same time with the help of parallelization techniques. This leads to an enormous reduction of the overall computation time. In addition, the method is stable and does not depend on the type

Table 5.1: Various integration rules and their convergence in terms of number of samples. MC is Monte Carlo, qMC quasi-Monte Carlo, FTPQ- full tensor product quadrature and SGSQ sparse grid Smolyak quadrature rule

Method	Sequence	Convergence
MC	random according to p.d.f.	$\mathcal{O}(N^{-1/2})$
qMC	low discrepancy sequence	$\mathcal{O}(\|\Psi_N\|_{BV}(\log N)^m N^{-1})$
FTPQ	deterministic	$\mathcal{O}(N^{-p/M})$
SGSQ	deterministic	$\mathcal{O}(N^{-r}(\log N)^{l^{(d-1)(r+1)}})$

of the problem being solved, i.e. whether the functional is of linear or nonlinear type. However, the integration is of the high-dimensional nature, and hence one requires a large amount of the integration points in order to achieve the desried convergence and accuracy of the solution. Due to this, the direct integration methods are often marked as impractical.

In the literature one may find various types of integration rules, which differ from each other by the way the integration points are chosen. The simplest and the most often used is the Monte Carlo (MC) method [205, 204, 36, 133] whose set of points $\{\boldsymbol{\theta}^{(j)}\}_{j=1}^{N}$ is built according to the probability distribution function (p.d.f.). Once the solution is evaluated in a deterministic fashion, one may extract the final statistics using Eq. (5.3) for which $w_j = 1/N, \forall j$. According to the central limit theorem and the law of large numbers the method converges towards Gaussian law $\varepsilon_N = \lim_{N\to\infty} \Psi_N - \Psi_u \approx \sigma_\Psi^2 N^{-1/2}\theta$, where θ is the standard Gaussian random variable with zero mean and unit variance, and $\sigma_\Psi = \|\Psi_N\|_{L_2}^2/N$ is a standard deviation of the functional Ψ [151]. In other words, the method converges under the weak regularity conditions[1] with probability one. In addition, the smoothness of the integrand is taken only through the variance, such that the small variance and low accuracy requirements characterise the most suitable conditions for this method. On the other side, the slow convergence rate is the biggest disadvantage of the method. Namely, the error reduces by one order of magnitude for the number of the evaluations increased by two orders, which makes the MC method fairly impractical.

The *variance reduction techniques* (e.g. antithetic variates, stratified sampling, importance sampling, control variates, etc.) try to improve the MC convergence rate

[1] Even when one does not know that the integrand is smooth and differentiable, the Monte Carlo method still performs very well

by manipulating the variance. The improvement is achieved by choosing the so-called low discrepancy (or quasi-random) instead of purely random sequence [36, 107, 133, 132] of numbers. By definition a low discrepancy sequence has a small measure of deviation (discrepancy) $D_N \leq c(\log N)^k N^{-1}$ of a given distribution from an ideal one, where c and k are the constants independent of N but possibly dependent on dimension M. Its asymptotic behaviour is described by the Koksma-Hlawka inequality [36], i.e. $\varepsilon \leq \sigma_\Psi^2 D_N$ where ε and σ_Ψ^2 represent the error and the total variation of the integrand, respectively. According to this, the variance reduction implies faster convergence rate than the standard MC method, i.e. the rate is $O(\|\Psi_N\|_{BV}(\log N)^M N^{-1})$, where $\|\Psi_N\|_{BV}$ denotes the bounded variation norm. However, in contrast to the MC sampling the convergence is problem dependent.

Besides random and pseudo-random sequences, one may use deterministic quadratures to integrate the functional in Eq. (5.3) [94, 233, 70, 34, 114]. As the number of the quadrature points strongly depends on the problem dimension, their (possibly ad-hoc) selection is often non-trivial especially in high-dimensional spaces. Namely, there are numerous ways to choose sampling points: full tensor quadrature, sparse grid Smolyak [114], cubature grid, etc. Each of them selects the points to achieve better convergence rates than MC or quasi-MC methods. However, both selection of points as well as convergence are strongly problem dependent.

The full tensor product quadrature grid—obtained as the simple product of the 1-D integration rules—numbers N^M points associated with the convergence rate $\mathcal{O}(N^{-p/M})$ [107]. The error exponentially decreases with the dimension M for the fixed polynomial order p, and results in $\mathcal{O}(N^{-1})$ (the best scenario) for $M = p$ (highly smoothed integrand). However, due to the exponential law (N^M) the number of points grows quickly with the dimension M, and thus the rule becomes impractical for large families of high dimensional problems. In order to reduce the number of points the Smolyak's algorithm combines the component rules into a single quadrature rule—sparse grid—such that the new abscissas are the set of the component abscissas; and the new weights are the component weights multiplied by the sparse grid coefficient [94, 233, 70, 34, 114, 109, 186, 219, 20]. The grids are often nested and hence reuse many of the points. Even though the number of points is the same in nested and non-nested case, the constants are much larger in the non-nested case for the same number of abscissas of univariate quadrature formulas. This means that the nested Smolyak approximation requires less function evaluations than the corresponding non-nested formula [172, 71]. Compared to previously introduced methods the sparse grid requires the fewest number of samples for the same accuracy. The method is associated with the logarithmic convergence law, i.e. $\mathcal{O}(N^{-r}(\log N)^{l^{(d-1)(r+1)}})$, where r represents the number of the bounded mixed par-

tial derivatives that the integrand can have.

Finally, the direct integration method, see Alogortihm 1, uses the KLE approximation of the random field for the evaluation of the current sample point. In such a case the random field realisation is not always smooth. This can break the regularity of the solution as assumed in the error estimates in Chapter 4. In addition, the random field in such a setting can violate the positive-definiteness property. This can be avoided by taking a large number of terms in the KLE [151].

5.4 Stochastic Galerkin method

The stochastic discretisation of the elastoplastic problem can be described by any finite dimensional subspace $(\mathcal{S})_{\mathcal{J}} \subset (\mathcal{S})$. Thus, the challenge is to find the most suitable $(\mathcal{S})_{\mathcal{J}}$ such that the high dimensional problem can be efficiently and accurately solved. According to literature the most promising way of doing this is a discretisation by stochastic finite elements, e.g. [78, 145, 151, 227, 107, 113]. Namely, by the initial proposal of Ghanem and Spanos [78] and later Matthies and Keese [145] the most suitable choice for the subspace $(\mathcal{S})_{\mathcal{J}} := L_2(\Omega, \Sigma(\theta), \mathbb{P})$ is the span of the multivariate orthogonal basis $H_\alpha(\boldsymbol{\theta}(\omega))$, i.e. $(\mathcal{S})_J :=$ span $\{H_\alpha(\boldsymbol{\theta}(\omega))\}_{\alpha\in\mathcal{J}} \subset (\mathcal{S})$, where $H_\alpha(\boldsymbol{\theta}(\omega))$ denotes the multivariate Hermite polynomial in the mutually independent Gaussian RVs $\boldsymbol{\theta}(\omega)$ (see Chapter 6), and $\mathcal{J}$ represents the set of multi-indices given in Eq. (6.11). As stated in [102, 98, 96], the Cameron-Martin theorem [37] guarantees that the algebra of Gaussian variables is dense in $L_2(\Omega)$. Still, the Gaussian variables and Hermite polynomials are not the only possible choice. Instead, one may use any other type of variables and polynomials declared in Askey scheme. For more information the reader is addressed to [248, 247, 246, 66, 243].

Once the spatial discretization has been done by the Galerkin projection, one strives to use the same procedure in the stochastic space as well [74, 150, 103, 17, 248, 140]. This can be achieved by using the Wiener's polynomial chaos expansion [74, 145, 152] for the solution ansatz:

$$\boldsymbol{u}(\boldsymbol{\theta}) = \sum_{\alpha\in\mathcal{J}} \boldsymbol{u}^{(\alpha)} H_\alpha(\boldsymbol{\theta}(\omega)), \tag{5.4}$$

$$\boldsymbol{\varepsilon}_p(\boldsymbol{\theta}) = \sum_{\alpha\in\mathcal{J}} \boldsymbol{\varepsilon}_p^{(\alpha)} H_\alpha(\boldsymbol{\theta}(\omega)), \tag{5.5}$$

$$\boldsymbol{\sigma}(\boldsymbol{\theta}) = \sum_{\alpha\in\mathcal{J}} \boldsymbol{\sigma}^{(\alpha)} H_\alpha(\boldsymbol{\theta}(\omega)), \tag{5.6}$$

where $\boldsymbol{u}^{(\alpha)} := [u_1^{(\alpha)}, \dots, u_{L_n}^{(\alpha)}]^T$, $\boldsymbol{\varepsilon}_p^{(\alpha)}$, and $\boldsymbol{\sigma}^{(\alpha)}$ denote the nodal vector of coefficients of polynomial chaos expansion gathered in a block-vector $\mathbf{u} = [..., \boldsymbol{u}^{(\alpha)}, ...]$, $\mathbf{e}_p$ and $\mathbf{s}$, respectively. Inserting Eqs. (5.4)–(5.6) back to the semi-discretised form in Eqs. (4.48)–(4.50), the full discretisation of the solution becomes

$$\hat{\boldsymbol{u}} := \sum_{j=0}^{L_n} \sum_{\alpha \in \mathcal{J}_Z} \boldsymbol{u}_j^{(\alpha)} \boldsymbol{N}_j(x) H_\alpha(\boldsymbol{\theta}(\omega)), \tag{5.7}$$

$$\hat{\boldsymbol{\varepsilon}}_p := \sum_{j=0}^{L_e} \sum_{\alpha \in \mathcal{J}_Z} \boldsymbol{\varepsilon}_j^{(\alpha)} \boldsymbol{V}_j(x) H_\alpha(\boldsymbol{\theta}(\omega)), \tag{5.8}$$

$$\hat{\boldsymbol{\sigma}} := \sum_{j=0}^{L_e} \sum_{\alpha \in \mathcal{J}_Z} \boldsymbol{\sigma}_j^{(\alpha)} \boldsymbol{V}_j(x) H_\alpha(\boldsymbol{\theta}(\omega)). \tag{5.9}$$

Here, the index set $\mathcal{J}_Z$ is taken as a finite subset of $\mathcal{J}$, the set of all finite non-negative integer sequences, i.e. multi-indices, see Eq. (6.11). Although the set $\mathcal{J}_Z$ is finite with cardinality $|\mathcal{J}_Z| = Z$ and $\mathcal{J}$ is countable, there is no natural order on it; and hence one does not impose one at this point. In addition, note that for simplicity of notation the same index set is used for all kinds of variables though one may assume that each of them is approximated by different polynomial orders.

Once the solution is discretised, the minimum of the convex cost functional in each time step n has to be found, whether one considers the small or large displacement elastoplasticity. To achieve this, one has first to resolve the nonlinear equilibrium equation for unknown displacement, see Eq. (4.61) for infinitesimal, or Eq. (4.38) for finite deformation case. In other words, one has to update the body configuration by solving the nonlinear residual equation:

$$\boldsymbol{Q}(\omega) \left(\sum_{\alpha \in \mathcal{J}_Z} \Delta \boldsymbol{u}_n^{(\alpha)} H_\alpha(\boldsymbol{\theta}(\omega)) \right) = \mathbf{0} \tag{5.10}$$

for the increment $\Delta \boldsymbol{u}_n$. The computation is performed by projecting the system in Eq. (5.10) in a Galerkin manner similar to the classical FEM

$$\forall \beta \in \mathcal{J}_Z : \quad \boldsymbol{Q}^{(\beta)} := \mathbb{E} \left(\boldsymbol{Q}(\omega) \left[\left(\sum_{\alpha \in \mathcal{J}_Z} \Delta \boldsymbol{u}_n^{(\alpha)} H_\alpha(\boldsymbol{\theta}) \right) \right] H_\beta(\boldsymbol{\theta}) \right) = \mathbf{0} \tag{5.11}$$

such that the error in the approximate solution is orthogonal to the space spanned

by $H_\beta(\boldsymbol{\theta})$. Due to the orthogonality of Hermite polynomials, Eq. (5.11) reduces to Z coupled problems $\boldsymbol{Q}^{(\beta)} = \mathbf{0}$, each of size of the "deterministic" problem. Furthermore, by gathering the left hand side of the equation in the block vector $\mathbf{Q} = (..., \boldsymbol{Q}^{(\beta)}, ...)^T$, Eq. (5.11) transforms to:

$$\mathbf{Q}(\Delta\mathbf{u}_n) = [\ldots, \mathbb{E}(H_\alpha(\cdot)\boldsymbol{Q}(\cdot)[\sum_\alpha \Delta\boldsymbol{u}_n^{(\beta)} H_\beta]), \ldots] = \mathbf{0}. \tag{5.12}$$

Let us assume that $\mathbf{Q}$ is Lipschitz continuous and differentiable except on a set of a measure 0. Then, in time step n and iteration (k) of the Newton-like method one may define an element $\mathbf{K} \in \partial\mathbf{Q}$ (indices are omitted for a simplicity of notation) with components:

$$\begin{aligned}(\mathbf{K})_{\alpha,\beta} &= (\mathrm{D}_{\mathbf{u}}\mathbf{Q})_{\alpha,\beta} = \mathrm{D}_{\mathbf{u}_\beta}(\mathbf{Q}_\alpha) \\ &= \frac{1}{\alpha!}\mathrm{D}_{\mathbf{u}_\beta}(\mathbb{E}(\mathbf{Q}H_\alpha)) \\ &= \int_{\mathcal{G}_h} \nabla\mathbf{N}^T(x)(\mathbf{A}_{ep})_{\alpha,\beta}(x)\nabla\mathbf{N}(x)\mathrm{d}x. \end{aligned} \tag{5.13}$$

Note that the stochastic and deterministic (see [21]) stiffness matrices have similar form with the only exception that the material properties $(\mathbf{A}_{ep})_{\alpha,\beta}(x)$ are given in a form of the mathematical expectation:

$$(\mathbf{A}_{ep})_{\alpha,\beta} := \mathbb{E}\left(H_\alpha(\theta)H_\beta(\theta)\boldsymbol{A}_{ep}(\sum_\gamma \boldsymbol{N}^T(x)\boldsymbol{u}^{(\gamma)}H_\gamma(\theta),\theta)\right). \tag{5.14}$$

Following this, the nonlinear system in Eq. (5.11) reduces to the symmetric and positive definite linear system of equations:

$$\mathbf{K}_n^{(k-1)}\delta\mathbf{u}_n^{(k)} = -\mathbf{Q}(\mathbf{u}_n^{(k-1)}) =: \mathbf{Q}_n^{(k-1)}, \quad \forall\delta\mathbf{u}_n^{(k)} \in \mathscr{U}_h \otimes (S)_J \tag{5.15}$$

which further can be solved by Krylov sub-space methods described in Section 5.4.1. Once the system is solved, the displacement increment can be udated to:

$$\Delta\mathbf{u}_n^{(k)} = \Delta\mathbf{u}_n^{(k-1)} + \delta\mathbf{u}_n^{(k)}, \quad k = 1, \ldots, m \tag{5.16}$$

i.e.

$$\mathbf{u}_n^{(k)} = \mathbf{u}_n^{(k-1)} + \delta\mathbf{u}_n^{(k)}, \text{ and } \mathbf{u}_n = \mathbf{u}_{n-1} + \Delta\mathbf{u}_n^{(m)}. \tag{5.17}$$

Note that in Eq. (5.15) one does not need to evaluate the Jacobian $\mathbf{K}_n^{(k-1)}$ in each iteration. Instead, by taking $\mathbf{y}^{(k)} := \mathbf{Q}_n^{(k)} - \mathbf{Q}_n^{(k-1)}$, the displacement correction can

be computed via:

$$\mathbf{p}^{(k)} := \Delta\mathbf{u}_n^{(k)} - \Delta\mathbf{u}_n^{(k-1)} = (\mathbf{K}_n^{(k)})^{-1}\mathbf{y}^{(k)}, \tag{5.18}$$

where the inverse matrix $(\mathbf{K}_n^{(k)})^{-1}$ is obtained as a rank-two update of the previous inverse $(\mathbf{K}_n^{(k-1)})^{-1}$. In other words,

$$\mathbf{K}_n^{(k)^{-1}} = (\mathbf{I} + \mathbf{q}^{(k)}\mathbf{v}^{(k)^T})\mathbf{K}_n^{(k-1)^{-1}}(\mathbf{I} + \mathbf{v}^{(k)}\mathbf{q}^{(k)^T}), \tag{5.19}$$

where $\mathbf{I}$ is an identity matrix and vectors $\mathbf{v}$ and $\mathbf{q}$ are defined as:

$$\mathbf{v}^{(k)} = \left(\frac{\mathbf{p}^{(k)^T}\mathbf{y}^{(k)}}{\mathbf{p}^{(k)^T}\mathbf{K}_n^{(k)^{-1}}\mathbf{p}^{(k)}}\right)^{1/2} \mathbf{K}_n^{(k)^{-1}}\mathbf{p}^{(k)} - \mathbf{y}^{(k)}, \quad \mathbf{q}^{(k)} = \frac{\mathbf{p}^{(k)}}{\mathbf{p}^{(k)^T}\mathbf{y}^{(k)}}. \tag{5.20}$$

This method is called BFGS [146, 138, 21] and belongs to a class of quasi-Newton methods. The initial value of matrix $\mathbf{K}_n^{(0)}$ is computed by taking the so-called mean stiffness matrix, which corresponds to the mean values of the random material parameters. As its estimation is rather simple, the matrix $\mathbf{K}_n^{(0)}$ is often seen as a preconditioner [107] for solving linear system of equations (see Section 5.4.1).

Previous discussions are drawing the principle behind the stochastic Galerkin method in a very general form. However, in order to perform actual computation one has to find the way to compute the residual in Eq. (5.11) and the stiffness matrix in Eq. (5.13), both given in a form of high-dimensional integrals over probability space. Basically, one may distinguish two approaches to this problem:

- *intrusive* Galerkin and
- *non-intrusive* Galerkin.

The intrusive method [244, 140] approximates the displacement via the polynomial chaos expansion (PCE) in the finite stochastic subspace, and further uses the polynomial chaos algebra (see Chapter 6) to compute the stress, the plastic strain, etc. locally in each FEM integration point (see Algorithm 2). The statistics are then easily evaluated in an algebraic way. Even though such an approach is numerically stable and feasible, its implementation is very demanding and requires very efficient procedures. Another possibility is to sample the residual in each iteration of the Newton-like methods by generating the set of samples for ω (i.e. $\boldsymbol{\theta}$)—the so-called non-intrusive Galerkin approach (see Section 5.4.2).

Algorithm 2: Stochastic Newton method via PCE algebra

Newton method

for each time step $n = 1 \rightarrow L_t$ **do**
  - set the initial values for $k = 0$
    $\mathbf{u}_n^{(0)} = \mathbf{u}_{n-1}$
  - set $k = k + 1$ and compute
    $\mathbf{Q}_n^{(k-1)} = \mathbf{f}^{int}(\mathbf{u}_n^{(k-1)}) - \mathbf{f}^{ext}$
  for each FEM Gauss point $i = 1 \rightarrow L_y$ **do**
    - evaluate consistent tangent matrix
      $\boldsymbol{A}_{ep}(\boldsymbol{y}_i)$ (see Algorithm 4)
    - compute PCE terms of element stiffness
      $\boldsymbol{K}^{(\alpha)}(\boldsymbol{y}_i) = \sum_\alpha (\nabla \boldsymbol{N}(\boldsymbol{y}_i))^T : \boldsymbol{A}_{ep}^{(\alpha)}(\boldsymbol{y}_i) : \nabla \boldsymbol{N}(\boldsymbol{y}_i) H_\alpha(\boldsymbol{\theta})$
  end for
  Set the mean based preconditioner
    $\mathbf{P} = \boldsymbol{I} \otimes \bar{\boldsymbol{K}}$
  for $i = 1 \rightarrow$ MAXITER **do**
    - solve by PCG (or GMRES) iterations
      $\delta \mathbf{u}_n^{(i+1),(k)} = \delta \mathbf{u}_n^{(i),(k)} + \mathbf{P}^{-1}(\mathbf{Q}_n^{(k-1)} - \mathbf{K}_n^{(k-1)} \delta \mathbf{u}_n^{(i),(k)})$
  end for
  - update displacement
    $\mathbf{u}_n^{(k)} = \mathbf{u}_n^{(k-1)} + \delta \mathbf{u}^{(k)}$
  for each FEM Gauss point $j = 1 \rightarrow L_y$ **do**
    -update strain
      $\hat{\boldsymbol{\varepsilon}}_n^{(k)}(\boldsymbol{y}_j) := \nabla \boldsymbol{N}(\boldsymbol{y}_j) \hat{\boldsymbol{u}}_n^{(k)}$
    - constitutive integration
      $\hat{\boldsymbol{\sigma}}_n^{(k)}(\boldsymbol{y}_j) = \hat{\boldsymbol{\sigma}}(\hat{\boldsymbol{\eta}}_{n-1}, \hat{\boldsymbol{\varepsilon}}_n^{(k)}), \quad \hat{\boldsymbol{\eta}}_n^{(k)} = \hat{\boldsymbol{\eta}}_n^{(k)}(\hat{\boldsymbol{\eta}}_{n-1}, \hat{\boldsymbol{\varepsilon}}_n^{(k)}),$
    - internal force
      $\boldsymbol{f}_{(e)}^{int} := \sum_e \varpi_i \nabla \boldsymbol{N}(\boldsymbol{y}_j))_i^T \hat{\boldsymbol{\sigma}}_n^{(k)}(\boldsymbol{y})$
  end for
  - assemble $\mathbf{f}^{int}$ and compute residual
    $\mathbf{Q} = \mathbf{f}^{int}(\mathbf{u}_n^{(k)}) - \mathbf{f}^{ext}$
  - check convergence
  if $\|\mathbf{Q}\| / \|\mathbf{f}^{ext}\| \leq \epsilon_{tol}$ **then**
    $(\cdot)_n = (\cdot)_n^{(k)}$
    EXIT
  else
    go to 4
  end if
end for

5.4.1 Instrusive Galerkin method

In order to solve the stochastic minimisation problem given in Theorem 4.3.3 one has to evaluate the high–dimensional integrals. According to previous sections this can be done by approximate computation of integrals using the random or deterministic sequences of numbers. However, such an approach can cause a possible computational overload due to slow convergence rates. To overcome this problem, one may evaluate the integral in an algebraic way in case that the integrand $\phi : \Omega \to \mathbb{R}$ is smooth enough. One such possibility would be to project ϕ onto a multivariate Hermite polynomial H_α (see Chapter 6) of unit norm [107], and then to define the mathematical expectation $\mathbb{E}(\phi(\omega)H_\alpha(\omega))$ in a following form:

$$\mathbb{E}(\phi(\omega)H_\alpha(\omega)) = \sqrt{\alpha!}\mathbb{E}(\mathrm{D}^\alpha\phi(\omega)), \tag{5.21}$$

where $\mathrm{D}^\alpha\phi(\omega)$ is the partial derivative of $\phi(\omega)$ corresponding to the multi-index α. Such an approach directly allows the evaluation of the elastoplastic solution in a purely deterministic (algebraic) way—known as the intrusive Galerkin method. This novel procedure does not require sampling at any stage of the computation. Instead, the method employs the polynomial chaos algebra coming from the polynomial chaos approximation of the input random fields Eq. (4.65) and the solution ansatz [140].

Approximation of a convex set

With the help of the Euler implicit difference scheme described in Section 4.2 one may pose the following optimisation problem:

$$\boldsymbol{\Sigma}_h = \underset{\boldsymbol{T}_h \in \mathscr{K}_h}{\arg\min}\, \Phi_{hn}(\boldsymbol{T}_h), \tag{5.22}$$

where $\mathscr{K}_h$ represents the convex elastic domain of admissible generalised stresses $\boldsymbol{\Sigma}_h$ described by a yield function ϕ_h as

$$\mathscr{K}_h = \{\boldsymbol{\Sigma}_h \in \mathcal{Y}_h \otimes (S) :\ \phi(\boldsymbol{\Sigma}_h) \leq 0 \text{ a.s.}\}. \tag{5.23}$$

Computationally, the process of solving Eq. (5.22) reduces to the iterative method of solving stochastic convex optimisation problem, which aims at finding the closest distance in the energy norm of a trial state to a convex set of elastic domain, known as a closest point projection. From Eq. (5.22) and Section 4.2.3 one may deduce the typical operator split of the closest point projection algorithm into two steps: the reversible (non-dissipative) and irreversible (dissipative), also called elastic predictor

and plastic corrector step.

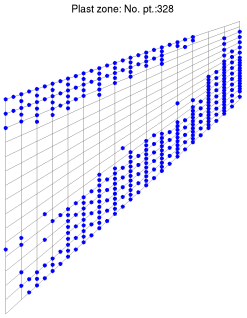

a) Direct integration p_{50} (328 ppts)

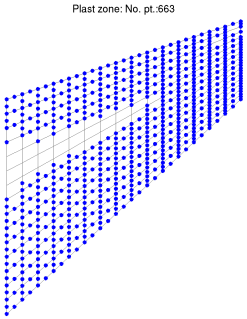

b) Markov p_{50} (663 ppts)

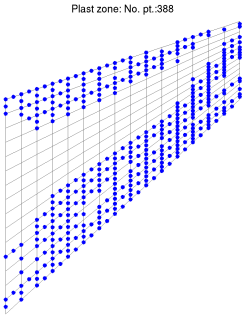

c) Chebyshev p_{50} (388 ppts)

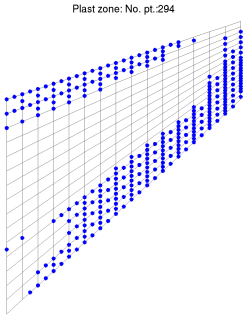

d) Mean (294 ppts)

Figure 5.1: Comparison of plastic zones obtained by different yield criteria decisions. Number of points that plastify is denoted by ppts.

Having that in each FEM-integration point the variables of consideration are essentially the RVs belonging to (S), one may use the methods presented in Chapter 6 for their discretisation. Such an approach yields to the representation of the convex domain $\mathscr{K}_h$ in terms of the finite PC approximation of the yield function $\hat{\phi}$, i.e.

$$\mathscr{K}_{h,\mathcal{J}} = \{\boldsymbol{\Sigma}_h \in \mathcal{Y}_h \otimes (S)_J \mid \hat{\phi} := \sum_{\alpha \in \mathcal{J}_Z} \phi^{(\alpha)} H_\alpha(\boldsymbol{\theta}) \leq 0\}. \tag{5.24}$$

This formulation is not “computationally simple” per se, because the decision cri-

terion is given in terms of the coefficients of the polynomial chaos expansion of ϕ. In order to satisfy the condition $\hat{\phi} \leq 0$ almost surely, one cannot simply convert Eq. (5.24) to the constraints on the coefficients $\phi^{(\alpha)}$. For example, by taking all coefficients to be greater than zero $\phi^{(\alpha)} > 0$ the positive definiteness of the random variable ϕ is not assured. Thus, the criterion in Eq. (5.24) has to be reformulated to anoter one, which uses the weaker version $\mathscr{K}_{\mathcal{J}}^{\star}$ of the set $\mathscr{K}_{h,\mathcal{J}}$. The choice of $\mathscr{K}_{\mathcal{J}}^{\star}$ depends on the general requirements of the system response on accuracy and computational cost.

The inequality in Eq. (5.24) can be relaxed such that the constraint is satisfied only for some finite number of points $\Xi := \{\boldsymbol{\theta}^j\}, j = 1, ..., N_p$, instead almost sure. Similar idea appeared in [11], where the domain $\mathscr{K}_{\mathcal{J}}^{\star}$ is defined as a set of the "deterministic" constraints:

$$\mathscr{K}_{\mathcal{J}}^{\star} = \{\boldsymbol{\Sigma}_h^j \in \mathcal{Y}_h \otimes (S)_J \mid \hat{\phi}(\boldsymbol{\theta}^j) \leq 0\} \quad j = 1, ..., N_p. \tag{5.25}$$

The number N_p is finite and corresponds to the full or sparse quadrature grid as described in Section 5.3. Note that this number may drastically grow with the dimension Z, not only for the full but also for sparse quadrature. This may on the other hand increase the overall computation time as the integration of the stress has to be performed over the set Ξ.

In order to avoid sampling as given in Eq. (5.24) we formulate another approximation $\mathscr{K}_{\mathcal{J}}^{\star}$ for $\mathscr{K}_{\mathcal{J}}$. The simplest and most natural choice would be

$$\mathscr{K}_{\mathcal{J}}^{\star} = \{\boldsymbol{\Sigma} \in \mathcal{Y}_h \otimes (S)_J \mid \phi^{(0)} \leq 0\}, \tag{5.26}$$

i.e. $\mathscr{K}_{\mathcal{J}}^{\star}$ taken as the mean of $\mathscr{K}_{\mathcal{J}}$. This corresponds to the case when the mean of ϕ is far from zero, and higher order moments of ϕ are relatively small compared to the mean value. Actually, they need to be such that the probability of ϕ to be zero or positive is equal to zero. As expected, this criterion can be used only when the von Mises σ_{VM} and yield σ_y stresses have non-overlapping probability density functions (e.g. initial elastic behaviour and strong plastyfing). However, in the critical region (also called *transition* zone) when two stresses are similar to each other (i.e. their probability densities are overlapping) one cannot use the mean based criteria to make the decision. If does, then the estimated plastifying zone is only mean accurate.

The mean convergence is not the scenario one would like to have, and hence another definition of Eq. (5.26) has to be provided. For this, let us consider the von Mises yield criterion in a form of $\phi = \sigma_{VM} - \sigma_y$, where both von Mises σ_{VM} and yield σ_y stresses are positive definite random variables. Then, the inequality $\phi \leq 0$ reduces

to the comparison $\sigma_{VM} \leq \sigma_y$ of two random variables σ_{VM} and σ_y in almost sure sense, i.e.

$$\hat{\sigma}_{VM} \leq \hat{\sigma}_y \tag{5.27}$$

in PCE terms. Assuming that the PC approximation of the RV σ_y admits the same properties as the original[2], both sides of Eq. (5.27) are divided by $\sigma_y > 0$ such that Eq. (5.27) transforms to inequality

$$\varphi := \frac{\hat{\sigma}_{VM}}{\hat{\sigma}_y} \leq 1. \tag{5.28}$$

This formulation is more convenient as one may employ the Markov inequality [129] to determine the upper bound on probability that RV φ satisfies Eq. (5.28):

Proposition 5.4.1. *Given the positive definite random variable φ one has*

$$\Pr(\varphi \geq 1) \leq \mathbb{E}(\varphi). \tag{5.29}$$

The Markov upper bound for cumulative distribution of random variables relates the probabilities to the expectation. The estimate provides useful but not tight bound on the probability of stress being outside of the convex elastic domain. Hence, the estimate cannot be considered as more sharp than the mean estimate given in Eq. (5.26). However, for further improvement, one may take into account the higher order moments of ϕ and paraphrase a one-sided Chebyshev inequality [129] (also known as Canolli's inequality):

Proposition 5.4.2. *Let φ be a random variable with mean $\mathbb{E}(\varphi)$ and variance* $\operatorname{var}\varphi$*, then for all $a > 0$ one has:*

$$\Pr[\tilde{\varphi} := \varphi - \mathbb{E}(\varphi) \geq a] \geq \frac{\operatorname{var}\varphi}{\operatorname{var}\varphi + a^2}. \tag{5.30}$$

[2] one may hope that the number of terms in PCE is large enough to keep the property of positive definiteness

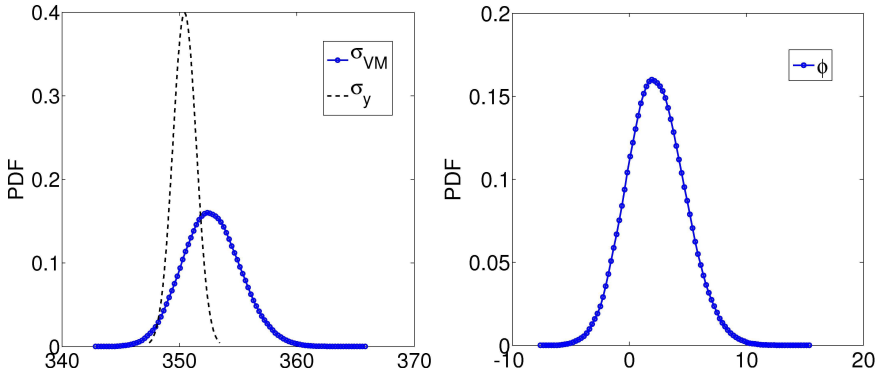

a) The plastic state is more probable than the elastic state

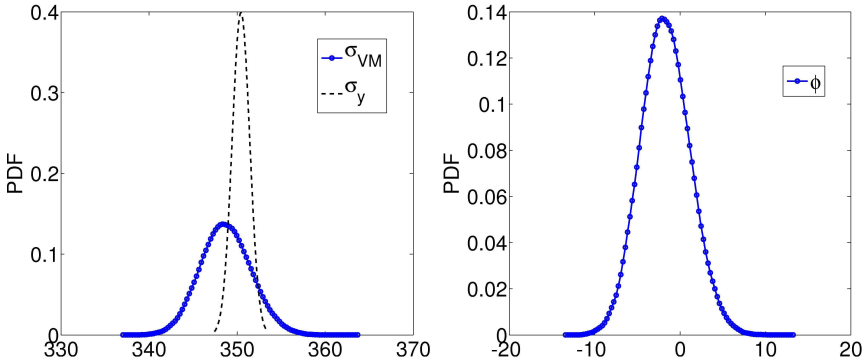

b) Plastic and elastic states are almost equally probable

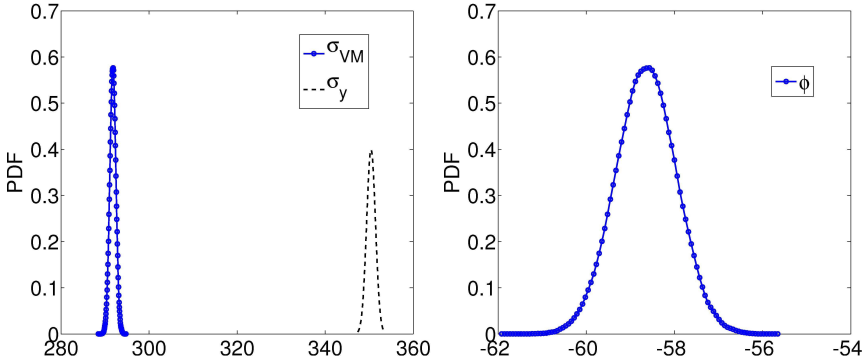

c) Fully elastic state

Figure 5.2: Probability distribution functions of von Mises stress σ_{VM}, yield stress σ_y, corresponding yield function ϕ, and description of state

Proof. Let us choose any $b > -a$ such that:

$$\begin{aligned} \Pr\ [\varphi \geq \mathbb{E}(\varphi) + a] &= \Pr\ [\varphi \geq a] \\ &= \Pr\ \left[\frac{\varphi + b}{a + b} \geq 1\right] \\ &\leq \Pr\ \left[\gamma := \left(\frac{\varphi + b}{a + b}\right)^2 \geq 1\right] \end{aligned} \tag{5.31}$$

holds. Applying the Markov estimate [129] on the last inequality, one may obtain the set of bounds parametrised by b:

$$\Pr\ [\varphi \geq a] \leq \mathbb{E}\left[\left(\frac{\varphi + b}{a + b}\right)^2\right] = \frac{\text{var}\ \varphi + b^2}{(a + b)^2}. \tag{5.32}$$

Note that from all possible bounds given in Eq. (5.32) one is particularly interested in the smallest possible $b = \text{var}\ \varphi / a$ satisfying

$$b = \arg\min_{v} \frac{\text{var}\ \varphi + v^2}{(a + v)^2}. \tag{5.33}$$

□

According to this, the stress stays in elastic area if the higher order moments of σ_y are bigger than the same for σ_{VM}, even though the von Mises stress has greater mean than the yield stress, see Fig. 5.2. The bound in Eq. (5.4.2) may be further improved with respect to the higher order moments of $\tilde{\varphi}$:

$$\Pr\ [\mathbb{E}(\tilde{\varphi}^n) \geq a] \geq \frac{\mathbb{E}((\tilde{\varphi} + b)^n)}{(a + b)^n}, \tag{5.34}$$

where n represents the even order of the moment and b is the optimisation parameter which minimises the bound (see Eq. (5.33)).

Following the previous defintions, one is able to construct the new set $\mathscr{K}^{\star}_{\mathcal{J}}$ in terms of the probability occurrence p_r :

$$\mathscr{K}^{\star}_{\mathcal{J}} = \{\boldsymbol{\Sigma} \in \mathcal{Y}_h \otimes (S)_J \mid \Pr\ (\hat{\phi} \leq 0) \geq p_r\}, \tag{5.35}$$

where the probability estimate $\Pr\ (\hat{\phi} \leq 0)$ follows from the Proposition 5.4.1 or Proposition 5.4.2. Here, p_r is the probability defining the occurrence of the elastic behaviour (the stress belongs to the convex set $\mathscr{K}_{\mathcal{J}}$). The choice of p_r depends on

the particular situation. For example, in some integration points it may happen that ϕ has 50% probability to be in the elastic and 50% to be in the plastic zone. This relates to the transition zone for which the proper choice has to be made.

Note that the set $\mathscr{K}_{\mathcal{J}}^{\star}$ in Eq. (5.35) does not require the previously introduced estimates. Another possibility would be to compute the probability of exceedance by a very cheap direct integration (see Section 5.3).

Closest point projection

The evolution equations described in Section 3.5.3 are further discretised by implicit Euler scheme, see Section 4.2. Their integration over time is done in a strain-driven manner by assuming that the stress and internal variables are updated from their values known at time t_{n-1} for a given strain increment in time (see Section 4.2.3). Following this, one may distinguish two steps in closest point projection algorithm as further described.

Elastic Predictor

Let be given the time interval of interest $\mathcal{T} = [0, T]$ such that the generalised total $\boldsymbol{E}_{n-1}(\omega) := (\boldsymbol{\varepsilon}_{n-1}(\omega), \mathbf{0})$ and plastic $\boldsymbol{E}_{p,n-1}(\omega) := (\boldsymbol{\varepsilon}_{p,n-1}(\omega), (\boldsymbol{\varepsilon}_{p,n-1}(\omega), \nu_{n-1}(\omega)))$ strains are known at time t_{n-1}. They represent the vector of random variables, each approximated by the polynomial chaos expansion (PCE) with Hermite transforms $\mathscr{H}(\boldsymbol{E}_{n-1}) = (\boldsymbol{E}_{n-1}^{(\alpha)})_{\alpha\in\mathcal{J}} =: (\boldsymbol{E}_{n-1}) \in \mathbb{R}^{a\times\mathcal{J}}$ and $\mathscr{H}(\boldsymbol{E}_{p,n-1}) := (\boldsymbol{E}_{p,n-1}) \in \mathbb{R}^{a\times\mathcal{J}}$, respectively. In order to perform the numerical computations these PCEs are truncated to a finite number of terms Z corresponding to the multi-index set $\mathcal{J}_Z := \mathcal{J}_{M,p}$ described by M random variables and polynomial order p. Thus, the variables are replaced by approximations $\hat{\boldsymbol{E}}_{n-1}$ and $\hat{\boldsymbol{E}}_{p,n-1}$, where $\hat{}$ denotes the projection on the finite subspace generated by $\{H_\alpha \mid \alpha \in \mathcal{J}_Z\}$. For simplicity, one may use the same finite subspace for $\boldsymbol{E}_{n-1}(\omega)$ and plastic strain $\boldsymbol{E}_{p,n-1}(\omega)$.

Besides the total and plastic strain, at time t_{n-1} are known the elastic strain $\boldsymbol{E}_e(\omega) = \boldsymbol{E}(\omega) - \boldsymbol{E}_p(\omega)$, i.e. $\hat{\boldsymbol{E}}_e$, and the generalized stress $\boldsymbol{\Sigma}_{n-1}(\omega)$, i.e. $\hat{\boldsymbol{\Sigma}}_{n-1}$. The main goal is to update these fields from t_{n-1} to t_n in a manner consistent with the constitutive equations previously described.

Given previously mentioned quantities one may first compute the increment of the displacement $\Delta \boldsymbol{u}_n(\omega)$ (i.e. its approximation $\Delta \hat{\boldsymbol{u}}_n$) by solving Eq. (5.15), and then the increment of the elastic strain as:

$$\Delta \hat{\boldsymbol{E}}_n = (\nabla_S(\Delta \hat{\boldsymbol{u}}_n), \boldsymbol{0}) = (\nabla_S(\Delta \boldsymbol{u}_n^{(\alpha)})_{\alpha \in \mathcal{J}_Z}, \boldsymbol{0}). \tag{5.36}$$

The last relation assumes the state of the plastic flow $\Delta \hat{\boldsymbol{E}}_{pn} = (0, ..., 0)$ to be frozen, i.e. the total strain increment is purely elastic with the corresponding stress $\Delta \hat{\boldsymbol{\sigma}}_n = \widehat{\mathbf{S}}_2(\widehat{\boldsymbol{A}}, \Delta \hat{\boldsymbol{E}}_n)$. Here, $\widehat{\mathbf{S}}_2$ denotes the dot product between random matrix $\widehat{\boldsymbol{A}}$ and vector $\Delta \hat{\boldsymbol{E}}_n$, (see Section 6.4). Following this, the generalised trial stress is defined as:

$$\hat{\boldsymbol{\Sigma}}_n^{trial} = \hat{\boldsymbol{\Sigma}}_{n-1} + \widehat{\mathbf{S}}_2(\widehat{\boldsymbol{C}}, \Delta \hat{\boldsymbol{E}}_n), \tag{5.37}$$

where $\widehat{\boldsymbol{C}}$ denotes the PCE representation of the general constitutive matrix $\boldsymbol{C}(\omega) := \text{diag}\,[\boldsymbol{A}(\omega), \boldsymbol{H}(\omega)]$ consisting from the Hooke's tensor $\boldsymbol{A}(\omega)$ and the hardening $\boldsymbol{H}(\omega) = \text{diag}[\boldsymbol{H}_{kin}(\omega), H_{iso}(\omega)]$. Its Hermite transform reads

$$\mathscr{H}(\boldsymbol{C}) = \text{diag}\,[\mathscr{H}(\boldsymbol{A}), \mathscr{H}(\boldsymbol{H})] = (\boldsymbol{C})_{\alpha \in \mathcal{J}}. \tag{5.38}$$

Once $\hat{\boldsymbol{\Sigma}}_n^{trial}$ is known, its admissibility (i.e. whether it belongs to $\mathscr{K}_J^\star$ or not) can be further investigated with respect to the yield condition $\phi(\omega)$ projected to $\hat{\phi}$. In this work the von Mises material is considered, i.e. the yield criterion in a form of:

$$\hat{\phi} = \|\text{dev}\,\hat{\boldsymbol{\sigma}} - \hat{\boldsymbol{\zeta}}\|_{J_2} + \sqrt{\frac{2}{3}}[\hat{\sigma}_y + \hat{\varsigma}], \tag{5.39}$$

where $\hat{\boldsymbol{s}} := \text{dev}\,\hat{\boldsymbol{\sigma}} = \hat{\boldsymbol{\sigma}} - \frac{1}{3}\sum_i \hat{\boldsymbol{\sigma}}_{ii}\boldsymbol{I}$ denotes the deviatoric part of the stress, while $\hat{\boldsymbol{\zeta}} = -\widehat{\mathbf{S}}_2(\widehat{\boldsymbol{H}}_{kin}, \hat{\boldsymbol{\varepsilon}}_p)$ and $\hat{\varsigma} = \widehat{H}_{iso} \bullet \hat{\nu}$ represent the back stress and isotropic conjugate force (corresponding to the equivalent plastic strain $\hat{\nu}$), respectively. The norm $\|\cdot\|_{J_2}$ in Eq. (5.39) is of the J_2 type

$$\|\boldsymbol{\sigma}\|_{J_2} = \sqrt{\hat{\boldsymbol{s}}_{ij} \bullet \hat{\boldsymbol{s}}_{ji}} = \sqrt{\hat{\tau}} =: \hat{\sigma}_{VM}, \tag{5.40}$$

in which one first computes the product $\hat{\tau} := \hat{\boldsymbol{s}}_{ij} \bullet \hat{\boldsymbol{s}}_{ji}$ and then the root $\hat{\sigma}_{VM} := \sqrt{\hat{\tau}}$, as discussed in Section 6.3.2. According to this the approximation of the yield function reads:

$$\hat{\phi} = \hat{\sigma}_{VM} - \sqrt{\frac{2}{3}}[\hat{\sigma}_y + \hat{\varsigma}], \tag{5.41}$$

and thus the yield criterion can be inspected. If the stress $\hat{\boldsymbol{\Sigma}}_n$ belongs to the elastic domain the minimization given in Eq. (5.22) is trivial since the step is purely elastic and $\hat{\boldsymbol{\Sigma}}_n = \hat{\boldsymbol{\Sigma}}^{trial}$. Otherwise, the value is corrected by projecting the stress back to

the elastic domain $\mathscr{K}_{\mathcal{J}}^{\star}$ — plastic corrector.

Algorithm 3: Spectral Stochastic Closest Point Projection (SSCPP)

I Non-dissipative predictor

Initialize $j = 0, \epsilon_1, \epsilon_2, \hat{\boldsymbol{E}}_{p,n}^{(0)} = \hat{\boldsymbol{E}}_{p,n-1}, \hat{\lambda}_n^{(0)} = 0$

1. Evaluate strain
   $\Delta\hat{\boldsymbol{E}}_{p,n}^{(j)} = \hat{\boldsymbol{E}}_{p,n}^{(j)} - \hat{\boldsymbol{E}}_{p,n-1}, \quad \Delta\hat{\boldsymbol{E}}_{e,n}^{(j)} = \Delta\hat{\boldsymbol{E}}_n - \Delta\hat{\boldsymbol{E}}_{p,n}^{(j)}$
2. Evaluate stress
   $\hat{\boldsymbol{\Sigma}}_n^{(j)} := \hat{\boldsymbol{\Sigma}}_{n-1} + \widehat{\mathbf{S}}_2(\hat{\boldsymbol{C}}_n^{(j)}, \Delta\hat{\boldsymbol{E}}_{e,n}^{(j)})$

II Dissipative corrector

3. Compute yield function $\hat{\phi}_n^{(j)} = \hat{\phi}(\hat{\boldsymbol{\Sigma}}_n^{(j)})$
4. Compute residual: $\hat{\boldsymbol{r}}_{sn}^{(j)} = \hat{\boldsymbol{E}}_{p,n-1} - \hat{\boldsymbol{E}}_{p,n}^{(j)} + \hat{\lambda}_n^{(j)} \bullet \partial\hat{\phi}_n^{(j)}$
5. Check the yield conidition and residual:

   if $\|\hat{\boldsymbol{\phi}}_n^{(j)}\|_{L_2(\Omega)} < \epsilon_1$ **and** $\|\hat{\boldsymbol{r}}_{sn}^{(j)}\|_{L_2(\Omega)} < \epsilon_2$ **then**
   the step is elastic; **exit**

   else

   6. Compute constitutive tensor $\hat{\boldsymbol{C}}_n^{(j)}$
   7. Compute consistent tangent moduli $\hat{\boldsymbol{A}}_{ep,n}^{(j)}$ (see Eq. (5.47))
   8. Solve linear system
      $\mathbf{A}_{ep,n}^{(j)} \Delta\boldsymbol{\Upsilon}_n^{(j)} = -\mathbf{r}_{ypl,n}^{(j)} \Rightarrow \Delta\hat{\lambda}_n^{(j)}, \Delta\hat{\boldsymbol{E}}_{p,n}^{(j)}$
   9. Update variables
      $\hat{\boldsymbol{E}}_{p,n}^{(j+1)} = \hat{\boldsymbol{E}}_{p,n-1}^{(j)} + \Delta\hat{\boldsymbol{E}}_{p,n-1}^{(j)}$
      $\hat{\lambda}_n^{(j+1)} = \hat{\lambda}_n^{(j)} + \Delta\hat{\lambda}_n^{(j)}$

   end

10. Set $j = j + 1$ and go to 1

Plastic Corrector

Let us project the Lagrangian $\mathcal{L}(\omega)$ from Eq. (4.20) onto the Hermitian basis in

a Galerkin manner such that the minimisation problem in one integration point in Eq. (5.22) reads:

$$\hat{\mathcal{L}}_n = \hat{\Phi}_n + \hat{\lambda}_n \hat{\bullet} \hat{\phi}_n(\hat{\boldsymbol{\Sigma}}_n). \tag{5.42}$$

Applying the standard optimality conditions the solution has to satisfy

$$0 \in \partial_{\boldsymbol{\Sigma}} \hat{\mathcal{L}}_n = \partial_{\boldsymbol{\Sigma}} \hat{\Phi}_n + \hat{\lambda}_n \hat{\bullet} \partial_{\boldsymbol{\Sigma}} \hat{\phi}_n, \tag{5.43}$$

i.e.

$$\begin{aligned} \hat{\boldsymbol{r}}_{sn} := \hat{\boldsymbol{A}}^{-1}(\hat{\boldsymbol{\Sigma}}^{trial} - \hat{\boldsymbol{\Sigma}}_n) + \hat{\lambda}_n \partial_{\boldsymbol{\Sigma}} \hat{\phi}(\hat{\boldsymbol{\Sigma}}_n) &= 0 \quad \text{a.s.} \\ \hat{\phi}_n := \hat{\phi}(\hat{\boldsymbol{\Sigma}}_n) &= 0 \quad \text{a.s.} \end{aligned} \tag{5.44}$$

Collecting the right hand side to $\hat{\boldsymbol{r}}_{ypl} := (\hat{\boldsymbol{r}}_{sn}, \hat{\phi}_n)^T$ and unknowns to $\hat{\Upsilon}_n := (\hat{\lambda}_n, \hat{\boldsymbol{E}}_{p,n})^T$, the linearisation of Eq. (5.44) in a Newton manner leads to the following block-system:

$$D_{\Upsilon} \mathbf{r}_{ypl,n}[\Delta \boldsymbol{\Upsilon}_n] = -\mathbf{r}_{ypl,n}, \tag{5.45}$$

where $D_{\Upsilon} \mathbf{r}_{ypl,n}$ represents the corresponding derivative, i.e. the Jacobian $\mathbf{A}_{ep}$ (the consistent tangent moduli). In other words, by linearising the previous equation the following system of equations is obtained:

$$\mathbf{A}_{ep} \Delta \boldsymbol{\Upsilon}_n = -\mathbf{r}_{ypl,n}, \quad \mathbf{A}_{ep} = \sum_{\alpha} \boldsymbol{A}_{ep}^{(\alpha)} \otimes \boldsymbol{\Delta}^{(\alpha)}, \tag{5.46}$$

where $\boldsymbol{\Delta}^{(\alpha)} = \mathbb{E}(H_\beta H_\alpha H_\gamma)$ (see Chapter 6). Here, the PCE of the consistent tangent moduli [215] reads:

$$\hat{\boldsymbol{A}}_{ep} = \begin{bmatrix} \hat{\boldsymbol{\Xi}}_1 & \hat{\lambda}_n \hat{\bullet} \partial^2_{\hat{\boldsymbol{\sigma}}\hat{\boldsymbol{\chi}}} \hat{\phi}_n \\ \hat{\lambda}_n \hat{\bullet} \partial^2_{\hat{\boldsymbol{\chi}}\hat{\boldsymbol{\sigma}}} \hat{\phi}_n) & \hat{\boldsymbol{\Xi}}_2 \end{bmatrix}^{-1}, \tag{5.47}$$

where $\hat{\boldsymbol{\Xi}}_1 = \hat{\xi}^{\circ} \hat{\div} \hat{\boldsymbol{A}}_n + \hat{\lambda}_n \hat{\bullet} \partial^2_{\hat{\boldsymbol{\sigma}}\hat{\boldsymbol{\sigma}}} \hat{\phi}_n$ and $\hat{\boldsymbol{\Xi}}_2 = \hat{\xi}^{\circ} \hat{\div} \hat{\boldsymbol{H}}_n + \hat{\lambda}_n \hat{\bullet} \partial^2_{\hat{\boldsymbol{\chi}}\hat{\boldsymbol{\chi}}} \hat{\phi}_n$.

After solving the system in Eq. (5.46) one obtains the plastic multiplier $\hat{\lambda}$ and the increment of the plastic strain $\Delta \hat{\boldsymbol{E}}_{p,n}$ necessary for the update of the corresponding values from time t_{n-1} to time t_n as shown in Algorithm 3.

Stiffness matrix

In order to solve the linear system of equations in Eq. (5.12) one has to compute the Jacobian, i.e. the stiffness matrix. In case of infinitesimal deformations the Jacobian

consists only of one term $\boldsymbol{K}^{(\alpha)}(x) := \int_{\mathcal{G}_h} \nabla \mathbf{N}(x) \boldsymbol{A}_{ep}^{(\alpha)}(x) (\nabla \mathbf{N}(x))^T \mathrm{d}x$, while in the finite deformation case it splits to two terms, linear $\boldsymbol{K}_L$ and geometrical $\boldsymbol{K}_{NL}$ stiffness matrices. Here, $\boldsymbol{A}_{ep}$ represents the tangent elastoplastic tensor, see [215]. The linear stiffness is computed in a similar way as $\boldsymbol{K}$, while the nonlinear part depends on the polynomial approximation of the second Piola-Kirchhoff stress:

$$[\boldsymbol{K}_{NL}]_{ij}^{(\alpha)} = \int_{\mathcal{G}_h} N_{i,I}(x) \boldsymbol{S}_{IJ}^{(\alpha)}(x) N_{j,J} \, \mathrm{d}x, \tag{5.48}$$

where index i, I denotes the partial derivative over coordinates and $\boldsymbol{S}_{IJ}^{(\alpha)}$ is the stress obtained in each FEM point via PCE algebra.

Algorithm 4: Consistent moduli computed via PCE algebra

Stochastic consistent tangent moduli in integration point y_j

Known: $\kappa = \{K, G, H_{iso}, H_{kin}\}$, $\boldsymbol{\Sigma} := (\boldsymbol{\sigma}, \boldsymbol{\chi})$

1. Express inputs in PCE format in Gauss point y_j
   $\hat{\kappa} = \sum_\alpha [\sum_j \varkappa_j(y_j) \xi_j^{(\alpha)}] H_\alpha(\boldsymbol{\theta}(\omega)) = \sum_\alpha \kappa^{(\alpha)}(y_j) H_\alpha(\boldsymbol{\theta})$
2. Evaluate deviatoric stress
   $\hat{\boldsymbol{s}} := \mathrm{dev}\, \hat{\boldsymbol{\sigma}} = \hat{\boldsymbol{\sigma}} - \frac{1}{3} \mathrm{tr}\, \hat{\boldsymbol{\sigma}} \mathbf{1} = \hat{\boldsymbol{\sigma}} - \frac{1}{3}(\hat{\sigma}_{11} + \hat{\sigma}_{22} + \hat{\sigma}_{33}) \mathbf{1}$
3. Compute J_2 norm by Newton method
   $\hat{b} = \|\hat{\boldsymbol{s}}\|_{J_2} = \sqrt{\frac{3}{2} \hat{s}_{ij} \hat{\bullet} \hat{s}_{ji}}$
4. Compute parameter ϑ
   $\hat{q}_2 = (2\hat{G} \hat{\bullet} \Delta\hat{\lambda}) \hat{\div} \hat{b} \Rightarrow \vartheta = \mathring{\xi} - \hat{q}_2$
5. Solve linear system for parameter ρ
   $\hat{\rho} \hat{\bullet} (\mathring{\xi} + (\hat{H}_{iso} + \hat{H}_{kin}) \hat{\div} (3\hat{G})) = \hat{\vartheta} - \mathring{\xi}$
6. Find normal $\hat{n}_i = \hat{s}_i \hat{\div} \hat{b}$
7. PCE multiplication:
   $q_3 = 2\hat{G} \hat{\bullet} \hat{\vartheta}, \quad q_4 = 2\hat{G} \hat{\bullet} \hat{\rho}$
8. Compute moduli
   $\boldsymbol{A}_{ep} = \hat{K} \mathbf{1} \otimes \mathbf{1} + \hat{q}_3 [\boldsymbol{I} - \frac{1}{3} \mathbf{1} \otimes \mathbf{1}] - \hat{q}_4 \hat{\boldsymbol{n}} \otimes \hat{\boldsymbol{n}}$

From previous definitions one may conclude that the stiffness matrix for the nonlinear problem is not as easy to compute as in linear problems. Namely, one looses the property of the linear dependence between Jacobian and input material parameters. This additionally complicates the problem since the KL/PCE of $\boldsymbol{K}$ cannot be computed using the black-box based deterministic software, but its stochastic coun-

terpart. In order to show this, the model of infinitesimal plasticity is chosen as a numerical example.

The essential motivation behind the intrusive Galerkin method is to employ the PCE methods for the estimation of the tangent elastoplastic moduli $\boldsymbol{A}_{ep}$. By PCE approximation of all RVs describing elastoplastic behaviour, one may use the favourable properties of PCE algebra (see Chapter 6) and compute the constitutive tensor in an integration point for the von Mises J_2 plasticity according to Algorithm 4. Here, the operations $\hat{\bullet}$, $\hat{\div}$ denote the PCE multiplication and division, see Chapter 6, and the term $\mathrm{dev}(\cdot)$ represents the deviator of the quantity. Note that Algorithm 4 formally has the same structure as the corresponding deterministic procedure in [215].

In order to evaluate the stiffness matrix in Eq. (5.13) one has to compute the Hermite transform $\mathcal{H}(\boldsymbol{A}) = (\boldsymbol{A}^{(\alpha)})_{\alpha\in\mathcal{J}}$ (see Chapter 6) of the parametric matrix $\boldsymbol{A}(x)$. The simplest way of doing this is to use the algebraic expression coming from the definition of the constitutive tensor and transform it (in each FEM integration point) via the polynomial chaos algebra to :

$$\mathcal{H}(\boldsymbol{A}) = \mathcal{H}(K)\mathbf{1}\otimes\mathbf{1} + 2\mathcal{H}(G)[\boldsymbol{I} - \frac{1}{3}\mathbf{1}\otimes\mathbf{1}]. \tag{5.49}$$

Here, $\mathcal{H}(K)$ and $\mathcal{H}(G)$ denote the Hermite transforms of random fields of bulk K and shear G moduli, respectively. They are computed by finite KL/PCE approximations in integration point x_ξ:

$$\hat{K}(x_\xi,\boldsymbol{\theta}) = \sum_{\alpha\in\mathcal{J}_{M_k,p_k}}\left[\sum_j^{M_k} K_j(x_\xi)\zeta_j^{(\alpha)}\right]H_\alpha(\boldsymbol{\theta}) = \sum_{\alpha\in\mathcal{J}_{M_k,p_k}} K^{(\alpha)}(x_\xi)H_\alpha(\boldsymbol{\theta}), \tag{5.50}$$

and

$$\hat{G}(x_\xi,\boldsymbol{\theta}) = \sum_{\alpha\in\mathcal{J}_{M_g,p_g}}\left[\sum_j^{M_g} G_j(x_\xi)\varsigma_j^{(\alpha)}\right]H_\alpha(\boldsymbol{\theta}) = \sum_{\alpha\in\mathcal{J}_{M_g,p_g}} G^{(\alpha)}(x_\xi)H_\alpha(\boldsymbol{\theta}). \tag{5.51}$$

Following Eq. (5.50) and Eq. (5.51) one may note that $\boldsymbol{K}$ is described in terms of two independent sets of RVs $\boldsymbol{\zeta}^{(\alpha)}$ and $\boldsymbol{\varsigma}^{(\alpha)}$ i.e. in $M = M_k + M_g$ RVs. Thus, its final approximation admits $p = \max(p_k, p_g)$ order in which the multi-index α may take the value in $\mathcal{J}_P$ obtained by gathering two multi-index sets $\mathcal{J}_{M_k,p_k}$ and $\mathcal{J}_{M_g,p_g}$. For simplicity reasons, one may assume that the solution set $\mathcal{J}_Z$ is identical to $\mathcal{J}_P$ [3].

[3] This assumption is not necessary. However, even in a more general case the analysis is formally the same.

Once the "material property" $\boldsymbol{A}_{ep}^{(\alpha)}$ has been estimated (Algorithm 4), the term $\boldsymbol{K}^{(\alpha)}$ is computed as a "usual" finite element stiffness matrix by calling the black-box deterministic code with $\boldsymbol{A}_{ep}^{(\alpha)}$ as input parameter. This results in the final form of the equilibrium Eq. (5.15):

$$\mathbf{K}\delta\mathbf{u} = \left[\sum_{\alpha\in\mathcal{J}_Z} \boldsymbol{K}^{(\alpha)} \otimes \boldsymbol{\Delta}^{(\alpha)}\right] \delta\mathbf{u} = \mathbf{Q}, \tag{5.52}$$

where the elements of the tensor $\boldsymbol{\Delta}^{(\alpha)}$ are given by $\Delta_{\beta\gamma}^{(\alpha)} := \mathbb{E}(H_\gamma H_\alpha H_\beta)$. Similarly, $\mathbf{u} = [..., \boldsymbol{u}^{(\alpha)}, ...] \in \mathbb{R}^{L_n} \otimes \mathbb{R}^Z$ and $\mathbf{Q} \in \mathbb{R}^{L_n} \otimes \mathbb{R}^Z$ are the block vectors of the nodal polynomial coefficients of the solution and the right hand-side, respectively. The concrete representation of Eq. (5.52) in terms of matrices and column vectors may be obtained by interpreting the symbol $\otimes$ everywhere as a *Kronecker* product [157, 192]. Namely, by exploiting the isomorphy between $\mathbb{R}^{L_n} \otimes \mathbb{R}^Z$ and $\mathbb{R}^{L_n \times Z}$ the term $(\boldsymbol{K}^{(\alpha)} \otimes \boldsymbol{\Delta}^{(\alpha)})$ acts as $\boldsymbol{K}^{(\alpha)}\delta\mathbf{u}(\boldsymbol{\Delta}^{(\alpha)})^T$.

The operator $\mathbf{K}$ in Eq. (5.52) inherits the properties of the corresponding deterministic operator in terms of symmetry and positive definiteness [145, 152, 192]. The symmetry may be verified directly from Eq. (5.52), while the positive definiteness follows from the Galerkin projection and the uniform convergence of the solution in Eq. (5.52) on the finite dimensional space $\mathbb{R}^{(L_n \times L_n)} \otimes \mathbb{R}^{(Z \times Z)}$ (see [150, 145, 107]). Due to the uniform convergence alluded to above the sum can be extended far enough such that the operators $\mathbf{K}$ in Eq. (5.52) are uniformly positive definite with respect to the discretisation parameters [145, 152]. This is in some way analogous to the use of the numerical integration in the usual FEM [225, 49, 250].

Solving linear systems of equations

Following the previous sections the fully discrete forward problem in each iteration becomes a linear, symmetric, and positive definite system of equations of size $L_n \times Z$, formally written as:

$$\mathbf{K}\mathbf{v} = \mathbf{Q}. \tag{5.53}$$

Here, $\mathbf{K}$ and $\mathbf{Q}$ represent the stiffness matrix and the residual at some time step n and Newton iteration (k), respectively; and $\mathbf{v}$ denotes the unknown variable. According to the discussion given in Chapter 3 the system is well-posed in the sense of Hadamard and admits the unique solution, which, however, may be difficult to find in an efficient computational manner for high-dimensional systems. Note that the knowledge on the system matrix $\mathbf{K}$ in this case may help to design the most suitable

numerical iterative procedure. For high-dimensional systems the application of the direct method (such as the sparse Gauss elimination [101]) is robust but computationally very expensive and thus impractical. Due to this the various approaches for solving Eq. (5.53) are developed. Most of them investigate the non-zero structure of $\mathbf{K}$ as well as its local matrices $\boldsymbol{K}$ before any computation is started. Namely, the matrix $\mathbf{K}$ has the block-sparse structure by virtue of the properties of the polynomial chaos approximations and the structure of $\boldsymbol{\Delta}$, while the local matrices have the identical sparse form coming from the finite element discretisation. Besides sparsity, the participating matrices also admit the symmetry which may advocate the use of the preconditioned MINRES [231, 67, 232] or CG [76, 183, 107] procedures for solving Eq. (5.53). MINRES is applied in a case when the stiffness matrix is described as symmetric, and CG when it is symmetric and positive definite. The preconditioning is suggested due to the large conditional numbers of the stiffness matrix and faster convergence. According to [231] one may distinguish two types of preconditioners: the mean based and Kronecker tensor product preconditioners. The choice strongly depends on the existing fluctuations. For small and moderate values the mean based preconditioner $\mathbf{P} = \mathbf{I} \otimes \mathbf{K}_0$ is recommended. Otherwise, one may employ the Kronecker type of preconditoner $\mathbf{P} = \mathbf{L} \otimes \mathbf{V}$, where $\mathbf{L}$ and $\mathbf{V}$ are found by solving the optimization problem $\|\mathbf{K} - \mathbf{L} \otimes \mathbf{V}\|_F$ in Frobenous norm [231]. Note that the use of the Kronecker preconditioner may lead to longer computational time than the use of the mean based due to the additional computational time necessary to solve the optimization problem. However, in both cases the computation cost does not include the assembling of the global stiffness matrix $\mathbf{K}$. Instead in each iteration:

$$\mathbf{v}^{(i+1)} = \mathbf{v}^{(i)} + \mathbf{P}^{-1}(\mathbf{Q} - \mathbf{K}\mathbf{v}^{(i)}) \tag{5.54}$$

one computes the corresponding matrix-vector products $\boldsymbol{w}_\alpha^{(\beta),(i)} := \boldsymbol{K}^{(\alpha)}\boldsymbol{v}^{(\beta),(i)}$ of "local" stiffness matrices $\boldsymbol{K}^{(\alpha)}$ with $\boldsymbol{v}^{(\beta)}$ such that $\mathbf{v}^{(i+1)} = \mathbf{v}^{(i)} + \mathbf{d}^{(i)}$, where $\boldsymbol{d}^{(\gamma),(i)} = \boldsymbol{K}_0^{-1}\left(\boldsymbol{Q}^{(\gamma)} - \sum_{\alpha,\beta} \boldsymbol{w}_\alpha^{(\beta),(i)} \Delta_{\beta,\gamma}^{(\alpha)}\right)$ [157, 107].

Besides the Krylov sub-space methods, any other type of numerical methods for solving large systems of equations (for review see [48]) can be used. For example, some of choices are: the multi-gird approach suggested by Le Maître [140], the incomplete block-diagonal preconditioner based on the domain decomposition FETI-PD solver [79], the hierarchical approach [183], and so forth. Furthermore, one may combine the standard iterative methods with low-rank tensor decompositions as in [118, 111, 157, 19], or one may use the non-overlapping domain Schur complement based geometric decomposition with two-level scalable preconditioners [226].

Convergence

The solution of the stochastic elastoplastic problem belongs to the tensor product space $\mathscr{U} := \mathcal{U} \otimes (S)$ numerically approximated by the separate discretisation of each of the subspaces $\mathcal{U}$ and (S), respectively. The approximation in this setting is important as one may construct the suitable error estimates of the additive type. Accordingly, the total resulting error in the numerical solution of elastoplastic problem summarises the time-, spatial- and stochastic discretisation errors. The time and spatial estimates are already discussed in Eq. (4.9) and Eq. (4.54), while the stochastic error estimate is given by Céa's lemma [49] for the Hermite approximation in Gaussian random variables. Finally, what one expects is that the closure $\cup_{M,p}(S)_{J_{M,p}}$ is dense in (S) [151] such that the solution $\boldsymbol{u}_{h,M,p}$ converges according to:

$$\|\boldsymbol{u} - \boldsymbol{u}_{h,M,p}\|_{\mathscr{U}_{h,J}} \leq C \inf_{\boldsymbol{v} \in \mathscr{U}_{h,J}} \|\boldsymbol{u} - \boldsymbol{v}\|_{\mathscr{U}_{h,J}}. \tag{5.55}$$

Note that in contrast to the finite element theory the regularity of the stochastic solution is not yet known. One may only specify the convergence rates as described further in Section 6.2.2.

5.4.2 Non-intrusive Galerkin method

The analytic evaluation of the problem in Section 5.4.1 is efficient in a case of small and moderate stochastic dimensions. However, the method is built upon the polynomial chaos algebra whose accuracy strongly depends on the number of terms used in the PCE. Thus, the method is intrusive and requires the knowledge of the full model and corresponding finite element code. However, when the deterministic code is not open sourced or the implementation of the intrusive method is expensive, one may substitute the direct approach with a more practically oriented technique called the non-intrusive Galerkin method [61, 109, 244, 16, 144, 245, 5].

Similar to the fully intrusive case, the solution ansatz is taken as the Hermite polynomial chaos expansion in Gaussian random variables (see Eq. (5.4)-Eq. (5.6)), and the residual is projected in Galerkin manner onto the finite dimensional subspace $(S)_J$ according to:

$$\mathbf{Q}(\mathbf{u}) = [\ldots, \mathbb{E}(H_\alpha(\cdot)\boldsymbol{Q}(\cdot)[\sum_\alpha \boldsymbol{u}_\beta H_\beta]), \ldots] = \mathbf{0}, \tag{5.56}$$

where $\mathbf{Q}(\mathbf{u}) = (..., \boldsymbol{Q}^{(\alpha)}(\mathbf{u})^T, ...)^T$ is the block-version of the residual. Eq. (5.56) has the same form as in the fully intrusive case, see Eq. (5.11). However, the process of evaluating the integral $\mathbb{E}(H_\alpha(\cdot)\boldsymbol{Q}(\cdot)[\sum_\alpha \boldsymbol{u}_\beta H_\beta])$ is significantly different. Instead of its analytical integration with the help of the complicated functional expressions in Section 5.4.1, the integral is computed numerically with the help of the direct integration techniques [152, 107] (see Section 5.3):

$$\int_\Omega H_\alpha \boldsymbol{Q}(\omega)[\sum_\beta \boldsymbol{u}^{(\beta)} H_\beta] \, \mathrm{d}\mathbb{P}(\omega) \approx \sum_{z=1}^{N_p} w_z H_\alpha(\boldsymbol{\theta}_z)\boldsymbol{Q}(\boldsymbol{\theta}_z)[\sum_\beta \boldsymbol{u}^{(\beta)} H_\beta(\boldsymbol{\theta}_z)], \tag{5.57}$$

where

$$\Xi = \{\boldsymbol{\theta}_z, 1 \leq z \leq N_p\}, \quad \boldsymbol{\theta} = \{\theta_1, ..., \theta_M\} \tag{5.58}$$

represents the set of the integration points and $\boldsymbol{w} := \{w_z\}_{z=1}^{N_p}$ corresponding weights. Note that the evaluation of the integral requires N_p evaluations of the residual, $\boldsymbol{Q}(\boldsymbol{\theta}_z),\ z = 1, ..., N_p$, each corresponding to the numerical integration over the spatial domain $\mathcal{G} \subset \mathbb{R}^d$ done in a classical FEM way. This could be seen as an advantage compared to the intrusive Galerkin method, because the FEM code is used in a black-box fashion. On the other side, the number of calls of the deterministic software increases drastically with the stochastic dimension which may lead to expensive or almost impractical procedures.

Closest point projection

The goal of the closest point projection is to minimise the stress

$$\boldsymbol{\Sigma}_h = \underset{\boldsymbol{T}_h \in \mathscr{K}_J^\star}{\arg\min}\, \Phi_{hn}(\boldsymbol{T}_h) \tag{5.59}$$

over the discretised set $\mathscr{K}_J^\star$, the weak formulation of the convex set $\mathscr{K}_J$. As discussed in Section 5.4.1, the weak construction is necessary in order to perform the actual computation. Moreover, in order to avoid the algebraic constraints given in Eq. (5.24), here the set

$$\mathscr{K}_J^\star = \{\boldsymbol{\Sigma}_h \in \mathcal{Y}_h \otimes (S)_J : \phi(\boldsymbol{\Sigma}_h(\boldsymbol{\theta}_z)) \leq 0, \quad \forall \boldsymbol{\theta}_z \in \Xi\}. \tag{5.60}$$

is introduced as a set of constraints on a finite number of the integration points Ξ.

Algorithm 5: Non-Intrusive Stochastic Closest Point Projection

I Non-dissipative predictor

1: Initialize $j = 0, \epsilon_1, \epsilon_2, \hat{\boldsymbol{E}}^{(0)}_{p,n} = \hat{\boldsymbol{E}}_{p,n-1}, \hat{\lambda}^{(0)}_n = 0$
2: **for** Sample point $\boldsymbol{\theta}^{(i)}, i = 1, ..., N_p$ **do**
3: - Evaluate strain
4: $\Delta \boldsymbol{E}^{(j)}_{p,n}(\boldsymbol{\theta}^{(i)}) = \hat{\boldsymbol{E}}^{(j)}_{p,n}(\boldsymbol{\theta}^{(i)}) - \hat{\boldsymbol{E}}_{p,n-1}(\boldsymbol{\theta}^{(i)})$;
5: $\Delta \boldsymbol{E}^{(j)}_{e,n}(\boldsymbol{\theta}^{(i)}) = \Delta \hat{\boldsymbol{E}}_n(\boldsymbol{\theta}^{(i)}) - \Delta \boldsymbol{E}^{(j)}_{p,n}(\boldsymbol{\theta}^{(i)})$;
6: - Evaluate stress
7: $\Delta \boldsymbol{\Sigma}^{(j)}_n(\boldsymbol{\theta}^{(i)}) := \boldsymbol{C}^{(j)}_n(\boldsymbol{\theta}^{(i)}) : \Delta \boldsymbol{E}^{(j)}_{e,n}(\boldsymbol{\theta}^{(i)})$;
8: $\boldsymbol{\Sigma}^{(j)}_n(\boldsymbol{\theta}^{(i)}) := \boldsymbol{\Sigma}^{(j)}_{n-1}(\boldsymbol{\theta}^{(i)}) + \Delta \boldsymbol{\Sigma}^{(j)}_n(\boldsymbol{\theta}^{(i)})$;
9:
10: **II Dissipative corrector**
11:
12: - Compute yield function
13: $\phi^{(j)}_n(\boldsymbol{\theta}^{(i)}) = \phi(\boldsymbol{\Sigma}^{(j)}_n(\boldsymbol{\theta}^{(i)}))$;
14: - Compute residual
15: $\boldsymbol{R}^{(j)}_n(\boldsymbol{\theta}^{(i)}) = -\Delta \boldsymbol{E}^{(j)}_{p,n}(\boldsymbol{\theta}^{(i)}) + \hat{\lambda}^{(j)}_n(\boldsymbol{\theta}^{(i)}) \partial \phi^{(j)}_n(\boldsymbol{\theta}^{(i)})$;
16: - Check the yield conidition and residual:
17: - **if** $\phi^{(j)}_n(\boldsymbol{\theta}^{(i)}) < \epsilon_1$ **and** $\|\boldsymbol{R}^{(j)}_n(\boldsymbol{\theta}^{(i)})\| < \epsilon_2$ **then**;
18: the step is elastic EXIT ;
19: - **end**
20: - Compute moduli $\boldsymbol{C}^{(j)}_n(\boldsymbol{\theta}^{(i)})$ and $\boldsymbol{A}^{(j)}_{ep,n}(\boldsymbol{\theta}^{(i)})$;
21: - Solve for $\Delta \Upsilon^{(j)}_n := [\Delta \boldsymbol{E}^{(j)}_{p,n}(\boldsymbol{\theta}^{(i)}), \Delta \lambda^{(j)}_n(\boldsymbol{\theta}^{(i)})]$
22: $\boldsymbol{A}^{(j)}_{ep,n}(\boldsymbol{\theta}^{(i)}) \Delta \Upsilon^{(j)}_n(\boldsymbol{\theta}^{(i)}) = -\boldsymbol{R}^{(j)}_{ypl,n}(\boldsymbol{\theta}^{(i)})$;
23: - Update the variables
24: $\boldsymbol{E}^{(j+1)}_{p,n}(\boldsymbol{\theta}^{(i)}) = \boldsymbol{E}^{(j)}_{p,n}(\boldsymbol{\theta}^{(i)}) + \Delta \boldsymbol{E}^{(j)}_{p,n}(\boldsymbol{\theta}^{(i)})$;
25: $\lambda^{(j+1)}_n(\boldsymbol{\theta}^{(i)}) = \lambda^{(j)}_n(\boldsymbol{\theta}^{(i)}) + \Delta \lambda^{(j)}_n(\boldsymbol{\theta}^{(i)})$;
26: **end for**
27: - Project to $\hat{\boldsymbol{E}}^{(j+1)}_{p,n}$ and $\hat{\lambda}^{(j+1)}_n$
28: $(\boldsymbol{E}^{(j+1)}_{p,n})^{(\beta)} \beta! = \sum_i^{N_p} w_i \boldsymbol{E}^{(j+1)}_{p,n}(\boldsymbol{\theta}^{(i)}) H_\beta(\boldsymbol{\theta}^{(i)})$;
29: $(\lambda^{(j+1)}_n)^{(\beta)} \beta! = \sum_i^{N_p} w_i \lambda^{(j+1)}_n(\boldsymbol{\theta}^{(i)}) H_\beta(\boldsymbol{\theta}^{(i)})$;
30: set $j = j + 1$ and goto line 2.

Such construction allows the decoupling of the problem in Eq. (5.59) into N_p smaller problems, which may be solved independently. Note that each of them corresponds to the normal deterministic optimization problem as presented in [215], for which the closest point projection consists of two steps called the predictor and the corrector step, respectively. Therefore, Algorithm 5 has a very similar structure to the one given in Section 5.4.1. Moreover, from the programming point of view Algorithm 5 has a less complex structure than Algorithm 3. Namely, the most of computation is done in the existing FEM part of the code.

Briefly, the procedure in Algorithm 5 consists of point evaluations of the trial stress and the yield function in time n in a black-box manner. For each stochastic integration point the von Mises stress is investigated with respect to the yield criteria. This may lead to two possible states of the trial stress $\boldsymbol{\Sigma}^{trial}(\boldsymbol{\theta}_z)$: inside of the convex domain $\mathscr{K}_J^\star(\boldsymbol{\theta}_z)$ when the step is elastic, or outside of the set when a correction has to be introduced. The correction is obtained by solving the Lagrangian problem decoupled into N_p smaller problems [4]:

$$\mathcal{L}(\boldsymbol{\theta}_z) = \Phi(\boldsymbol{\theta}_z) + \lambda(\boldsymbol{\theta}_z)\phi(\boldsymbol{\theta}_z), \quad \boldsymbol{\theta}_z \in \Xi, \tag{5.61}$$

for which the optimality conditions read $\partial_{\boldsymbol{\Sigma}}\mathcal{L}(\boldsymbol{\theta}_z) = \mathbf{0}$. The corresponding system of equations is then point-wise solved for each $\lambda(\boldsymbol{\theta}_z)$ by deterministic solver. In this way the update of the variables from the state $n-1$ to state n is numerically performed (see Algorithm 5).

5.5 Stochastic collocation

The stochastic collocation approach can be broadly classified into: interpolation and regression techniques. The basic idea of interpolation is to find the polynomial $\boldsymbol{u}(\boldsymbol{\theta})$ such that

$$\boldsymbol{u}(\boldsymbol{\theta}_z) = \boldsymbol{u}_z \tag{5.62}$$

for a set of points $\Xi = \{\boldsymbol{\theta}_z\}_{z=1}^{L}$. In other words, each RV $\boldsymbol{u}(\omega) = [u_1(\omega), \ldots, u_{L_N}(\omega)]^T$ that belongs to the space of RVs with finite variance $L_2(\Omega)$ can be approximated by a polynomial function (PCE)

$$\hat{\boldsymbol{u}}(\boldsymbol{\theta}) = \sum_{\alpha \in \mathcal{J}_Z} \boldsymbol{u}^{(\alpha)} \Psi_\alpha(\boldsymbol{\theta}) \tag{5.63}$$

[4] N_p is the number of samples

in a finite dimensional subspace $(S)_{\mathcal{J}}$ spanned by the multi-dimensional interpolating polynomials $\{\Psi_\alpha\}_{\alpha\in\mathcal{J}_Z}$ of high degree [244, 16]. Once the approximation is prescribed, one may compute PCE coefficients from a given data set $\{\boldsymbol{u}_z\}_{z=1}^{L}$ by solving

$$\hat{\boldsymbol{u}}(\boldsymbol{\theta}_z) = \boldsymbol{u}_z, \tag{5.64}$$

i.e. the linear system of equations

$$\mathbf{V}\mathbf{u} = \mathbf{v} \tag{5.65}$$

where

$$\mathbf{V} := [\Psi_{\alpha,z}] = \begin{bmatrix} \Psi_1(\boldsymbol{\theta}_1) & \Psi_2(\boldsymbol{\theta}_1) & \cdots & \Psi_Z(\boldsymbol{\theta}_1) \\ \Psi_1(\boldsymbol{\theta}_2) & \Psi_2(\boldsymbol{\theta}_2) & \cdots & \Psi_Z(\boldsymbol{\theta}_2) \\ \vdots & \vdots & \ddots & \vdots \\ \Psi_1(\boldsymbol{\theta}_L) & \Psi_2(\boldsymbol{\theta}_L) & \cdots & \Psi_Z(\boldsymbol{\theta}_L) \end{bmatrix} \in \mathbb{R}^{L\times Z} \tag{5.66}$$

is the Vandermode-like matrix of coefficients, and

$$\mathbf{u} := [\boldsymbol{u}_1, \ldots, \boldsymbol{u}_Z]^T, \tag{5.67}$$

$$\mathbf{v} := [\boldsymbol{u}_1, ..., \boldsymbol{u}_L]^T \tag{5.68}$$

are the unknown PCE coefficients and sample values, respectively. The system in Eq. (5.65) further can be solved by some of existing methods for solving linear system of equations.

On the other side, the regression approach searches for the function that minimises some cost, usually the mean square error. In this particular case, the goal of regression is to find the multivariate polynomial expansion which fits the data by minimising the following error in each FEM point [242]:

$$\min_{\hat{\boldsymbol{u}}\in(S)_{\mathcal{J}}} \epsilon \quad = \quad \min_{\hat{\boldsymbol{u}}\in(S)_{\mathcal{J}}} \int_\Omega \left[\boldsymbol{u}(\omega) - \hat{\boldsymbol{u}}(\omega)\right]^2 \mathbb{P}(\mathrm{d}\omega), \tag{5.69}$$

where $\hat{\boldsymbol{u}}(\omega)$ denotes the polynomial approximation of the solution. As the distance squared is minimised, this computes the orthogonal projection in the corresponding inner product. The function $\hat{\boldsymbol{u}}$ approximates the solution by a finite number of uncorrelated and independent RVs $\boldsymbol{\theta} := \{\theta_j\}_{j=1}^{M}$, and hence the integration in Eq. (5.69) may be evaluated numerically (see Section 5.3):

$$\min_{\hat{\boldsymbol{u}}\in(S)_{\mathcal{J}}} \hat{\epsilon} = \min_{\hat{\boldsymbol{u}}\in(S)_{\mathcal{J}}} \sum_{z=1}^{L} \left[\boldsymbol{u}(\boldsymbol{\theta}_z) - \sum_\alpha \boldsymbol{u}^{(\alpha)}\Psi_\alpha(\boldsymbol{\theta}_z)\right]^2 w(\boldsymbol{\theta}_z). \tag{5.70}$$

Further on, the solution of Eq. (5.70) can be found from the optimality condition:

$$\mathbf{u} := (\boldsymbol{u}^{(\alpha)})_{\alpha\in\mathcal{J}} \in \partial_{\boldsymbol{u}^{(\alpha)}}\hat{\epsilon} = \mathbf{0}, \tag{5.71}$$

which in component form becomes:

$$\sum_{\beta}\sum_{\alpha}\sum_{z=1}^{L}\boldsymbol{u}^{(\alpha)}\Psi_{\alpha}(\boldsymbol{\theta}_z)\Psi_{\beta}(\boldsymbol{\theta}_z)w_z = \sum_{\beta}\sum_{z=1}^{L}\boldsymbol{u}_z\Psi_{\beta}(\boldsymbol{\theta}_z)w_z, \tag{5.72}$$

where $w_z := w(\boldsymbol{\theta}_z)$ denote the integration weights and $\boldsymbol{u}_z := \boldsymbol{u}(\boldsymbol{\theta}_z)$ the sample points. In matrix notation the previous equation reduces to:

$$\begin{aligned}\mathbf{J}\mathbf{u} &:= \mathbf{H}^T\mathbf{W}\mathbf{H}\mathbf{u}\\ &= \mathbf{H}^T\mathbf{W}\mathbf{v},\end{aligned} \tag{5.73}$$

where $\mathbf{J}$ is the Gram matrix, $\mathbf{u}$ and $\mathbf{v}$ have same meaning as before, and

$$\mathbf{H} := [\Psi_{\alpha}(\boldsymbol{\theta}_z)] \in \mathbb{R}^{L\times Z}, \tag{5.74}$$

$$\mathbf{W} := \operatorname{diag}[w_k] \in \mathbb{R}^{L\times L}. \tag{5.75}$$

In previous equations the data set $\mathbf{u}$ is computed by solving the deterministic residual equation at each independent grid point $\boldsymbol{\theta}_z$. This means that the collocation approach already decouples the system into L smaller independent systems of equations before the linear system is solved. These solutions are obtained by available deterministic solvers, while the solution of the linear system is computed using the Krylov preconditioned techniques or any other type of methods for large systems of linear equations.

The displacement $\boldsymbol{u}$ is not the only solution one wants to have information about, but also about stress, elastic and plastic strain, etc. The process of their computing is greatly similar to Eq. (5.73). Formally one may write:

$$\begin{aligned}\mathbf{J}\boldsymbol{\sigma}_b &= \mathbf{H}^T\mathbf{W}\mathbf{H}\hat{\boldsymbol{\sigma}}_b\\ &= \mathbf{H}^T\mathbf{W}\boldsymbol{\tau}_b,\end{aligned} \tag{5.76}$$

where $\boldsymbol{\sigma}_b$ is the unknown block-vector of PCE coefficients of the stress, $\boldsymbol{\tau}_b := [\boldsymbol{\sigma}_z]^T \in \mathbb{R}^L$ is the vector consisting of the FEM integrated stresses $\boldsymbol{\sigma}_z$ in each collocation point $\boldsymbol{\theta}_z$, and $\mathbf{H}$ is of the same meaning as in Eq. (5.73). The stress $\boldsymbol{\sigma}_z$ is obtained by solving the corresponding deterministic minimisation problem Eq. (5.59) in each $\boldsymbol{\theta}_z$, which corresponds to the closest point projection algorithm as described

in Section 5.4.2. Similar is valid for the plastic or elastic strain.

Finally, the greatest difference between the non-intrusive Galerkin and the interpolation approach lies in the way of computing the corresponding polynomial chaos coefficients. In the latter case one uses interpolation to fit the polynomial chaos expansion to the data set obtained by sampling, while the non-intrusive Galerkin projects the residual error onto the subspace spanned by orthogonal Hermite polynomials and computes the corresponding expectation by sampling. The linearised system is then further solved in a classic "intrusive way".

5.5.1 Convergence

The full tensor product convergence results are studied in ([16]), while the sparse tensor product convergence results for the isotropic and anisotropic Smolyak method can be found in [172] and [171], respectively. According to this, an isotropic full tensor product interpolation with Clenshaw-Curtis abscissas converges with rate $C(\sigma, M)\exp(-\sigma p)$, where σ describes the analyticity of a solution, M denotes the number of RVs, and p the polynomial order. Another expression for the same convergence rate can be given in terms of the number of collocation points L, i.e. $C(\sigma, M)L^{-\sigma/M}$ [172]. Obviously the rate increases with L, and thus the full tensor grid interpolation is rarely used in practice. Practically more suitable Smolayk interpolation has a much better performance advocated by convergence rate $\mathcal{O}(\sigma/\log(2M))$ for Clenshaw-Curtis and $\mathcal{O}(\sigma/\log M)$ for Gaussian abscissas.

5.6 Adaptivity

The stochastic Galerkin and non-intrusive Galerkin methods face the problem of resolving a huge amount of equations for which the computational cost grows with the number of deterministic as well as stochastic dimensions. In order to afford the computation in real time one has to study the sparsity structure of the solution with respect to which possible reduction techniques shall be designed. As the solution belongs to the space $\mathcal{Z} \otimes (S)$ obtained as a tensorial product of the deterministic $\mathcal{Z}$ and stochastic (S) spaces, one may try to cut down the computational cost by reducing or reformulating the basis in both of mentioned spaces. In this way one may search for the optimal subspace $\mathscr{Z}_o \subset \mathcal{Z} \otimes (S)$ with the help of the prior or posterior error estimates.

The system in Eq. (5.52) immediately reduces if one succeeds to find the most suitable basis for the discretisation of the deterministic space $\mathcal{Z}$. In such a situation the computational effort for both, the Galerkin based methods and sampling techniques, reduces. Furthermore, by choosing the appropriate stochastic basis with respect to the probability distribution of the base RV the system in Eq. (5.52) admits sparse form. Both mentioned alternatives are exploited in stochastic multi-element or multi-wavelet techniques [141]. Another possibility would be to compute the solution of the problem on the coarse mesh, to decompose it in a KLE manner, and further to apply it on the fine mesh [60].

In recent years several approaches for the reduction of the stochastic space have appeared. Most of them exploit the structure of the solution using the a priori estimates or indicators, while others try to find the optimal subspace already during the process of solving—on the run. For example, one may show that the solution of the stochastic linear elliptic PDE admits sparse form after some appropriate conditions have been fulfilled [230]. Moreover, the mentioned non-zero structure can be discovered by studying the so-called zero-dimensional stochastic problem [27], which corresponds to the Galerkin solution of the PDE for one stochastic degree of freedom. Another approach is to use the variational low-rank approach with the successive rank-one update based on the minimum energy principle [119]. In this case the reduction of the basis is done with respect to the a posteriori error indicator given in terms of the suitable residual norm. By adding new terms of PCE one may immediately quantify its influence on the solution. The residual type of the estimate is also fundamental for the method published in [164, 165]. The basic idea behind the method lies in the singular value decomposition of the solution which further transforms the large linear system Eq. (5.52) into a much smaller nonlinear one. Moreover, one may compress the solution in a low-rank tensor product format [156, 157] and keep it as such during the computation, thereby not only reducing the amount of data to be handled but also the computational cost. Such representation can be found adaptively during the solution process by alternating iteration and compression with the help of the truncated singular value decomposition (SVD). A similar approach, though not exactly adaptive, is to use the alternating least-squares algorithm (ALS) for the separated representation of the solution with the low rank [61]. In this way all d-dimensional algebraic operations transform to much cheaper one dimensional operations.

Besides the reduction of Eq. (5.52), one may try to reduce the initialy nonlinear system by optimizing it with respect to the equations, and not to the solution [174, 173]—the generalised spectral decomposition approach. This method relies on solving the eigen-like problems by one of two basic ad-hoc algorithms: the basic power type or the improved power type method.

5.7 Conclusion

The present work develops numerical techniques for the solution of the problem of infinitesimal and finite J_2 elastoplasticity described by uncertain parameters. Starting with the approximation techniques such as the Karhunen Loève and polynomial chaos expansions the intrusive and non-intrusive numerical methods are proposed. Their efficiency strongly depends on the approximation properties of the ansatz spaces and the stochastic regularity of the response.

In order to compute the functional of the solution, three different numerical techniques are proposed: the first based on the direct integration, the second employing the properties of the Galerkin projection, and the third done in a full collocation manner. With respect to the use of the deterministic solver all mentioned approaches are classified into intrusive and non-intrusive methods. The former do not use the deterministic solver (FEM code) in a "black box" manner. Instead, the deterministic solver is adopted to work with new kinds of variables. On the other side, the non-intrusive approaches, such as direct integration and collocation, allow the use of the FEM code as delivered by companies. This is an important advantage. However, with respect to the computation time those methods are not very favourable.

To handle the discretised stochastic evolution law, a stochastic closest point projection algorithm is introduced. The method minimises the energy functional in a purely algebraic manner via polynomial chaos algebra. In such a setting the algorithm efficiency as well as accuracy are highly affected by the choice of the ansatz spaces, as well as the approximation of the input material uncertainties. For later comparison purposes, the projection algorithm is also constructed in a sampling (non-intrusive) setting. Its difference to the direct intrusive procedure lies in the approximation of the convex domain and the way of computing the residual. Namely, the direct approach computes the integrals over the probability space in purely algebraic way; and functionally approximates the random inequalities via Markov, Chebyshev or other kinds of probability estimates. In contrast to this, the samling non-intrusive approach weakly decouples the variational inequality on a set of integration points with the help of pseudo-Galerkin projection or the least square estimate.

Finally, as PCE oriented approaches both the stochastic Galerkin and collocation method greatly depend on the regularity of the solution, and their convergence rates strongly relate to the number of random variables and polynomial order.

Chapter 6

Polynomial chaos algebra

One person's constant is another person's variable.

S. Gerhart

In order to simplify the analysis of a complex random problem one may try to express the uncertain solution in some system of idealised elementary random variables—the technique called the "white noise analysis"—as already discussed in Chapter 5. The basis is usually chosen with respect to the probability distribution of the involved random quantities, for example the Hermite polynomial basis is used for the approximation of the lognormally distributed random fields, see Chapter 5. According to this, the chapter studies the idea of the polynomial chaos expansion and corresponding algebra in detail. This will hopefully give a more detailed description of the numerical methods presented in Section 5.4.1.

The chapter is organized as follows: in Section 6.1 and Section 6.2 are given short definitions of the white noise and the polynomial chaos expansion together with its numerical computation. Furthermore, the elemental and nonlinear operations on random variables, as well as their numerical computations are studied in Section 6.3. This is then generalised to the algebra of the matrix-valued random variables used in the package PLASTON (see Chapter 7). For most of operations small numerical examples are provided. They may further help to understand the study of the accuracy and computation cost of the numerical algorithms presented in Chapter 8.

6.1 White noise analysis

A random field may be interpreted in two ways: as a mapping $\omega \to \kappa(\cdot, \omega),\ \omega \in \Omega$, known as the distribution-valued random field, or the function $x \to \kappa(x, \cdot),\ x \in \mathbb{R}^d$ in the suitable space of the stochastic distributions. If the random variables constructing the field are of the square integrable type then this space is known as a Schwartz space S, otherwise, in a more general case, Hida and Kondratiev space [96, 98]. This further means that the random field definition given in Section 3 is not general enough. Hence, its application in some specific cases such as the white noise problem is not possible at all. Therefore, a more general definition has to be introduced.

Let $S(\mathbb{R}^d)$ be a Schwartz space of all infinitely differentiable real functions $f(x), x \in \mathbb{R}^d$ on a d-dimensional Euclidean space $\mathbb{R}^d$ [58] decreasing at infinity, together with all their derivatives, more rapidly than any negative power $|x|^{-k},\ k = \{1, 2, ...\}$. This space is a Fréchet space under the family of seminorms:

$$\|f\|_{k,\alpha} = \sup\{(1 + |x|^k)|\partial^\alpha f(x)|\}, \tag{6.1}$$

where k represents integer [98] and $\alpha := (\alpha_1, \alpha_2, ..\alpha_n)$ the multi-index set of non-negative integers such that $|\alpha| = \alpha_1 + \alpha_2 + ... + \alpha_d$ and $\partial^\alpha f = \partial^{|\alpha|} f / \partial x_1^{\alpha_1} \partial x_2^{\alpha_2} ... \partial x_d^{\alpha_d}$ with an obvious modification when some $\alpha_i = 0,\ i = \{1, ..., d\}$. In this topology $S(\mathbb{R}^d)$ is a locally convex nuclear space. The dual space of $S(\mathbb{R}^d)$ is the space $S'(\mathbb{R}^d)$ of all real linear continuous functionals on $S(\mathbb{R}^d)$ equipped with a weak topology. The elements of the space $S'(\mathbb{R}^d)$ are said to be the real tempered generalised functions (distributions), which, taken for the realisations of the random variables, are called the generalised random field.

With previous definitions of the Schwartz space one may identify the probability space with the triple $(S'(\mathbb{R}^d), \mathcal{B}, \mathbb{P}_\gamma)$, where $\mathcal{B}$ represents the family of the Borel subsets of $S'(\mathbb{R}^d)$ and $\mathbb{P}_\gamma$ the *white noise* (or the normalized Gaussian) measure specified by a Bochner-Minlos theorem. The theorem states the existence of a unique probability measure $\mathbb{P}_\gamma$ on $\mathcal{B}(S'(\mathbb{R}^d))$ with the following property [58]:

$$\mathbb{E}[e^{i(\cdot,\phi)}] = \int_{S'} e^{i<\omega,\phi>}\, \mathrm{d}\mathbb{P}_\gamma(\omega) = e^{-\frac{1}{2}\|\phi\|^2} \tag{6.2}$$

for all $\phi \in S(\mathbb{R}^d)$, where $\|\phi\|^2 = \|\phi\|^2_{L^2(\mathbb{R}^d)}$. Here, $< \omega, \phi >= \omega(\phi)$ represents the action of $\omega \in S'(\mathbb{R}^d)$ on $\phi \in S(\mathbb{R}^d)$. Following this, for any $\varphi \in S(\mathbb{R}^d)$ the random variable $\langle \cdot, \varphi \rangle : L_2(\mathbb{R}^d) \mapsto S'(\mathbb{R}^d)$ is normally distributed with the zero mean and the variance equal to $\|\varphi\|^2$. According to these definitions, the

triplet $(S'(\mathbb{R}^d), \mathcal{B}(S'(\mathbb{R}^d)), \mathbb{P}_\gamma)$ becomes the one-dimensional white noise probability space corresponding to the one dimensional white noise:

$$w : S(\mathbb{R}^d) \times S'(\mathbb{R}^d) \to \mathbb{R}. \tag{6.3}$$

Similarly, the triplet $(S', \mathcal{B}, \mathbb{P}_\gamma)$ becomes the multidimensional space with $S := \prod_{i=1}^m S(\mathbb{R}^d)$, $S' := \prod_{i=1}^m S'(\mathbb{R}^d), \mathcal{B} := \prod_{i=1}^m \mathcal{B}(S'(\mathbb{R}^d))$ and $\mathbb{P}_\gamma^m = \mathbb{P}_\gamma \times \mathbb{P}_\gamma \times ... \times \mathbb{P}_\gamma$ to which corresponds the multi-dimensional case of the white noise

$$w : S \times S' \to \mathbb{R}^m. \tag{6.4}$$

6.2 Decomposition by homogeneous chaos

Following the previous section, the space $L_2(S'(\mathbb{R}^d), \mathcal{B}, \mathbb{P}_\gamma)) =: L_2(\Omega, \mathcal{B}, \mathbb{P})$ can be directly decomposed to a so-called *homogeneous chaos* (Wiener's polynomial chaos, the Wiener chaos, or the Wiener Ito Chaos) introduced by Wiener [238] and proved by Segal [207]. Note that the word "chaos" has nothing to do with the modern term "chaos" in mathematics where it characterizes the unpredictable behaviour of dynamical systems. Formally, the polynomial chaos can be seen as a functional approximation of a given random variable [149, 151]. Its definition starts with the Hilbert space Θ (see Chapter 3) and the family of the multivariate polynomials $X(\theta_1, \theta_2, .., \theta_m)$ up to order p:

$$\mathcal{P}_p := \{X(\theta_1, \theta_2, .., \theta_m), X \text{ is a polynomial of degree } p, m < \infty\}, \tag{6.5}$$

where $\theta_1, \theta_2, .., \theta_m$ are orthonormal RVs belonging to Θ. Following this, a homogeneous chaos of order p represents a vector space $\mathcal{H}_p$ given as:

$$\mathcal{H}_p := \bar{\mathcal{P}}_p \ominus \bar{\mathcal{P}}_{p-1}, \quad p \in \mathbb{N}, \tag{6.6}$$

with $\bar{\mathcal{P}}_p$ being the closure of the linear space $\mathcal{P}_p$ in $L_2(\Omega, \mathcal{B}, \mathbb{P})$. In addition, the vector space $\mathcal{H}_p$ generates the polynomial chaos $\mathcal{H}_{\leq p} = \bigcup_{i=0}^p \mathcal{H}_p$ such that L_2 can be orthogonally decomposed [96] to

$$L_2(\Omega, \mathcal{B}(\Theta), \mathbb{P}) := \bigoplus_{p=0}^{\infty} \mathcal{H}_p, \tag{6.7}$$

where the space of polynomials $\mathcal{P}(\Theta) = \cup_o^\infty \mathcal{P}_p(\Theta)$ is dense in $L_p(\Omega, \mathcal{B}(\Theta), \mathbb{P})$ [102]. As the RVs $\{\theta_i\}_{i=1}^\infty$ are problem specified, the orthogonal polynomials in

Table 6.1: The Wiener-Askey Chaos table

Type	RV $\xi(\omega)$	Basis $X(\xi)$	Support
Continuous	Gaussian	Hermite	$\{-\infty, \infty\}$
	Gamma	Laguerre	$[0, \infty\}$
	Beta	Jacobi	$[a, b]$
	Uniform	Legendre	$[a, b]$
Discrete	Poisson	Charlier	$\{0, 1, 2, ...\}$
	Binomial	Krawtchouk	$\{0, 1, ..., N\}$
	Negative Binomial	Meixner	$\{0, 1, 2, ..\}$
	Hypergeometric	Hahn	$\{0, 1, ..., N\}$

Eq. (6.5) are chosen in such a way that their weight function in the orthogonality relation has the same form as the probability distribution function of the underlying random variables. In case of Gaussian random varaibles that means that the polynomials are Hermitain as the weighting function of m-dimensional Hermite polynomial is the same as the probability density function of the m-dimensional Gaussian random variable. Following this, each function κ in the Gaussian Hilbert space $L_2(\Omega, \mathcal{B}(\Theta), \mathbb{P})$ obtains a unique representation:

$$\kappa(\omega) = \sum_{\alpha \in \mathcal{J}} \kappa_\alpha H_\alpha(\omega), \tag{6.8}$$

where the multivariate polynomials $H_\alpha(\omega)$ are given via the product of the corresponding univariate Hermite polynomials $h_{\alpha_j}(\theta_j)$ [150]:

$$H_\alpha(\boldsymbol{\theta}) := \prod_{j \in \mathbb{N}} h_{\alpha_j}(\theta_j), \tag{6.9}$$

and the orthogonality relation:

$$\mathbb{E}(H_\alpha H_\beta) = \alpha! \delta_{\alpha\beta}, \text{ with } \|H_\alpha\|_{L_2}^2 = \alpha!. \tag{6.10}$$

Here, $\alpha := (\alpha_i)_{i \in \mathcal{J}}$ and similarly β denote the multi-indices, i.e. the sequence of non-negative integers with only finitely many non-zero elements:

$$\alpha = (\alpha_1, ..., \alpha_j, ...) \in \mathcal{J} := \mathbb{N}_0^{(\mathbb{N})} \tag{6.11}$$

for which $|\alpha| := \sum_{j=1}^{\infty} \alpha_j$ and $\alpha! := \prod_{j=1}^{\infty} \alpha_j!$. The length of the multi-index is the largest $j \in \mathbb{N}$ for which $\alpha > 0$. Even though in this work the basis is chosen to be Hermitian, see Eq. (6.8), other possible choices do exist and hence the polynomial expansion may be generalised to:

$$\kappa(\omega) = \sum_{\mathcal{J}} \kappa^{(\alpha)} X_\alpha(\xi(\omega)), \tag{6.12}$$

where X_α denotes the generalised basis and $\xi(\omega)$ corresponding RVs [248, 244]. For example, the density result similar to Gaussian random variables may be achieved by Possion random variables and the corresponding orthogonal Charlier polynomials. The choice of the suitable CONS depends mostly on the type of the problem one is solving as shown in Table 6.1.

According to Cameron and Martin [37] and later Xiu [248, 244], an expansion as given in Eq. (6.8) or Eq. (6.12) converges in the L_2 sense for any arbitrary stochastic process with the finite second moment. This requirement means that the L_2 norm of Eq. (6.8)

$$\|\kappa\|_{L_2}^2 = \sum_{\alpha \in \mathcal{J}} \kappa_\alpha^2 \alpha!, \quad \kappa_\alpha^2 = \langle \kappa_\alpha | \kappa_\alpha \rangle, \tag{6.13}$$

satisfies the growth condition $\sum_\alpha \alpha! \kappa_\alpha^2 < \infty$ [98]. Note that this condition may be posed in a slightly different way. However, in such a case one requires the definition of more generalised stochastic test function spaces and the spaces of the stochastic distributions called Kondratiev spaces. For more information please see [98].

6.2.1 Estimation of PCE coefficients

The number of terms (also known as the cardinality of the index set $\mathcal{J}_\mathcal{Z}$) of the p-th order Hermite polynomial expansion in M Gaussian RVs is determined by

$$Z := \begin{pmatrix} M+p \\ M \end{pmatrix} = \frac{(M+p)!}{M!p!} \tag{6.14}$$

and grows rapidly with the polynomial degree, see Fig. 6.1. Note that if PCE terms are not chosen in an addaptive manner as presented in Section 5.6, the polynomial chaos approximation may become computationally hard for large M. Since this issue has been already addresed before (see Section 5.6), the following text will consider only the estimation of PCE coefficients without any further introduction of adaptive techniques.

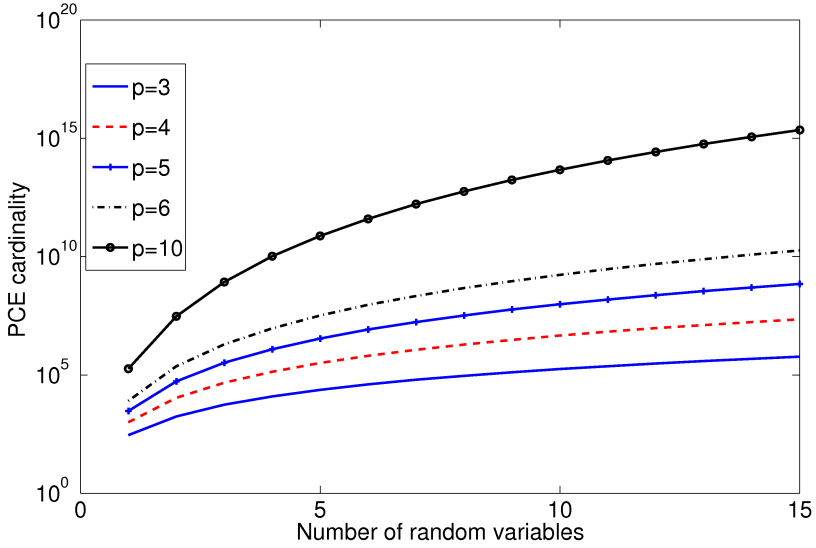

Figure 6.1: The number of terms of PCE as a function of the number of random variables and polynomial degree

For a given orthonormal basis $\boldsymbol{\theta} := \{\theta_i\}_{i=1}^{\infty}$ of Θ and the function $\kappa \in L_2(\Omega, \Sigma(\theta), \mathbb{P})$ of Gaussian RV $\boldsymbol{\theta}$, the expansion in Eq. (6.8) can be evaluated with the help of the Galerkin projection:

$$\forall \alpha \in \mathcal{J}: \quad \kappa^{(\alpha)} = \mathbb{E}(\kappa(\cdot)H_\alpha(\cdot))/\langle H_\alpha | H_\alpha \rangle = \frac{1}{\alpha!}\mathbb{E}(\kappa(\cdot)H_\alpha(\cdot)) \tag{6.15}$$

i.e. the high-dimensional integration. The integral in Eq. (6.15) can be estimated

Table 6.2: The approximation of lognormal RV ξ with the order of polynomial

Order	Error	PCV
1	19.1%	[3.7434 2.9947]
2	4.70%	[3.7434 2.9947 1.1979]
3	0.89%	[3.7434 2.9947 1.1979 0.3194]
4	0.12%	[3.7434 2.9947 1.1979 0.3194 0.0639]
5	0%	[3.7434 2.9947 1.1979 0.3194 0.0639 0.0102]

in both numerical and analytical ways. The analytical computation is only possible

when the function $\kappa(\theta)$ is smooth enough, i.e. if all partial derivatives of κ belong to L_2. In such a case the coefficients $\kappa^{(\alpha)}$ follow from the differentiation rule:

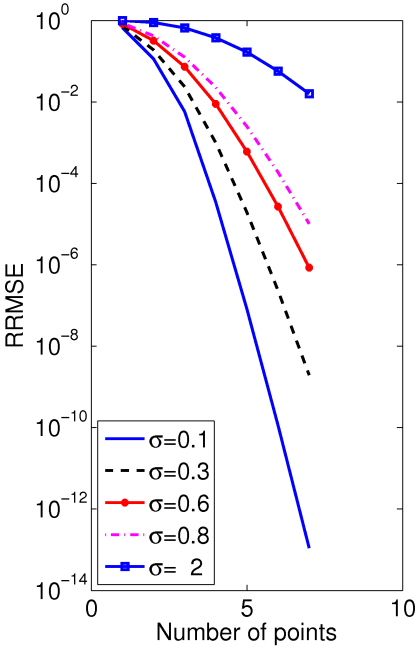

Figure 6.2: Convergence of the PCE of lognormal RV obtained by Gauss-Hermite quadrature for different values of the standard deviation σ of base Gaussian RV

$$\kappa^{(\alpha)} = (\alpha!)^{-1}\mathbb{E}(\mathrm{D}^{(\alpha)}\kappa), \tag{6.16}$$

where $\mathrm{D}^{(\alpha)}$ is the partial derivative with respect to the multi-index [107]. For example, the coefficients of the lognormal random variable $\kappa = \exp(\mu + \sigma\theta)$ are given as:

$$\kappa^{(\alpha)} = \frac{1}{\alpha!}\sigma^{\alpha}\mathbb{E}(e^{\mu+\sigma\theta}) = \frac{1}{\alpha!}\sigma^{\alpha}e^{\mu_\theta+\frac{1}{2}\sigma_\theta^2}. \tag{6.17}$$

On the other side, the numerical integration can be performed in a way as described in Section 5.3. This is usually done when the function is not smooth enough or the partial derivatives are too complicated.

Example 6.2.1. *The accuracy of the polynomial chaos approximation of the lognor-*

mal random variable $\xi = \exp(1 + 0.8\theta)$ analyticaly expanded in PCE of order 1 up to 5 is estimated with respect to the true value, see Eq. (6.16). According to Table 6.2 the relative root mean square error (RRMSE)

$$\epsilon_{rms} = \frac{\sqrt{\sum_{\alpha \in \mathcal{J}_M} [(\kappa_{IR}^{(\alpha)} - \kappa_{AN}^{(\alpha)}]^2 \alpha!}}{\sqrt{\sum_{\alpha \in \mathcal{J}_Z} [(\kappa_{AN}^{(\alpha)}]^2 \alpha!}} \tag{6.18}$$

decreases with the number of terms in PCE. In Eq. (6.18) the index $_{IR}$ denotes the PCE of the current order and $_{AN}$ the true value of the variable. Note that this error measure considers only $p + 1$ lowest order modes [56], and hence evaluates the accuracy of the PCE within the space covered by basis functions up to order p. Besides the analytical method, one may compute the coefficients of PCE numerically by Gauss-Hermite (GH) quadrature rule. Fig. 6.2 shows that GH for PCE of order 5 has monotonic convergence and requires very few functional evaluations. However, the number of necessary evaluations (i.e. sample points) strongly depends on the input variance and grows with its increase.

6.2.2 PCE convergence

In contrast to deterministic the stochastic regularity is not yet completely investigated. The rates of the optimal approximation are known [23, 38] although in norms of stochastic distribution spaces [96] weaker than $L_2(\Omega)$ norm. The error estimate is provided by Benth and Gjerde [23] and further improved by Cao et al. [38]. The latter error estimate prognoses the error:

$$\|\xi - \hat{\xi}\|_{S^{(\rho,-q,\mathcal{V})}} \leq \|\xi\|_{S^{(\rho,-q+d,\mathcal{V})}} \sqrt{C_1(d) M^{1-d} + C_2(d) 2^{-dp}}, \tag{6.19}$$

valid for the generalised random variable $\xi \in (S)^{(\rho,-q+d,\mathcal{V})}$ with $q > 0$, $d > 1$. Here, $S^{(\rho,-q,\mathcal{V})}$ is the stochastic analogue of the spatial Sobolev space as described in [96], and the terms $C_1(d)$ and $C_2(d)$ are functions of $w = 1/(1-d)$ and $s = d-1$, respectively, such that $C_1(d) = \exp(2w)dw$ and $C_2(d) = \exp((s2^s)^{-1})(2^{-s-1}w)$. From previous expression one may conclude that the convergence is exponential in p and algebraic in M. This means that the error reduces with the increase of both the maximum stochastic dimension M and the polynomial degree p.

6.3 Polynomial chaos algebra

The representation of the random variable in a form of polynomial chaos expansion allows us to use the algebra of RVs as primitive objects in stochastic calculations, see Chapter 5 for example. Note that some of existing publications (e.g. [56, 140]) are already discussing this topic, but only in its basic form. In order to provide a deeper understanding of the problem this work offers the detailed study of the linear and nonlinear PCE algebra. In this regard the section uses unified notation $\xi \in L_2(\Omega, \mathbb{R})$ for a scalar-valued RV and

$$\hat{\xi}(\boldsymbol{\theta}) = \sum_{\alpha \in \mathcal{J}_{\mathcal{Z}}} \xi^{(\alpha)} H_\alpha(\boldsymbol{\theta}) \tag{6.20}$$

for its corresponding projection onto the Hermitian basis (i.e. approximation), also called the *polynomial chaos variable* (PCV).

6.3.1 Elementary operations on scalar valued RVs

The algebra of RVs represents a collection of operations such as addition, subtraction, multiplication and division with the same priority as in the algebra of real numbers. Elementary operations play a crucial role in defining more complex operations such as inverse, square root, etc. However, in contrast to real numbers, RV arithmetics is not an easy task. The difficulties are reflected in the choice of suitable algorithms and their convergence in terms of existing polynomial chaos approximations.

Addition: Let be given two RVs ξ_1 and ξ_2 in $L_2(\Omega, \mathbb{R})$ with the corresponding Hermite transform:

$$\mathscr{H}(\xi_i) = (\xi_i^{(\alpha)})_{\alpha \in \mathcal{J}} =: (\xi_i), \quad i = 1, 2 \tag{6.21}$$

and finite projections $\hat{\xi}_1$ and $\hat{\xi}_2$ belonging to the subspace spanned by the Hermite polynomials $\mathcal{P} := \text{span}\{H_\alpha, \alpha \in \mathcal{J}_{\mathcal{Z}}\}$. Here, $\mathscr{H}(\xi_i)$ denotes the Hermite transform, i.e. a linear (unitary) transformation compatible with addition and scalar multiplication:

$$\mathscr{H}(\xi_1 \pm \xi_2) = \mathscr{H}(\xi_1) \pm \mathscr{H}(\xi_2), \quad \mathscr{H}(c\xi_1) = c\mathscr{H}(\xi_1) \tag{6.22}$$

for any RVs ξ_1 and ξ_2 in $L_2(\Omega, \mathbb{R})$ and a scalar c [150, 151, 192].

Following preceding definitions, one may define addition as operation of adding two sequences of coefficients, i.e. polynomial approximations $\hat{\xi}_1$ and $\hat{\xi}_2$. The operation

is commutative, associative and characterised by a neutral (identity) element $\check{\xi}$. The neutral element is a constant function $\check{\xi} : \omega \mapsto 0$ (described by a Hermite transform $(0, 0, ...0)$) such that when added to any arbitrarly chosen RV $\hat{\xi}_1$, the RV $\hat{\xi}_1$ does not change. In other words, $\mathscr{H}(\check{\xi} + \xi_1) = \mathscr{H}(\xi_1)$ for all $\xi_1 \in L_2(\Omega, \mathbb{R})$.

Multiplication. The product of two RVs lies in a bigger subspace than the terms entering the multiplication. This further means that the PCE cardinality of the product increases with every new multiplication. However, this issue can be resolved with the help of Cameron-Martin theorem [37] and properties of the polynomial chaos representation. Namely, the dimension of the product of two random variables ξ_1 (i.e. $\hat{\xi}_1$) and ξ_2 (i.e. $\hat{\xi}_2$) can be reduced by a Galerkin projection onto the Hermite basis [56], i.e.

$$\xi_3^{(\gamma)} = \frac{1}{\gamma!}\mathbb{E}(\xi_3 H_\gamma) = \mathbb{E}(\xi_1 \cdot \xi_2 H_\gamma) = \sum_{\alpha\in\mathcal{J}} \sum_{\beta\in\mathcal{J}} \xi_1^{(\alpha)} \xi_2^{(\beta)} c_{\alpha\beta}^{\gamma}, \tag{6.23}$$

where $c_{\alpha\beta}^{\gamma} = \mathbb{E}(H_\alpha H_\beta H_\gamma)/\gamma!$ [150] represents the element of the three dimensional tensor. More formally, the operation of multiplication represents the Hermite transform:

$$\mathscr{H}(\xi_3) = \left((\xi_1) Q_2^{\gamma} (\xi_2)^T)\right)_{\gamma\in\mathcal{J}}, \quad Q_2^{\gamma} := (c_{\alpha\beta}^{\gamma}), \tag{6.24}$$

where each coefficient is a bilinear form in the coefficient sequences of the factors. The collection of the bilinear forms $\mathbf{Q}_2 = (Q_2^{\gamma})_{\gamma\in\mathcal{J}}$ is a bilinear mapping that maps the coefficient sequences of ξ_1 and ξ_2 into the coefficient sequence of the product

$$\mathscr{H}(\xi_3) =: \mathbf{Q}_2((\xi_1), (\xi_2)) = \mathbf{Q}_2\left(\mathscr{H}(\xi_1), \mathscr{H}(\xi_2)\right). \tag{6.25}$$

For computational purposes one truncates the Hermite transform by replacing the random variables by their finite representations denoted by $\widehat{\ }$, which, for simplicity reasons, are here assumed to belong to the same subspace $\mathcal{P}$. However, as previously discussed, the product $\mathbf{Q}_2((\hat{\xi}_1), (\hat{\xi}_2))$ does not necessarily lie in the same subspace as the terms entering the product. This may cause the growth of the problem dimension on the expense of the actual computation [56], e.g. successive multiplication. To overcome this issue, the product $\mathbf{Q}_2((\hat{\xi}_1), (\hat{\xi}_2))$ is simply projected onto the subspace $\mathcal{P}$ in a Galerkin manner such that:

$$\hat{\xi}_3 = \widehat{\mathbf{Q}_2}(\hat{\xi}_1, \hat{\xi}_2) =: \hat{\xi}_1 \,\hat{\bullet}\, \hat{\xi}_2. \tag{6.26}$$

Note that in other sections of this thesis the symbol $\widehat{\mathbf{Q}_2}$ is shortly denoted by $\hat{\bullet}$.

Due to the symmetry of the tensor (Q_2^{γ}) the multiplication is the commutative and associative operation, characterised by a neutral element $\mathring{\xi}$—the constant function $\omega \mapsto 1$—with the Hermite transform $\mathscr{H}(\mathring{\xi}) = (1, 0, 0, ..., 0)$, such that $\xi = \xi \cdot \mathring{\xi}$.

Considering multiplication one may notice that the total accuracy consist of two different truncation errors. The first one occurs in the truncation of the input approximations and the second in the final Galerkin projection. However, it may be shown that those truncation errors are negligible if the order of the polynomial chaos expansion is chosen sufficiently high to describe properly the result of the multiplication (e.g. see the following example).

Example 6.3.1. *The square χ of the skewed random variable represented by the polynomial chaos coefficients* $[1\ 0.7\ 0.1\ 0.02]$ *is computed by the Galerkin projection* $\hat{\chi} := \widehat{\mathbf{Q}_2}(\hat{\xi}, \hat{\xi})$ *onto the Hermite basis of different orders. As expected, the product accuracy improves with the increase of the polynomial order, see Table 6.3. This further means that the product cannot be in general simply projected onto the basis of one of input RVs. The reason is the skewness of the input which cannot be properly described by the small order PCE. In this specific case, the 4th order approximation can be used for the actual computation since the RRMSE:*

$$\epsilon = \frac{\sqrt{(\chi_p^{(\alpha)} - \chi_6^{(\alpha)})^2 \alpha!}}{\sqrt{(\chi_6^{\alpha})^2 \alpha!}} \tag{6.27}$$

is smaller than 2%. Here, $\chi_p^{(\alpha)}$ denotes the coefficients of the p-order PCE approximation of the random variable χ and $\chi_6^{(\alpha)}$ the analytic result obtained for the polynomials of the sixth order (the true value).

Table 6.3: The square of RV ξ and its accuracy with the order of polynomial approximation of result

Order	Error	PCV
1	43.73%	[1.4900 1.4000 0 0 0 0]
2	17.78%	[1.5100 1.6800 0.7300 0 0 0 0]
3	5.03%	[1.5124 1.7040 0.8212 0.2040 0 0 0]
4	1.062%	[1.5124 1.7040 0.8212 0.2040 0.0416 0 0]
5	0.21%	[1.5124 1.7040 0.8212 0.2040 0.0416 0.0040 0]
6	0%	[1.5124 1.7040 0.8212 0.2040 0.0416 0.0040 0.0004]

Remark: the lognormal random variable is the exponential transformation of the Gaussian RV, and thus is a *group* under multiplication since the Gaussian RVs form a vector space. This means that after multiplication of two lognormal RVs one again obtains the lognormal RV.

Table 6.4: The accuracy of RVs division with respect to the order of polynomial approximation of result

Order	Error	PCV
1	16.83%	[1.2240 1.0000 0 0 0]
2	2.68%	[1.2465 0.8873 0.2705 0]
3	0.19%	[1.2447 0.8964 0.2486 0.0335]
4	0%	[1.2448 0.8960 0.2496 0.0320 0.0016]

Division. In contrast to multiplication the division of two RVs cannot be done in a completely straightforward way by the direct projection of the formula $\xi = \xi_3/\xi_1$ onto the polynomial chaos basis [56]. Instead, one reformulates the problem to $\xi_1 \cdot \xi = \xi_3$, i.e. the system of equations with the unknown ξ. Taking the results of Eq. (6.25) the system becomes:

$$\mathscr{H}(\xi_3) =: \mathbf{Q}_2(\xi_1), (\xi)) = \mathbf{Q}_2\left(\mathscr{H}(\xi_1), \mathscr{H}(\xi)\right) \tag{6.28}$$

or in a matrix notation:

$$\mathbf{C}\xi = \xi_3, \tag{6.29}$$

where $\mathbf{C} = [..., \sum_{\beta\in\mathcal{J}} \xi_1^{(\beta)} c_{\alpha\beta}^{(\gamma)}, ...]_{\gamma\in\mathcal{J}}^T$, $\xi = (..., \xi^{(\alpha)}, ...)^T$ and $\xi_3 = (..., \xi_3^{(\gamma)}, ...)^T$. Projecting the system in the Galerkin manner to $\hat{\xi}_1 \hat{\bullet} \hat{\xi} = \hat{\xi}_3$, Eq. (6.29) becomes:

$$\widehat{\mathbf{C}}\hat{\xi} = \hat{\xi}_3 \tag{6.30}$$

with the corresponding vectors and matrices described by the index set $\mathcal{J}_\mathcal{Z}$. This system may be solved by Krylov subspace methods, such as the preconditioned conjugate gradient method, SOR, GMRES, etc. In order to simplify the notation the division of two PCVs is denoted as:

$$\hat{\xi} = \hat{\xi}_3 \hat{\div} \hat{\xi}_1, \tag{6.31}$$

where the symbol $\hat{\div}$ indicates the linear system of Eq. (6.30) which has to be solved.

Example 6.3.2. *Let us take the RV described by the PCE coefficients* $[1.4240\ 1.2448\ 0.4480\ 0.0832\ 0.0080\ 0.0003]$ *and divide it by the Gaussian RV* $[1\ 0.2]$. *As the first variable is of the fifth order and the second of order one, one expects that the result has order* 4. *This is proven in Table 6.4 where the convergence of the division with respect to the polynomial order is shown. The error is computed*

Table 6.5: Error [%] of n-th division of non-Gaussian RV by Gaussian RV θ. The non-Gaussian RV has: a) small, b) high coefficient of variation.

a) $\theta = (1, 0.1)$	Division/ Order	1	2	3	4
	$1st$	5.08	0.36	0.01	0.00
	$2nd$	3.86	0.24	0.01	0.00
	$3rd$	2.97	0.23	0.01	0.00
	$4th$	2.65	0.31	0.01	0.00
b) $\theta = (1, 0.3)$	Division/Order	1	2	3	4
	$1st$	31.88	8.99	1.40	0.00
	$2nd$	49.02	22.71	6.70	0.00
	$3rd$	85.81	66.55	33.58	0.00
	$4th$	157.95	192.69	156.41	0.00

according to Eq. (6.27), i.e. the relative root mean square error with respect to the given analytical result.

Example 6.3.3. *Let us divide the RV ξ with $\mathscr{H}(\xi) = [1.1015\ 0.5302\ 0.1030\ 0.0101\ 0.0005]$ by the Gaussian RV $[1\ 0.1]$ (case a) in Table 6.5) and the RV χ with $\mathscr{H}(\chi) = [2.0215\ 2.3464\ 1.1430\ 0.2943\ 0.0405\ 0.0024]$ by the Gaussian RV $[1\ 0.3]$ (case b) in Table 6.5). These two cases represent the "good" and "bad" scenario with respect to the value of the coefficient of variation (i.e. the ratio of the standard deviation to the mean) of numerator [1]. In the first case the coefficient is 0.27, while in the second 4.29. The goal is to investigate the RMSE behaviour of the result with respect to the order of its polynomial chaos approximation. According to Table 6.5 the approximation error: a) reduces, b) grows with every new division. The reason for this lies in the piece of information each of the PCE terms of numerator carry over to the division. Namely, if the coefficient of variation is small (as for ξ) the higher order terms do not carry much information, and the truncated division is close to the truth. However, this initial error is then reduced through the successive division since it gets divided by Gaussian RV. On the other side, if the variance of the RV is not so small and the higher order terms are not negligible, as in case of χ, the low order truncations will produce large error. This error transforms the initial problem to another one, and one does not divide χ, but some other RV by Gaussian. This phenomenon becomes worse with every new successive division. However, if the proper order is used (4th in this case) one obtains the correct result and the error does not alter any more.*

[1] Note that the Gaussian RVs are already accurately approximated by the first order PCE

Table 6.6: Error [%] of n-th power of Gaussian RV θ with the order of PCE

$\theta = (1, 0.1)$	Power/ Order	1	2	3	4
	$2nd$	0.82	0	0	0
	$3rd$	2.42	0.07	0	0
	$4th$	4.74	0.29	0.06	0
	$5th$	7.72	0.69	0.03	5.8e-4
$\theta = (1, 0.5)$	Power/Order	1	2	3	4
	$2nd$	10	0	0	0
	$3rd$	25	2.78	0	0
	$4th$	41.30	8.69	0.72	0
	$5th$	56.45	17.38	2.69	0.18
$\theta = (1, 2)$	Power/Order	1	2	3	4
	$2nd$	30.77	0	0	0
	$3rd$	57.14	12.7	0	0
	$4th$	76.52	27.83	4.64	0
	$5th$	88.11	46.21	11.75	1.57

Power function. This function is a generalisation of the product of RV with itself. Going one step further from the product given in Eq. (6.25), one may define the product of three RVs with finite variance as $\chi := \xi_1 \cdot \xi_2 \cdot \xi_3$ (the cube $\chi := \xi \cdot \xi \cdot \xi$ is a special case):

$$\chi^{(\delta)} = \sum_{\alpha \in \mathcal{J}} \sum_{\beta \in \mathcal{J}} \sum_{\gamma \in \mathcal{J}} \xi_1^{(\alpha)} \xi_2^{(\beta)} \xi_3^{(\gamma)} \frac{1}{\delta!} \mathbb{E}(H_\alpha H_\beta H_\gamma H_\delta). \tag{6.32}$$

However, such representation is not comfortable for practical computation due to the definition of the forth order tensor $\mathbb{E}(H_\alpha H_\beta H_\gamma H_\delta)$. To avoid its computation, one may employ the associativity of the product and sequentially calculate the power:

$$\mathscr{H}(\chi) := \mathbf{Q}_3((\xi_1), (\xi_2), (\xi_3)) := \mathbf{Q}_2(\mathbf{Q}_2((\xi_1), (\xi_2)), (\xi_3)). \tag{6.33}$$

After the Galerkin projection on the subspace $\mathcal{P}$, Eq. (6.36) becomes:

$$\hat{\chi} := \widehat{\mathbf{Q}}_3((\hat{\xi}_1), (\hat{\xi}_2), (\hat{\xi}_3)) \tag{6.34}$$

i.e.

$$\hat{\chi} = \hat{\xi}_1 \bullet (\hat{\xi}_2 \bullet \hat{\xi}_3) = \hat{\xi}_1 \bullet \hat{\eta}, \tag{6.35}$$

Table 6.7: Error [%] of n-th power of non-Gaussian RV with the order p of PCE

n/p	1	2	3	4	5	6	7	8
2	43.73	17.78	5.03	1.06	0.21	0	0	0
3	73.47	44.65	20.68	8.45	2.84	0.76	0.11	0.03
4	90.23	70.22	44.67	25.25	12.38	5.16	1.80	0.46
5	97.08	86.87	67.68	47.35	29.20	15.64	7.03	2.29

where $\hat{\eta}$ follows from Eq. (6.25) [150]. This definition requires the computation of the third order tensor $c_{\alpha\beta}^{(\gamma)}$, which may be precomputed and stored in the memory for any further multiplication.

Similarly to this procedure, one may compute the product of n variables as:

$$\mathscr{H}(\chi) := \mathbf{Q}_n((\xi_1),(\xi_2),\dots,(\xi_n)) := \mathbf{Q}_{n-1}(\mathbf{Q}_2((\xi_1),(\xi_2)),\dots,(\xi_n)). \quad (6.36)$$

Each $\mathbf{Q}_n$ is again composed of a sequence of k-linear forms $\{Q_n^\gamma\}_{\gamma\in\mathcal{J}}$. The sequence defines each coefficient of the Hermite transform of the n-fold product [150].

Example 6.3.4. *In this example one investigates the RRMSE of the n-th power of some arbitrary chosen RV projected on the subspace spanned by the Hermite polynomials of different orders. For simplicity, let us take the Gaussian RV with the mean $\mu = 1$ and different values of the standard deviations $\sigma = \{0.1, 0.5, 2\}$, respectively. In such a case one may observe the drastic change of the RRMSE with the polynomial order. Namely, if one takes a small standard deviation, e.g. $\sigma = 0.1$, the error of the 5th power for the 2nd order approximation is just 0.69%, while for $\sigma = 2$ this error becomes ca. 46%. This behaviour is shown in Table 6.6 for different degrees of the power function. The analytical (true) value is obtained by the PCE of the 5th order (as the input variable has order 1).*

Similarly, one may compute the power of the non-Gaussian RV with the PCE $\mathscr{H}(\xi) = [1\ 0.7\ 0.2\ 0.08]$ (see Table 6.7). Namely, the second power is already well approximated by the PCE of the order 4, while 3rd power requires the PCE of the order 5. As the exponent increases, one has to use more terms in PCE to keep the accuracy. For example, the projection onto the same basis as the term entering the power delivers much higher error for the 5th power than for the 3rd power.

Negative n-th power of RV. The inverse of the RV ξ, denoted by χ, could be seen as a division between the neutral element $\overset{o}{\xi}$ and ξ, i.e. $\hat{\chi} = \hat{\overset{\circ}{\xi}} \hat{\div} \hat{\xi}$, see Eq. (6.31).

Similarly, one may define the second negative power as $\hat{\eta} := \hat{\xi}^{-2} = \hat{\overset{\circ}{\xi}} \hat{\div} \hat{\chi}$, as well as the further ones by sequential dividing by $\hat{\chi}$. Another way would be to first compute the power $\hat{\xi}^2$ and then to divide $\hat{\eta} = \hat{\overset{\circ}{\xi}} \hat{\div} \hat{\xi}^2$.

6.3.2 Nonlinear functions of RVs

The nonlinear functions of RVs are much more difficult to compute compared to basic operations. The reason is that one is not able to apply the Galerkin projection on the "formula" directly, but only on its linearised form. The process of linearisation can be done with the help of the *stochastic version of the Newton-like methods*, which is the subject of this section.

Square root. In order to find the square root of a RV ξ one has to solve the nonlinear equation:

$$f(\chi) = \mathscr{H}(\xi) - \mathbf{Q}_2((\chi),(\chi)) = 0, \tag{6.37}$$

where the function $f(\chi)$ is differentiable with respect to χ. Regarding the smoothnes condition one may define the Jacobian $J = 2\chi$ and compute the solution in Newton iterative manner. In such a case the linearised version of Eq. (6.37) becomes

$$\mathscr{H}(r^{(k)}) = \mathbf{Q}_2(J^{(k)}, \Delta\chi^{(k)}), \tag{6.38}$$

where $r^{(k)} := f(\chi^{(k)}) - f(\chi^{(k-1)})$ is the residual in iteration k. Once the linearisation is performed, the system in Eq. (6.38) is projected onto the finite polynomial basis such that

$$\hat{r}^{(k)} = \widehat{\mathbf{Q}}_2(\hat{J}^{(k)}, \Delta\hat{\chi}^{(k)}) \tag{6.39}$$

holds. This system is now easy to solve and the solution has a form of

$$\hat{\chi}^{(k)} = \frac{1}{2}(\hat{\chi}^{(k-1)} \hat{+} \hat{\kappa}^{(k-1)}) = \frac{1}{2}\left(\hat{\chi}^{(k-1)} \hat{+} (\hat{\xi} \hat{\div} \hat{\chi}^{(k-1)})\right), \tag{6.40}$$

where $\kappa^{(k-1)} := \frac{\xi}{\chi^{(k-1)}}$. The iterations repeat as long as the fraction of the probabilistic norms is such that:

$$\frac{\|J^{(k)}\Delta\chi^{(k)} + r^{(k)}\|_{L_2(\Omega)}}{\|r^{(k)}\|_{L_2(\Omega)}} > \epsilon, \tag{6.41}$$

with ϵ being the specified tolerance. Note that the approximation of RV $\kappa^{(k-1)}$ is obtained by division $\hat{\kappa}^{(k-1)} = \hat{\xi} \hat{\div} \hat{\chi}^{(k-1)}$ which requires another Galerkin projection

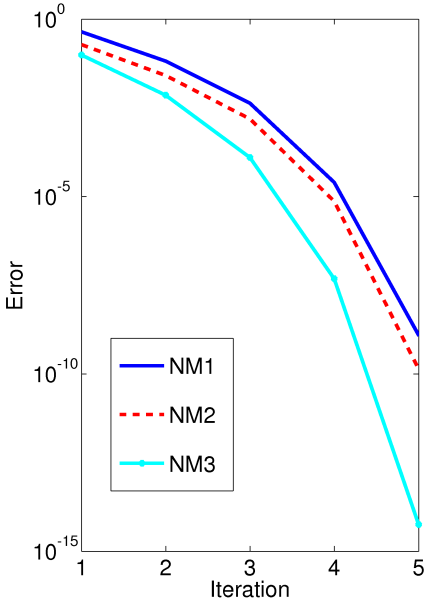

Figure 6.3: The square root of Gaussian RV $(\mu = 1, \sigma = 0.2)$ *obtained by Newton method for different initial points: NM1 starts with RV* $(0.8, 0)$*, NM2 with RV* $(1, 0)$ *and NM3 with* $(1, 0.1)$*. The last one is the closest to the solution.*

and possibly another iterative process.

The Newton method converges quadratically if the initial point $\chi^{(0)}$ is close enough to the solution (see Fig. 6.3). However, if the initial value is not taken properly, the method diverges. To satisfy this condition, the initial point of the PCV square root has to be taken in the form of PCV close enough to the PCV of root. This choice greatly depends on the variance of RV ξ. For the small and moderate values one may assume that the initial point is PCV with the mean value equal to the square root of μ_ξ (the mean value of ξ) and higher order terms equal to zero. However, if the input variance is large enough this assumption is not good and one has to precompute the initial point by some sampling technique (see Fig. 6.5). In such situation, of course, it is recommended to use a small number of sampling points, much less than necessary for the integration method to converge.

The Newton method as given in Eq. (6.40) is relatively inefficient since in each itera-

tion one has to compute κ as a solution of a linear system of equations of dimension $Z \times Z$. This may harm the efficiency of the algorithm. In order to avoid this issue one may try to find the reciprocal square root of ξ, i.e. $\mathring{\xi}/\sqrt{\xi}$; and then to compute the root $\sqrt{\xi}$ by simple multiplication $\xi \cdot \mathring{\xi}/\sqrt{\xi}$.

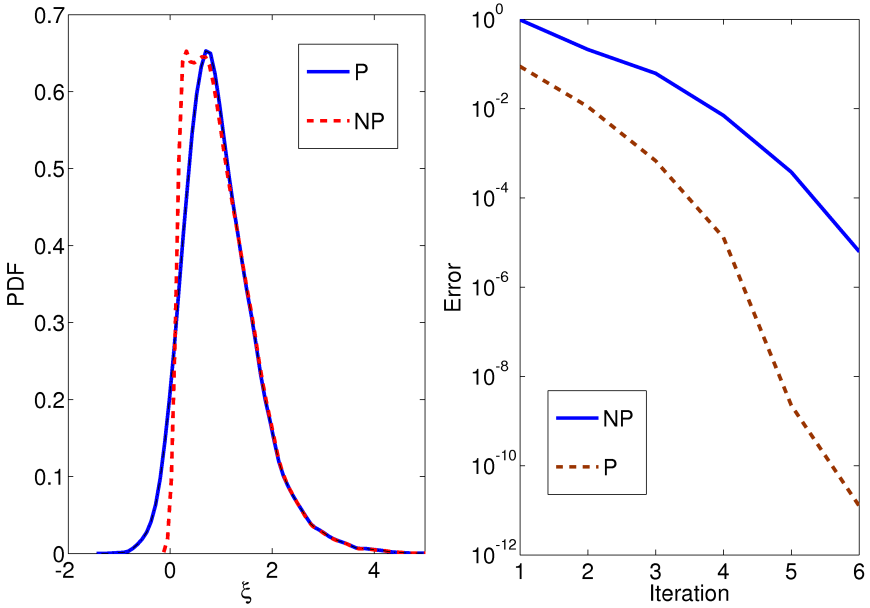

Figure 6.4: a) The square root of RV with coefficients χ = [1.5124 1.7040 0.8212 0.2040 0.0416 0.0040 0.0004] obtained by non-preconditioned (NP) and preconditioned (P) Newton method b) Convergence of methods

Example 6.3.5. *Let us take the RV* $\mathscr{H}(\chi) = [1.5124\ 1.7040\ 0.8212\ 0.2040\ 0.0416\ 0.0040\ 0.0004]$ *whose square root represents the RV* $\mathscr{H}(\xi) = [1\ 0.7\ 0.1\ 0.02]$. *The example is chosen to show the performance of the Newton method when the input variance is not so small. To investigate the influence of the initial point on the convergence of the Newton method, one may consider two different scenarios: 1) the initial point is deterministic and 2) the initial point is stochastic. The first scenario takes for a starting point the mean value* $\sqrt{1.5124}\mathring{\xi}$ *which produces the result* $\mathscr{H}(\hat{\xi}_1) = [1.0230\ 0.6478\ 0.1504\ -0.0053\ \ 0.0059\ 0.0001\ -0.0003]$, *close to the correct solution but not the same. This happens because the initial point is deterministic, not random. To overcome this issue, the initial point is chosen in another way by preconditioning, i.e. by collocating the solution in a very small number*

of samples. In this way the mean value and the standard deviation of the initial point become closer to the real solution (see Fig. 6.4 b)). With such initial point the Newton method delivers the exact solution $\hat{\xi}_2 = \hat{\xi}$ up to the error defined by the convergence tolerance. This can be observed in Fig. 6.4 a), where one clearly sees the deviation of the root $\hat{\xi}_1$ from the correct result $\hat{\xi}_2$.

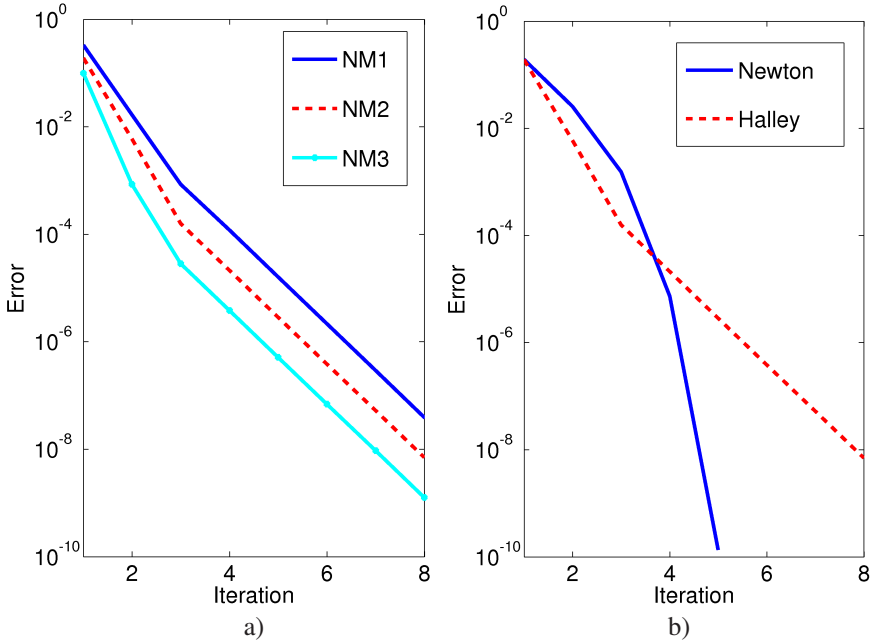

Figure 6.5: a) The square root of Gaussian RV $(\mu = 1, \sigma = 0.2)$ obtained by Halley's method for different initial points: NM1 starts with RV $(\mu = 0.8, \sigma = 0)$, NM2 with RV $(1, 0)$, and NM3 with $(1, 0.1)$; b) Comparison of Newton and Halley's method

Another way to compute the square root of PCV is to use the Halley's method, the Householder's method of order two (see Fig. 6.5). The method consists of the sequence of iterations:

$$\chi^{(k+1)} = \chi^{(k)} - \frac{2f(\chi^{(k)})f'(\chi^{(k)})}{2[f'(\chi^{(k)})]^2 - f(\chi^{(k)})f''(\chi^{(k)})}, \tag{6.42}$$

where f is given in Eq. (6.37). After the Galerkin projection the final system of

equations has a form:

$$\hat{\chi}^{(k+1)} = [\hat{\chi}^{(k)} \hat{\bullet} (\hat{\kappa}^{(k)} \hat{-} \hat{\xi})] \hat{\div} [3\hat{\hat{\xi}} \hat{\bullet} (\hat{\kappa}^{(k)} \hat{+} \hat{\xi})], \tag{6.43}$$

where $\hat{\kappa} = \hat{\chi}^{(k)} \hat{\bullet} \hat{\chi}^{(k)}$. The method converges cubically (see Fig. 6.5 a)), and involves more operations per iteration than the corresponding Newton method (see Fig. 6.5 b)). However, the sensitivity on the initial point is similar.

n-th square root. Similar to the square root, one may compute the n-th square root by solving the nonlinear system $\mathscr{H}(\chi) := \mathbf{Q}_n((\chi),(\chi),\dots,(\chi)) := \mathbf{Q}_{n-1}(\mathbf{Q}_2((\chi),(\chi)),\dots,(\chi))$ (see Eq. (6.36)) by the Newton method:

$$\chi^{(k+1)} = \frac{1}{n}\left((n-1)\chi^{(k)} + \frac{\xi}{(\chi^{(k)})^{n-1}}\right). \tag{6.44}$$

Inverse square root. The inverse square root is described by a nonlinear function $f(\eta) = \frac{1}{\eta^2} - \xi = 0$, whose linearised form is given by $\eta^{(k+1)} = 0.5\eta^{(k)}\left(3 - \xi \cdot (\eta^{(k)})^2\right)$, where k represents the Newton iteration. Taking notation $\kappa^{(k)} := (\chi^{(k)})^2$ and $\varsigma^{(k)} := \xi \cdot \kappa^{(k)}$, and further projecting the linear system in a Galerkin manner one obtains:

$$\hat{\eta}^{(k+1)} = \frac{\hat{\eta}^{(k)}}{2} \hat{\bullet} (3\hat{\hat{\xi}} \hat{-} \hat{\varsigma}^{(k)}). \tag{6.45}$$

Note that the method requires only the operations of multiplication and summation, not the division. The initial point is chosen in a similar way as for the direct Newton method. However, the method is not stable, and thus is even more sensitive on the choice of the initial point compared to the direct procedure. If the initial value is not close to the reciprocal square root, the iterations diverge from it rather than converge to it. To overcome this issue, one may run one iteration of the direct method in order to precompute the solution, i.e. to find the initial point.

Exponential function. The exponential function is one of the functions which often appear in computational problems describing nonlinear behaviour of the structure. It may be characterized in a variety of equivalent ways, of which the most known is the power series method. Let us find the exponential of some RV ξ with the mean $\bar{\xi}$ and the fluctuating part $\tilde{\xi}$:

$$\chi := \exp\xi = \exp(\bar{\xi} + \tilde{\xi}) = \exp\bar{\xi}\exp\tilde{\xi} \tag{6.46}$$

As $\exp\bar{\xi}$ is constant, one expands the fluctuating part according to:

$$\exp\tilde{\xi} := \overset{o}{\xi} + \sum_{i=1}^{n} \frac{\tilde{\xi}^n}{n!} \tag{6.47}$$

where $\tilde{\xi}^n$ is the power function as previously described (see Eq. (6.36)). With the help of the Galerkin projection one may compute $\exp\tilde{\xi}$ in a finite number of terms and then multiply it by $\exp\bar{\xi}$. However, the power series method is not the best approximation for RVs with large input variance—the values can be far from the mean. For such cases [56] proposes the integral method where the solution is found via equation $\xi = \int_1^{\chi} t^{-1}\mathrm{d}\,t$. Another possibility is to compute the value with the help of the Newton approach, similarly to before.

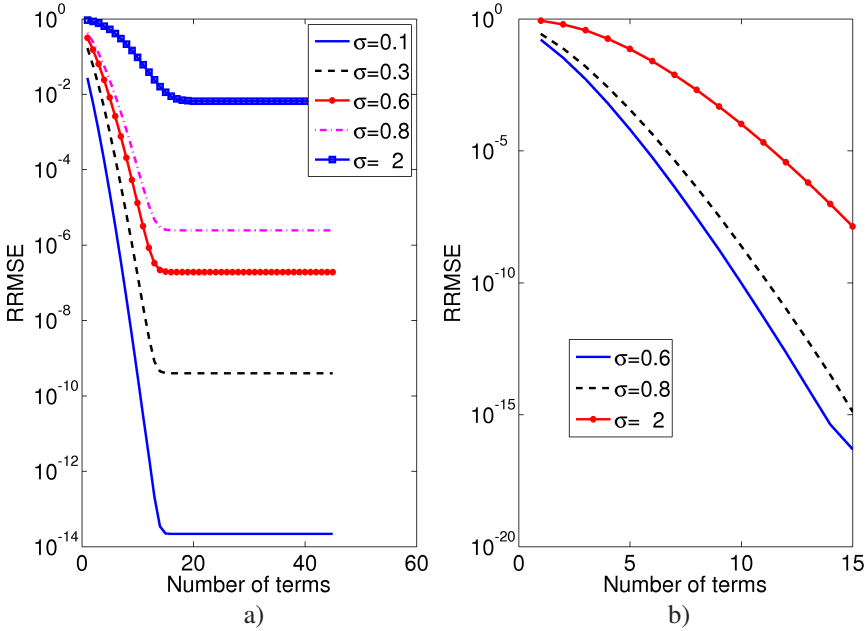

Figure 6.6: The convergence of the Taylor method for exp(θ): a) with respect to the number of terms b) with respect to the polynomial order

Example 6.3.6. *The numerical properties of Taylor expansion applied on RV exp*$(1+\sigma\theta)$ *are tested on the example of the Gaussian RV* $\theta = \mathcal{N}(1,\sigma)$*, where* σ

takes the value in the interval $[0.1\ 2]$. *The analytic solution, evaluated according to Eq. (6.16), is compared to the numerical solution in Fig. 6.6. The comparison shows that the Taylor expansion with* 20 *terms and PCE operations in the space spanned by the polynomials of order* 7 *are enough to get the error of ca.* 1*e-14 for* $\sigma = 0.1$ *(see Fig. 6.6a)), or similar for moderate deviations. However, by applying the same procedure to the RV with the large standard deviation* $\sigma = 2$*, the error is not negligible any more. This can be reduced with the increase of the polynomial order as shown in Fig. 6.6b). For example, going from order 7 to order 15 the approximation error reduces from 1e-2 to 1e-8.*

Logarithm. This function is an isomorphism from the group of positive RVs under multiplication to the group of random variables under addition, i.e. $\ln(\xi_1\xi_2) = \ln\xi_1 + \ln\xi_2$. The function is inverse to the exponential, i.e. $\exp(\ln\xi) = \xi$ and $\ln(\exp\xi) = \xi$, and hence admits similar properties of the Taylor expansion:

$$\ln\hat{\xi} = \ln\hat{\xi}^{(0)} + \sum_{i=1}^{n}(-1)^{n+1}\frac{(\hat{\xi}/\hat{\xi}^{(0)})^n}{n}. \tag{6.48}$$

Here, $\hat{\xi}^{(0)}$ denotes the first coefficient in the PCE approximation of ξ.

Table 6.8: The convergence of the logarithm of RV with the order of PCE

Order	PCE
1	$[0.9996\ 0.2027\ 0\ 0]$
2	$[1.0000\ 0.1999\ 0.0004\ 0]$
3	$[1.0000\ 0.2000\ 0.0000\ 0.0000]$

Example 6.3.7. *Let* $[2.7732\ 0.5546\ \ 0.0555\ 0.0037\ 0.0002]$ *be the PCE coefficients of the random variable whose logarithm represents the Gaussian RV with the PCE coefficients* $[1\ 0.2]$. *The accuracy of the numerical solution computed with the help of the Taylor expansion with* 20 *terms is investigated in Table 6.8. The expansion is evaluated via the Galerkin projection onto the Hermite basis of different polynomial orders. According to the results in Table 6.8, the exact solution is already achieved with the third order approximation. However, if one reduces the number of terms in the Taylor expansion, the polynomial order has to grow in order to achieve the same accuracy. This is valid only for moderate input variances. However, in case of large input variances the method is not accurate enough and one has to use another procedure, such as the Newton method.*

Sinus function. The sinus function of the random variable ξ can be approximated by the Taylor expansion:

$$\sin(\xi) = \sum_{n=0}^{\infty} (-1)^n \frac{\xi^{2n+1}}{(2n+1)!}, \tag{6.49}$$

where ξ^{2n+1} denotes the power function of RV ξ.

Example 6.3.8. *Let be given the Gaussian RV with the mean equal to* 1 *and the standard deviation belonging to the interval* $[0.1\ 2]$. *To evaluate its sinus, the Taylor expansion with* 20 *terms and the PCE of order* 1 *up to* 14 *are used, see Fig. 6.7. The convergence error is computed with respect to the* 15*th order approximation, taken as a reference solution. For more proper analysis, the reference is compared to the solution obtained by the Monte Carlo simulation with* $2 \cdot 10^6$ *samples. The relative error in the mean and variance for* $\sigma = 0.8$ *are* 4.2*e-*04 *and* 1.83*e-*04*, respectively.*

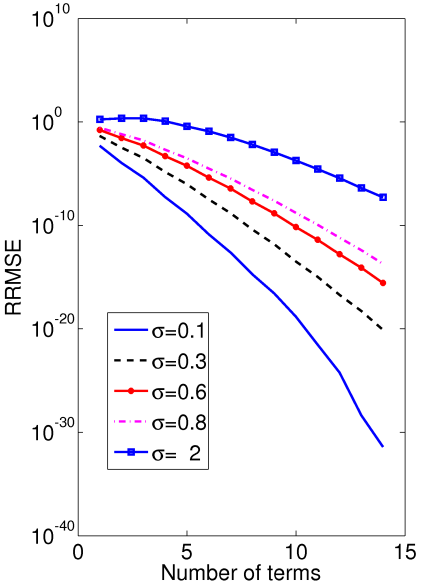

Figure 6.7: The convergence of the sinus function of the Gaussian RV

General nonlinear function. In general, nonlinear functions are approximated by the Taylor expansion around the mean when the variance is small or has moderate

values. In case of large input variances, one has to use some iterative technique, such as the Newton-Raphson method as previously described.

6.4 Algebraic operations on vector and matrix valued RVs

In the previous sections the algebra of RVs belonging to $L_2(\Omega, \mathbb{R})$ was considered. However, this can be generalised to a case when RVs belong to $L_2(\Omega, \mathbb{R}^N)$ or, more generally, $L_2(\Omega, \mathbb{R}^{M\times N})$, as shortly described in this section.

The dot product. Let us take the vector of RVs

$$\boldsymbol{r}(\omega) = \sum_{\alpha\in\mathcal{J}} \boldsymbol{r}^{(\alpha)} H_\alpha(\theta(\omega)), \quad \boldsymbol{r}^{(\alpha)} \in \mathbb{R}^n, \tag{6.50}$$

represented by the Hermite transform $\mathscr{H}(\boldsymbol{r}) = (\boldsymbol{r}^\alpha) := (\boldsymbol{r}) \in \mathbb{R}^{n\times\mathcal{J}}$. Similarly to this, let us take the vector $\boldsymbol{s} \in L_2(\Omega, \mathbb{R}^n)$. Then, the dot product between these two vectors is the scalar-valued RV $b \in L_2(\Omega, \mathbb{R})$ given by the Hermite transform:

$$\mathcal{H}(b) = \left(\sum_{i=1}^{n} \mathbf{Q}_2((r_i),(s_i))\right) =: \mathbf{S}_1((\boldsymbol{r}),(\boldsymbol{s})), \tag{6.51}$$

where $\mathbf{S}_1$ represents the linear combination of the bilinear forms $\mathbf{Q}_2((r_i),(s_i))$. In a computational sense, one applies the projection such that $\hat{b} = \hat{\mathbf{S}}_1((\hat{\boldsymbol{r}}),(\hat{\boldsymbol{s}}))$. The element-wise product may be defined similarly.

Matrix-vector product. The more general case is the product of the matrix-valued random variables $\boldsymbol{R}(\omega)$ and the vector-valued random variables $\boldsymbol{r}(\omega)$ via the classical dot product. Let be given the Hermite transforms of those variables as $\mathscr{H}(\boldsymbol{R}) = (\boldsymbol{R}^{(\alpha)}) := (\boldsymbol{R}) \in \mathbb{R}^{m\times n\times\mathcal{J}}$ and $\mathscr{H}(\boldsymbol{r}) = (\boldsymbol{r}^{(\alpha)}) := (\boldsymbol{r}) \in \mathbb{R}^{n\times\mathcal{J}}$, respectively. Then, the matrix-vector dot product $\boldsymbol{b}(\omega) = \boldsymbol{R}(\omega)\cdot\boldsymbol{r}(\omega)$ has the Hermite transform $\mathscr{H}(\boldsymbol{b}) = (\boldsymbol{b}) \in \mathbb{R}^{m\times\mathcal{J}}$ with the elements (RVs):

$$\mathscr{H}(\boldsymbol{b}) = \left(\sum_{j=1}^{n} \mathbf{Q}_2((R_{ij}),(r_j))\right)_i =: \mathbf{S}_2((\boldsymbol{R}),(\boldsymbol{r})),$$

where the form $\mathbf{S}_2$ represents the linear combination of the bilinear forms

$\mathbf{Q}_2((R_{ij}),(r_j))$ with the summation done over the second index (index 2 in notation of $\mathbf{S}$). Notation $\mathbf{S}_1$ is used for the summation over the first index, i.e. for the product $\boldsymbol{r}\cdot\boldsymbol{R}$, where $\boldsymbol{r}$ is the vector of the length m. The rest of operations such as addition, summation, n-th power, etc. one may define with the help of the previous two operations in a similar manner as in previous sections.

Matrix product. By generalizing the formula in Eq. (6.52) one may define the inner product $\Xi \in L_2(\Omega,\mathbb{R}^{M\times L})$ of two matrix-valued RVs $\Phi \in L_2(\Omega,\mathbb{R}^{M\times N})$ and $\Sigma \in L_2(\Omega,\mathbb{R}^{N\times L})$, respectively :

$$\mathscr{H}(\Xi)=\left(\sum_{J=1,..,N}\mathbf{Q}_2((\Phi_{IJ}),(\Sigma_{JL}))\right)_{IJ} =: \mathbf{S}_2(\Phi,\Sigma). \tag{6.52}$$

In the further text the notation $\hat{\Xi}=\hat{\mathbf{S}}_2(\hat{\Phi},\hat{\Sigma}) =: \hat{\Phi}_1\hat{\circ}\hat{\Sigma}$ is used to denote the matrix product due to simplicity reasons.

Hadamards pointwise product. The pointwise product $\Xi \in L_2(\Omega,\mathbb{R}^{M\times N})$ of Φ and Σ in $L_2(\Omega,\mathbb{R}^{M\times N})$ is given as:

$$\mathscr{H}(\Xi)=(\mathbf{Q}_2((\Phi_{IJ}),(\Sigma_{IJ})))_{IJ} \tag{6.53}$$

which after the projection gives $\hat{\Xi}=[\left(\widehat{\mathbf{Q}}_2((\hat{\Phi}_{IJ}),(\hat{\Sigma}_{IJ}))\right)_{IJ}] =: \hat{\Phi}\hat{*}\hat{\Sigma}$.

Double dot product. Another product to be defined is the double dot product in its two variants: the first

$$\mathscr{H}(\xi)=\left(\sum_{I=1}^{N}\sum_{J=1}^{N}\mathbf{Q}_2((\Phi_{IJ}),(\Sigma_{JI}))\right), \quad \xi\in L_2(\Omega,\mathbb{R}) \tag{6.54}$$

after the projection denoted as:

$$\hat{\xi} := \hat{\Phi}_1 \hat{:} \hat{\Sigma} \tag{6.55}$$

and the second

$$\mathscr{H}(\xi)=\left(\sum_{I=1}^{N}\sum_{J=1}^{N}\mathbf{Q}_2((\Phi_{IJ}),(\Sigma_{IJ}))\right), \quad \xi\in L_2(\Omega,\mathbb{R}) \tag{6.56}$$

denoted as:

$$\hat{\xi} = \hat{\Phi}_1 \hat{\cdot\cdot} \hat{\Sigma}. \tag{6.57}$$

The product fulfills the same law of contraction as in the matrix algebra of the real numbers. Namely, the order of the result is reduced to two in case of the double dot product, and for one in case of the inner (dot) product.

Matrix Determinant. In linear algebra of random variables the scalar valued determinant $\chi := \det \Xi$ is a value associated with a square matrix valued RV $\Xi \in L_2(\Omega, \mathbb{R}^{N\times N})$. Its value can be computed by the Leibniz or Laplace formula. However, if the matrix dimension N is large these methods require many stages of computation and are very inefficient. Thus, another type of approach has to be used. Namely, for a given matrix-valued RV Ξ one may try to compute its determinant by factorizing the matrix as a product of matrices whose determinants can be more easily calculated—the so-called decomposition approach. This idea comes from the matrix algebra of the real numbers, where one may find the determinant of a positive definite matrix $\boldsymbol{A} \in \mathbb{R}^{N\times N}$ by its LDU decomposition:

$$\det(\boldsymbol{A}) = \det(\boldsymbol{L}) \det(\boldsymbol{D}) \det(\boldsymbol{U}) = \det(\boldsymbol{D}), \tag{6.58}$$

where $\boldsymbol{U}$ is the unit upper triangular, $\boldsymbol{D}$ the diagonal, and $\boldsymbol{L}$ the unit lower triangular matrix with the same memory requirements as in a case of LU decomposition. Matrix $\boldsymbol{D}$ is diagonal and hence the determinant of $\boldsymbol{A}$ reduces to the product of N diagonal elements:

$$\det(\boldsymbol{A}) = \prod_{i=1}^{N} D_{ii}, \tag{6.59}$$

which is further easy to compute fast. Let us now suppose that LDU decomposition $\Xi = \Sigma\Lambda\Phi$ of a matrix-valued random variable $\Xi \in L_2(\Omega, \mathbb{R}^{N\times N})$ exists (i.e. that Ξ is positive definite), where again Σ is the unit lower, Φ the unit upper and Λ the diagonal matrix. After the Galerkin projection the matrix becomes $\hat{\Xi} = \hat{\Sigma} \mathbin{\hat{\circ}} \hat{\Lambda} \mathbin{\hat{\circ}} \hat{\Phi}$ such that the determinant represents a product of scalar valued RVs $\hat{\chi} = \widehat{Q}_N(\hat{\lambda}_1, \ldots, \hat{\lambda}_N)$, according to Eq. (6.59). Here, $\hat{\lambda}_i$ are the projections of the diagonal elements of the matrix valued RV Λ.

Matrix inverse. The inversion is the process of finding the matrix RV $\Phi := \Xi^{-1} \in L_2(\Omega, \mathbb{R}^{N\times N})$ that satisfies $\Xi\Phi = \boldsymbol{I}$ for a given invertible matrix RV $\Xi \in L_2(\Omega, \mathbb{R}^{N\times N})$. If the matrix-valued RV takes the values in $\mathbb{R}^{2\times 2}$ or $\mathbb{R}^{3\times 3}$ one may compute the matrix of co-factors (adjugate matrix) and calculate the inverse directly. However, such recursive method is not optimal for large matrices due to reasons of computational cost. Instead, one usually solves N linear systems of equations $\Xi\boldsymbol{\phi}_j = \boldsymbol{e}_j,\ j = 1, .., N$, where $\Phi_{:,j} =: \boldsymbol{\phi}_j$ is the unknown vector of RVs, and $\boldsymbol{e}_j$ the corresponding j-th unit element, i.e. the vector of zero random variables with $\mathring{\xi}$ on j-th position. The term $\Phi_{:,j}$ represents the jth column of a matrix Φ. Here,

one should not forget that each element of the column is given by the PCV. After the Galerkin projection one obtains N linear systems of equations, which further may be solved by Krylov subspace methods.

6.5 Conclusion

This chapter studies the functional approximation of random variables in a form of polynomial chaos expansion, and develops the powerful algebraic tool for uncertainty quantification of nonlinear materials. Even though elementary operations as defined in Section 6.3.1 are not so frequently used in practice, their accurate representation is of primary importance in choosing an approximation technique for the nonlinear counterparts. Namely, after linearisation and Galerkin projection, the computation of nonlinear operator is shown to be the simple evaluation of elementary operations in a Galerkin manner. Such an approach is characterised by a high accuracy in low order approximation for the functions with moderately fluctuating variables (i.e. the variance is small or moderate) as arguments. However, if the argument variance is high, the polynomial approximation can fail, especially in case when the Taylor expansion is used.

Chapter 7

Numerical implementation — PLASTON

The central enemy of reliability is complexity.

Geer et al.

PLASTON (PLAsticity–STOchastic aNalysis) is a general-purpose MATLAB library for the numerical simulation of elastoplastic behaviour described by uncertain parameters. The library supports a wide range of tasks, from finite element calculations to numerical methods for solving stochastic partial differential equations. The package contains procedures for simulation of linear and nonlinear problems in small and large displacement regimes. The functions are written in open source code with permission to be re-used and modified.

7.1 Overall design

The PLASTON library is a stochastic finite element program for the elastoplastic analysis. The library is written in MATLAB (version 6.1 release 12.1) and represents a tool for solving 2-D stochastic partial differential equations specified by uncertain coefficients, boundary conditions, or the right hand side. The package numerically solves the partial differential equations with the help of direct integration, stochastic collocation, and Galerkin methods. In preprocessing step PLASTON is coupled with FEAP [228] for higher accuracy in meshing. The input data are separated in three .txt files: *input_coordinates*, *input_elements*, and *input_boundary*. However, the communication with external software is only in the preprocessing phase, the rest of the

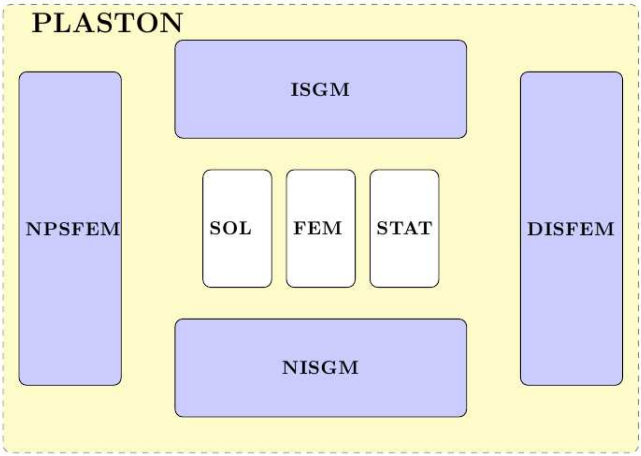

Figure 7.1: The PLASTON module structure

FEM program is done inside of the PLASTON library. There are several reasons for this. First of all, the significant communication overhead is avoided, and second and more important the FEM subroutines are redesigned to work with random variables. Still, an possibility to connect PLASTON with the external software such as PAK [237] exists.

The key features of the PLASTON code are four modules for the stochastic analysis: ISGM, NISGM, DISFEM, and NPSFEM, see Fig. 7.1. The rest of the code consists of the solver (SOL), the finite element program FEM, and the statistic toolbox STAT.

FEM is the finite element program library for solving the elasto-plastic problems. It consists of two modules: SFEM and LFEM, for small and large displacement analysis, respectively. Each of these modules contains the functions describing shape functions, integration, the stiffness and mass matrices, internal forces, elastic and plastic constitutive equations, the closest point projection algorithm, corresponding linear and nonlinear solvers, etc. Most of linear solvers that library offers are already built-in in MATLAB, while the nonlinear solvers are developed additionally. One may choose between the Newton-Raphson, the modified Newton-Raphson (with or without line search) and the BFGS algorithms. The time discretisation is done by a backward Euler method. Basically, the FEM modules represent the efficient numerical implementation of

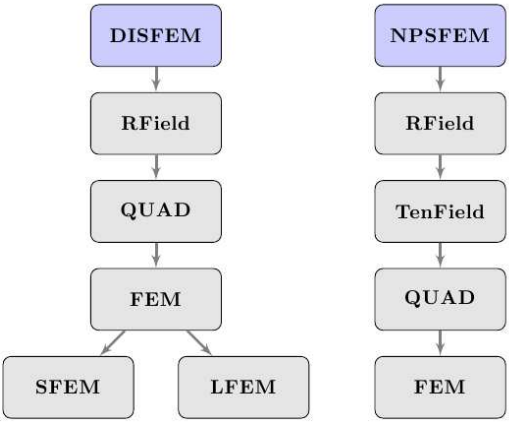

Figure 7.2: The DISFEM and NPSFEM scheme of communication

models shortly reviewed in Chapter 2. The toolbox is fully vectorised as described in Section 7.2.1.

DISFEM is the module for the direct integration of stochastic partial differential equations. It integrates the solution over the probability space as described in Section 5.3 with the help of the random or quasi-random sequences, or sparse Smolayk grid delivered from the QUAD package. Once the type of integration is chosen, DISFEM imports the KLE of the base Gaussian random field from RField and hands it in to QUAD, where the expansion is sampled and nonlinearly transformed in a point-wise fashion. These samples are then forwarded to FEM as a parametric input. After solving, the deterministic solution (realisation) is transferred to STAT which computes the desired statistics.

NPSFEM is the module (see Section 3.3) that has similar structure to the DISFEM. The only difference lies in the process of constructing input random fields. Namely, the normalized non-Gaussian random field is built in RField, and transformed to the heterogeneous non-Gaussian random field (TenField) in a set of points obtained from QUAD. Once the samples are initialised, the module calls the deterministic software FEM and calculates the desired statistics in STAT.

ISGM is the module for the intrusive stochastic Galerkin method, as described in Section 5.4.1. After spatial discretisation has been performed in FEM, the

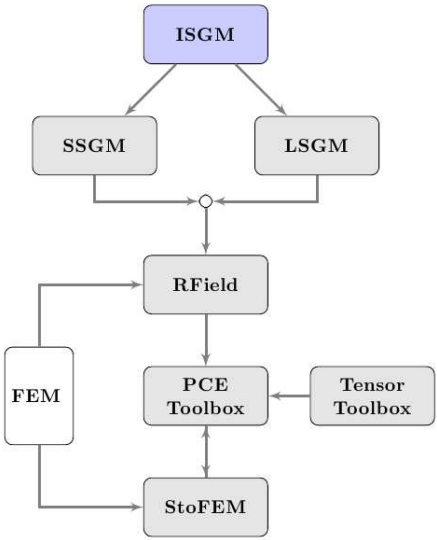

Figure 7.3: Schematic representation of intrusive Galerkin method

modul discretises the random fields in RField by applying the KLE followed by PCE. The KLE part is built in RField which communicates with FEM module. The evaluation of the PCE is done in the PCE Toolbox in an algebraic or numerical way. The direct algebraic method requires the KLE of the Gaussian base random field from RField, while the numerical integration calls the procedures from QUAD. Furthermore, the random fields are compressed in a Tensor Toolbox [116] with the help of the Tucker (or canonical) decomposition. This toolbox provides an efficient way of computing tensor-matrix, tensor-vector, and matrix-matrix products, see Section 7.2.1. Such prepared data are then handed over to StoFEM which preforms stochastic analysis using the PCE algebra (see Section 5.4.1) (PCE Toolbox). However, the connection with the FEM is not completely abandoned. The ISGM computes the solution with the help of iterative methods which require the knowledge on the preconditioners (usually the mean model). These are possibly obtained from the FEM. In addition, the FEM vectorisation procedures are fully employed during the ISGM run.

NISGM represents the modul for the non-intrusive integration of the stochastic elastplastic problem. The module highly communicates with the FEM package, and offers two solution strategies: the stochastic Galerkin and collocation

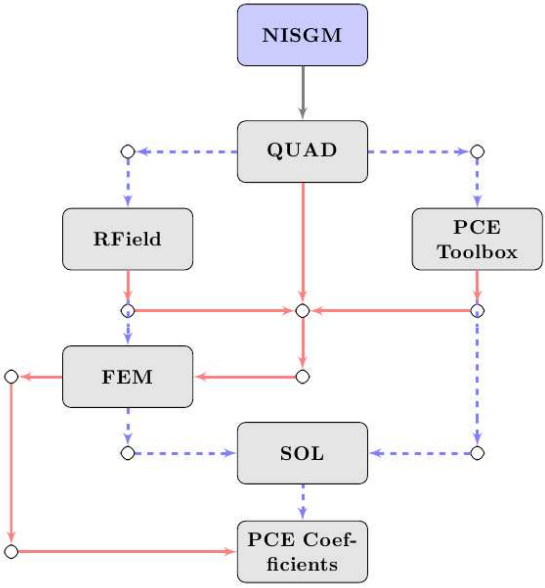

Figure 7.4: Schematic representation of stochastic Galerkin and collocation methods

approaches. In case of stochastic Galerkin, the FEM is used for the evaluation of the residual realisations (QUAD), as well as for building preconditioners of nonlinear solver. However, the process of solving stochastic system of equations is done outside of FEM in SOL sub-module. Interpolation is designed in a similar way. Namely, one calculates the solution (FEM solve), computes the PCE basis (PCE Toolbox) with the help of the quadrature (QUAD), and then solves the linear system (SOL) of equations right before the delivery. Both procedures are schematically represented in Fig. 7.4 where the Galerkin projection is denoted by the red full line and the interpolation by the blue dashed line.

SOL consists of procedures for solving the linear or nonlinear system of equations in both the deterministic and stochastic case. For the linear system there are several possibilities such as the Gauss-Seidel method, GMRES with SSOR, GMRES with ILU, CG, PCG method and so on. In case of nonlinearities the Newton-Raphson, modified Newton-Raphson and BFGS are offered.

STAT post-processes the solution. The method of computing the statistics depends on the form of the data delivered to STAT. If the output is an ensemble of samples, one computes the statistics in usual way. However, one may also project the data onto the polynomial chaos basis, and then compress PCE via the singular value decomposition for future saving. If the data are already in PCE format the statistics are computed in a straightforward manner.

7.1.1 The PCE toolbox

The polynomial chaos algebra as described in Chapter 6 plays a very important role in the algorithm structure of ISGM. The algebra is implemented in the PCE Toolbox module in a form of METHODS, i.e. functions that operate on PCE and its index, and OPERATIONS executing the mathematical operations on a given PCE, also called polynomial chaos variable (PCV). The linear and nonlinear operations are of the general type and may be applied on the PCV or the MPCV (matrix valued PCV). Each mathematical operation has its own function which directly computes the resulting PCV. For example, in case of division one may use $dpcet$, where the corresponding system of equations is solved in the direct way, or using PCG iterations via $dpcetpcg$. All functions that carry $quad$ in the name are functions which numerically compute the coefficients using some sampling rule from QUAD. Similarly, all functions which end on mc are of the Monte Carlo type. A typical example is the function for computing the square root of PCV. Its implementation is done in several forms such as $pcsqrtnew$ for the Newton method, $pcsqrthalley$ for Halley's method, $pcsqrtinv$ for the inverse Newton, $pcsqrtinvhalley$ for the inverse Halley's method, and finally functions which compute roots numerically: $sqrtmc$ and $sqrtquad$.

The second important part of the PCE Toolbox is the part which computes the coefficients of the PCE for some specified random field, or random variables in KLE. The computation can be done in a purely algebraic way: get_pce or numerically $pce\_numerical$. Similarly, if one would like to project the ensemble of data on the PCE basis then the functions $mc2pce$ or $quad2pce$ can be used. The group of functions *Set PCE* evaluates efficiently the PCE basis in a finite number of points with the help of the vectorisation techniques described in Section 7.2. Finally, the group of functions INDEX operates with Hermite polynomials and corresponding indices.

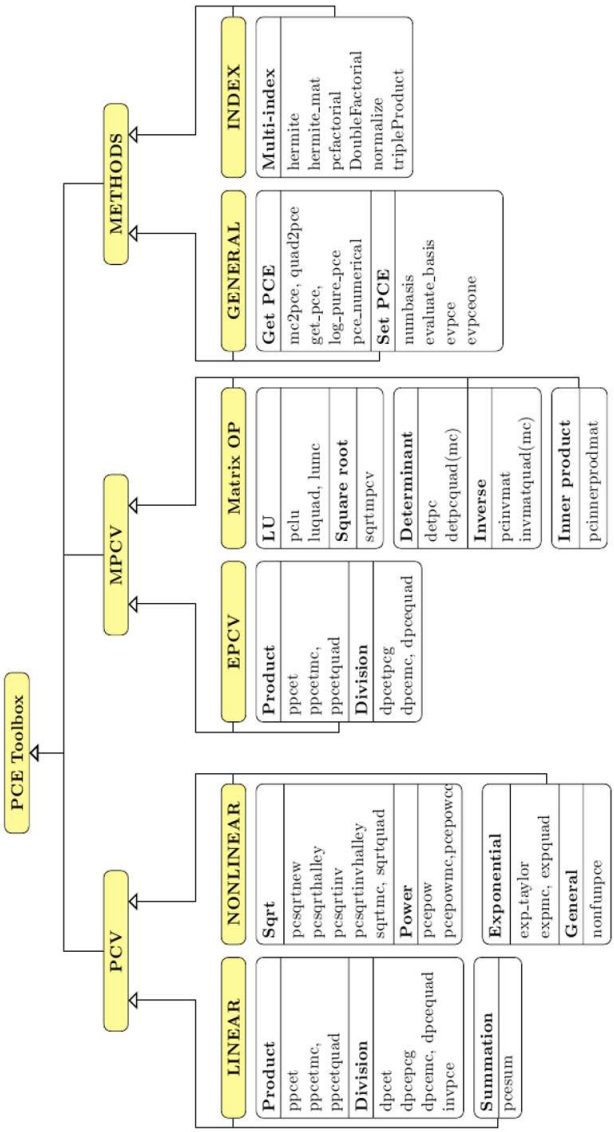

Figure 7.5: The polynomial chaos algebra toolbox

7.2 Storage and vectorisation

In order to reduce the memory requierements, the fully dense tensors are stored in sparse format. The sparsity increases with the polynomial order, see Table 7.1 on the examples of the global stiffness matrix $\mathbf{K}$ and the stochastic tensor Δ. The PLASTON library uses the so-called coordinate storage, i.e. the tensor $\mathbf{A} \in \mathbb{R}^{N_1 \times N_2 \ldots \times N_n}$ is uniquely stored as a vector $a \in \mathbb{R}^P$ and a matrix $A \in \mathbb{R}^{P \times R}$. In this manner the memory requirement reduces to $(R+1)\text{nnz}(\mathbf{A})$ [18, 117]. Similarly, the computation cost drastically decreases. For example, the cost of the inner product of two tensors reduces from $\mathcal{O}(\text{nnz}(\mathbf{A})\text{nnz}(\mathbf{B}))$ to $\mathcal{O}(P \log P)$, where $P = \text{nnz}(\mathbf{A}) + \text{nnz}(\mathbf{B})$. For tensor-vector multiplication the cost is $\mathcal{O}(\text{nnz}(\mathbf{A})$, and for tensor-tensor multiplication the cost depends on the mode. It can be high $\mathcal{O}(\text{nnz}(\mathbf{A})\text{nnz}(\mathbf{B}))$ or low $\mathcal{O}(\text{nnz}(\mathbf{A})\log \text{nnz}(\mathbf{A}) + \text{nnz}(\mathbf{B}) \log \text{nnz}(\mathbf{B}))$.

Table 7.1: The number of elements and sparse density ρ of stochastic matrices with the polynomial order. The deterministic matrix $\mathbf{K}$ has size 117649 and density $\rho = 0.0720$.

p	$\mathcal{J}_{M,p}$		$\mathbf{K}$		Δ	
	Num	ρ	Num	ρ	Num	ρ
2	30	0.4	1176490	0.0354	1000	0.0820
3	60	0.5	2352980	0.0248	8000	0.0478
4	115	0.571	4117715	0.0182	42875	0.0356
5	168	0.625	6588344	0.0139	175616	0.0272
6	252	0.6667	9882516	0.0110	592704	0.0229

Compressing the tensors in a Tucker format, the computational cost decreases according to [18]. The Tucker tensor requires much less memory than the full tensor, i.e. the storage of the core plus the storage of the matrices entering the sum vs. the storage of the full tensor (the number of elements is equal to the product of the tensor dimensions). In case of the tensor-matrix multiplication the cost is of the matrix-matrix multiplication; for the tensor-vector multiplication the multiplication of the matrix with vector and the core with the vector. Similarly, one may find the costs of the tensor-tensor multiplication, leading to the considerable time savings [18].

In PLASTON those operations are implemented via the Tensor Toolbox package, see [116].

7.2.1 Vectorisation of the deterministic solver

Extending the idea of the paper [185] on quadrilateral elements, an effective vectorised finite element code is implemented in PLASTON. The algorithm substitutes all element-wise arithmetic operations carried out element by element by the matrix-wise vector operations. The efficiency improvement of such implementation may be seen in Table 7.2. The table compares the computation times of the classical algorithm with the newly improved (vectorised). Note that the assembling of the stiffness and mass matrices are the most improved, while the element calculations are not influenced so much. The reason for this is that the element calculations are characterized by matrices and vectors of small size (deterministic case).

Table 7.2: Improvement in computation time with vectorisation

Term	**Vectorised [s]**	**Classical [s]**	**Size**	**Factor**
Mass assembling	0.15	36.66	2260	238.80
Stiffness assembling	0.80	293.19	2260	367.10
Element calculations	0.13	5.17	2260	40.48
Mass assembling	0.12	0.15	176	1.22
Stiffness assembling	0.05	0.20	176	3.97
Element calculations	0.11	0.22	176	1.94

The speed-up of the computation run of the deterministic code greatly influences all PLASTON procedures, especially the non-intrusive methods such as the non-intrusive Galerkin, the direct integration and collocation. In addition, the vectorisation contributes much more to the nonlinear than linear problems. Namely, by vectorisation the time for the matrix assemble in each integration point and each iteration of the Newton method reduces from 290 to 0.8 seconds. This is achieved by using only the matrix-vector products and avoiding point-wise multiplications. The vectorisation is basically done such that all the variables are memorised in the tensor format. The tensor dimensions are specified by the number of the components, integration points (in FEM), elements, and PCE coefficients. Such formed tensors are then stored in sparse format such that the Tensor Toolbox [116] or special functions in vectorisation toolbox can be used.

7.3 Algorithmic scheme

Fig. 7.6 shows the simple scheme of the PLASTON algorithm. The preprocessing step reads the input data from the $.txt$ files and builds three data structures: $geom$, rhs and $elem$. The first one stores the nodal information: the coordinates, the total number of nodes, boundary conditions, the element integration rule, etc. The structure $elem$ provides the information about elements and boundary conditions such as the connectivity array, the total number of the elements, etc., while rhs describes the loading conditions. During this phase the mass matrix is computed and the material parameters are initialized in corresponding structures. They describe the input random fields via the type of the distribution, the second order statistics and polynomial order. As the material characteristics are in general of the non-Gaussian type, the function *base_randomfield()* maps them back to the Gaussian base field and outputs the corresponding characteristics in *rfg*. In addition, the function *base_randomfield()* computes the KLE decomposition of both the Gaussian (*rfg*) and non-Gaussianl random field (*rfgl*). After this, the KLE random variables are expanded to the PCE via *get_pce()*, which outputs the coefficients of the combined KLE/PCE expansion. The combined expansion does not correspond to the integration point level, but nodal. Thus, the suitable transformation is performed. However, if the random fields are positive definite (lognormal) the interpolation is not done directly. Instead, the fields are mapped by a lognormal transformation from the cone to the vector space in which the straightforward interpolation is possible. Finally, the preprocessing step ends by computing the triple product of the Hermite polynomials *triple_product()*, which is then stored in the memory for the later use. Note that depending on the type of the analysis the preprocessing step may be slightly different than presented. Namely, instead of *get_pce* one may have function *set_pce* which computes the realisation of KLE or PCE necessary for the methods that use the stochastic integration rules.

After all the input data have been prepared, the function *force()* computes the right hand side from the loading conditions memorized in *rhs*. This means that the time integration is performed and the loading step in time n evaluated. Once the loading and the number of the steps are known, the iterative loop over n is activated. This is then followed by the iterative loop over k coming from the nonlinear solver. Before the loop is started, all random fields and variables are initialised in function *initialise*, which takes for the initial conditions the values from the previous converged time step. The iterative method calls classical functions such as *epl_matrix*, *build_tenstiff*, and *apply_force* which compute the tangent modulus, the factorisation of the stochastic stiffness matrix, and the residual, respectively. The linear system of equations is solved inside of *solve_linsys*, which further handles the solution to *update_disp* for the configuration update (i.e. the displacement update). As schematic diagram in

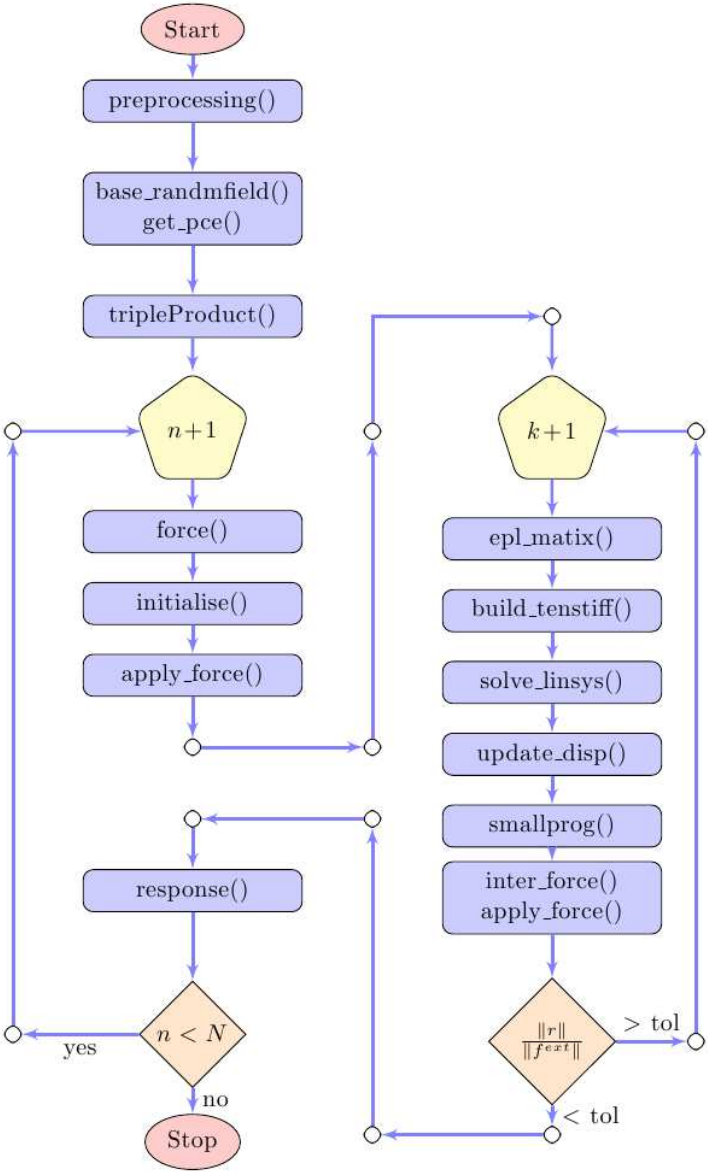

Figure 7.6: The schematic diagram of PLASTON

Fig. 7.6 is made for the small displacement analysis, the elastoplastic state is evaluated by function *smallprog*, and the internal force by *inter_force* and *apply_force*. Note that the presented ISGM scheme is similar to those in classical finite element programs. The difference lies in the pre-processing and post-processing step and the way of treating the variables (not deterministic any more).

7.4 Summary

This chapter briefly summarises the construction of the MATLAB library PLASTON with the special focus on the description of the overall design, implementation of the polynomial chaos algebra operations, and the code vectorisation. Some specific and the most important parts of the code are already given in previous chapters, for example the stochastic Newton method. In order to graphically describe the computational process the schematic form of the main algorithm is also presented and shortly described.

Chapter 8

Numerical results

The numerical study will start with a relatively simple example describing material properties in a form of random variables independent of spatial coordinates, i.e. the homogenous case. Such an example is suitable for further numerical analysis because the number of the stochastic degrees of freedom one has to deal with is relatively small. Later on the author will progress to the more difficult case illustrating the properties of the stochastic Galerkin method applied on a more realistic material description in a form of random fields, as introduced in Section 8.2.

8.1 Random variable case

In order to do the proper numerical analysis of the stochastic Galerkin method a simple test example in 2D conditions is chosen, see Fig. 8.1. The plate with a

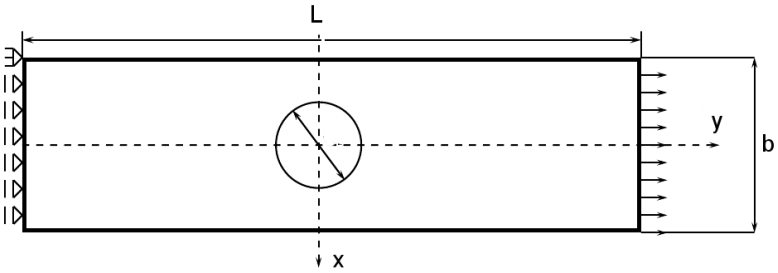

Figure 8.1: Geometrical setup of the problem

hole (dimensions $L = 56$[mm], $b = 20$[mm], $d = 10$[mm], and unit thickness) in plane strain conditions is constrained at one edge and loaded by uniform tension $f = 2t$[kN] at the opposite. The material is described by uncertain bulk K[GPa]

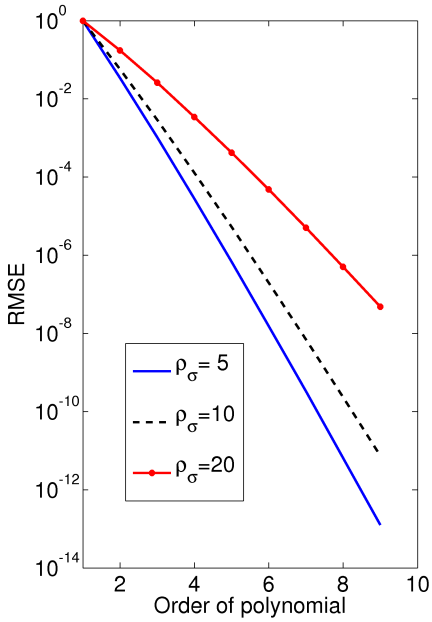

Figure 8.2: The RMSE of the input approximation

modulus, shear G[GPa] modulus and yield stress σ_y[GPa]; all three taken to be log-normally distributed random variables according to the maximum entropy principle (homogeneous case). In addition, the yield criterion is chosen to be of the von Mises type with the linear isotropic hardening $H_{iso} = 2.24$[GPa] as a deterministic parameter. To be more specific, the random parameters are modelled as:

$$\begin{aligned} K &= 10 + 15 \cdot \exp(1 + \sigma_1 \theta_1), \\ G &= 10 + 5 \cdot \exp(1 + \sigma_2 \theta_2), \\ \sigma_y &= 0.1 + 0.25 \cdot \exp(\sigma_3 \theta_3), \end{aligned} \tag{8.1}$$

where $\{\theta_i\}_{i=1}^3$ are the standard Gaussian RVs and $\{\sigma_i\}_{i=1}^3$ are the input standard deviations. The modified lognormal distributions in Eq. (8.1) are the right choice with respect to the positive-definitness of properties they model, however only if one presumes that the variables have finite variance, see Section 3.3.

To start numerical computations the random variables $\kappa \in \{K, G, \sigma_y\}$ are effectively approximated by polynomial chaos expansions (PCEs) whose coefficients are obtained by simple projection $\kappa^{(\alpha)} = \mathbb{E}(\kappa H_\alpha(\theta(\cdot))$. The accuracy of this approximation strongly depends on the polynomial order, see Chapter 6. The proper choice has to be made with respect to the input variance of κ, i.e. of σ_i according to Eq. (8.1). The dependence can be shown by computing the relative root mean square error:

$$\epsilon = \|\kappa_a - \kappa_t\|_{L_2(\Omega\times\mathcal{G})} / \|\kappa_t\|_{L_2(\Omega\times\mathcal{G})} \tag{8.2}$$

versus the polynomial order of κ_a, where κ_a and κ_t represent the PCE approximation and the true (analytical) value of κ, respectively. The plotted results in Fig. 8.2 discover that the RVs with large input variance, or coefficient of variation $\rho_\sigma = \text{std}(\kappa)/\mathbb{E}(\kappa) \cdot 100\%$, require higher polynomial order than the RVs with small ρ_σ for the same accuracy. Due to this the following section studies three different test scenarios: $\rho_\sigma = 5\%$, $\rho_\sigma = 10\%$, and $\rho_\sigma = 20\%$, each of them representing a higher level of difficulty. Notice that $\rho_\sigma = 20\%$ is not so often met in practice as the uncertainties in engineering problems are not so strong. However, this case is of great numerical importance, and thus will be considered further.

8.1.1 Reference solution

To compare the methods described in Chapter 5 the result of the Monte Carlo simulation with $N = 10^6$ samples is introduced as the reference solution. According to the law of large numbers, this method displays $1/\sqrt{N}$ convergence. In other words, regardless of the number of the stochastic dimensions the MC method reduces the error three times by increasing the number of samples nine times. This is apparent in Fig. 8.3 where the root mean square error (RMSE) is plotted across the number of samples. Note that both the stress and the plastic strain RMSE are slowly converging with the number of samples. The same is valid for the mean value.

In addition to these, Table 8.1 plots the convergence in variance for the stress components, and Table 8.2 for the strain components. Apparently very few samples ($\approx 10^3$) are not sufficient to accurately represent the solution as expected. However, from these data one can see that the error in the strain is smaller than the error in the stress. This happens as the coefficient of variation of strain $\rho_\sigma(\varepsilon)$ is smaller than the coefficient of variation of stress $\rho_\sigma(\sigma)$ (as will be shown later). Graphically the convergence in variance is shown in Fig. 8.4, where the variance is plotted across the number of the finite element node. By comparing plots on the left and right hand side

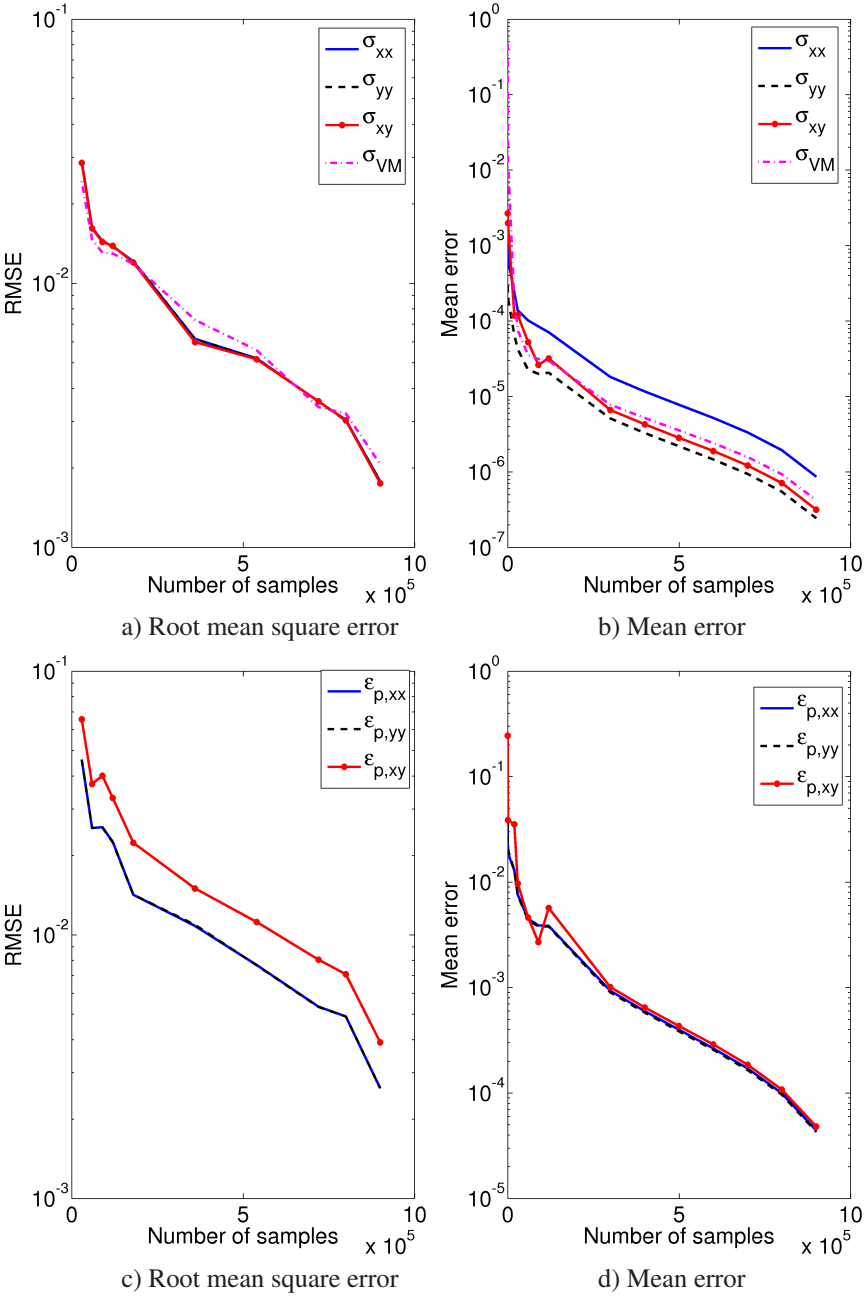

Figure 8.3: The stress and plastic strain convergence obtained by MC. The test is performed for $\rho_\sigma = 5\%$.

Table 8.1: Relative error in stress variance with the number of samples used in the Monte Carlo integration. The results are given for the input uncertainty equal to $\rho_\sigma = 5\%$.

No. samp.	σ_{xx}	σ_{yy}	σ_{xy}	σ_{VM}
10^3	6.6e+01	2.9e+02	2.1e+01	1.6e+02
$3 \cdot 10^4$	1.4e+00	7.5e+00	1.7e-01	2.8e+00
$1.2 \cdot 10^5$	2.9e-01	1.4e+00	1.3e-02	7.1e-01
$5.4 \cdot 10^5$	5.2e-02	3.0e-01	5.8e-03	9.0e-02
$8 \cdot 10^5$	2.1e-02	5.0e-02	4.0e-03	4.1e-02
$9 \cdot 10^5$	3.0e-03	1.0e-02	4.0e-03	4.0e-02

Table 8.2: Relative error in strain variance with the number of samples used in the Monte Carlo integration. The results are given for the input uncertainty equal to $\rho_\sigma = 5\%$.

No. samp.	ε_{xx}	ε_{yy}	ε_{xy}	$\varepsilon_{p,xx}$	$\varepsilon_{p,yy}$	$\varepsilon_{p,xy}$
$3 \cdot 10^4$	1.3e-01	9.7e-01	5.9e-01	6.0e-02	6.0e-02	1e-01
$1.2 \cdot 10^5$	7.0e-02	4.5e-01	2.9e-01	2.0e-03	2.0e-03	2.0e-03
$5.4 \cdot 10^5$	1.0e-02	8.0e-02	5.0e-02	1.9e-03	1.9e-03	6.0e-03
$8 \cdot 10^5$	3.0e-03	1.2e-02	8.0e-03	3.0e-03	3.0e-03	4.0e-03
$9 \cdot 10^5$	2.0e-03	1.0e-02	4.0e-03	5.0e-04	5.0e-04	1.3e-03

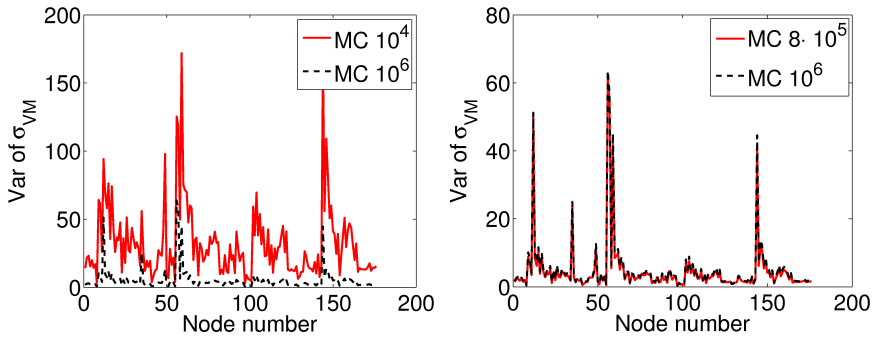

Figure 8.4: The MC solution compared to the reference solution

Table 8.3: The uncertainty in the response ρ_σ in $[\%]$ obtained by the direct integration in plastic (P) and elastic (E) points of domain.

State	ρ_σ	σ_{xx}	σ_{yy}	σ_{xy}	ε_{xx}	ε_{yy}	ε_{xy}	ε_{pxx}	ε_{pyy}	ε_{pxy}
P	5	17.3	1.7	4.0	6.2	3.1	3.9	90.7	90.2	75.5
P	20	42.4	5.9	4.9	30.3	14.8	19.3	137.8	132.5	123
E	5	1.0	0.6	2.9	4.9	3.1	3.6	-	-	-
E	20	4.9	2.5	2.0	23.6	14.6	17.0	-	-	-

of Fig. 8.4 one may notice that the variance converges to the reference solution with the increase of the number of samples used in integration.

Finally, Table 8.3 provides the results of the uncertainty quantification in the structure response represented by the appropriate coefficient of variation ρ_σ. The coefficients are computed in two points in the domain, one with elastic (E) and one with plastic (P) response. As one may notice, the plastic deformation has the largest uncertainty ratio ρ_σ in both cases, i.e. it is the most sensitive on the uncertainties in the input characteristics. If the input uncertainty increases (ρ_σ of material properties) the output uncertainty will increase too, not only for the plastic deformation but also for other quantities. In addition, the elastic response has a much smaller coefficient of variation than the plastic one, as already expected.

8.1.2 Intrusive Galerkin method

The intrusive Galerkin method as described in Section 5.4.1 is a purely direct "deterministic" method and does not require sampling at any stage. Instead, the method employs the polynomial chaos algebra (see Chapter 6) and delivers the surrogate solution in a form of the polynomial chaos expansion. Due to this the input properties are approximated in a form of the PCE of order p_κ, and the ansatz of the solution is assumed to be the PCE of order p_u. This further means that in each time step and each iteration one has to solve the linear system of equations of size $N \times Z$, where N represents the number of the spatial degrees of freedom and Z the cardinality of the solution PCE determined by the number of input RVs and polynomial order p_u. In order to properly investigate the convergence of the method and sesnitivity of the system, the input parameters are assumed to be random separatelly, i.e. each at the time.

Only through this analysis one may investigate the sensitivity of the output on the input uncertainty. Later on the study will be done for all three uncertain parameters as a more realistic scenario.

Let us assume that the bulk modulus K is described by a lognormal distribution as in Eq. (8.1). In order to investigate its influence on the system response two values of $\rho_\sigma(K) = \{5\%, 20\%\}$ are observed, as previously described. According to Fig. 8.2, the polynomial expansion of order $p_K = 6$ can be safely used for the approximation of the bulk modulus with $\rho_\sigma = 5\%$. On the other side, for the same accuracy $\rho_\sigma = 20\%$ requires a higher polynomial order. However, the question is which polynomial order p_u is necessary to achieve the desired accuracy in the stress-or strain-like variables. In order to answer this question, the root mean square error is plotted versus the polynomial order p_K as well as p_u, see Table 8.4. The "reference" solution is computed with the polynomial order $p_u = 9$. According to Table 8.4 the relative RMSE decreases with the polynomial order and approaches the error of circa 10^{-11} for the polynomial order 6. Interestingly, the error is already small for a polynomial order $p_K = p_u = 2$ in both the stress and plastic strain case. This could be explained by a very small input variance which can be accurately approximated with only few polynomial terms. On the other side, the fact that $p_u = 2$ delivers satisfactory results shows that the uncertainty in the bulk modulus is not so drastically influencing the uncertainty in the response, as will be discussed later in the text. Note that the solution of order one is not computed as the input in this case would be normally distributed and not positive-definite any more.

The uncertainty in the shear modulus G gives similar results to those obtained for K. This is expected as the bulk and shear moduli are constructing the more general random parameter—constitutive tensor $\boldsymbol{A}$. Therefore, the table with the calculated RMSE for uncertain G is not provided. Instead, the influence of the uncertainty in σ_y on the system response is investigated. Namely, the yield stress (together with the material hardening) can have huge impact on the system response since it defines the starting point of the plastic flow. This is proven in Table 8.5, which discovers that the same amount of uncertainty ($\rho_\sigma = 5\%$) in σ_y and K produces different results. Namely, for the same polynomial approximation σ_y delivers larger RMSE. To be more specific, the error in stress does not change drastically compared to Table 8.4, while the error in plastic strain grows. In this situation the polynomial order 2 cannot be any more successfully used for the computation of the final solution. Instead, one has to use the double polynomial order to get the same accuracy in the plastic strain as for K. The reason can be found in the approximation of the convex set which strongly depends on the yield condition and σ_y. As in this case both the von Mises and the yield stress are uncertain, the state of the material point (whether is plastic or elastic) is greatly influenced by the adopted probability level.

Table 8.4: The response RMSE (see Eq. (8.2)) for uncertain K with $\rho_\sigma = 5\%$. The error is computed with respect to the solution obtained using polynomial order 9. The input is approximated by order p_K and the response by p_u.

p_K	p_u	σ_{xx}	σ_{yy}	σ_{xy}	$\varepsilon_{p,xx}$	$\varepsilon_{p,yy}$	$\varepsilon_{p,xy}$
2	2	1.1e-05	1.8e-06	1.0e-05	7.0e-05	1.5e-05	1.3e-05
3	3	2.8e-07	3.9e-08	8.0e-07	7.6e-08	7.8e-08	7.9e-08
4	4	1.3e-09	2.2e-10	3.6e-09	2.0e-10	1.9e-10	1.6e-10
6	6	5.3e-11	8.5e-12	1.9e-11	9.7e-14	2.3e-13	8.2e-13

Table 8.5: The response RMSE (see Eq. (8.2)) for uncertain σ_y with $\rho_\sigma = 5\%$. The error is computed with respect to the solution obtained using polynomial order 9. The input is approximated by order p_k and the response by p_u.

p_{σ_y}	p_u	σ_{xx}	σ_{yy}	σ_{xy}	$\varepsilon_{p,xx}$	$\varepsilon_{p,yy}$	$\varepsilon_{p,xy}$
2	2	2.9e-05	8.5e-06	2.3e-05	8.4e-04	1.3e-03	6.1e-02
3	3	1.1e-06	4.4e-07	1.5e-06	1.9e-05	6.3e-05	4.3e-03
4	4	5.1e-08	2.7e-08	1.1e-07	1.1e-07	3.4e-06	2.5e-05
6	6	1.9e-12	6.5e-11	8.6e-11	4.7e-12	1.1e-09	2.4e-09

Table 8.6: The response RMSE (see Eq. (8.2)) for all three uncertain parameters with $\rho_\sigma = 5\%$. The error is computed with respect to the solution obtained using polynomial order 9. The input is approximated by order p_κ and the response by p_u.

p_κ	p_u	σ_{xx}	σ_{yy}	σ_{xy}	$\varepsilon_{p,xx}$	$\varepsilon_{p,yy}$	$\varepsilon_{p,xy}$
2	2	3.9e-05	9.2e-06	3.8e-05	1.7e-03	1.8e-03	6.9e-02
4	4	1.3e-07	4.2e-08	1.3e-07	1.0e-06	3.7e-06	4.4e-05
6	6	9.3e-10	3.9e-10	3.5e-10	4.5e-11	6.7e-10	2.1e-08

Table 8.7: The root mean square error (see Eq. (8.2)) for uncertain K with $\rho_\sigma = 20\%$. The error is computed with respect to the solution obtained using polynomial order 9. The input is approximated by order p_k and the response by p_u.

p_K	p_u	σ_{xx}	σ_{yy}	σ_{xy}	$\varepsilon_{p,xx}$	$\varepsilon_{p,yy}$	$\varepsilon_{p,xy}$
2	2	1.6e-03	2.9e-04	3.4e-03	1.8e-02	1.7e-02	2.2e-02
3	3	1.9e-04	3.7e-05	7.8e-04	5.4e-03	6.1e-03	4.9e-03
4	4	7.1e-05	1.2e-05	1.2e-04	1.1e-03	6.0e-04	3.4e-03
6	6	9.8e-06	1.7e-06	6.5e-06	1.4e-06	3.7e-06	8.1e-06

Table 8.8: The root mean square error (see Eq. (8.2)) for uncertain σ_y with $\rho_\sigma = 20\%$. The error is computed with respect to the solution obtained using polynomial order 9. The input is approximated by order p_{σ_y} and the response by p_u.

p_{σ_y}	p_u	σ_{xx}	σ_{yy}	σ_{xy}	$\varepsilon_{p,xx}$	$\varepsilon_{p,yy}$	$\varepsilon_{p,xy}$
2	2	9.3e-02	2.6e-02	3.6e-02	4.6e-01	5.3e-01	9.6e-01
3	3	9.3e-02	2.6e-02	3.6e-02	4.6e-01	5.3e-01	9.5e-01
4	4	9.3e-02	2.6e-02	3.6e-02	4.6e-01	5.3e-01	9.5e-01
6	6	9.3e-02	2.6e-02	3.6e-02	4.6e-01	5.3e-01	9.5e-01

Table 8.9: The root mean square error (see Eq. (8.2)) for all three uncertain parameters with $\rho_\sigma = 20\%$. The error is computed with respect to the solution obtained using polynomial order 9. The input is approximated by order p_κ and the response by p_u.

p_κ	p_u	σ_{xx}	σ_{yy}	σ_{xy}	$\varepsilon_{p,xx}$	$\varepsilon_{p,yy}$	$\varepsilon_{p,xy}$
2	2	8.3e-03	2.0e-03	7.8e-03	7.3e-02	8.0e-02	4.7e-01
4	4	4.8e-03	1.2e-03	1.4e-03	3.9e-02	3.4e-02	1.8e-01
6	6	4.7e-03	1.1e-03	1.1e-03	3.8e-02	3.4e-02	1.6e-01

Surprisingly, the results for RMSE for all three uncertain parameters in Table 8.6 are very much similar to those in Table 8.5. The only difference is that the error slightly grows in both stress-and strain-like variables due to the increase of the input uncertainty. This further means that the final response is mostly influenced by σ_y for the same level of uncertainty in all three parameters.

Even though the material properties in practice do not exceed the uncertainty percentage of 5%, the ratio $\rho_\sigma = 20\%$ is further considered due to its numerical importance. Namely, with the increase of the input ratio ρ_σ the convergence of the intrusive Galerkin method (ISGM) slows down in all three case studies, see Table 8.7 to Table 8.9. For example, if ρ_σ of the bulk modulus increases four times, the corresponding error increases by multiple two, see Table 8.7. The same applied on ρ_σ of σ_y (Table 8.8), or on ρ_σ of all three uncertain parameters (Table 8.9), results in even bigger errors. The reason for this lies in the truncation errors of the PCEs approximations of the input properties and the ansatz. In other words, the truncation errors grow with the increase of the input variance if the polynomial orders p_κ and p_u do not change. Furthermore, one may investigate the sensitivity of the method on the input uncertainty. While the sixth polynomial order gives accuracy of circa 10^{-6} in the response for the uncertain K (see Table 8.7), the same or even higher polynomial order produces much bigger error in the output for uncertain σ_y, see Table 8.8. Adding K and G as uncertain the algorithm becomes more stable, and thus the error in Table 8.9 reduces. However, in order to get the accurate solution, one has to use high polynomial order approximations.

The previous analysis reveals that not all uncertain parameters have the same type of influence on the result. This is also apparent from Table 8.10 and Table 8.11 which provide the variation coefficient ρ_σ of the output data. Tables show the results for two points in the domain: P in the plastic and E in the elastic area. Namely, Table 8.10 discovers that when the uncertainty in the input grows the response ratio ρ_σ increases. The largest value belongs to the first stress component σ_{xx} and the smallest to the shear stress. This is expected due to the properties of the external force. One may notice that the ratio ρ_σ is much bigger for the plastic than elastic stress response because the stress is strongly nonlinear in input parameters. However, the change in the deformation ratio ρ_σ is not so drastic. Fig. 8.5 depicts a clear trend of the variance increase of the von Mises stress with the increase of the input uncertainty in both the elastic and plastic zone.

What is interesting in the data presented in Table 8.11 is that the first and the second stress component, as well as the plastic strain, are strongly influenced by the uncertainty in σ_y. On the other side, the shear modulus G propagates the most of the uncertainty in the total strain ε. A similar behaviour is shown in Fig. 8.6, where the

Table 8.10: The uncertainty in the response obtained by the intrusive Galerkin approach for the plate with a hole under the extension and assuming the yield stress, bulk and shear modulus as uncertain according to Eq. (8.1). The order of polynomials used in calculation equals 6. The yield condition in the material point is computed according to p_{90} criteria.

IU	σ_{xx} [%]	σ_{yy} [%]	σ_{xy} [%]	ε_{xx} [%]	ε_{yy}[%]	ε_{xy} [%]
plastic						
5%	23.17	1.80	4.19	6.13	2.95	3.81
10%	39.18	3.02	2.51	10.21	4.92	6.34
20%	142.34	9.62	9.98	30.34	14.65	18.65
elastic						
5%	0.88	0.23	2.91	4.80	2.94	3.44
10%	1.46	0.38	0.05	7.98	4.89	5.72
20%	4.58	1.19	0.20	23.43	14.40	16.78

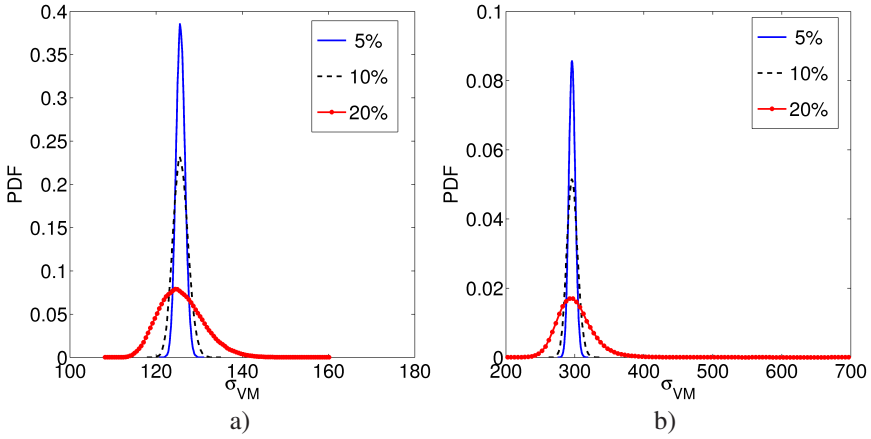

Figure 8.5: Influence of the input uncertainty ρ_σ on the PDF of the von Mises stress σ_{VM}: a) elastic zone b) plastic zone. All parameters are considered as uncertain.

Table 8.11: Comparison of the uncertainty in the response obtained by the intrusive Galerkin approach for the plate with the hole under the extension and assuming yield stress, bulk and shear modulus separately or all as uncertain according to Eq. (8.1). The order of polynomials used in the calculation equals 6 and the input uncertainty equals 5%. The yield condition is computed according to p_{90} criteria in each material point.

RV	σ_{xx}	σ_{yy}	σ_{xy}	ε_{xx}	ε_{yy}	ε_{xy}	$\varepsilon_{p,xx}$	$\varepsilon_{p,yy}$	$\varepsilon_{p,xy}$
P									
all	23.17	1.80	4.19	6.13	2.95	3.81	125.07	125.26	229.63
K	3.23	0.27	2.90	2.52	1.33	0.17	9.11	10.24	6.21
G	2.31	0.19	2.08	5.25	2.50	3.57	3.11	3.92	1.02
σ_y	22.86	1.78	2.18	1.89	0.84	1.30	124.75	125.08	226.89
E									
all	0.88	0.23	2.91	4.80	2.94	3.44	-	-	-
K	0.71	0.18	2.36	1.53	0.94	0.02	-	-	-
G	0.51	0.13	1.69	4.55	2.78	3.43	-	-	-

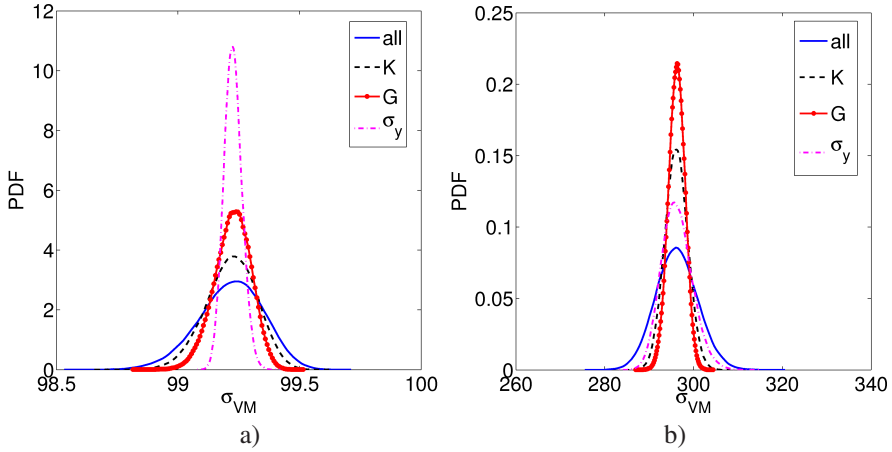

Figure 8.6: Influence of the input uncertainty on the PDF of the von Mises stress σ_{VM} in: a) elastic zone b) plastic zone

Table 8.12: The yield point: comparison of different decision criteria for one point in the domain and input uncertainty 20%.

Rule	σ_{xx}	σ_{yy}	σ_{xy}
Direct p_{50}	39.18	3.02	7.03
Direct p_{75}	17.22	3.89	6.26
Direct p_{90}	12.23	0.25	6.56
Direct p_{99}	12.23	0.25	6.56
Mean	39.18	3.02	7.033
Markov p_{75}	17.22	3.89	6.26
Markov p_{90}	26.65	3.45	7.49
Markov p_{99}	39.18	3.02	7.03
Chebyshev p_{50}	26.65	3.45	7.49
Chebyshev p_{75}	26.65	3.45	7.49
Chebyshev p_{90}	12.23	0.25	6.56
Chebyshev p_{99}	12.23	0.25	6.56

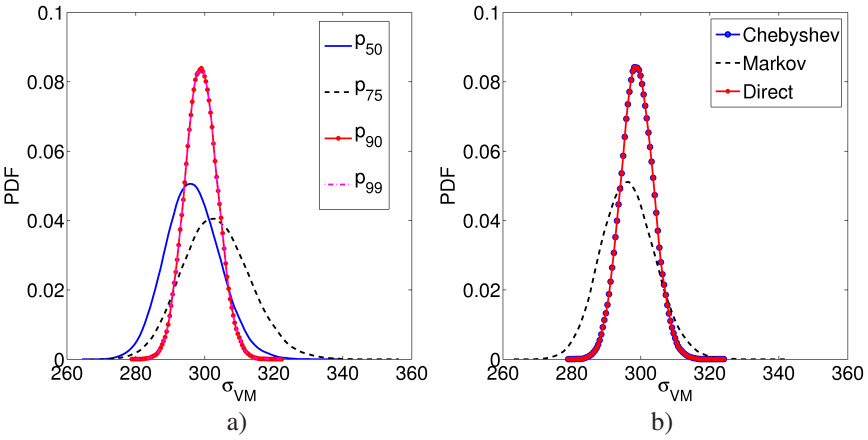

Figure 8.7: Influence of the decision criteria on the von Mises stress: a) the direct integration approach b) the direct integration, Chebyshev and Markov criteria for p_{90}. *All parameters are considered as uncertain with* $\rho_\sigma = 10\%$

probability density function (PDF) of the von Mises stress σ_{VM} is plotted versus input parameters. In the elastic zone the bulk and shear modulus shape the PDF of the von Mises stress σ_{VM}, while σ_y does not have any influence. The variance of σ_{VM} given σ_y exists only due to the truncation errors introduced by the algorithm. On the other side, in the plastic zone, see Fig. 8.6 b), the yield stress σ_y has the largest effect on σ_{VM}.

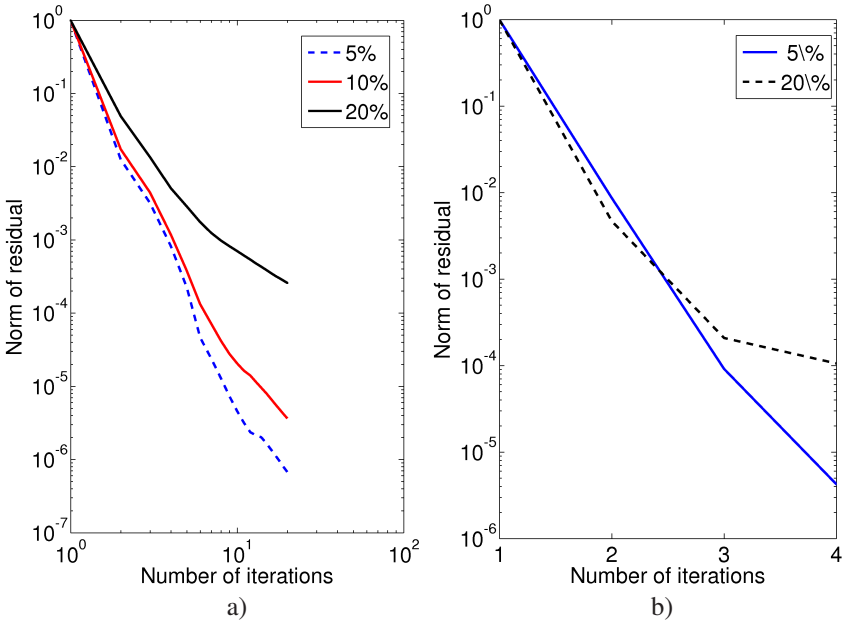

Figure 8.8: The residual convergence for different values of input ratio ρ_σ and a) all three random parameters b) uncertain bulk modulus

The previous analysis examined the impact of the input uncertainties on the system response without taking into consideration the type of the variational inequality criteria used to measure the distance between the von Mises stress and the elastic convex domain. The study in one material point in the domain reveals that not all criteria produce the same plastic zone, see Table 8.12. Namely, by increasing the probability level from p_{50} up to p_{99} the considered decision criteria reduce the plastic zone to a certain area. This means that the adopted probability level directly influences the output uncertainty ρ_σ. Additionally, ρ_σ is affected by decision making as different criteria may not deliver the matching plastic zone for the same probability level. For example, the Markov limit (p_{99}) and the mean criteria give the same result as the p_{50}

direct integration limit. However, they overestimate the response variance and give a larger ρ_σ than the p_{99} direct integration result. In contrast to this, the Chebyshev p_{99} criterion gives the same result as the direct integration. This is expected as the Chebyshev criterion takes into account the variance during the decision making, not only the mean as the Markov rule. Graphically this phenomenon is illustrated in Fig. 8.7 where the PDF of σ_{VM} is plotted against the decision rule.

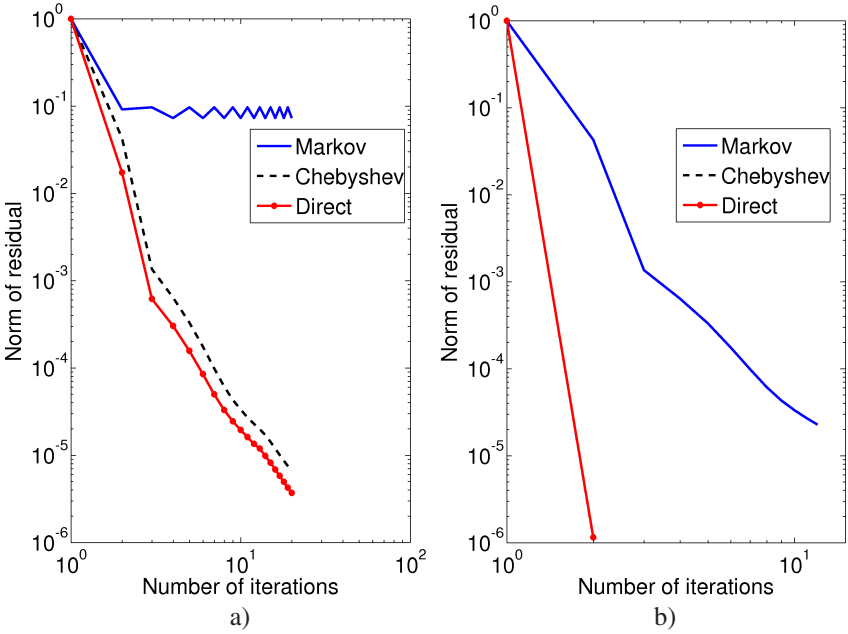

Figure 8.9: The residual convergence as a function of the decision criteria with: a) p_{50} level b) p_{90} level

Previous results do not reveal much the properties of the intrusive stochastic Newton method. Therefore, in order to investigate the convergence of the method, the L_2-norm of residual is plotted in Fig. 8.8. The polynomial order of input is taken to be $p_\kappa = 6$, while the polynomial order of the solution is $p_u = 9$. Clearly, the residual requires more iterations to converge with the increase of variance. On the other side, the fast convergence is observed only when one of the parameters is uncertain, e.g. K or G. However, in this case one may notice that the stochastic Newton method converges quadratically to the value of 10^{-4} when the convergence rate slightly changes. The reason for this lies in the frequent use of the Galerkin projec-

tions in PCE algebra, i.e. the existence of the local truncation errors. Such behaviour will be explained further in the following sections. Note that the convergence of the residual is also greatly affected by the decision criteria as shown in Fig. 8.9. For example, the Markov criterion with the p_{50} flow limit is diverging, while the mean criterion (direct) and Chebyshev converge. For the flow limit equal to p_{90} the direct integration and Chebyshev criteria converge fast, while the Markov criterion overestimates the state by predicting more plastic points than they really exist.

Comparison to the reference solution

The previous section demonstrated the properties of the intrusive Galerkin solution by comparing it to the "best achieved" intrusive solution of relatively high polynomial order. Even though this kind of analysis is proper, it is not sufficient to judge the method. Therefore, the ISGM solutions are compared to the reference solution described in Section 8.1.1.

The comparison of the ISGM algorithm to the direct integration technique is not an easy process. Namely, these two methods are not estimating the same problem, though on the first look it may seem so. The difference lies in the approximation of the convex set, i.e. in the prediction of the plastic state in each integration point. While the direct integration technique samples the variational inequality and estimates the plastic zone point-wise, the intrusive method uses the surrogate model (see Section 5.4.1) and predicts the plastic zone with respect to some probability level p_q. Hence, the following comparison has to be analysed carefully.

Table 8.13: The root mean square error of the intrusive Galerkin compared to the MC method for 10^6 *samples and all three uncertain parameters*

Order	σ_{xx}	σ_{yy}	σ_{xy}	σ_{VM}
2	5.6e-01	0.4947	5.4e-01	5.0e-01
3	5.2e-01	5.0e-01	5.3e-01	5.1e-01
4	5.6e-01	5.0e-01	5.3e-01	5.0e-01
6	1.3e-02	6.6e-03	6.5e-03	8.4e-03
9	1.3e-02	6.6e-03	6.5e-03	8.4e-03

In order to check the convergence of the ISGM algorithm Table 8.13 plots the root mean square error between the two solutions for all three uncertain parameters with

Table 8.14: The root mean square error of the intrusive Galerkin compared to the MC method for 10^6 samples and all three uncertain parameters

Order	ε_{xx}	ε_{yy}	ε_{xy}	$\varepsilon_{p,xx}$	$\varepsilon_{p,yy}$	$\varepsilon_{p,xy}$
2	6.3e-01	5.4e-01	5.6e-01	6.2e+00	6.0e+00	1.5e+00
3	6.2e-01	5.4e-01	5.5e-01	2.7e+00	2.9e+00	1.5e+00
4	6.1e-01	5.3e-01	5.5e-01	1.0e+00	1.0e+00	1.0e+00
6	6.0e-03	6.0e-03	7.0e-03	4.1e-01	4.2e-02	9.9e-01
9	6.0e-03	6.0e-03	7.0e-03	4.1e-01	4.2e-02	9.9e-01

$\rho_\sigma = 5\%$. The data clearly indicate that the polynomial orders higher than 4 have to be used in order to get 10^{-2} accuracy in the stress components. However, the same order is not enough to get the desired accuracy in the plastic strain components as the error is only reduced to 40% as shown in Table 8.14. This behaviour could be explained by the different sizes of the plasticity zones the two methods produce in each iteration of the Newton method. The size of the plastic zone directly influences the values of the plastic strain and thus the error. The drastic change in accuracy is revealed in Table 8.15. Namely, one may see that the presence of the uncertainty in material characteristics such as the bulk modulus is very well quantified by the polynomial order 9. However, the uncertainty in the yield condition is more problematic since σ_y produces larger errors than K for the same polynomial approximations.

Table 8.15: The root mean square error of the intrusive Galerkin (polynomial order 9) compared to the MC method for 10^6 samples and different number of uncertain parameters

RV	σ_{VM}	ε_{xx}	ε_{yy}	ε_{xy}	$\varepsilon_{p,xx}$	$\varepsilon_{p,yy}$	$\varepsilon_{p,xy}$
K	5.4e-3	5.5.e-3	5.6e-3	5.5e-3	5.5e-3	5.6 e-3	5.5e-3
σ_y	6.8e-3	6.3e-3	5.3e-3	7.1e-3	4.1e-01	4.2e-01	9.9e-01
all	1.3e-2	6.0e-3	6.0e-3	7.1e-3	4.1e-02	4.2e-01	9.9e-01

Besides the root mean square error, two more results are at least significant: the mean value and the variance. As indicated in Fig. 8.10 the mean value of components σ_{xx} and σ_{xy} match well the reference mean, while the variance of σ_{xx} is underestimated due to presence of the local truncation errors. On the other side, the strain estimates

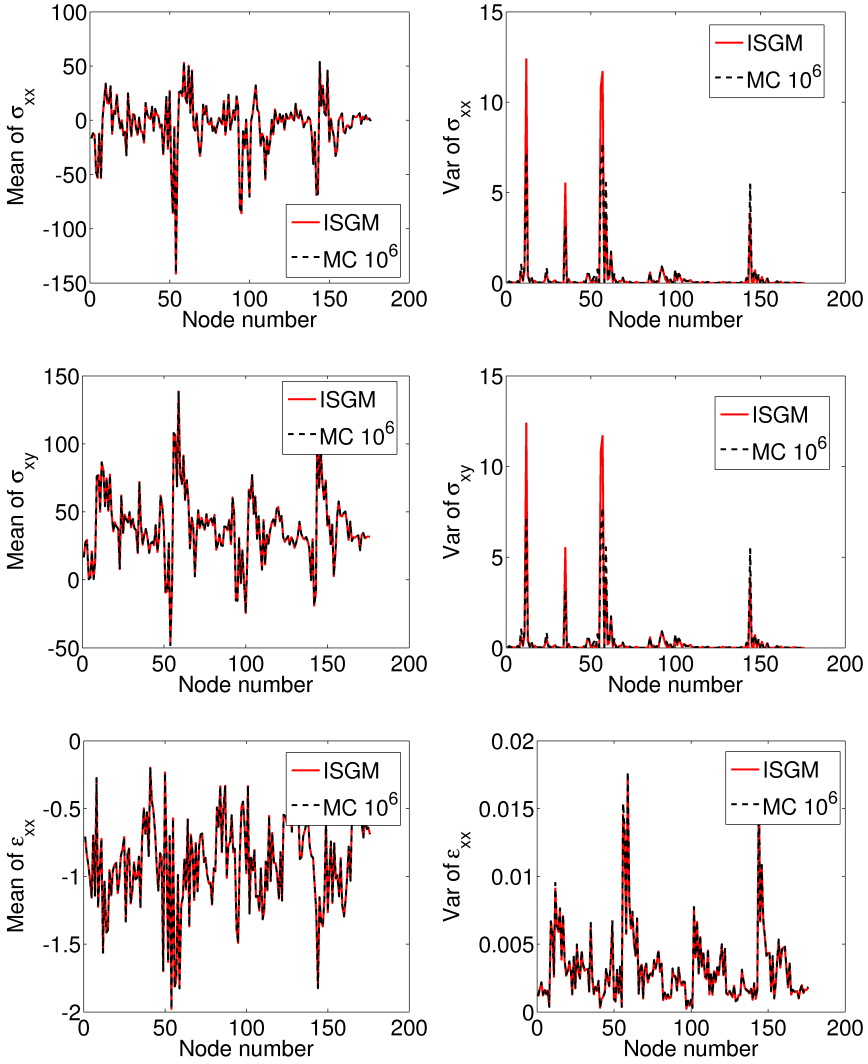

Figure 8.10: The second order statistics (mean and variance) of the intrusive stochastic Galerkin method (ISGM) and the Monte Carlo (MC) method. Comparison is done for the input uncertainty of 5%

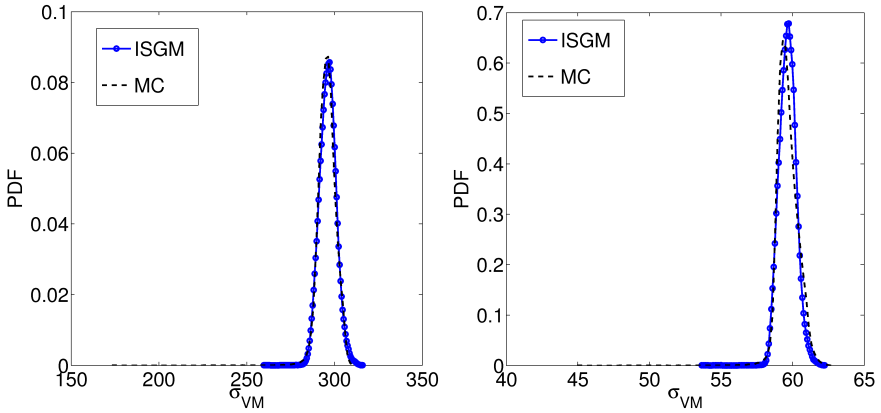

a) plastic point b) elastic point

Figure 8.11: Comparison of probability density functions of von Mises stress obtained by intrusive stochastic Galerkin method (ISGM) and Monte Carlo (MC) for points with plastic and elastic state

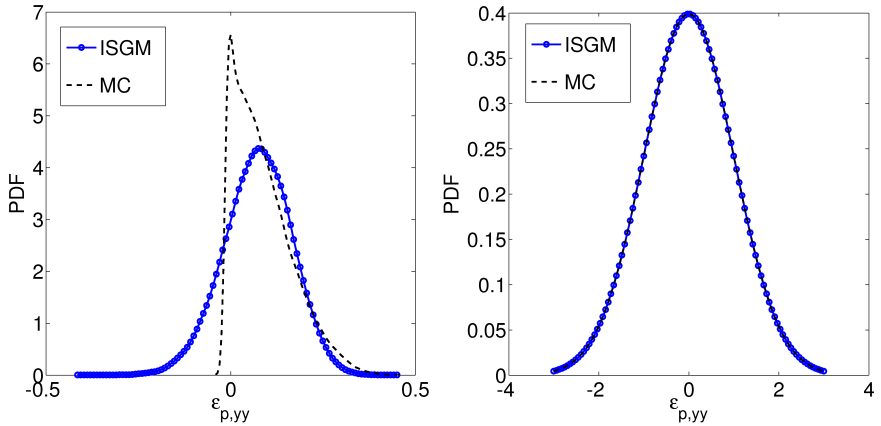

a) plastic point 1 b) plastic point 2

Figure 8.12: The probability density function comparison of the plastic strain obtained by the intrusive stochastic Galerkin method (ISGM) and Monte Carlo (MC) for two different points with plastic state

are coinciding. This can be seen in Fig. 8.11 and Fig. 8.12 where the PDF comparisons of the von Mises stress and the plastic strain in one FEM integration point are presented. In contrast to stress, the plastic deformation is not accurately approximated in both the elastic and plastic cases. The PDF obtained by the MC solution in the first plot of Fig. 8.12 is narrower and more skewed than the PDF computed by the ISGM. This means that the order used in the ISGM is not yet high enough to accurately approximate the reference PDF.

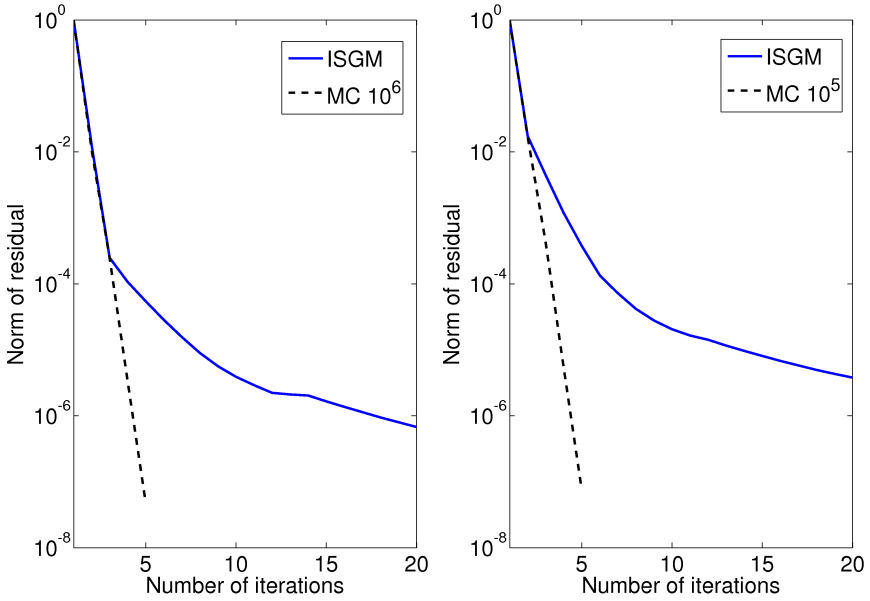

a) $\rho_\sigma = 5$ % b) $\rho_\sigma = 20$ %

Figure 8.13: The residual convergence of the intrusive stochastic Galerkin method (ISGM) compared to Monte Carlo (MC) for different values of the input uncertainty ρ_σ

Finally, the algorithm is tested with respect to the L_2-norm of the residual plotted in Fig. 8.13 for both uncertainty ratios, $\rho_\sigma = 5$ and $\rho_\sigma = 20\%$. While the reference Newton method converges quadratically, this trend characterizes the ISGM only until some point, i.e. the accuracy of 10^{-4} for $\rho_\sigma = 5\%$ and 10^{-2} for $\rho_\sigma = 20\%$. Then the convergence rate changes and becomes slower as the higher order terms in the ISGM residual do not disappear with the increase of the number of the iterations. This happens due to the existence of the numerical truncation errors in polynomial

chaos algebra (see Chapter 6), which cannot be reduced if the polynomial order is not increased.

Table 8.16: The response root mean square error for all three uncertain parameters with $\rho_\sigma = 5\%$. The error is computed with respect to the solution obtained using 10^6 MC samples. The input is approximated by order p_k and response by p_u.

p_K	p_u	σ_{xx}	σ_{yy}	σ_{xy}	ε_{xx}	ε_{yy}	ε_{xy}
2	2	0.5636	0.4949	0.5418	0.6313	0.5424	0.5631
mccmp 65		0.9651	0.9534	1.0232	1.0355	0.9481	0.9724
4	4	0.5616	0.5001	0.5331	0.6102	0.5312	0.5511
mccmp 150		0.5356	0.5316	0.5535	0.5564	0.5301	0.5375
6	6	0.0132	0.0066	0.0065	0.0060	0.0060	0.0070
mccmp 520		0.2530	0.2517	0.2526	0.2517	0.2509	0.2514

However, the previous analysis is not completely honest because the MC method needs a much longer computation time than the ISGM method for the same values of the input uncertainty. Namely, as one can see in Table 8.1, in order to achieve 10^{-3} accuracy one has to run circa one million samples (runs of deterministic code). On the other side, the ISGM method requires only one run. To do the proper comparison one has to compare the ISGM solution to the MC solution for the same computation time, as shown in Table 8.16. Here the time factors are not discussed because the time analysis will be given later in Section 8.3. Namely, for one ISGM run of order 6 one may compute only 520 response samples with the MC method. In average both methods give similar results, while the higher order moments of the ISGM solution are closer to the reference. The MC solution obtained from 520 samples overestimates the PCE coefficients for both the stress- and strain-like components. In this manner, ISGM outperforms MC.

8.1.3 Non-intrusive Galerkin method

Besides the intrusive Galerkin method, the polynomial chaos expansion of the solution can be also found with the help of the non-intrusive Galerkin (NSGM) approach as described in Section 5.4.2. This method avoids the employment of the polynomial chaos algebra and accompanying numerical errors, and uses the numerical integration for the computation of the Galerkin projection. However, this brings another type of the error into the story as further investigated. By comparing the relative

Table 8.17: The streess root mean square error of the non-intrusive Galerkin compared to the MC method for 10^6 *samples and all three uncertain parameters*

p_u	# of points	σ_{xx}	σ_{yy}	σ_{xy}	σ_{VM}
2	25	1.47e-02	6.2e-03	7.7e-03	6.3e-03
3	69	8.8e-03	5.8e-03	6.1e-03	6.2e-03
4	351	7.6e-03	5.6e-03	5.9e-03	6.1e-03
	1233	6.6e-03	5.5e-03	5.7e-03	6.1e-03
	7973	5.9e-03	5.5e-03	5.6e-03	6.2e-03
	16535	5.8e-03	5.5e-03	5.6e-03	6.2e-03

Table 8.18: The strain root mean square error of the non-intrusive Galerkin compared to the MC method for 10^6 *samples and all three uncertain parameters*

p_u	# points	ε_{xx}	ε_{yy}	ε_{xy}	$\varepsilon_{p,xx}$	$\varepsilon_{p,yy}$	$\varepsilon_{p,xy}$
2	25	7.4e-03	6.2e-03	8.2e-03	4.4e-01	4.5e-01	5.9e-01
3	69	6.0e-03	5.7e-03	6.3e-03	2.3e-01	2.4e-01	5.1e-01
4	351	5.9e-03	5.6e-03	6.1e-03	1.8e-01	1.9e-01	4.3e-01
	1233	5.6e-03	5.6e-03	5.8e-03	1.1e-01	1.1e-01	2.6e-01
	7973	5.5e-03	5.6e-03	5.6e-03	6.8e-02	7.0e-02	1.4e-01
	16535	5.5e-03	5.5e-03	5.6e-03	6.2e-02	6.3e-02	1.2e-01

Table 8.19: The root mean square error of the non-intrusive Galerkin compared to the MC method for 10^6 *samples and different number of uncertain parameters. The number of sample points is* 681.

RV	σ_{VM}	ε_{xx}	ε_{yy}	ε_{xy}	$\varepsilon_{p,xx}$	$\varepsilon_{p,yy}$	$\varepsilon_{p,xy}$
K	5.0e-03	5.5e-03	5.6e-03	5.5e-03	5.7e-03	5.8e-03	5.6e-03
σ_y	4.7e-03	5.3e-03	5.0e-03	5.5e-03	1.9e-01	2.0e-01	4.4e-01
all	7.6e-03	5.6e-03	6.1e-03	1.8e-01	1.8e-01	4.3e-01	4.2e-01

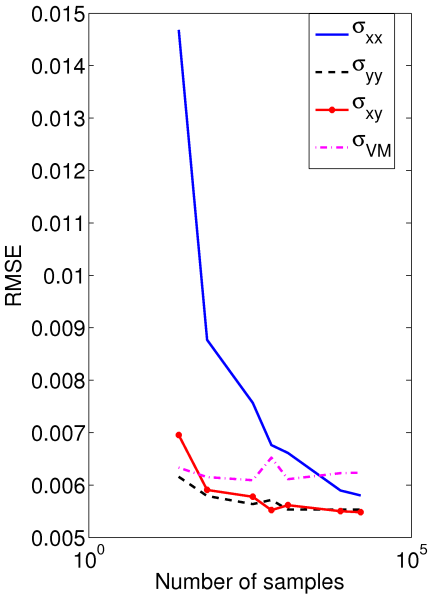

a) RMSE in stress for $\rho_\sigma = 5\%$

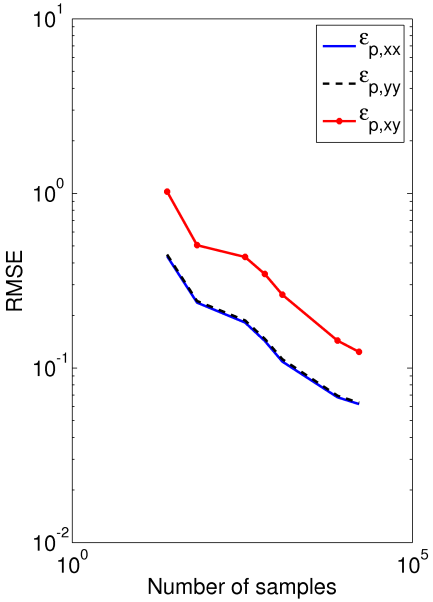

b) RMSE in strain for $\rho_\sigma = 5\%$

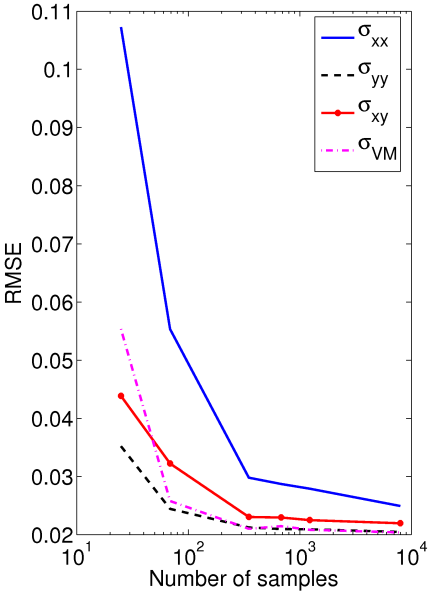

c) RMSE in stress for $\rho_\sigma = 20\%$

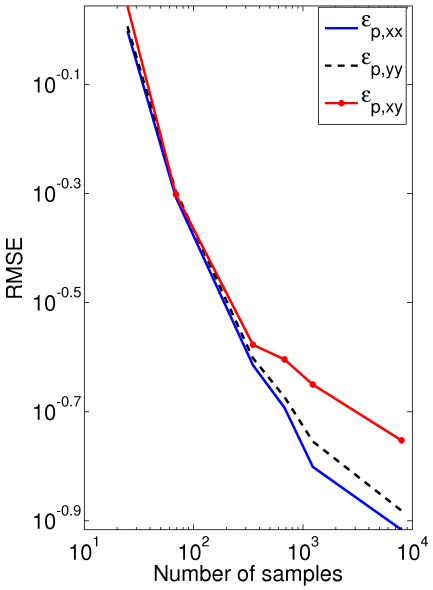

d) RMSE in strain for $\rho_\sigma = 20\%$

Figure 8.14: The convergence of the non-intrusive Galerkin compared to the MC method.

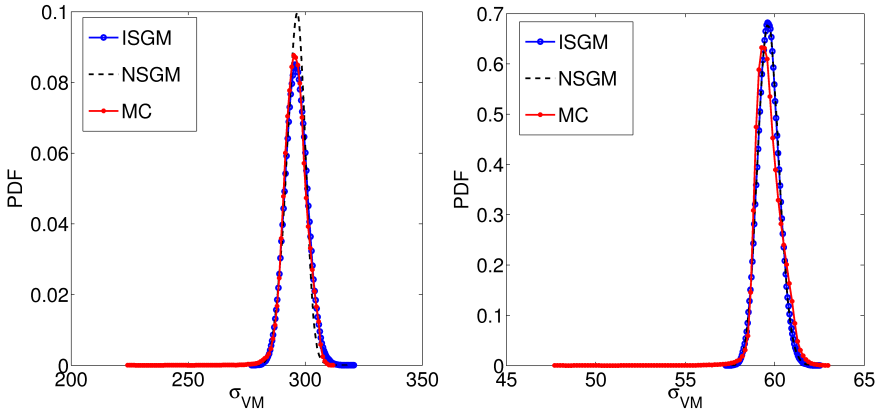

a) point with plastic state b) point with elastic state

Figure 8.15: Comparison of the probability density function of the von Mises stress obtained by the intrusive stochastic Galerkin method (ISGM), the non-intrusive stochastic Galerkin method (NSGM), and the Monte Carlo (MC) method in points with plastic and elastic state

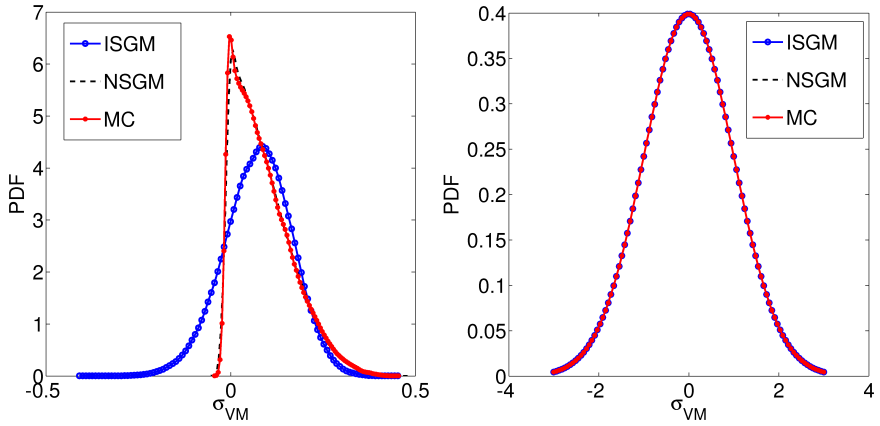

a) point 1 with plastic state b) point 2 with plastic state

Figure 8.16: Comparison of the probability density function of the plastic strain obtained by the intrusive stochastic Galerkin method (ISGM), the non-intrusive stochastic Galerkin method (NSGM), and the Monte Carlo (MC) method in two different points in the plastic zone

Table 8.20: The uncertainty in the response obtained by the direct integration in plastic (P) and elastic (E) points

State	ρ_σ	σ_{xx} [%]	σ_{yy} [%]	σ_{xy} [%]	ε_{xx} [%]	ε_{yy}[%]	ε_{xy} [%]
P	5%	17.14	1.50	3.99	6.21	2.96	3.74
E	5%	0.87	0.24	0.04	4.80	2.94	3.43

root mean square error of the stress components in Table 8.17—computed with respect to the reference MC solution— one may notice that the error decreases with the increase in a polynomial order and the number of integration points, as expected. Similarly, the data indicate that the polynomial order 4 provides better accuracy than the polynomial order 9 for ISGM, see Table 8.13. However, one has to bear in mind that this conclusion may change with the increase of the input variance.

Compared to the ISGM results (see Table 8.14), the NSGM error in the strain components converges much faster and has better accuracy in both the total and the plastic components if the number of the sample points is large enough, see Table 8.18 and Fig. 8.14. The only component that still has error larger than 10% is the shear component of the plastic strain. Namely, while the stress components almost immediately have an error of circa 1% (see Table 8.17), the plastic strain still experiences problems. If the number of points increases the error drops to circa 6%, see Table 8.18. This happens due to the presence of uncertainty in all three input parameters and possible skewness of the plastic strain. On the other side, if the uncertainty of each parameter is introduced into the algorithm separately, the error decreases as given in Table 8.19.

The previously described behaviour can also be seen in Fig. 8.14, where the errors are plotted against the number of samples. As one may notice in Fig. 8.14 c) and d) the error does not drop as quickly for the input ratio $\rho_\sigma = 20\%$ as for $\rho_\sigma = 5\%$ (see Fig. 8.14 a) and b)). Thus, one requires much more than 10^4 samples to accurately represent the solution.

As a comparison to the ISGM the probability density functions of the von Mises stress and the plastic strain are plotted in two randomly chosen points inside the domain, one in plastic and one in elastic zone, see Fig. 8.15 and Fig. 8.16. While the stress PDFs are similar in all three cases, the plastic strain response is much better for the non-intrusive Galerkin method. The possible reason is that the truncation in PCE algebra delivers a higher numerical error than the corresponding local integration.

Finally, the estimation of the response uncertainty in plastic and elastic points of the domain is illustrated in Table 8.20, and as one may notice it is comparable to those in Table 8.3.

8.1.4 Stochastic collocation

With the help of the stochastic collocation approach as described in Section 5.4.2 one may choose the appropriate sparse grid and collocate the solution in a set of sample points, the number of which has a great influence on the solution accuracy.

Table 8.21: The RMSE error of the stress obtained by stochastic collocation

ρ_σ	# of points	σ_{xx}	σ_{yy}	σ_{xy}	σ_{VM}
5	69	2.2e-02	6.5e-03	7.9e-03	9.9e-03
	165	8.0e-03	2.3e-03	2.6e-03	3.6e-03
	351	3.2e-03	9.0e-04	1.1.e-03	1.4e-03
20	69	1.5e-01	5.3e-02	6.0e-02	1.1e-01
	165	4.4e-02	1.4e-02	1.6e-02	1.8e-02
	351	1.4e-02	4.0e-02	6.1e-03	5.9e-03

Table 8.22: The RMSE error of the strain obtained by stochastic collocation

ρ_σ	# of points	$\varepsilon_{p,xx}$	$\varepsilon_{p,yy}$	$\varepsilon_{p,xy}$
5	69	8.2e-01	8.2e-01	1.6e+00
	165	2.5e-01	2.5e-01	3.0e-01
	351	6.4e-02	6.6e-02	8.5e-02
20	69	2.1e+00	2.1e+00	2.2e+00
	165	4.5e-01	4.7e+00	4.6e-01
	351	1.5e-01	1.5e-01	1.9e-01

To analyse this method, Table 8.21 and Table 8.22 plot the convergence of the solution (stress and plastic strain) with the number of points for different values of the

input uncertainty ρ_σ. The reference is computed using 1233 points. As one may notice the error decreases with the increase of the number of points. In contrast to this, the error grows with the increase of the input uncertainty, as already expected. The larger the input variance is, the more difficult it is to accurately represent the higer order moments of the solution. The root mean squared error as defined in Eq. (8.2) is used as the corresponding error indicator.

However, the real comparison of the solution can be only done with respect to the reference solution, see Section 8.1.1. As the projection is already compared with the huge Monte Carlo run, here we choose to compare the collocated solution with the non-intrusive Galerkin. The data in Table 8.23 represent the RMSE between the collocation and projection approach for the quadrature rules with the same number of points. As the error is of order 10^{-15} for 681 sample points one may conclude that the collocation gives a pretty similar results as the projection by integration.

Table 8.23: The comparison of the stochastic collocation to the non-intrusive Galerkin method for 5% *and* 20% *of the input uncertainty*

ρ_σ	# points	σ_{xx}	σ_{yy}	σ_{xy}	$\varepsilon_{p,xx}$	$\varepsilon_{p,yy}$	$\varepsilon_{p,xy}$
5	69	2.3e-02	5.6e-03	1.0e-02	4.5e-01	4.5e-01	6.0e-01
	681	6.3e-15	6.3e-15	6.5e-15	4.5e-15	4.2e-15	2.9e-15
	1233	4.1e-15	4.3e-15	4.5e-15	2.9e-15	2.9e-15	2.9e-15
20	69	1.6e-01	5.9e-02	9.5e-02	2.0e+00	2.0e+00	2.2e+00
	681	5.9e-15	6.4e-15	6.1e-15	3.4e-15	3.2e-15	3.1e-15
	1233	4.2e-15	4.4e-15	4.4e-15	2.9e-15	3.0e-15	2.6e-15

8.2 Random field case

The main goal of previous sections was to show the advantages and disadvantages of the numerical methods presented in Chapter 5. However, the material properties modelled as scalar valued random variables are not proper for the practical utilisation. Namely, the material characteristics are in essence heterogeneous and change their values from one point in the domain to the next. Such behaviour, for example, can be described with the help of the random field theory, which is the subject of this section.

8.2.1 Input random fields

Going one step further from the problem considered in Section 8.1 one may model the material properties as positively distributed random fields:

$$\kappa(x,\omega) = \exp(\mu + \sigma\gamma(x,\omega)), \tag{8.3}$$

i.e. the exponential transformation of the Gaussian random field $\gamma(x,\omega)$ with zero mean, unit variance and covariance function:

$$\text{cov}_\gamma = \exp\left(-|x-y|/l_c\right) \text{ or } \text{cov}_\gamma = \exp\left(-|x-y|^2/l_c^2\right). \tag{8.4}$$

Here $l_c := (l_x, l_y)$ represents the vector of the correlation lengths and x and y the spatial coordinates.

Table 8.24: The relative error in the mean and the variance of the approximated Gaussian random field with the number of terms used in KLE

Error	10	20	40	50	70	90
Mean	1.8e-03	6.6e-04	1.1e-04	4.6e-05	4.0e-06	1.8e-06
Var	3.6e-01	1.3e-01	2.3e-02	9.4e-03	8.1e-04	3.7e-04

Following the discussion in Section 4.4 the field κ is first approximated by the Karhunen-Loève and then by the polynomial chaos expansion both resulting in PCE in FEM integration point. The PCE is described by M Gaussian random variables and Hermite polynomials of order p:

$$\kappa(x_{gp},\theta) = \sum_{\alpha\in\mathcal{J}} \kappa^\alpha(x_{gp}) H_\alpha(\theta). \tag{8.5}$$

The KLE of the lognormal random field can be computed directly using the transformation of the covariance function from cov_γ to cov_κ. In such a case the corresponding PCE can be evaluated by the direct integration. However, a much easier way is to compute the KLE of the Gaussian random field and then to compute the final PCE of the lognormal random field [231] via:

$$\kappa^{(\alpha)} = \frac{\mathbb{E}(\kappa)}{\sqrt{\alpha!}} \prod_{m=1}^{\infty} (\sqrt{\lambda_m}\gamma_m(x))^{\alpha_m}. \tag{8.6}$$

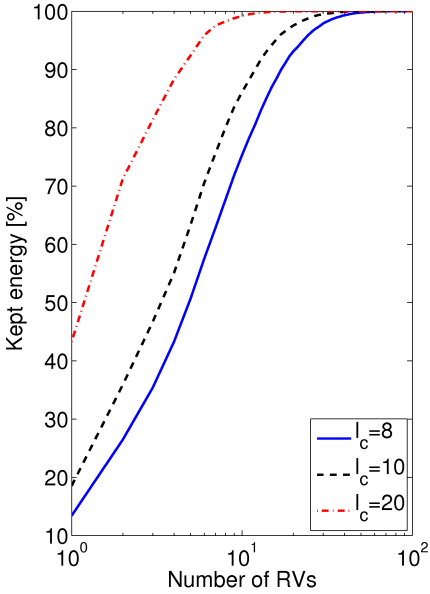

a) The energy kept by the KLE approximation of the RF

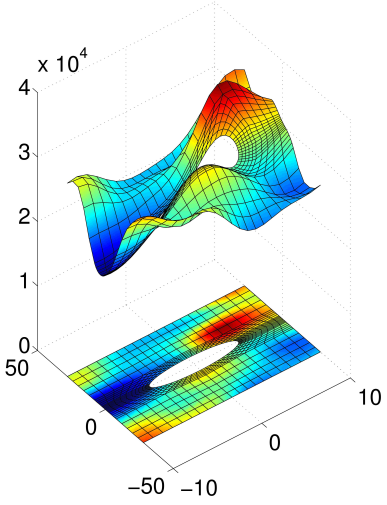

b) One realisation of the lognormal random field

Figure 8.17: The accuracy of the input approximation and the realisation of the random field for 100 *RVs*

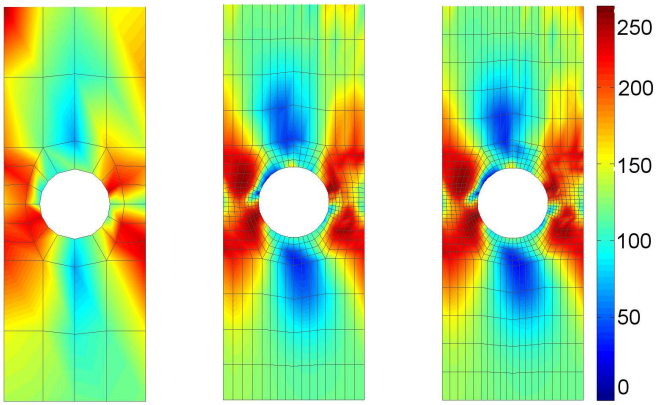

a) 44 elements b) 448 elements c) 700 elements

Figure 8.18: The influence of the mesh refinement on the von Mises stress σ_{vm}. Elements are taken to be the eight-noded quadrilaterals.

Here λ_m and $\gamma_m(x)$ are the eigenvalues and the eigenfunctions of the KLE of the Gaussian random field.

Following the previous discussion the approximation accuracy of the random field with the mean value $\mathbb{E}(\kappa) = 28000$ and $\rho_\sigma = \text{std}\,\kappa/\mathbb{E}(\kappa) = 10\%$ can be computed as shown in Table 8.24. Here the relative mean and the variance errors are plotted across the number of terms used in the KLE expansion. As one may notice, the relative errors decrease with the increase of the number of KLE terms. A similar behaviour can be seen in Fig. 8.17 where the total kept energy is illustrated. The plot indicates that one has to take into account a large number of RVs in order to properly model the material. This number depends on the values of the input variance and the correlation lengths of considered RF. If the input variance increases or the correlation lengths decrease, the number of the KLE terms (RVs) has to increase. Besides this, the approximation accuracy strongly depends on the spatial discretisation of the RF, see Fig. 8.18. Namely, one has to use a higher-order basis and more elements (finer mesh) to achieve the desired accuracy [1]. This, however, immediately influences the efficiency of algorithms, as will be seen later.

[1] Connected to this, one may note that the field realisations are not symmetric for the deterministic response. The reason lies in the absence of material symmetry.

8.2.2 Plate with a circular hole

Let us consider the same numerical example, i.e. a plate with a circular hole, as in the random variable case. The input parameters are taken with the following statistics: the bulk modulus K (mean 4.6667e+04 MPa, standard deviation 10%), the shear modulus (mean 28000 MPa, standard deviation 10%), the yield stress σ_y (mean 243 MPa, standard deviation 10%) and the hardening modulus (mean 2240 MPa, standard deviation 0%). The total applied load is $3000t$[N]. In order to describe the input parameters the different values of the correlation lengths for the yield stress, bulk and shear moduli are adopted. For an accurate representation we took the KLE/PCE with the maximal number of random variables 100 and the order of polynomial 3, where the spatial discretisazion is done with the help of 700 quadrilateral eight-noded elements, i.e. 2290 spatial degrees of freedom. With respect to such discretisation the coupled system in Eq. (5.53) is considered as a system of large dimension, i.e. 404988790 of the total degrees of freedom. However, as the correlation lengths are relatively large, the number of RVs in the KLE can be reduced to much less than 100. Fig. 8.19 and Fig. 8.20 illustrates the approximation accuracy of the shear modulus in the mean value and the standard deviation compared to the reference solution obtained by 10^5 Monte Carlo samples.

In order to compare the non-intrusive and intrusive methods the simpler version of the problem considers only the shear modulus to be uncertain on the relatively coarse FEM-mesh (i.e. 176 spatial degrees of freedom—eight-noded elements). The modulus is assumed to be lognormal RF with previously described statistics and correlation lengths $l_c = [20\ 20]$. This allows us to use only 5 RVs and the polynomial order 3 for modelling 89.06% of the total energy of the field. However, if the correlation lengths are taken as smaller one has to take more RVs into consideration to maintain the desired accuracy. In Table 8.25 the stress and strain RFs obtained by the direct Galerkin (ISGM), stochastic collocation (SCOL) and pure Monte Carlo methods are compared for the same number $M = 5$ of RVs used in the KLE approximation and the polynomial order $p = 3$. The number of samples used in the Monte Carlo integration is equal to $3 \cdot 10^5$, while the number of the collocating points is 13073. According to the plotted RMSE both methods (ISGM and SCOL) deliver approximately the same result, while the mean error is slightly better for the direct Galerkin method than the collocation.

Another comparison between the direct Galerkin method and the reference solution computed with 10^5 latin-hypercube samples is presented in Table 8.26. Interestingly, the error is pretty similar for all the stress and strain components and amounts to circa 5%. This means that RMSE quantifies the sampling error in the MC method

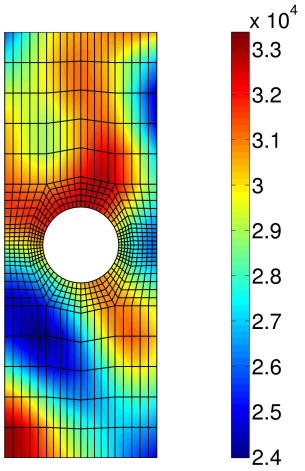

Figure 8.19: Realisation of the input random field G (shear modulus)

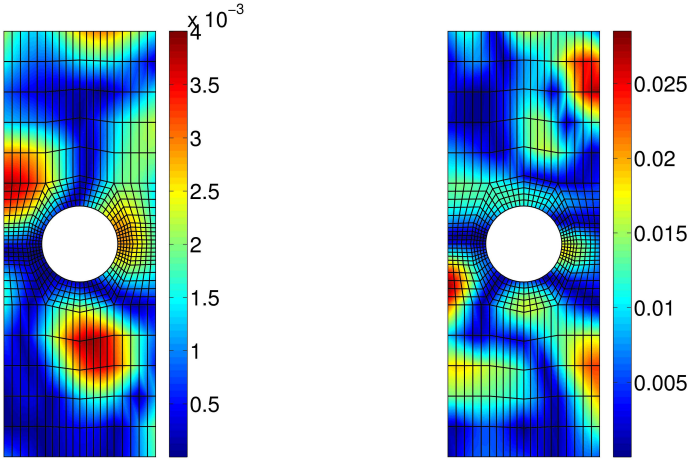

a) ϵ_μ b) ϵ_σ

Figure 8.20: Relative errors in the approximation of the random field: ϵ_μ in the mean and ϵ_σ in the standard deviation.

and not the Galerkin solution. In other words, the Galerkin solution is more trustful. This phenomenon already appeared in previous examples, see Section 8.1.

Table 8.25: Comparison of the intrusive (IM) and non-intrusive (NM) methods to the MC solution with $3 \cdot 10^5$ *samples*

	Error	σ_{xx}	σ_{yy}	ε_{yy}	ε_{pxx}	ε_{pyy}	ε_{pxy}
IM	rmse	1.5e-02	1.4e-02	1.4 e-02	1.5 e-02	1.5e-02	1.4e-02
	mean	1.3e-04	3.2e-05	1.2e-04	5.9e-04	5.1e-04	5.0e-04
NM	rmse	1.5e-02	1.4e-02	1.4e-02	2.1e-02	2.0e-02	2.0e-02
	mean	6.9e-04	1.6e-04	3.6e-04	2.9e-03	2.5e-03	2.4e-03

Table 8.26: The RMSE error between the direct Galerkin (10RVs, polynomial order 3) and 10^5 *latin hypercube samples*

Error	σ_{xx}	σ_{yy}	σ_{xy}	ε_{xx}	ε_{pxx}	ε_{pyy}	ε_{pxy}
rmse	5.2e-02	5.3e-02	5.3e-02	5.3e-02	5.3e-02	5.2e-03	5.2e-03
mean	1.3e-04	5.1e-05	3.0e-05	3.0e-05	5.6e-05	6.2e-05	4.0e-05

As the correlation lengths strongly influence the obtained results, the direct Galerkin solution is compared to the collocation response by plotting the root mean square error in Table 8.27. Clearly, as the correlation lengths reduce, the error becomes larger. The reasons are fluctuations of the random field, which cannot be covered by polynomial order $p = 3$ and $l = 13073$ sampling points. This behaviour can also be seen in Fig. 8.21 where the probability density function of the von Mises stress is plotted with respect to the correlation lengths in a randomly chosen point inside the plastic zone.

Now let the RF has a correlation length equal $l_c = 20$ and let us compute the Galerkin solutions with a different number of RVs as shown in Table 8.28. Clearly, the RMSE decreases with the number of the input RVs.

However, the previous comparison is done with respect to the small number of RVs. In order to give the more accurate error analysis, the RMSE results comparing the collocation solution with the reference solution obtained by 10^5 latin-hypercube

Table 8.27: The RMSE between the direct Galerkin and the reference solution as a function of the correlation lengths

l_c	σ_{xx}	σ_{yy}	σ_{xy}	ε_{yy}	$\varepsilon_{p,xx}$	$\varepsilon_{p,yy}$
[20 20]	4.3e-03	9.9e-04	2.4e-03	1.9e-03	1.7e-02	1.4e-02
[10 10]	6.5e-03	1.5e-03	4.3e-03	2.5e-03	2.5e-02	2.2e-02
[5 5]	4.7e-02	1.1e-02	4.1e-02	9.4e-03	1.8e+00	1.7e+00

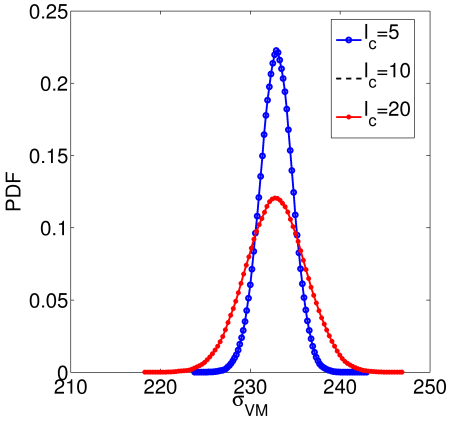

Figure 8.21: Influence of the correlation lengths on the von Mises stress

Table 8.28: The RMSE between the direct and the non-intrusive Galerkin methods for M RVs and polynomial order 3

Error	M	σ_{xx}	σ_{yy}	σ_{xy}	ε_{xx}	ε_{yy}	ε_{xy}
rmse	10	1.4e-03	5.4e-04	2.7e-04	5.4e-04	6.0e-04	2.3e-04
mean	10	3.1e-04	1.2e-04	6.2e-05	1.2e-04	1.3e-04	4.8e-05
var	10	1.2e-02	2.7e-02	3.9e-03	2.4e-03	3.3e-03	3.5e-03
rmse	5	8.4e-04	3.4e-04	1.7e-04	3.3e-04	3.7e-04	1.4e-04
mean	5	2.6e-04	1.0e-04	5.1e-05	1.0e-04	1.1e-04	3.9e-05
var	5	1.1e-02	5.3e-02	3.5e-04	1.8e-04	2.3e-04	3.3e-04

Table 8.29: The RMSE between the collocation and the reference solution (MC 10^5). The number of used RVs is 100 and order 3

Error	σ_{VM}	ε_{xx}	ε_{yy}	ε_{xy}	ε_{pxx}	ε_{pyy}	ε_{pxy}
mean	2.8e-04	5.9e-04	4.2e-04	4.2e-04	3.8e-04	3.8e-04	3.6e-04
var	2.7e-02	7.1e-03	6.9e-03	6.9e-03	2.1e-02	2.1e-02	1.5e-02

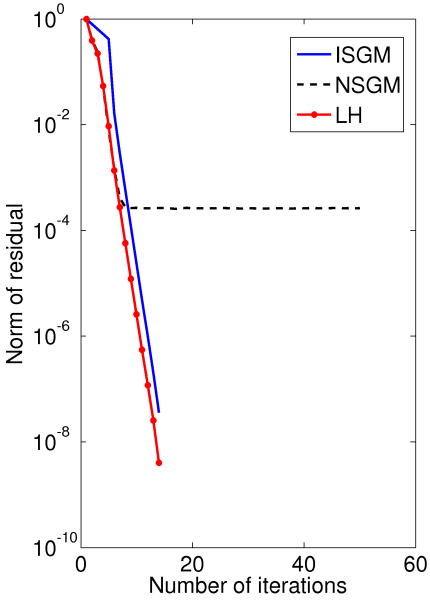

Figure 8.22: The residual convergence: intrusive (ISGM) and non-intrusive (NSGM) Galekin method, LH- latin hypercube integration

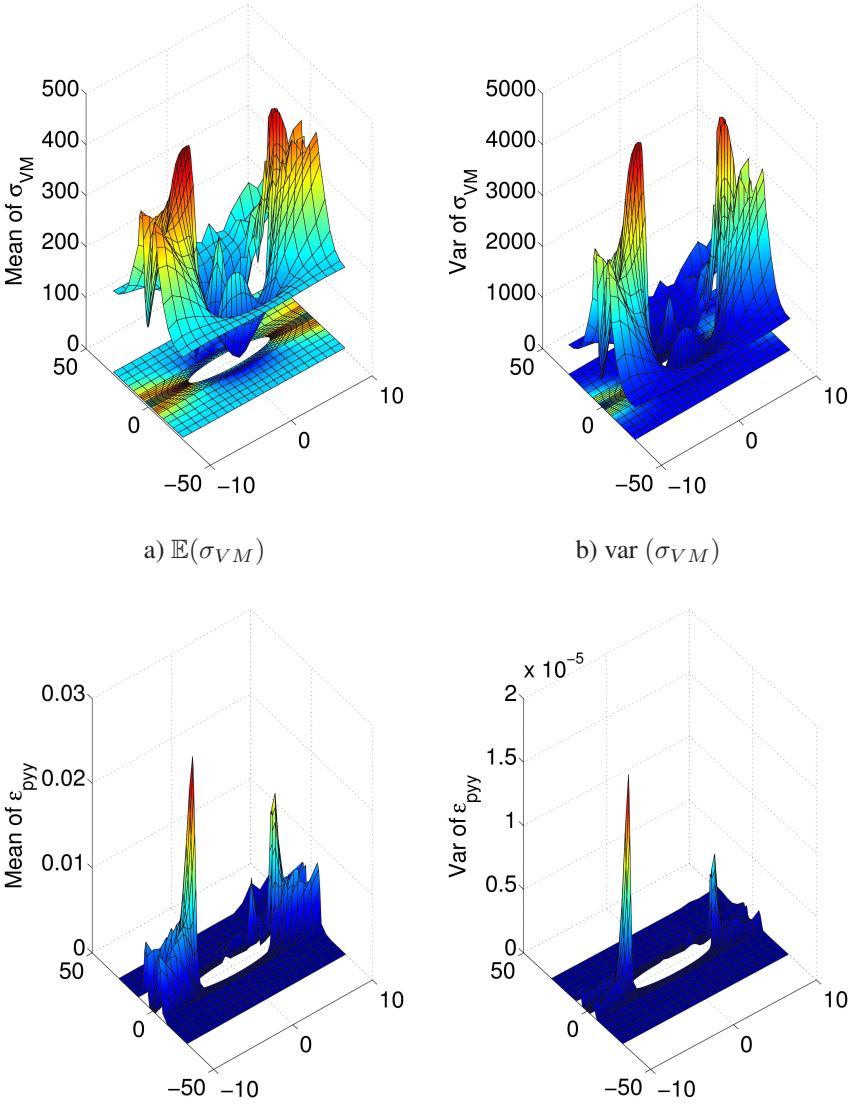

a) $\mathbb{E}(\sigma_{VM})$

b) var (σ_{VM})

c) $\mathbb{E}(\varepsilon_{pyy})$

d) var (ε_{pyy})

Figure 8.23: Mean and variance of von Mises stress and plastic strain

Monte Carlo samples are provided in Table 8.29 for inputs approximated by 100 RVs. The number of terms in polynomial chaos expansion used to approximate the solution is 176 851.

This error estimate is different from the one given in Table 8.26 as the number of the KLE terms used in the MC integration is equal to 100 and the correlation lengths are taken to be equal to $l_c = 5$. This means that the collocation method is stable with the increase of the number of RVs. However, the question is how big error one makes by assuming only 5 RVs in the input approximation. With this respect the RMSE between the PCE solution with 5 RVs and the one with 100 RVs is computed. For example, the error in the first stress component is already around 80%. The reason is that 5 random variables for $l_c = 5$ keep less than 30% of the total energy, and thus the solutions of those two problems are completely different.

Similar to the RV example, the comparison of the convergence of the residual in Fig. 8.22 shows that the non-intrusive method has better convergence than the direct variant.

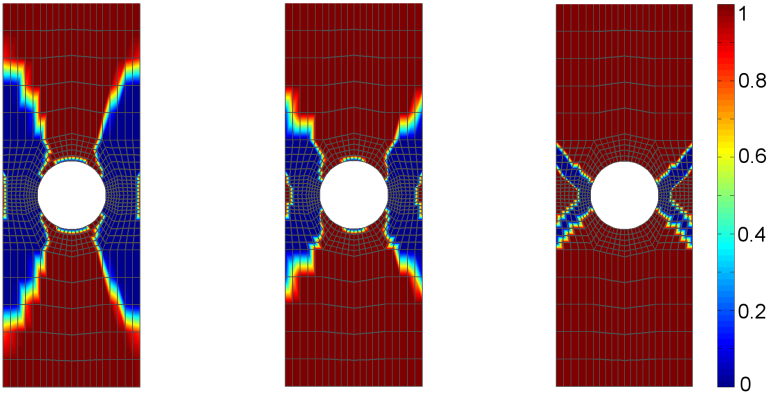

a) Prob($\sigma_{vm} < 150$) b) Prob($\sigma_{vm} < 200$) c) Prob($\sigma_{vm} < 250$)

Figure 8.24: Probability exceedance of the von Mises stress

The previous discussion has focused more on the method properties, however, for the engineering practice are more important the statistics of the output response (i.e. the actual value of the mean and the variance of the response, etc.). Due to this,

Fig. 8.23 plots the mean and the variance of the von Mises stress, as well as the mean and the variance of the plastic strain. As indicated and expected, both the mean and the variance achieve their maximal values exactly in the plasticity zone around the hole. Their uncertainty is given by a ratio of 20% for the von Mises stress, and of 60% for the plastic strain component.

However, the probability exceedance of maximal stress occurence can be even more important information for engineers than the second order statistics. Namely, one is the most interested in zones of materials where the maximal value of the von Mises stress occurs. Via stochastic analysis one is able not only to give the mathematical expectation where this happens, but also the probability of such an outcome. For example, in Fig. 8.24 the regions in which the von Mises stress crosses 150, 200 or 250 [MPa] (possible yield stress) are plotted. This information immediately can help engineers to decide whether a material in such conditions can be employed or not.

8.2.3 Cook's membrane

The Cook's membrane in a finite deformation is clamped on one end and excited by a shear force $F = 2t$[kN] in y-direction on the second as shown in Fig. 8.25. The plate is discretised via the finite element method into 225 quadrilateral eight-noded elements (regular mesh). The statistics of the input parameters are given as: the bulk modulus (mean 164.2068 [GPa], standard deviation 10%), shear modulus (mean 80.1940 [GPa], standard deviation 10%), yield stress (mean 0.2 [Gpa], standard deviation 10%) and the istotropic hardening (mean 0.129[GPa], standard deviation 0).

For such defined input parameters the membrane deforms according to Fig. 8.26, where the obvious difference between the response obtained by deterministic (red line) and stochastic (blue line) simulations can be seen. This means that the presence of the uncertainty has a great influence on the output response, and thus cannot be neglected.

The uncertainty in response greatly alters with the variation of the input uncertainty. For example, if one compares the direct Galerkin solutions for uncertain shear modulus (see Fig. 8.27) and all three parameters, one may notice that the second order statistics are bigger in case of uncertain shear modulus G. This can be explained by the number of RVs used in simulation. When all three fields are uncertain, each of them is modelled only by 6 RVs. Otherwise, the uncertain shear modulus alone is modelled with the help of 20 RVs. This shows that the approximation of the input has

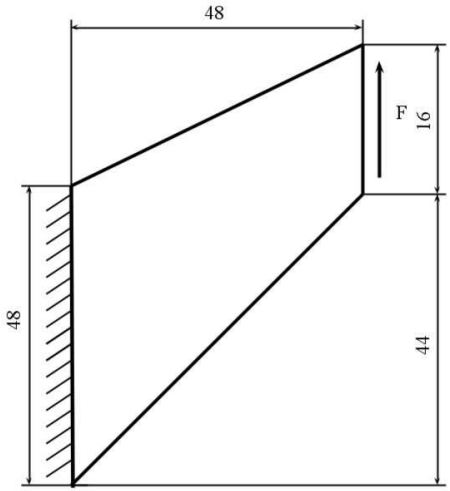

Figure 8.25: The geometrical setup of Cooke's membrane

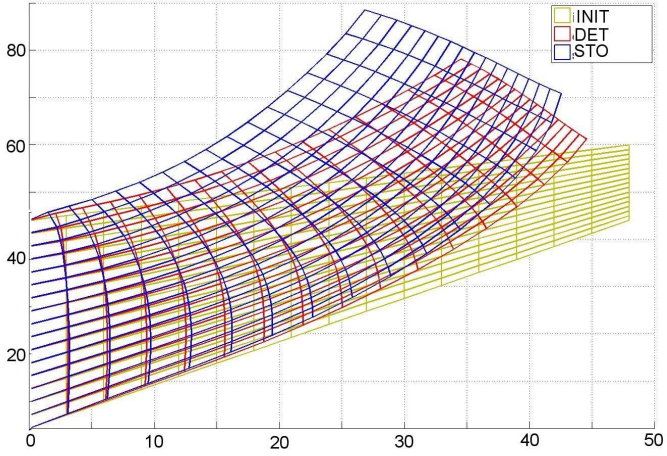

Figure 8.26: The comparison of the deformed configurations obtained by pure deterministic (DET) and stochastic approach (STO) with the initial undeformed configuration.

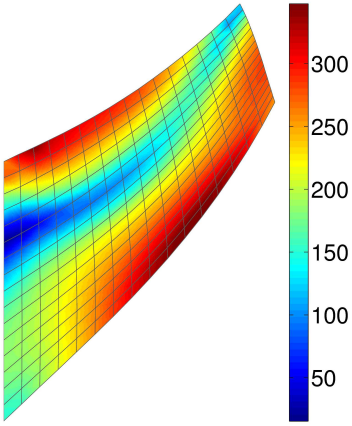

a) $\mathbb{E}(\sigma_{VM})$ (uncertain K, G, σ_y)

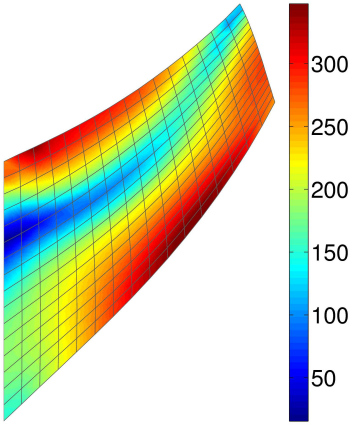

b) $\mathbb{E}(\sigma_{VM})$ (uncertain G)

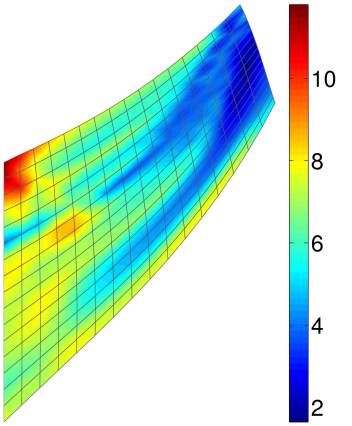

a) std (σ_{VM}) (uncertain K, G, σ_y)

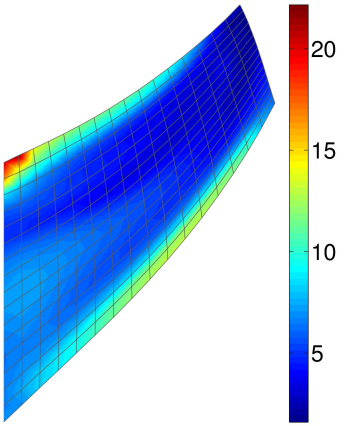

b) std (σ_{VM})(uncertain G)

Figure 8.27: The comparison of second order statistics of the von Mises stress when K, G and σ_y are taken as uncertain, or only G.

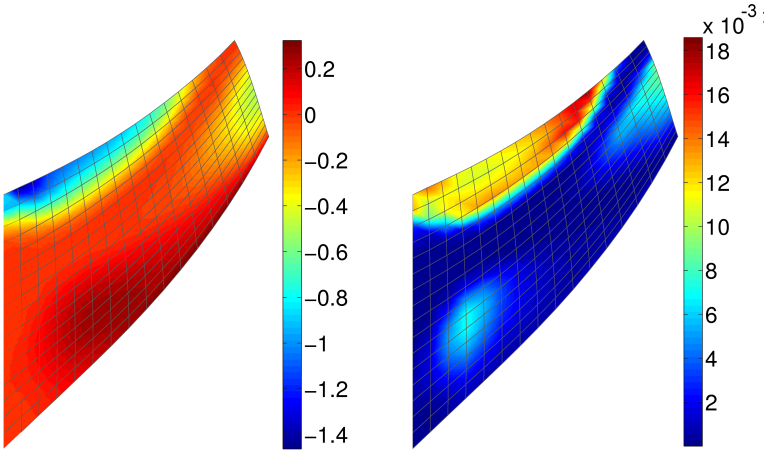

a) $\mathbb{E}(\varepsilon_p)$ b) std (ε_p)

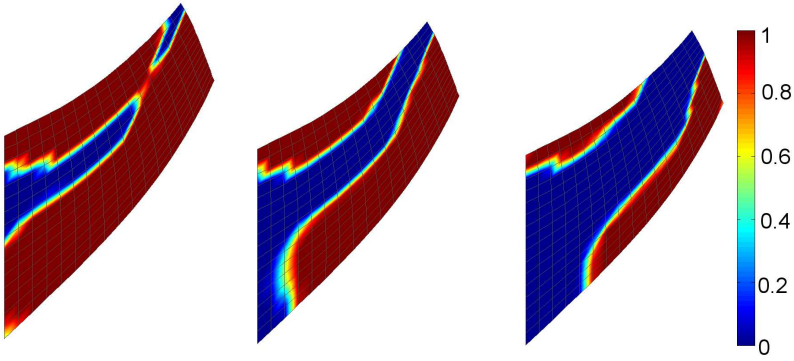

c) $\sigma_{VM} > 150$ d) $\sigma_{VM} > 200$ e) $\sigma_{VM} > 250$

Figure 8.28: The plastic strain statistics and the probability exceedance of the von Mises stress for 100 *RV and order* 3.

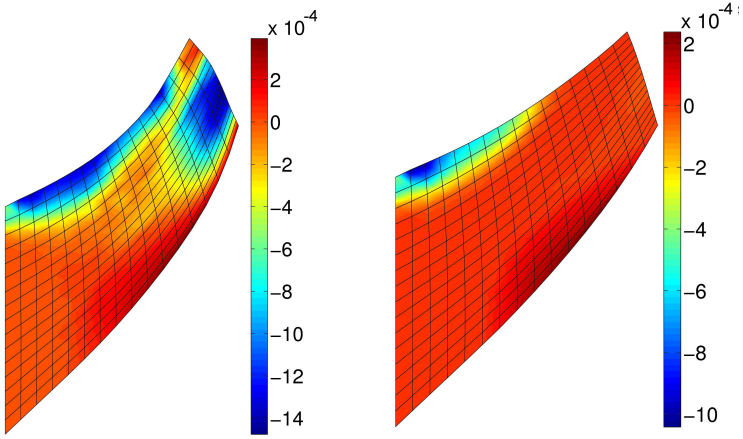

a) $\mathbb{E}(\varepsilon_p)$ (l_c) b) $\mathbb{E}(\varepsilon_p)$ $(2l_c)$

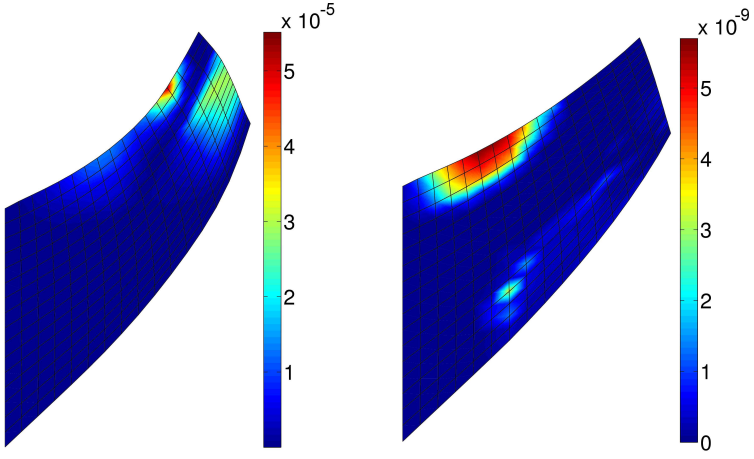

c) var(ε_p) (l_c) d) var(ε_p) $(2l_c)$

Figure 8.29: The mean and the variance of the response plastic strain with the correlation lengths. l_c is taken to be 10. The number of RVs is 100 *and order* $p = 3$.

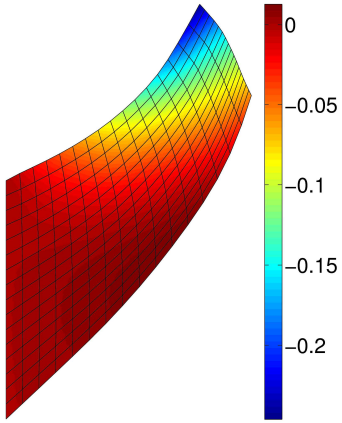

a) $\mathbb{E}(u)$ (l_c)

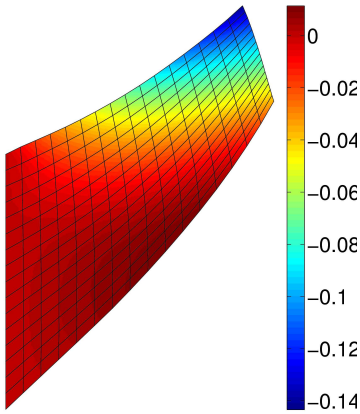

b) $\mathbb{E}(u)$ $(2l_c)$

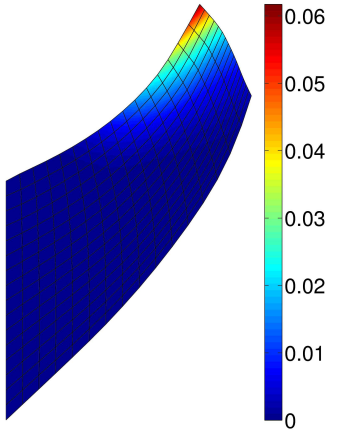

c) var(u) (l_c)

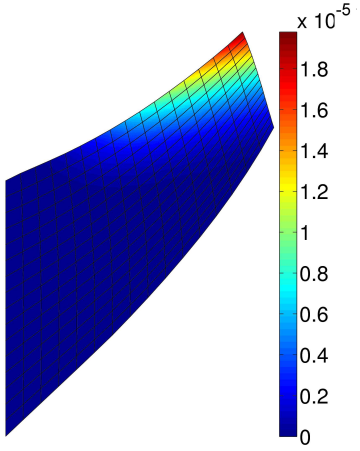

d) var(u) $(2l_c)$

Figure 8.30: The mean and the variance of the response displacement with the correlation lengths. l_c is taken to be 10. The number of RVs is 100 *and order* $p = 3$

a great influence on the accuracy of the solution. Although the statistics in Fig. 8.27 are not really comparable, one may still make conclusion about the influence zone of the uncertainty. Namely, the zone is much wider when the three mentioned parameters are random than only one of them—shear modulus. This is already indicated in Fig. 8.28 a) and b) where the mean and the variance of the plastic strain are plotted. As expected, the plastic zone concentrates in the specific region of the domain exposed to compression. In a similar manner one may compute the probability exceedance statistics, see Fig. 8.28 c)–e), and distinguish the zones in which the stress exceeds some already known value with probability one.

The previous study has been done for the constant values of the correlation lengths. However, without measurements one cannot be sure how large they can be for the specific input parameters. As the goal of the identification problem [191] is to find their accurate levels, here one may only assume some values. According to the data in Fig. 8.29 for smaller correlation lengths the plasticity zone spreads wider than for large correlation lengths. This happens due to the existing fluctuations in the field with smaller correlation lengths. A similar behaviour can be observed in the displacement field in Fig. 8.30. If the correlation lengths are smaller the input fields are varying more and the statistics of the output are bigger than for large correlation lengths.

8.2.4 Reduced parametric approach

The random fields in previous simulation are taken to be lognormally distributed, and the constitutive tensor isotropic in the mean. However, the constitutive tensor can be modelled in another way with the help of the reduced parametric approach (see Chapter 3).

Following the mathematical theory given in Chapter 3 the constitutive tensor $\boldsymbol{A}$ is constructed with the help of the Gamma distribution and by assuming the isotropic tensor

$$\bar{\boldsymbol{A}} = \begin{pmatrix} 271.1322 & 110.7441 & 0 \\ 110.7441 & 271.1322 & 0 \\ 0 & 0 & 80.1940 \end{pmatrix} \tag{8.7}$$

for the mean. Furthermore, $l_c = 20$ is adopted for the correlation lengths of the corresponding Gaussian random field γ, whose kernel is the exponential covariance function. Similarly, the dispersion of the base non-Gaussian random field $\boldsymbol{T}$ is adopted to be $\delta_T = 0.1$. Note that $\boldsymbol{A}$ is only isotropic in the mean and not in its fluctuation part,

as can be seen in Fig. 8.32 and Fig. 8.33. Namely, in each realisation the constitutive tensor owns the components A_{13},A_{23} etc. even though the isotropic model does not.

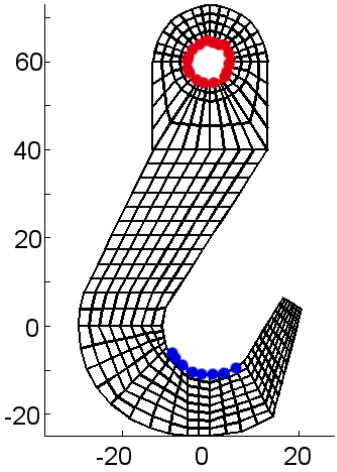

Figure 8.31: The geometrical set up

The response statistics obtained for such a defined model are given in Figs. 8.34–8.37. The results clearly show that the plastic zone is much wider compared to the results of the lognormally distributed random fields given in the previous section. Apparently the uncertainty in the stress components is not as high as it goes up to circa $\rho_\sigma = 5\%$. However, the uncertainty in the elastoplastic strain is much bigger and similar to the one obtained by the direct parametric approach.

Another example is made by considering the test with the geometrical domain of the hook shape constrained on the top (red area) and loaded by the concentrated force (blue area) $f = 130t$ in the arc area as shown in Fig. 8.31. The mean matrix is modelled by Young modulus $E = 7 \cdot 10^4$ [MPa] and $\nu = 0.25$. The yield stress is 243 [MPa] and isotropic hardening $H_{iso} = 2000$ [MPa]. All other parameters are the same as in the previous example. As one may see in Figs. 8.38–8.41 the stress concentration appears to be in the arc area where it is expected. The highest uncertainty of circa 40% happens in the first stress component, while others have a much lower ratio of the uncertainty.

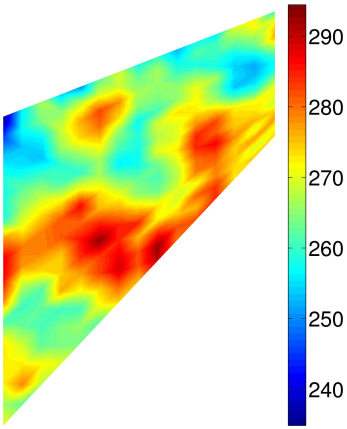

a) A_{11}

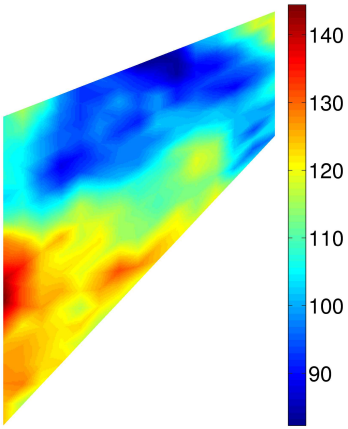

b) A_{12}

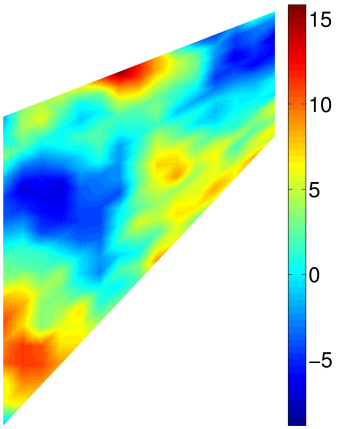

c) A_{13}

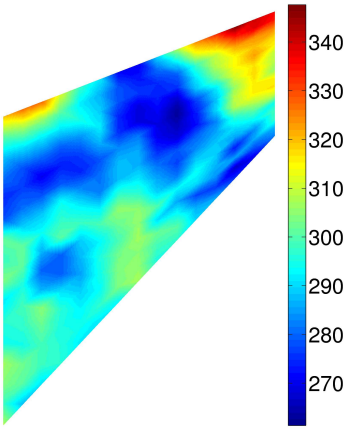

d) A_{22}

Figure 8.32: Realisations of components of the elastic constitutive tensor

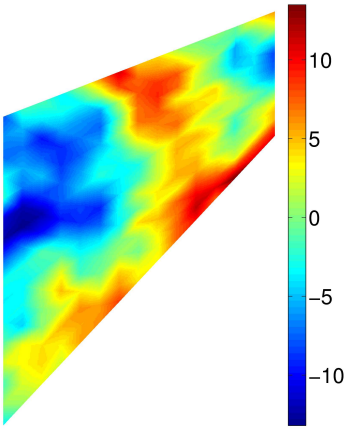

e) A_{23}

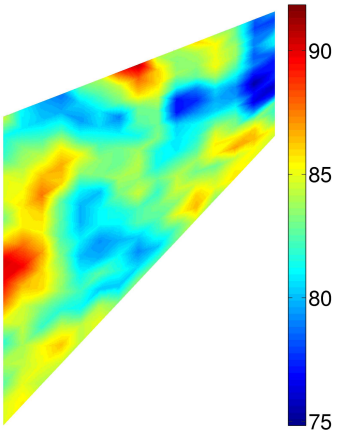

f) A_{33}

Figure 8.33: Realisations of components of the elastic constitutive tensor

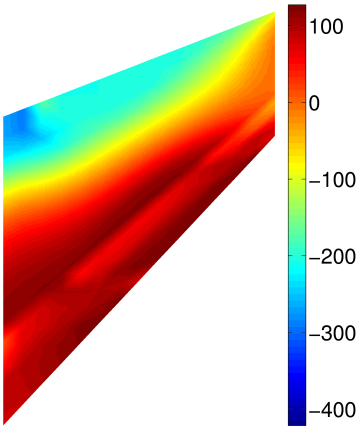

a) $\mathbb{E}(\sigma_{xx})$

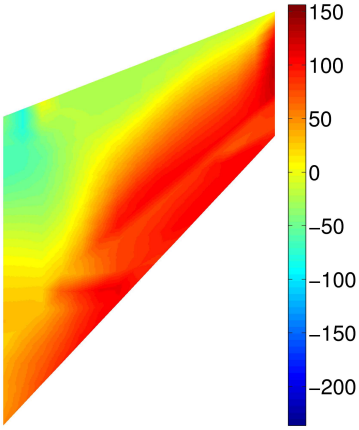

b) $\mathbb{E}(\sigma_{yy})$

Figure 8.34: The mean values of the stress and plastic strain components

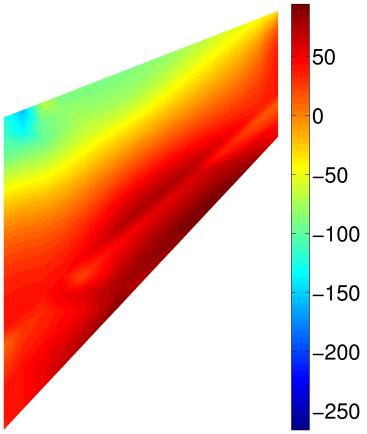

c) $\mathbb{E}(\sigma_{xy})$

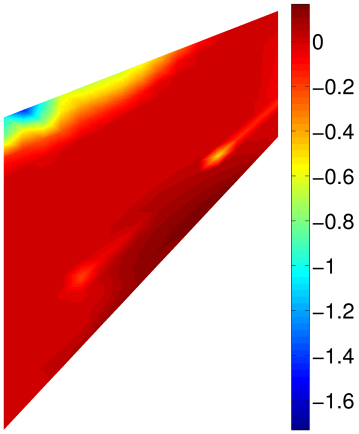

d) $\mathbb{E}(\varepsilon_{pxx})$

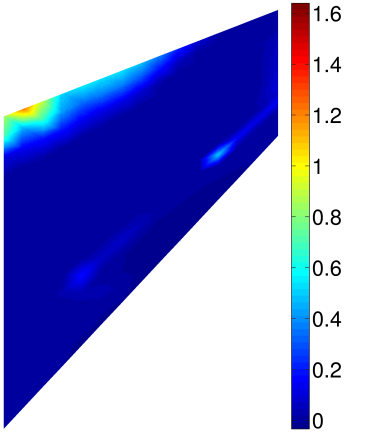

e) $\mathbb{E}(\varepsilon_{pyy})$

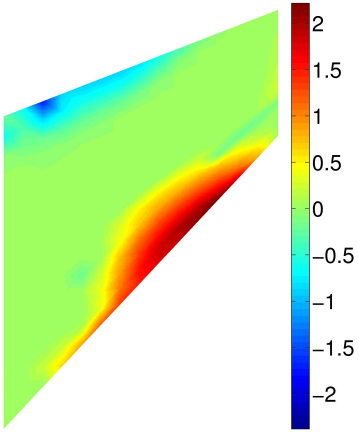

f) $\mathbb{E}(\varepsilon_{pxy})$

Figure 8.35: The mean values of the stress and plastic strain components

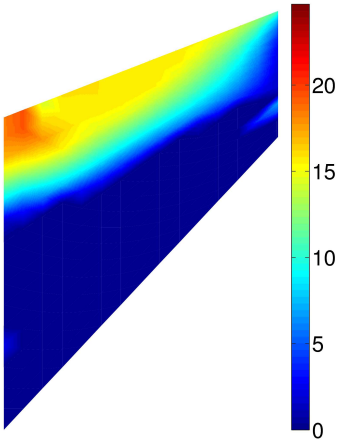

a) std (σ_{xx})

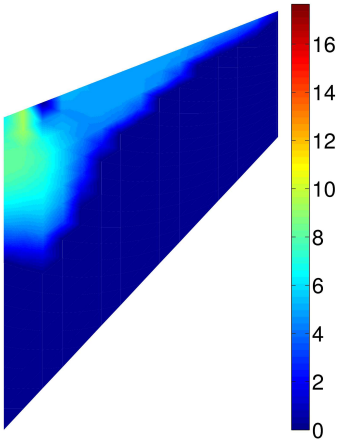

b) std (σ_{yy})

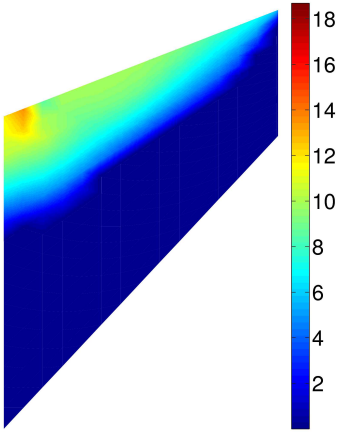

c) std (σ_{xy})

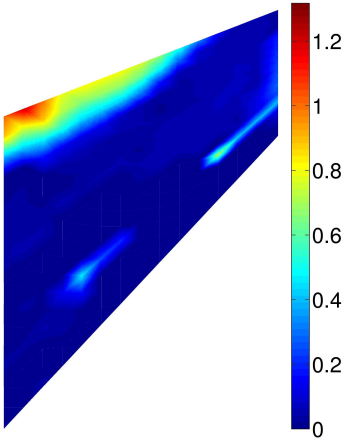

d) std (ε_{pxx})

Figure 8.36: Standard deviation of the stress and plastic strain components

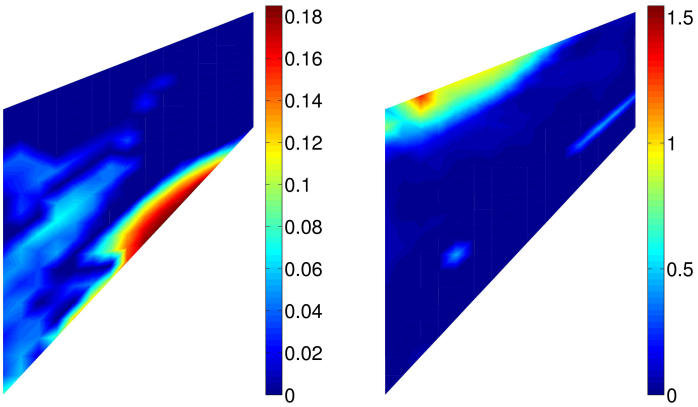

e) std (ε_{pyy}) f) std (ε_{pxy})

Figure 8.37: Standard deviation of the stress and plastic strain components

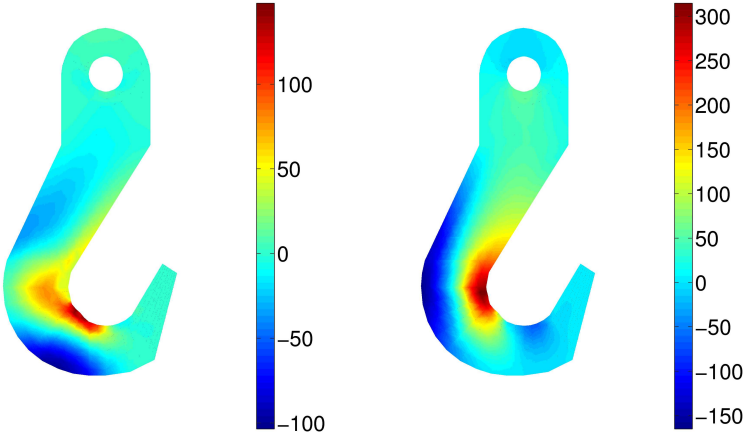

a) $\mathbb{E}(\sigma_{xx})$ b) $\mathbb{E}(\sigma_{yy})$

Figure 8.38: The mean values of the stress and plastic strain components

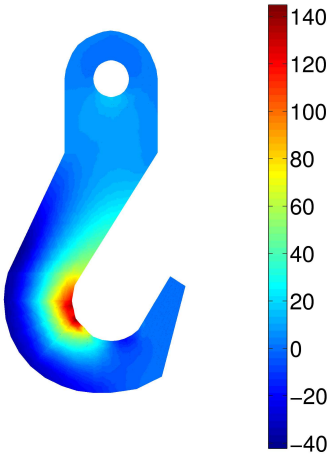

c) $\mathbb{E}(\sigma_{xy})$

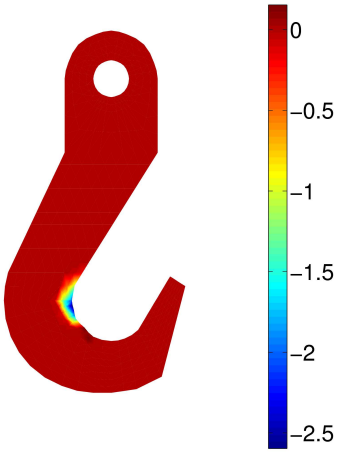

d) $\mathbb{E}(\varepsilon_{pxx})$

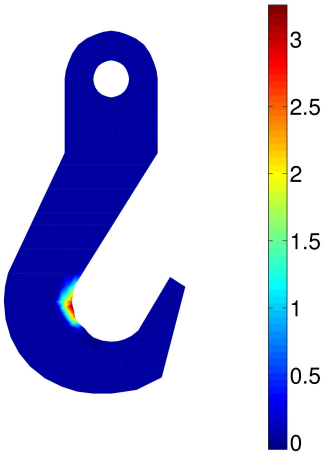

e) $\mathbb{E}(\varepsilon_{pyy})$

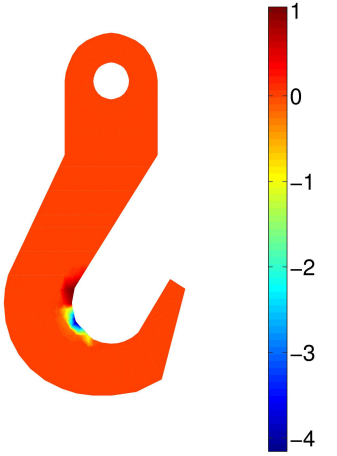

f) $\mathbb{E}(\varepsilon_{pxy})$

Figure 8.39: The mean values of the stress and plastic strain components

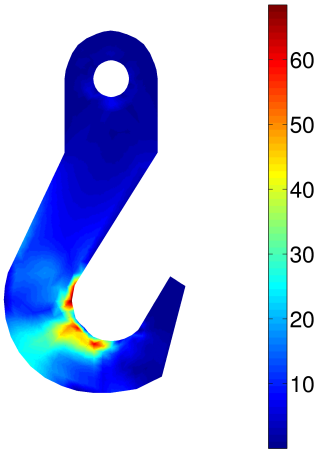

a) std (σ_{xx})

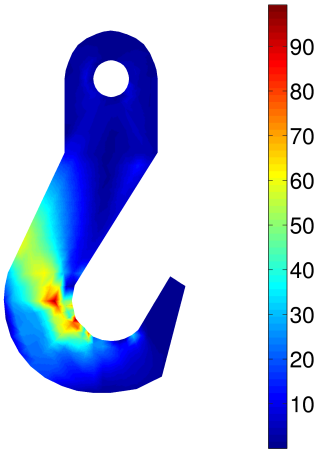

b) std (σ_{yy})

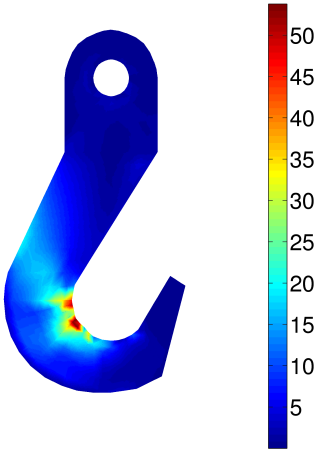

c) std (σ_{xy})

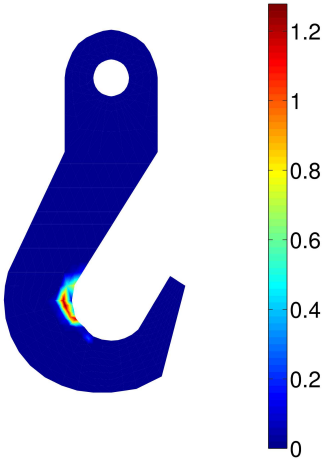

d) std (ε_{pxx})

Figure 8.40: Standard deviation of the stress and plastic strain components

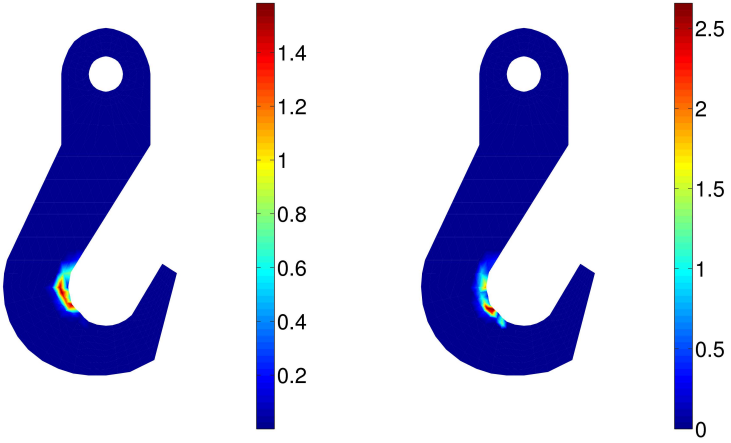

e) std (ε_{pyy}) f) std (ε_{pxy})

Figure 8.41: Standard deviation of the stress and plastic strain components

8.3 Complexity and computation cost

In order to decide which method is best applicable in practice one has to provide the proper analysis of the accuracy and the computation cost. As the accuracy is already considered, here we try to provide the time and the memory requirements of the PLASTON package for the various methods presented in this work.

As discussed in Chapter 5, the stochastic Galerkin and collocation method differ in the way they are solving the final system of equations. The direct Galerkin solves the coupled system of equations at once by the preconditioned Krylov subspace method, while the stochastic collocation decouples the system into the finite number of small deterministic systems. This number depends on the number and the type of the collocation points being selected for the numerical integration.

The direct integration methods, as purely sampling based procedures, are working in a similar manner. For comparison Table 8.30 collects the data representing the number of the total stochastic degrees of freedom for each of the previously mentioned methods. They are constructed for 179 deterministic degrees of freedom and

Table 8.30: The number of stochastic degrees of freedom

M	p	Z	L_S	L_{NS}	L_{TP}
3	3	20	25	19	27
	5	56	165	93	243
5	3	56	61	51	125
	5	252	781	401	3125
20	3	1771	841	801	8000
	5	53130	120321	90601	3200000

the problem described in Section 8.1. Thus, the computation times are compared for the uncertainties represented by RVs, not RFs. However, a similar conclusion can be made for the more general case of random fields, as will be discussed later. The first and the second column in Table 8.30 represent the number of the stochastic degrees of freedom M (i.e. the number of RVs) and the polynomial order of the Hermite basis, respectively. In the third column is listed the number Z of the PCE terms used in the Galerkin projection, i.e. this number multiplied with the number of the deterministic degrees of freedom N gives us the size of the coupled system which needs to be solved in each iteration. Note that Z grows with the dimension M and order p exponentially, see Chapter 6. Similarly, in columns L_S, L_{NS}, and L_{TP} are given the number of points used in the non-nested Smolayk, the nested Smolyak, and full tensor product rule, respectively. This number corresponds to the number of the decoupled deterministic systems of size $N \times N$ which the direct integration and collocation methods have to solve in each iteration. Note that this number grows much faster than the number of terms in PCE. This is especially the case for the full tensor product rule, which delivers a huge amount of the integration points for already small number of stochastic dimensions. Due to this the full tensor grid is never used in practice, but mostly the nested Smolayk rule which compared to the previous two delivers the smallest number of points. Note that the number of the Monte Carlo samples in Table 8.30 is not listed as it is very well-known that more than $1\ 000\ 000$ samples are necessary for the accuracy of 1e-3 according to the law of large numbers.

Even though the ISGM has the smallest dimension according to Table 8.30, that does not necessary mean that its computation time is also the shortest. The algorithms based on the stochastic Galerkin have to solve a much bigger system of equations in each iteration of the Newton-like methods compared to the other presented methods.

Table 8.31: ISGM overall computation time with the order p: t_p total time, t_{sol} time spent on solving the linear system of equations in [%], t_{ppcet} time spent on the multiplication of the matrix-valued PCEs in [%], t_{ttm} time spent on the sparse matrix multiplications in [%], t_{dpcet} time spent on the division of the matrix valued PCEs in [%], t_{sqrt} time spent on finding the square root of matrix-valued RVs in [%]

p	t_p [s]	t_{sol} [%]	t_{ppcet} [%]	t_{ttm} [%]	t_{dpcet} [%]	t_{sqrt} [%]
2	55.43	27.04	47.70	20.75	2.78	0.47
4	124.30	28.42	54.20	30.84	1.75	0.32
6	438.88	21.43	68.24	56.11	1.72	0.36
9	4905.443	10.70	84.94	86.30	2.12	0.45
10	10771.275	10.16	85.48	87.79	2.13	0.47

The solving time is around 30% of the overall computation time for small polynomial orders (see Table 8.31).

Table 8.32: The number of PCE algebra operations with the increase of the polynomial order. N_{ppcet} is the number of products, N_{ttm} the number of the sparse matrix multiplications, N_{dpcet} the number of divisions, N_{sqrt} the number of square root operations

Order	N_{ppcet} [s]	N_{ttm} [%]	N_{dpcet} [%]	N_{sqrt} [%]
2	18503	40191	486	130
4	20465	44465	626	141
6	20465	44465	626	141
9	20465	44465	626	141
10	20465	44465	626	141

Besides, the computation time strongly depends on the time neccessary to perform the PCE algebra calculations. For example, the multiplication can take more than 80% of the overall time. This is due to the tensor multiplications (see time t_{ttm}) which are mostly used in the product procedure. In contrast to this, the division and the square root are relatively fast as their number of calls is relatively small, see Table 8.32. The number of the tensor-product calls is twice compared to the number of the product calls. On the other side, the square root function is the least frequent

Table 8.33: The number of PCE operations with the number of iterations

PC products	PC divisions	Tensor Products	Iterations
3105	425	8615	5
4968	680	13784	8
6210	850	17230	10
9315	1275	25845	15
15525	2125	43075	25
22977	3145	63751	40

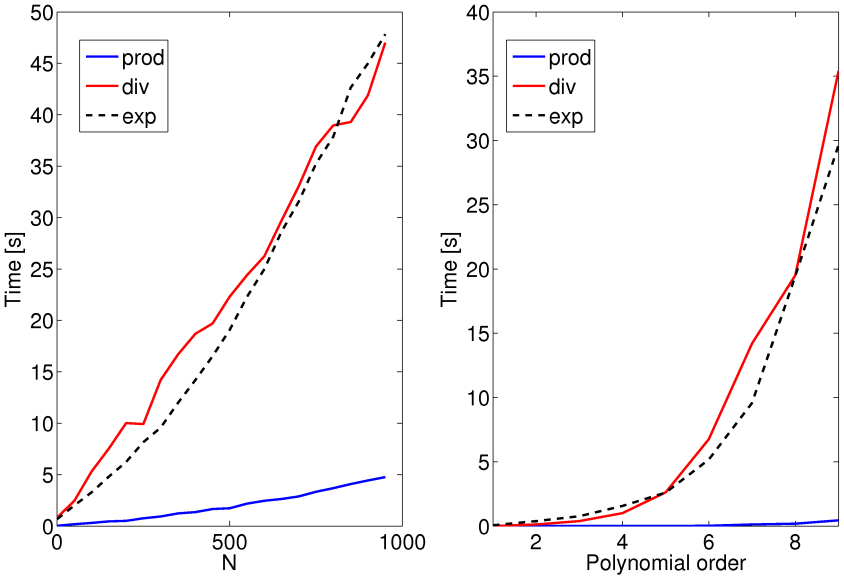

a) Number of elements b) Polynomial order

Figure 8.42: Computation time as a function of: a) number of elements b) polynomial order

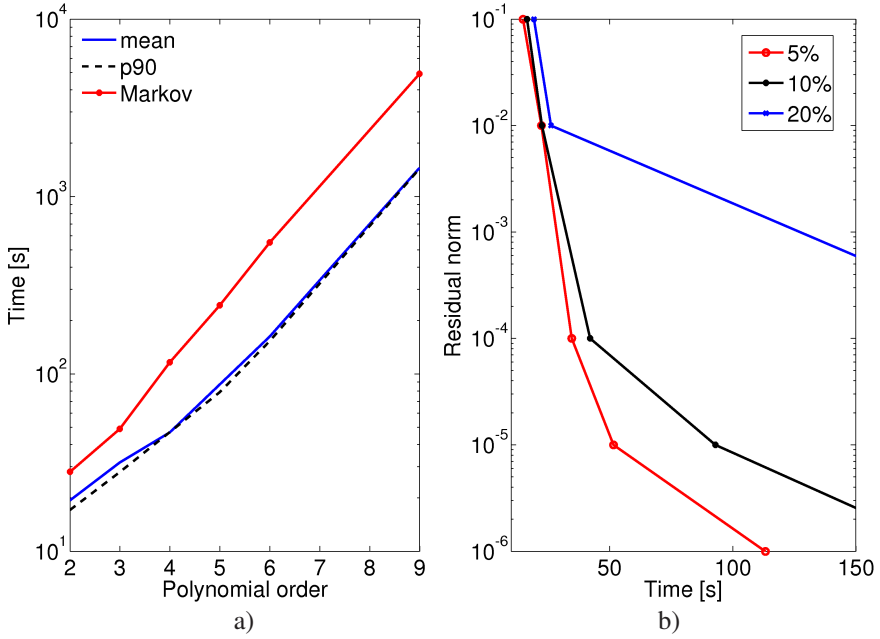

Figure 8.43: Computation time: a) for the same number of iterations b) same accuracy

Table 8.34: Overall computation time t_p and time spent on solving the system of equations t_{sol}: ISGM compared to the sparse Smolayk method (SMOL-non-nested, NSMOL-nested)

	ISGM		SMOL			NSMOL		
Z	t_p	t_{sol}	L	t_p	t_{sol}	L	t_p	t_{sol}
10	26.91	5.58	25	34.63	19.8	19	20.98	11.23
20	44.02	11.92	69	97.92	56.78	39	42.74	22.82
35	69.96	23.83	165	235.36	135.28	93	102.54	53.27
56	117.79	41.81	351	499.86	262.14	165	203.23	86.60
84	225.20	68.81	681	972.05	512.72	237	300.93	122.66

as it is called just once in each iteration. Similarly, the division is not often used and the number of calls is circa 3 times smaller than the number of product calls.

Table 8.35: Overall computation time with the number of integration points. ISGM - intrusive Galerkin, NPRO- integration by projection (sparse grid), NSOL- collocation by nested Smolyak

Order	ISGM	L	NPRO	NSOL
2	26.91	19	20.00	20.98
		39	40.02	40.35
		93	92.39	93.64
		165	165.56	166.11
6	26.91	237	249.03	300.93
		381	369.81	449.20
		513	507.44	566.34
		703	710.43	761.03

The overall time of the ISGM procedure strongly depends on the polynomial order (see Table 8.32) and the number of the iterations of the nonlinear solver (see Table 8.33), or, more precisely, on the number of points in which the stress lies outside of the admissibility region and for which the closest point projection has to be performed. Namely, the number of the polynomial operations grows with the increase of the points in plastic state. It is interesting to note that the division as well as other PCE operations are not so often called during the program run. After multiplication the division is on the second place with only 425 divisions in 5 iterations. Of course these numbers depend on the nature of the problem (as previously said) as well as on the deterministic dimension (the number of nodes). In order to recognize the dependence Fig. 8.42 a) and b) depicts the time neccessary to compute the product of two PCEs of dimension $N \times Z$ with respect to N and Z. The PCE product is the most frequently called operation, but also the cheapest one. For $Z = 120$ the PCE product of 1000×120 requires 5.54s. This means that in circa 6 seconds one can multiply two PCEs describing 1000 elements in one integration point. In contrast to this for the same PCEs the division and the exponent take circa 50 times more. However, by luck they are not as often called as multiplication. This may mutually compensate. In contrast to the linear dependence on the deterministic dimension, the PCE operations are exponentially dependent on the stochastic dimension, as shown in Fig. 8.42 b) where the time necessary to multiply, divide, and exponentially transform the matrix valued PCE is plotted. The multiplication is again the most efficient operation, while

the division and the exponent are more expensive due to employment of the iterative methods in their implementation.

Table 8.36: Overall computation time t_p and time spent on solving the system of equations t_{sol}: ISGM compared to the stochastic collocation (SCOL) and non-intrusive Galerkin (NSGM)

	ISGM		SCOL			NSGM	
Z	t_p	t_{sol}	L	t_p	t_{sol}	t_p	t_{sol}
10	26.91	5.58	19	20.00	11.06	283.61	11.25
20	44.02	11.92	39	39.93	21.64	319.39	127.89
35	69.96	23.83	93	92.89	51.38	458.42	385.62
56	117.79	41.81	165	170.45	83.27	623.3	510.76
84	225.20	68.81	237	249.03	111.49	881.9	779.93

Another study of the computation time can be done regarding the decision criteria used to estimate the yield point. As shown in Fig. 8.43 a) the Markov criterion appears to be much slower than the direct integration or the mean criteria for the same probability level.

The reason is that the Markov plasticity zone is over-estimated, and thus more iterations are necessary to achieve the same accuracy. The dependence of the computation time on the achieved accuracy is plotted in Fig. 8.43 b). As expected, the bigger the input variance is, the more computation time is needed.

The ISGM method has similar computation time as the projection by nested Smolyak grid, see Table 8.34. However, this comparison is done for a very small system in both the deterministic and stochastic sense, and hence it cannot be generalised. With the increase of the number of the stochastic dimensions the number of the integration points in the stochastic collocation grows, as well as the system size in the ISGM. Therefore, the computation time increases, as shown in Table 8.35. Similar conclusion can be made for the stochastic collocation method, see Table 8.36. However, compared to the non-intrusive Galerkin method, ISGM only wins in computation time but not in accuracy. Due to numerical errors caused by integration, the non-intrusive Galerkin requires more iterations for solving the linear system of equations than ISGM, and hence it is slower. To overcome this problem one may increase the number of the integration points on the cost of overall computation time.

Table 8.37: Overall computation time in case of material properties modelled as random fields: ISGM -intrusive Galerkin, SCOL-stochastic collocation and MC-Monte Carlo

Random fields computation time		
ISGM	SCOL	MC
≈ 5h	≈ 15h	≈ 53days

Finally, if the material properties are modelled as random fields the total computation time grows drastically. For example for the problem with 2290 spatial degrees of freedom, 20 RVs and the polynomial order 3 the total computation time of the stochastic Galerkin method is around 5 hours. Here one has to take into account the time for solving the KLE problems for all three uncertain RFs, the time of computing the mathematical expectation of the triple Hermitian product, and the rest of the FEM procedures. On the other side, for the collocation with circa 13000 points one needs approximately 15 hours, while the Monte Carlo solution, if not implemented in parallel, requires around 53 days for 10^6 samples.

8.4 Conclusion

In the previous chapter the group of methods proposed in Chapter 5 is tested on a few numerical examples in plane strain conditions. Even though the considered problems are not of the three-dimensional type, nothing drastically would change in the latter case, only the number of degrees of freedom would grow. The presented study was designed to determine the effect of the input uncertainty on the system response by considering two groups of methods: those based on the Galerkin projection of the residual onto polynomial basis and those collocating the elastoplastic solution on the sparse Smolayk grid. Both methods are contrasted to the reference solution obtained by direct integration with the help of 10^6 Monte Carlo samples. More particularly two variants of the stochastic Galerkin method are considered: intrusive and non-intrusive procedures. Both use the KLE/PCE approximation of the input random fields and the PCE ansatz for the response solution. The difference lies in the numerical computation of the stochastic residual: in the first case the solution is obtained using polynomial chaos algebra, while in second the numerical integration is purchased.

In order to investigate the influence of the individual uncertain parameters on the system response, the simple example describing the homogenous material properties in a form of scalar valued RVs is first considered. The analysis suggest that the intrusive Galerkin method is able to deliver the solution with the desired accuracy only if the polynomial order of the solution is high enough. Lower polynomial orders can be used only when the uncertainty entering the system is not too high. However, even in such cases the method is greatly sensitive on the presence of the uncertainty in the yield stress. There are several possible explanations for this. In general the algorithm overestimates or underestimates the plasticity zone due to the weak approximation of the convex domain and the existence of the local numerical errors which accumulate with time. Only high polynomial orders can help to overcome this problem. However, the present results are significant in at least two major respects: the intrusive Galerkin method compared to the Monte Carlo solution gives more accurate results for the same computational load, and the computation of the statistics is much easier than in the sampling case. In addition, the ISGM is robust with respect to the stochastic dimension M. Namely, even if the random variables are substituted by the corresponding random fields, the algorithm still behaves in a similar manner. Its accuracy strongly depends on the polynomial order. However, compared to the random variable example the computational time increases. It is interesting to note that the stress and strain-like solutions are alike to those obtained by the MC solution, while the approximation of the possible non-smooth elasto-plastic deformation can be a problem. In contrast to stress and strain, the plastic deformation admits huge variance, and hence cannot be approximated by small polynomial orders.

In contrast to ISGM, the non-intrusive Galerkin method is not so sensitive to the presence of uncertainty in the yield stress. At the same time, the method is more accurate at the expense of computational cost. To keep the desired accuracy the method increases the number of integration points with the increase of stochastic dimension. Therefore, the method may become impractical in high stochastic dimensions. Besides, the integration error affects the accuracy of the global stiffness matrix, which further leads to the slower convergence of the Newton-like iterations than in case of ISGM. This can be overcome by increasing the number of integration points, which on the other side influences the efficiency of the algorithm.

The intrusive and non-intrusive variant of Galerkin method can be generally considered as “intrusive” since both require a certain modification in the finite element code. While the intrusive method is completely invasive, the non-intrusive requires only slight changes in the code. In this aspect, the stochastic collocation method and the direct integration techniques are completely non-intrusive with the only difference that the collocation approach converges faster. When the elastoplastic problem is described by random variables, this approach is maybe the most efficient as the

computational load is similar to the ISGM one, and the accuracy is better. However, the stochastic collocation approach only wins in small dimensions. With the increase of the stochastic dimension the number of the integration points grows, and hence the computational cost. This could be a problem if the cost of one deterministic run is high enough.

Note that the conclusions drawn here are made for results validated with the help of the Monte Carlo solution for 10^6 samples, even though this number is possibly not large enough to be yet considered as the reference solution. Namely, the results in this study show that the stochastic Galerkin and the collocation method detect the error in the sampling produced by MC for low-dimensional problems.

From the aspect of computational cost and accuracy it is difficult to say which method is the best applicable in practice. This strongly depends on the number of stochastic dimensions and the properties of the posed problem. On the other side, with respect to the accessibility to the finite element code, the stochastic Galerkin methods are not recommended as they can be used only in combination with open-source codes.

Chapter 9

Conclusion

The present work introduces the idea of parameters describing the irreversible nonlinear behaviour as the incompletely known quantities whose probability distribution functions can be determined with the help of the maximum entropy principle and available a priori information. By favour of such modelled constitutive and hardening tensors the classical deterministic approach has been extended to the stochastic resolution of the inelastic problem described by uncertain parameters or an uncertain right-hand side. Furthermore, with the help of the convex analysis and the theory of variational inequalities, the mathematical similarity between the deterministic abstract variational formulation and its stochastic counterpart has been illustrated. In this regard the thesis provides the complete description of the stochastic variational structure behind the inelastic phenomena with the focus on the infinitesimal as well as the finite deformation elastoplasticity. By exhibiting the structure of the stochastic evolutionary equations in a convex setting, the mathematical description of an abstract primal variational formulation is carried over to the computationally more suitable mixed variational description for which the existence and uniqueness of the solution have been shown. With the help of proper convexity assumptions the mixed problem is transformed to the numerically more comfortable minimisation of the smooth convex functional on the discrete tensor product space, whose unique miniser is obtained via the well-posed closest point projection method. To this end, a description in the language of non-dissipative and dissipative operators has been presented and the relation between the global mixed and the local dual problem clarified.

The time and space discretisation of obtained stochastic evolutionary equations is performed in a usual manner with the help of the implicit Euler scheme and the finite element method, while the stochastic dependence is resolved with the help of the functional approximation of random variables via white noise analysis (stochastic Galerkin and collocation) or by representing random variables in a more classical

way by sampling (direct integration techniques). The former type of discretisation, i.e. the idea of random variables as functions in an infinite dimensional space approximated by elements of finite dimensional spaces, is used to develop a completely novel procedure— the stochastic closest point projection algorithm. The proposed algorithm computes the functionals of the solution (given in some form of mathematical expectation) in a purely algebraic manner if certain assumptions regarding the smoothness of the integrand are made. Particularly, this thesis provides an extension of stochastic finite element methods and related numerical procedures in the Galerkin context from the linear to the nonlinear case. These methods can be understood in a sense of model reduction techniques due to the applied Karhunen-Loève and polynomial chaos expansions, the truncation error of which is minimised by Galerkin projection. To this end, the coupled nonlinear system of equations is solved via stochastic Newton-like methods. In each iteration of these methods the correction of the solution is computed with the help of polynomial chaos algebra operations and the preconditioned Krylov sub-space methods used to solve the corresponding coupled linear system of equations. The present study separates two ways of computing the residual in a Galerkin manner: fully intrusive or non-intrusive variant. The former method represents the direct, purely algebraic way of computing the response in each iteration of Newton-like methods, while the latter evaluates the residuum in each iteration via high-dimensional integration rules based on random or deterministic sampling, e.g. Monte Carlo and related techniques. Besides the Galerkin method, the thesis provides another version of a functional approximation approach, already known as a stochastic collocation.

This research also aimed to identify the pros and cons of various computational algorithms described in this work. Even though the detailed comparison is provided, it is still difficult to clarify which method is the most suitable to use. The intrusive Galerkin method would be the proper choice if the main requirement is the computational efficiency. However, the method achieves accuracy in the plastic strain solution only when the polynomial order is sufficiently high. Also, the method cannot be considered efficient in case when the problem dimension is too high. When efficiency is not the primary condition, but accuracy, the direct integration techniques by Monte Carlo are considered as a suitable choice. However, if the integrand has large variance the Monte Carlo method may show not so good convergence. On the other side, the stochastic collocation method and the non-intrusive Galerkin may be well suited when the ISGM procedure cannot be applied. Finally, one may say that the choice depends on the particular problem and the number of the stochastic dimensions.

9.1 Outlook

The direct stochastic Galerkin method seems to be a promising way of computing the response statistics of the solution. However, the method is fully intrusive and requires the complete modification of the finite element codes. In addition, the convergence of the method is greatly influenced by local errors in Galerkin projections used in polynomial chaos algebra. This means that the higher order polynomial basis has to be used in order to accurately represent the solution. However, such requirement is difficult to fulfill as the number of terms of polynomial chaos expansion grows rapidly with the polynomial order, and thus the efficiency of the algorithm is affected. In order to prevent this the adaptive discretisation of the supported space can help to reduce the curse of dimensionality. Thus, the next step in any following analysis is to construct the numerical algorithm in an adaptive fashion similarly to [27, 119, 174, 173].

An assumption of the probability distributions for model uncertainties is not sufficient in order to realistically represent the practical problems. Instead, one has to quantify the uncertainty in the input with the help of the provided measurement data. In order to improve the description of the material one may apply the identification techniques in a probabilistic manner [180, 192, 191] onto the problem considered in this paper. Some of these issues have already been addressed in [191]. Besides, further reduction of the number of material parameters describing the problem can be considered. In this respect one may use the existing theory of non-Gaussian symmetric tensor-valued random fields [221, 222] in order to model the fully anisotropic constitutive tensor.

Another interesting view on the problems presented in this thesis would be to considerate the nonlinear elastic response in combination with the linear or nonlinear mixed hardening plasticity. In a deterministic sense some of those models are already considered in [189] where the elastic energy is assumed to be of the hyperelastic type.

List of Figures

List of Tables

List of Algorithms

List of Symbols

Abbrevation

SVI	Stochastic variational inequality
RVI	Random variational inequality
$CSYS$	coordinate system
a.e.	almost everywhere
a.s.	almost surely
KLE	Karhunen-Loève expansion
FEM	Finite element method
PC	Polynomial chaos
PCE	Polynomial chaos expansion
PDE	Partial differential equation
SPDE	Stochastic partial differential equation
SVD	Singular value decomposition
PCV	Polynomial chaos variable
MC	Monte Carlo method
CG	Conjugate gradient method
PCG	Preconditioned conjugate gradient method
ISGM	Intrusive stochastic Galerkin method
NSGM	Non-intrusive stochastic Galerkin method
RMSE	Root mean square error
RRMSE	Relative root mean square error
RV	Random variable
RF	Random field
FP	Fockker-Planck
PDF	Probability density function

General notation

		$\mathbf{A}$	Block-matrix
a	Scalar	$\mathcal{A}$	Deterministic space
$\boldsymbol{a}$	Vector	$\mathscr{A}$	Stochastic space
$\mathbf{a}$	Block-vector	a_h	Spatial discretisation
$\boldsymbol{A}$	Tensor	a_n	Time discretisation
		$\hat{a}$	Truncated PCE approximation

Symbols

$\mathcal{G}$	The spatial domain
$\Gamma = \partial\mathcal{G}$	The boundary
Γ_D	Dirichlet boundary conditions
Γ_N	Neumann boundary conditions
$\mathbb{R}^3$	Euclidean space
$\mathcal{T} = [0, T] \subset \mathbb{R}_+$	The time interval of interest
$\mathcal{G}_0$	Initial body configuration
$\mathcal{G}_t$	Current body configuration
$\varphi(X, t)$	The path of material point X
X	Material coordinates
$x = \varphi(X, t)$	Spatial coordinates
$\boldsymbol{F} = \nabla\varphi$	Deformation gradient
$GL_+(d)$	General linear group
s	Local entropy of the system
$\boldsymbol{\eta}$	Internal variable
∇_M	Differential operator with respect to X
∇_s	Differential operator with respect to x
∇_S	Symmetric differential operator
ψ	Helmholtz free energy
U	Internal energy
T	Temperature
$\boldsymbol{P}$	First Piola-Kirchhoff stress
$\boldsymbol{\chi}$	Conjugate force
j	Reduced dissipation
$\boldsymbol{u}$	The displacement
$\boldsymbol{\sigma}$	The stress tensor
$\boldsymbol{f}$	The loading

$\boldsymbol{\sigma}_N$	The prescribed traction on Γ_N
$\boldsymbol{u}_0$	The prescribed displacement on Γ_D
$\mathrm{Sym}(\mathbb{R}^d)$	Symmetric tensors in $\mathbb{R}^d$
$\boldsymbol{\varepsilon}$	The strain tensor
σ_y	The yield stress
$\boldsymbol{\varepsilon}_e$	The elastic strain
$\boldsymbol{\varepsilon}_p$	The plastic strain
ψ_e	The reversible part of the free energy
ψ_{irr}	The irreversible part of the free energy
A	The elastic operator
H	The hardening operator
$\langle \cdot, \cdot \rangle$	The duality pairing
$\langle \cdot \vert \cdot \rangle$	The inner product
$\boldsymbol{A}$	The elastic constitutive tensor
$\boldsymbol{H}$	The hardening constitutive tensor
$\boldsymbol{\varsigma}$	The kinematic stress
ζ	The isotropic stress
$\boldsymbol{H}_{kin}$	Kinematic hardening
H_{iso}	Isotropic hardening
$\boldsymbol{E}_p$	Generalised plastic strain
$\boldsymbol{\Sigma}$	Generalised stress
$\mathcal{K}$	The convex elastic domain
$\boldsymbol{N}_{\mathcal{K}}$	The normal cone of $\mathcal{K}$
$\Psi_{\mathcal{K}}$	The indicator function of $\mathcal{K}$
$\Psi^*_{\mathcal{K}}$	Conjugate dual of $\Psi_{\mathcal{K}}$
$g_{\mathcal{K}}$	The gauge function
$\phi_{\mathcal{K}}$	The yield function
$\dot{\boldsymbol{E}}_p$	The flow of the plastic strain
λ	The Lagrangian multiplier
$\mathcal{K}^\infty$	The barrier cone (the effective domain of $\mathcal{K}$)
j^*	The dissipation dual
$\mathcal{V}$	Hilbert space
L_p	The space of the Bochner-Lebesgue p-integrable functions
$\mathcal{U}$	Deterministic space of displacement
$H^1(\mathcal{G})$	Hilbert space of one times differentiable functions
$\mathcal{F} := \mathcal{U}^*$	Deterministic space of forces
$\mathcal{E}$	Deterministic space of total strain
$\mathcal{E}_p$	Deterministic space of the plastic strain
$\mathcal{R}$	Deterministic space of Causchy stress
$\mathcal{Q}$	Deterministic space of internal variables
$\mathcal{C}$	Deterministic space of conjugate forces
$\mathcal{P}$	Deterministic space of generalised strain
$\mathcal{Q}$	Deterministic space of internal variables
$\mathcal{C}$	Deterministic space of conjugate forces

$\mathcal{P}$	Deterministic space of generalised strain
$\mathcal{Y} := \mathcal{R} \times \mathcal{C}$	Deterministic space of generalised stress
$\boldsymbol{w} := (\boldsymbol{u}, \boldsymbol{E}_p)$	Primal variable
$\boldsymbol{w}^* := (\boldsymbol{f}, \boldsymbol{\Sigma})$	Dual variable
$H^m(\mathcal{T}, \mathcal{V})$	Sobolov space
$l(\boldsymbol{v})$	The linear functional of $\boldsymbol{v}$
$a(\boldsymbol{u}, \boldsymbol{u})$	The bilinear form of $\boldsymbol{u}$
$\|\boldsymbol{u}\|_A$	The energy norm
$\|\boldsymbol{u}\|_1$	Norm in space $H^1(\mathcal{G})$
$\|\boldsymbol{u}\|$	Euclidean norm
A^*	The dual operator of A
a^*	The dual bilinear form
$b(\boldsymbol{\tau}, \boldsymbol{v})$	The mixed bilinear form
B	The operator corresponding to b
$\Phi(\boldsymbol{v})$	The cost minimisation functional
S	Statistically admissible set
$\boldsymbol{F}^p$	Plastic deformation gradient
$\boldsymbol{F}^e$	Elastic deformation gradient
$SL(d)$	Special linear group
$\boldsymbol{C}$	The right Cauchy deformation tensor
$\boldsymbol{b}$	The left Cauchy deformation tensor
$\boldsymbol{C}^e$	Elastic part of right Cauchy deformation tensor
$\boldsymbol{C}^p$	Plastic part of right Cauchy deformation tensor
$\boldsymbol{b}^e$	The elastic part of left Cauchy deformation tensor
$\boldsymbol{b}^p$	The plastic part of left Cauchy deformation tensor
$\boldsymbol{E}$	The Green-Lagrangian strain tensor
$\boldsymbol{e}$	The Almansi strain tensor
φ_*	Push-forward operator
$\boldsymbol{S}$	Second Piola-Kirchhoff stress tensor
$\boldsymbol{\tau}$	Kirchhoff stress tensor
$\boldsymbol{d}$	Rate of deformation
$\boldsymbol{l}$	Velocity gradient
$\Pi := \boldsymbol{F}^{p\,-1}$	The inverse of plastic gradient
Ξ_p	The generalised plastic strain
D_p	Plastic dissipation
$\tilde{\boldsymbol{\varsigma}}$	The invariant back stress
Υ	The Gâteaux derivative of $\boldsymbol{E}$
ψ_v	Volumetric energy
ψ_d	Deviatoric energy
ψ_h	Stored plasic energy

$\boldsymbol{f}(t,x,\omega)$	Random loading
$\boldsymbol{A}(x,\omega)$	Random elastic constitutive tensor
$K(x,\omega)$	Random bulk modulus
$G(x,\omega)$	Random shear modulus
$H_{iso}(x,\omega)$	Random isotropic hardening
$\boldsymbol{H}_{kin}(x,\omega)$	Random kinematic hardening
$(\Omega,\mathcal{F},\mathbb{P})$	Probability space
ω	The event
Ω	The space of all events ω
$\mathcal{F}\subset 2^{\Omega}$	σ-algebra
$\mathcal{B}$	Borel algebra
$\mathbb{P}$	The probability measure
$\kappa(\omega)$	The random variable
$\kappa(x,\omega)$	The random field
$\mathcal{V}$	Vector space of definition of κ
F_{κ}	Probability distribution function of κ
f	The probability density function
$W(f)$	Entropy
$\bar{\kappa}:=\mathbb{E}(\kappa)$	The mean value of κ
$\mathrm{cov}_{\kappa}(x_1,x_2)$	The covariance function
$\widetilde{\kappa}:=\kappa-\mathbb{E}(\kappa)$	The fluctuation of κ
erf	The Gaussian distribution function
μ	The mean of Gaussian base field
σ	The standard deviation of Gaussian base field
$\theta(x,\omega),\gamma(x,\omega)$	Gaussian random field
$\boldsymbol{U}_A(x)$	Cholesky factor of the mean matrix $\bar{\boldsymbol{A}}$
$\boldsymbol{T}(x,\omega)$	Non-Gaussian normalized random tensor
$\Gamma(x,\omega)$	Standard Gaussian random tensor
$\boldsymbol{U}$	Cholesky factor of $\boldsymbol{T}(x,\omega)$
δ_T	Dispersion of $\boldsymbol{T}(x,\omega)$
δ_A	Dispersion of $\boldsymbol{A}$
$L_p(\Omega,\mathcal{F},\mathbb{P})$	The space of RVs
$L_0(\Omega,\mathcal{F},\mathbb{P})$	The space of RVs with topology of convergence in probability
$L_1(\Omega,\mathcal{F},\mathbb{P})$	The space of integrable RVs
$(S):=L_2(\Omega,\mathcal{F},\mathbb{P})$	The space of square integrable RVs
$\langle\langle u\|v\rangle\rangle=\mathbb{E}(\langle u\|v\rangle_{\mathcal{V}})$	Inner product of two RVs
$\\|\kappa\\|_1$	Norm in $L_1(\Omega,\mathcal{F},\mathbb{P})$
$\\|\kappa\\|_2$	Norm in $L_2(\Omega,\mathcal{F},\mathbb{P})$
$\boldsymbol{\theta}$	Vector of Gaussian random variables
Θ	Gaussian Hilbert space

$\mathscr{V} \simeq \mathcal{V} \otimes (S)$	The stochastic tensor product space
$\langle\langle u, v \rangle\rangle = \mathbb{E}(\langle u, v \rangle_{\mathcal{V}})$	The duality pairing
$\mathscr{K}$	The stochastic convex domain
$\phi_{\mathscr{K}}$	The stochastic yield function
$\boldsymbol{\nabla}_S$	The linear bounded operator
$\mathscr{U}$	The stochastic space of displacement
$\mathscr{F}$	The stochastic space of forces
$\mathscr{E}$	The stochastic space of deformation
$\mathscr{R}$	The stochastic space of Cauchy stress
$\mathscr{C}$	The stochastic space of conjugate stresses
$\mathscr{P}$	The stochastic space of plastic strain
$\mathscr{Y}$	The stochastic space of generalised stress
$\mathscr{Z}$	The stochastic space of primal variable
$\mathscr{Z}^*$	The stochastic space of dual variables
a^m	The bilinear form in material description
L_t	The number of time increments
Δt	The time step size
Δq_n	The backwards difference
δq_n	The backward divided difference
$\boldsymbol{w}_n$	The primal solution in time n
ϑ	The time integration parameter
a^g	The bilinear form describing the general hardening
$\boldsymbol{C}$	The generalised constitutive tensor
$\boldsymbol{\Sigma}^{trial}$	The trial stress
$\mathscr{V}_h := \mathcal{V}_h \otimes (S)$	Space discretisation of tensor product space
$\mathcal{G}_h$	The FEM discretisation of geometrical domain
$\boldsymbol{N}$	Vector of shape functions
$\boldsymbol{u}$	Vector of nodal displacements
$(\cdot)_h$	General notation for FEM discretisation
$(\cdot)_{hn}$	General notation for FEM-time discretisation
$\xi_k(\omega)$	Random variables in KLE
λ_k	KLE eigenvalues
M	The number of RVs in KLE
p	Order of polynomial
$\boldsymbol{M}$	Gram matrix
l_c	Correlation length
$\kappa^{(\alpha)}$	PCE coefficient
α	Multiindex
$\mathcal{J}$	Multiindex set
$\mathcal{J}_{M,p}$	Truncated multiindex set
$H_\alpha(\boldsymbol{\theta}(\omega))$	Hermite polynomials

Ψ_u	Functional of solution
$(S)_J$	Discretisation of stochastic space (S)
$\hat{\boldsymbol{u}}$	Variable represented by PCE
$\mathcal{J}_Z$	Finite subset of $\mathcal{J}$
σ_{VM}	Von Mises stress
$\mathcal{H}(\cdot)$	Hermite transform
$\mathbf{S}_2$	Product of PCE matrices
$\hat{\mathbf{S}}_2$	Projection of $\mathbf{S}_2$ on Hermite basis
Σ^{trial}	Trial stress
$\bullet$	Product of RVs
$\hat{\bullet}$	Projection of $\bullet$ on Hermite basis
$\mathcal{K}_J^\star$	Approximation of $\mathcal{K}_J$
$L(\omega)$	Lagrangian
λ	Lagrangian multiplier
Φ	Convex energy functional
$\boldsymbol{A}_{ep}$	Elastoplastic constitutive tensor
Δq	Increment of quantity q
$\mathbf{K}_n^{(k)}$	Stiffness matrix in time n and iteration k
$\boldsymbol{f}^{int}$	Vector of internal forces
$\boldsymbol{f}^{ext}$	Vector of external loading
$\mathbf{K}_{NL}$	Nonlinear stiffness matrix
$\boldsymbol{\Delta} = \mathbb{E}(H_\alpha H_\beta H_\gamma)$	Stochastic tensor
$\mathbf{P}$	Preconditioner
$\|\cdot\|_F$	Frobenious norm
$\mathbb{E}(\cdot)$	Mathematical expectation
Ξ	Set of integration points
$\mathbf{H}$	Matrix of Hermite polynomials
$\mathbf{W} = \text{diag}\,(w_k)$	Matrix of weights
$S(\mathbb{R}^d)$	Schwartz space
$\mathcal{P}_p$	Linear space of polynomials
$\mathcal{H}_p$	Homogenous chaos of order p
$\mathbf{Q}_2$	Bilinear map of PCE product
$\mathring{\xi}$	Neutral element of PCE algebra
$\div$	PCE division
$\hat{\div}$	Projected PCE division
$:$	Double dot product of PCE matrices
$\hat{:}$	Projected double dot product of PCE matrices

Bibliography

[1] R. Abraham, J. E. Marsden, and T. Ratiu. *Manifolds, Tensor Analysis, and Applications. Second edition*. Springer, New York, 1983.

[2] P. Abrahamsen. A review of Gaussian random fields and correlation functions. Technical Report 917, Norwegian Computing Center, Oslo, 1997. Available from: http://publications.nr.no/917_Rapport.pdf.

[3] S. Acharjee. *Stochastic and Deterministic Techniques for Computational Design of Deformation Process*. PhD thesis, Faculty of the Graduate School of Cornell University, 2006. Available from: http://mpdc.mae.cornell.edu/Publications/PDFiles/THESES/SAcharjee/SAcharjeeThesis.pdf.

[4] S. Acharjee and N. Zabaras. Uncertainty propagation in finite deformations—a spectral stochastic Lagrangian approach. *Computer Methods in Applied Mechanics and Engineering*, 195(19–22):2289–2312, 2006. doi:10.1016/j.cma.2005.05.005.

[5] S. Acharjee and N. Zabaras. A non-intrusive stochastic Galerkin approach for modeling uncertainty propagation in deformation processes. *Computers and Structures*, 85(5–6):244–254, 2007. doi:10.1016/j.compstruc.2006.10.004.

[6] R. J. Adler. *The Geometry of Random Fields*. John Wiley & Sons, Chichester, 1981.

[7] D. L. Allaix and V. I. Carbone. Discretization of 2D random fields: a genetic algorithm approach. *Engineering Structures*, 31(5):1111–1119, 2009. doi:10.1016/j.engstruct.2009.01.008.

[8] M. Anders and M. Hori. Stochastic finite element methods for elasto-plastic body. *International Journal for Numerical Methods in Engineering*, 46(11):1897–1916, 1999. doi:10.1002/(SICI)1097-0207(19991220)46:11<1897::AID-NME758>3.0.CO;2-3.

[9] M. Anders and M. Hori. Three-dimensional stochastic finite element method for elasto-plastic bodies. *International Journal for Numerical Methods in Engineering*, 51(4):4927–4948, 2002. doi:10.1002/nme.165.

[10] J. Arghavani, F. Auricchio, and R. Naghdabadi. A finite strain kinematic hardening constitutive model based on Hencky strain: General framework, solution algorithm and application to shape memory alloys. *International Journal of Plasticity*, 27(6):940–961, 2011. doi:10.1016/j.ijplas.2010.10.006.

[11] M. Arnst and R. G. Ghanem. A variational-inequality approach to stochastic boundary value problems with inequality constraints and its application to contact and elastoplasticity. *International Journal for Numerical Methods in Engineering*, 89(13):1665–1690, 2011. doi:10.1002/nme.3307.

[12] E. Artioli, F. Auricchio, and L. Beirao da Veiga. Generalized midpoint integration algorithms for J2 plasticity with linear hardening. *International Journal of Numerical Methods in Engineering*, 72(4):422–63, 2007. doi:10.1002/nme.2019.

[13] E. Artioli, F. Auricchio, and V. L. Beirao da Veiga. A novel 'optimal' exponential-based integration algorithm for von-Mises plasticity with linear hardening: theoretical analysis on yield consistency, accuracy, convergence and numerical investigations. *Journal of Numerical Methods in Engineering*, 67(4):449–98, 2006. doi:10.1002/nme.1637.

[14] R. B. Ash and C. A. Doleans-Dade. *Probability and Measure Theory*. Academic Press, San Diego, California, USA, 2000.

[15] S. N. Atluri. On constitutive relations at finite strain: hypo-elasticity and elasto-plasticity with isotropic or kinematic hardening. *Computer Methods in Applied Mechanics and Engineering*, 43(2):137–171, 1984. doi:10.1016/0045-7825(84)90002-1.

[16] I. Babuška, F. Nobile, and R. Tempone. A stochastic collocation method for elliptic partial differential equations with random input data. *SIAM Journal on Numerical Analysis*, 45(3):1005–1034, 2007. doi:10.1137/100786356.

[17] I. Babuška, R. Tempone, and G. E. Zouraris. Galerkin finite element approximations of stochastic elliptic partial differential equations. *SIAM Journal on Numerical Analysis*, 42(2):800–825, 2004. doi:10.1137/S0036142902418680.

[18] B. W. Bader and T. G. Kolda. Efficient MATLAB computations with sparse and factored tensors. *SIAM Journal on Scientific Computing*, 30(1):205–231, 2007. doi:10.1137/060676489.

[19] J. Ballani and L. Grasedyck. A projection method to solve linear systems in tensor format. Technical Report 1324, Institut für Geometrie und Praktische Mathematik, RWTH Aachen, 2010. doi:10.1002/nla.1818.

[20] N. E. Barthelmann and K. Ritter. High dimensional polynomial interpolation on sparse grids. *Advances in Computational Mathematics*, 12(4):273–288, 2000. doi:10.1023/A:1018977404843.

[21] K. J. Bathe. *Finite elment procedures in engineering analysis*. Prentice Hall, New Jersey, 1982.

[22] K. J. Bathe. *Finite element procedures (Part 1-2)*. Prentice Hall, New Jersey, 2nd edition, June 1995.

[23] F. E. Benth and J. Gjerde. Convergence rates for finite element approximations of stochastic partial differential equations. *Stochastics and Stochastic Reports*, 63(3-4):313–326, 1998. doi:10.1080/17442509808834153.

[24] A. Bertram. *Elasticity and plasticity of large deformations — an introduction*. Springer Berlin, Heidelberg, 2008.

[25] J. Betancort-Rijo. Structures in random fields: Gaussian fields. *Physical Review A*, 45(6):3447–3466, 1992. doi:10.1103/PhysRevA.45.3447.

[26] M. Bieri and C. Schwab. Sparse high order FEM for elliptic SPDEs. Technical Report 22, Eidgenössische Technische Hochschule Zürich, 2008. Available from: ftp://ftp.sam.math.ethz.ch/pub/sam-reports/reports/reports2008/2008-22.pdf.

[27] M. Bieri and C. Schwab. Sparse high order FEM for elliptic SPDEs. *Computer Methods in Applied Mechanics and Engineering*, 198(13–14):1149–1170, 2009. doi:10.1016/j.cma.2008.08.019.

[28] P. Billingsley. *Probability and measure*. John Wiley & Sons, New York, 1995.

[29] P. Bochev and M. Gunzburger. *Least-squares finite element methods*. Springer, Berlin, 2009.

[30] J. Bonet and R. D. Wood. *Nonlinear continuum mechanics for finite element analysis*. Cambridge University Press, 2008.

[31] M. Bonnet and S. Mukherjee. Implicit BEM formulations for usual and sensitivity problems in elasto-plasticity using the consistent tangent operator concept. *International Journal of Solids and Structures*, 33(30):4461–4480, 1996. doi:10.1016/0020-7683(95)00279-0.

[32] C. Bucher. Adaptive sampling — an iterative fast Monte Carlo procedure. *Structural Safety*, 5(2):119–126, 1988. doi:10.1016/0167-4730(88)90020-3.

[33] C. Bucher and M. Macke. Stochastic computational mechanics. In *Proceedings of International Conference on Safety, Risk and Reliability—Trends in Engineering, Malta*, 2001.

[34] H. J. Bungartz and S. Dirnstorfer. Multivariate quadrature on adaptive sparse grids. *Computing*, 71(1):89–114, 2003. doi:10.1007/s00607-003-0016-4.

[35] J. Büttner and B. Simeon. Runge–Kutta methods in elastoplasticity. *Applied Numerical Mathematics*, 41(4):443–458, 2002. doi:10.1016/S0168-9274(01)00133-7.

[36] R. E. Caflisch. Monte Carlo and Quasi-Monte-Carlo methods. *Acta Numerica*, 7:1–49, 1998. doi:10.1017/S0962492900002804.

[37] R. H. Cameron and W. T. Martin. Transformations of Wiener integrals under translations. *The Annals of Mathematics*, 45(2):386–396, 1944. Available from: http://www.jstor.org/stable/1969276.

[38] Y. Cao. On convergence rate of Wiener-Ito expansion for generalized random variables. *An International Journal of Probability and Stochastic Processes*, 78(3):179–187, 2006. doi:10.1080/17442500600768641.

[39] C. Carstensen. Convergence of adaptive finite element methods in computational mechanics. *Applied Numerical Mathematics*, 59(9):2119–2130, 2009. doi:10.1016/j.apnum.2008.12.006.

[40] C. Carstensen, K. Hackl, and A. Mielke. Non-convex potentials and microstructures in finite-strain plasticity. *Proceedings of the Royal Society A Mathematical Physical and Engineering Sciences*, 458(2018):299–317, 2002. doi:10.1098/rspa.2001.0864.

[41] C. Carstensen, A. Orlando, and J. Valdman. A convergent adaptive finite element method for the primal problem of elastoplasticity. *International Journal for Numerical Methods in Engineering*, 67(13):1851–1887, 2006. doi:10.1002/nme.1686.

[42] J. Chaboche. Constitutive equations for cyclic plasticity and cyclic viscoplasticity. *International Journal of Plasticity*, 5(3):247–302, 1989. doi:10.1016/0749-6419(89)90015-6.

[43] J. Chakrabarty. *Theory of plasticity*. McGraw-Hill Book Company, New York, 1987.

[44] H. S. Chen and M. A. Stadtherr. A modification of Powell's Dogleg method for solving systems of nonlinear equations. *Computers & Chemical Engineering*, 5(3):143–150, 1981. doi:10.1016/0098-1354(81)85003-X.

[45] W. F. Chen and A. F. Saleeb. *Constitutive equations for engineering materials*. Wiley InterScience, New York, 1982.

[46] G. Christakos. *Random field models in earth sciences*. Academic Press, New York, 1992.

[47] D. B. Chung, M. A. Gutierrez, and R. de Borst. The development of an object-oriented stochastic finite element package for the analysis of fibre-metal laminates. *Computational Methods in Stochastic Mechanics and Reliability Analysis*, 194:1427–1446, 2005. Available from: http://www.imamod.ru/~serge/arc/conf/ECCOMAS_2004/ECCOMAS_V1/proceedings/pdf/29.pdf.

[48] D. B. Chung, M. A. Gutiérrez, L. L. Graham-Brady, and F. J. Lingen. Efficient numerical strategies for spectral stochastic finite element models. *International Journal for Numerical Methods in Engineering*, 64(10):1334–1349, 2005. doi:10.1002/nme.1404.

[49] P. G. Ciarlet. *The finite element method for elliptic problems*. SIAM, Philadelphia, 2002.

[50] A. P. Cisilino and M. H. Aliabadi. A boundary element method for three-dimensional elastoplastic problems. *Engineering Computations*, 15(8):1011–1030, 1998. doi:10.1108/02644409810244110.

[51] T. F. Coleman and Y. Li. On the convergence of interior-reflective Newton methods for nonlinear minimization subject to bounds. *Mathematical Programming*, 67(2):189–224, 1994. doi:10.1007/BF01582221.

[52] K. Conrad. Probability distributions and maximum entropy. *Entropy*, 6(10):1–20, 2004. Available from: http://www.math.uconn.edu/~kconrad/blurbs/analysis/entropypost.pdf.

[53] Y. Dafalias. Issues on the constitutive formulation at large elastoplastic deformations, part 1: Kinematics. *Acta Mechanica*, 69(1):119–138, 1987. doi:10.1007/BF01175717.

[54] Y. Dafalias. Issues on the constitutive formulation at large elastoplastic deformations, part 2: Kinetics. *Acta Mechanica*, 73(1):121–146, 1988. Available from: http://dx.doi.org/10.1007/BF01177034.

[55] E. A. de Souza Neto, D. Perić, and R. J. Owen. *Computational Methods for Plasticity: Theory and Applications*. John Wiley & Sons, Singapore, 2008.

[56] B. J. Debusschere, H. N. Najm, Ph. P. Pebay, O. M. Knio, R. G. Ghanem, and O. P. Le Maître. Numerical challenges in the use of polynomial chaos representations for stochastic processes. *SIAM Journal on Scientific Computing*, 26(2):698–719, 2005. doi:10.1137/S1064827503427741.

[57] P. M. Dixit and U. S. Dixit. *Modeling of metal forming and machining processes by finite element and soft computing methods*. Springer Verlag, London, 2008.

[58] R. L. Dobrushin and R. A. Minlos. An investigation of the properties of the generalized Gaussian random fields. *Selecta Mathematika Sovietica*, 1(3):215–263, 1981. Available from: http://www.cpt.univ-mrs.fr/dobrushin/papers/108.pdf.

[59] J. L. Doob. *Stochastic Processes*. John Wiley & Sons, New York, 1990.

[60] A. Doostan, R. G. Ghanem, and J. Red-Horse. Stochastic model reduction for chaos representations. *Computer Methods in Applied Mechanics and Engineering*, 196(37-40):3951–3966, 2007. doi:10.1016/j.cma.2006.10.047.

[61] A. Doostan and G. Iaccarino. A least-squares approximation of partial differential equations with high-dimensional random inputs. *Journal of Computational Physics*, 228(12):4332–4345, 2009. doi:10.1016/j.jcp.2009.03.006.

[62] G. Duvaut and J. L. Lions. *Inequalities in mechanics and physics*. Springer Verlag, Berlin, 1976.

[63] F. Ebobisse and B. Daya Reddy. Some mathematical problems in perfect plasticity. *Computer Methods in Applied Mechanics and Engineering*, 193(48–51):5071–5094, 2004. doi:10.1016/j.cma.2004.07.002.

[64] S. Eckert, H. Baaser, D. Gross, and O. Scherf. A BDF2 integration method with step size control for elasto-plasticity. *Computational Mechanics*, 34(5):377–386, 2004. doi:10.1007/s00466-004-0581-1.

[65] I. Ekeland and R. Temam. *Convex analysis and variational problems*. North-Holland, Amsterdam, 1976.

[66] O. G. Ernst, A. Mugler, H. J. Starkloff, and E. Ullmann. On the convergence of generalised polynomial chaos expansions. *ESAIM:Mathematical Modelling and Numerical Analysis*, 46(2):317–339, 2012. doi:10.1051/m2an/2011045.

[67] O. G. Ernst and E. Ullmann. Stochastic Galerkin matrices. *SIAM Journal on Matrix Analysis and Applications*, 31(4):1848–1872, 2010. doi:10.1137/080742282.

[68] R. Forster and R. Kornhuber. A polynomial chaos approach to stochastic variational inequalities. *Journal of Numerical Mathematics*, 18(4):235–255, 2010. doi:10.1515/JNUM.2010.012.

[69] D. Y. Gao. General analytic solutions and complementary variational principles for large deformation nonsmooth mechanics. *Meccanica*, 34(3):169–198, 1999. doi:10.1023/A:1004651503537.

[70] J. Garcke. Sparse grid tutorial. Technical report, TU Berlin, Institut für Mathematik, 2011. Available from: http://page.math.tu-berlin.de/~garcke/paper/sparseGridTutorial.pdf.

[71] T. Gerstner and M. Griebel. Numerical integration using sparse grids. *Numerical Algorithms*, 18(3–4):209–232, 1998. Available from: http://wissrech.ins.uni-bonn.de/research/pub.php4?abstract=Gerstner.Griebel:1998.

[72] R. G. Ghanem. Hybrid stochastic finite elements and generalized Monte Carlo simulation. *Journal of Applied Mechanics ASME*, 65(4):1004–1009, 1998. doi:10.1115/1.2791894.

[73] R. G. Ghanem. Ingredients for the general purpose stochastic finite elements implementation. *Computer Methods in Applied Mechanics and Engineering*, 168:19–34, 1999. doi:10.1016/S0045-7825(98)00106-6.

[74] R. G. Ghanem. Stochastic finite elements for heterogeneous media with multiple random non-Gaussian properties. *Journal of Engineering Mechanics*, 125(1):24–40, 1999. doi:10.1061/(ASCE)0733-9399(1999)125:1(26).

[75] R. G. Ghanem and S. Dham. Stochastic finite element analysis for multiphase flow in heterogeneous porous media. *Transport in Porous Media*, 32(3):239–262, 1998. doi:10.1023/A:1006514109327.

[76] R. G. Ghanem and R. Kruger. Numerical solution of spectral stochastic finite element systems. *Computer Methods in Applied Mechanics and Engineering*, 129(3):289–303, 1996. doi:10.1016/0045-7825(95)00909-4.

[77] R. G. Ghanem and J. Red-Horse. Propagation of probabilistic uncertainty in complex physical systems using a stochastic finite element approach. *Physica D*, 133(1–4):137–144, 1999. doi:10.1016/S0167-2789(99)00102-5.

[78] R. G. Ghanem and P. D. Spanos. *Stochastic finite elements: a spectral approach*. Springer Verlag, New York, 1991.

[79] D. Ghosh, P. Avery, and C. Farhat. A feti-preconditioned conjugate gradient method for large-scale stochastic finite element problems. *International Journal for Numerical Methods in Engineering*, 80(6-7):914–931, 2009. doi:10.1002/nme.2595.

[80] M. K. Ghosh and K. S. M. Rao. A probabilistic approach to second order variational inequalities with bilateral constraints. *Proceedings of the Indian Academy of Science*, 113(4):431–442, 2003. Available from: http://arxiv.org/pdf/math/0406076.pdf.

[81] R. Glowinski, J. L. Lions, and R. Tremolieres. *Numerical analysis of variational inequalities*. North-Holland Amsterdam, 1981.

[82] M. Grigoriu. *Applied Non-Gaussian processes*. Englewood Cliffs, NY, 1995.

[83] M. Grigoriu. Non-Gaussian models. *Probabilistic Engineering Mechanics*, 14(4):236–239, 1997.

[84] J. Guilleminot and C. Soize. Stochastic modelling of the mesoscopic elasticity tensor random field for composite materials. In *Proceedings of the 17th International Conference on Composite Materials (ICCM17), Edinburgh, United Kingdom*, 2009.

[85] J. Guilleminot and C. Soize. Non-Gaussian positive-definite matrix-valued random fields with constrained eigenvalues: Application to random elasticity tensors with uncertain material symmetries. *International Journal for Numerical Methods in Engineering*, 88(11):1128–1151, 2011. doi:10.1002/nme.3212.

[86] J. Gwinner. A class of random variational inequalities and simple random unilateral boundary value problems - existence, discretization, finite element approximation. *Stochastic Analysis and Applications*, 18(6):967–993, 2009. doi:10.1080/07362990008809706.

[87] J. Gwinner and F. Raciti. On a class of random variational inequalities on random sets. *Numerical Functional Analysis and Optimization*, 27(5–6):619–636, 2006. doi:10.1080/01630560600790819.

[88] J. Gwinner and F. Raciti. On monotone variational inequalities with random data. *Journal of Mathematical Inequalities*, 3(3):443–453, 2009. doi:10.7153/jmi-03-44.

[89] K. Hackl. Generalized standard media and variational principles in classical and finite strain elastoplasticity. *Journal of the Mechanics and Physics of Solids*, 45(5):667–688, 1997. doi:10.1016/S0022-5096(96)00110-X.

[90] K. Hackl and F. D. Fischer. On the relation between the principle of maximum dissipation and inelastic evolution given by dissipation potentials. *Proceedings of the Royal Society A: Mathematical, Physical and Engineering Science*, 464(2089):117–132, 2008. doi:10.1098/rspa.2007.0086.

[91] B. Halphen and Q. S. Nguyen. Sur les matériaux standards généralisés. *J. de Mécanique*, 14:39–63, 1975.

[92] W. Han and B. Daya Reddy. *Plasticity: mathematical theory and numerical analysis*. Springer, New York, 1999.

[93] W. Han and M. Sofonea. *Quasistatic contact problems in viscoelasticity and viscoplasticity*. Studies in Advanced Mathematics, American Mathematical Society, 2001. Available from: http://epub.ub.uni-muenchen.de/916/1/HeissWinschel2006.pdf.

[94] F. Heiss and V. Winschel. Estimation with numerical integration on sparse grids. Technical Report 2006-15, Department of Economics, University of Munich, 2006. Available from: http://epub.ub.uni-muenchen.de/916/1/HeissWinschel2006.pdf.

[95] V. Hernandez, J. E. Roman, A. Tomas, and V. Vidal. A survey of software for sparse eigenvalue problems. Technical report, Universidad Politecnica de Valencia, 2009. Available from: http://www.grycap.upv.es/slepc/.

[96] T. Hida, H. H. Kuo, J. Potthoff, and L. Streit. *White noise analysis-an infinite dimensional calculus*. Kluwer, Dordrecht, 1993.

[97] I. Hlavaček, J. Haslinger, J. Nečas, and J. Lovíšek. *Solution of variational inequalities in mechanics*. Springer Verlag New York, 1988.

[98] H. Holden, B. Oksendal, J. Uboe, and T. Zhang. *Stochastic Partial Differential Equations. A Modeling, White Noise, Functional Approach*. Birkhäuser, Boston, 1996.

[99] S. Huang, S. Quek, and K. Phoon. Convergence study of the truncated Karhunen-Loève expansion for simulation of stochastic processes. *International Journal for Numerical Methods in Engineering*, 52(9):1029–1043, 2001. doi:10.1002/nme.255.

[100] J. E. Hurtado and A. H. Barbat. Monte Carlo techniques in computational stochastic mechanics. *Archives of Computational Methods in Engineering*, 5(1):3–30, 1998. doi:10.1007/BF02736747.

[101] A. Ibrahimbegović. *Nonlinear solid mechanics*. Springer, Berlin, 2009.

[102] S. Janson. *Gaussian Hilbert Spaces*. Cambridge University Press, Cambridge, 1997.

[103] M. Jardak, C. H. Su, and G. E. Karniadakis. Spectral polynomial chaos solutions of the stochastic advection equation. In *Proceedings of the Fifth International Conference on Spectral and High Order Methods (ICOSAHOM-01) (Uppsala)*, volume 17, pages 319–338, 2002. doi:10.1023/A:1015125304044.

[104] E. T. Jaynes. Information theory and statistical mechanics. *Physical Review*, 106(4):620–630, 1957. Available from: http://bayes.wustl.edu/etj/articles/theory.1.pdf.

[105] B. Jeremić, K. Sett, and M. Kavvas. Probabilistic elasto-plasticity: formulation in 1d. *Acta Geotechnica*, 2(3):197–210, 2007. doi:10.1007/s11440-007-0036-x.

[106] M. L. Kavvas. Nonlinear hydrologic processes: Conservation equations for determining their means and probability distributions. *Journal of Hydrologic Engineering*, 8(2):44–53, 2003. doi:10.1061/(ASCE)1084-0699(2003)8:2(44).

[107] A. Keese. *Numerical solution of systems with stochastic uncertainties. A general purpose framework for stochastic finite elements*. PhD thesis, Department of Mathematics and Computer Science, TU Braunschweig, Germany, 2003. Available from: http://opus.tu-bs.de/opus/volltexte/2004/595.

[108] A. Keese. A review of recent develpoments in the numerical solution of stochastic partial differential equations. Technical Report 2003-6, Institute of Scientific Computing, Department of Mathematics and Computer Science, TU Braunschweig, Germany, 2003. Available from: http://www.digibib.tu-bs.de/?docid=00001504.

[109] A. Keese and H. Matthies. Numerical methods and Smolyak quadrature for nonlinear stochastic partial differential equations. Technical Report 2003-5, Institute of Scientific Computing, TU Braunschweig, Germany, 2003. Available from: http://www.digibib.tu-bs.de/?docid=00001471.

[110] B. N. Khoromskij, A. Litvinenko, and H. G. Matthies. Application of hierarchical matrices for computing the Karhunen-Loève expansion. *Computing*, 84(1–2):49–67, 2009. doi:10.1007/s00607-008-0018-3.

[111] B. N. Khoromskij and C. Schwab. Tensor-structured Galerkin approximation of parametric and stochastic elliptic PDEs. *SIAM Journal on Scientific Computing*, 33(1):364–385, 2011. doi:10.1137/100785715.

[112] D. Kinderlehrer and G. Stampacchia. *An introduction to variational inequalities and their applications*. Academic Press, New York, 1990.

[113] M. Kleiber and T. D. Hien. *The stochastic finite element method—basic perturbation technique and computer implementation*. John Wiley & Sons, New York, 1992.

[114] A. Klimke. Sparse grid interpolation toolbox user's guide. Technical report, Universität Stuttgart, 2007. Available from: http://www.ians.uni-stuttgart.de/spinterp/.

[115] M. Kojić and K. Bathe. *Inelastic analysis of solids and structures*. Springer, Berlin, 2004.

[116] T. G. Kolda. Tensor toolbox, 2012. Available from: http://www.sandia.gov/~tgkolda/TensorToolbox/index-2.5.html.

[117] T. G. Kolda and B. W. Bader. Tensor decompositions and applications. *SIAM Review*, 51(3):455–500, 2009. doi:10.1137/07070111X.

[118] D. Kressner and C. Tobler. Low-rank tensor Krylov subspace methods for parametrized linear systems. Technical report, Seminar for Applied Mathematics, ETH Zürich, 2010. Available from: http://www.math.ethz.ch/~kressner/pub/param.pdf.

[119] M. Krosche and R. Niekamp. Low rank approximation in spectral stochastic finite element method with solution space adaption. Technical report, Institut für Wissenschaftliches Rechnen, Technische Universität Braunschweig, Germany, 2010. Available from: http://www.digibib.tu-bs.de/?docid=00036351.

[120] R. Kubos. Stochastic Liouville equations. *Journal of Mathematical Physics*, 4(2):174–183, 1963. doi:10.1063/1.1703941.

[121] A. D. Kuireghian and J. B. Kee. The stochastic finite element method in structural reliability. *Journal of Engineering Mechanics*, 3(2):83–91, 1988. doi:10.1016/0266-8920(88)90019-7.

[122] A. Kučerova, J. Sýkora, B. V. Rosić, and H. G. Matthies. Acceleration of uncertainty updating in the description of transport processes in heterogeneous materials. *Journal of Computational and Applied Mathematics*, 236(18):4862–4872, 2012. doi:10.1016/j.cam.2012.02.003.

[123] H. Lang. *The difference of the solutions of the elastic and elastoplastic boundary value problem and an approach to multiaxial stress-strain correction*. PhD thesis, Technische Universität Kaiserslautern, 2007. Available from: http://nbn-resolving.de/urn:nbn:de:hbz:386-kluedo-21314.

[124] P. D. Lax and A. N. Milgram. Parabolic equations. In Peter Sarnak and Andrew Majda, editors, *Selected Papers Volume I*, pages 8–31. Springer, New York, 2005.

[125] R. B. Lehoucq and D. C. Sorensen. *ARPACK user's guide: solution of large scale eigenvalue problems with implicitly restarted Arnoli methods.* SIAM, Philadelphia, 1998.

[126] R. LeVeque. *Finite difference methods for ordinary and partial differential equations: steady-state and time-dependent problems*. Classics in Applied Mathematics. Society for Industrial and Applied Mathematics, Philadelphia, PA, USA, 2007.

[127] R. D. Levine and M. Tribus. *Maximum entropy formalism*. The MIT Press, Cambridge, 1979.

[128] R. C. Lin, W. Brocks, and J. Betten. On internal dissipation inequalities and finite strain inelastic constitutive laws: Theoretical and numerical comparisons. *International Journal of Plasticity*, 22(10):1825–1857, 2006. doi:10.1016/j.ijplas.2006.01.002.

[129] Z. Lin and Z. Bai. *Probability inequalities*. Springer, 2010.

[130] A. Lion. Constitutive modelling in finite thermoviscoplasticity: a physical approach based on nonlinear rheological models. *International Journal of Plasticity*, 16(5):469–494, 2000. doi:10.1016/S0749-6419(99)00038-8.

[131] J. L. Lions and L. Stampacchia. Variational inequalities. *Communications on Pure and Applied Mathematics*, 20(3):493–519, 1967. doi:10.1002/cpa.3160200302.

[132] D. Liu. *Uncertainty quantification with shallow water equations*. PhD thesis, Institute of Scientific Computing, TU Braunschweig, 2010. Available from: http://www.digibib.tubs.de/?docid=00032048.

[133] J. S. Liu. *Monte Carlo strategies in scientific computing*. Springer, corrected edition, January 2008.

[134] W.-K. Liu, T. Belytschko, and A. Mani. Random field finite elements. *International Journal for Numerical Methods in Engineering,*, 23(10):1831–1845, 1986. doi:10.1002/nme.1620231004.

[135] J. Lof and A. H. von den Boogard. Adaptive return mapping algorithms for J2 elasto-viscoplastic flow. *International Journal of Numerical Methods in Engineering*, 51(11):1283–1298, 2001. doi:10.1002/nme.203.

[136] J. Lubliner. A maximum-dissipation principle in generalized plasticity. *Acta Mechanica*, 52(3):225–237, 1984. doi:10.1007/BF01179618.

[137] D. G. Luenberger. *Optimization by vector space methods*. John Wiley & Sons, New York, Chichester, Weinheim, 1981.

[138] D. G. Luenberger. *Introduction to linear and nonlinear programming*. Addison-Wesley, Reading, Massachusetts, 1984.

[139] X. Ma and N. Zabaras. An adaptive hierarchical sparse grid collocation algorithm for the solution of stochastic differential equations. *Journal of Computational Physics*, 228(8):3084–3113, 2009. doi:10.1016/j.jcp.2009.01.006.

[140] O. P. Le Maître and O. M. Knio. *Spectral methods for uncertainty quantification with applications to computational physics*. Springer Dordrecht Heidelberg London New York, 2010.

[141] O. P. Le Maître, H. N. Najm, P. P. Pebay, R. G. Ghanem, and O. M. Knio. Multi-resolution-analysis scheme for uncertainty quantification in chemical systems. *SIAM Journal of Scientific Computing*, 29(2):864–889, March 2007. doi:10.1137/050643118.

[142] L. E. Malvern. *Introduction to the mechanics of a continuous medium*. Prentince Hall, Englewood Cliffs, N.J., 1969.

[143] J. Mandel. Equations constitutives et directeurs dans les milieux plastiques et viscoplastiques. *International Journal of Solids and Structures*, 9(6):725–740, 1973. doi:10.1016/0020-7683(73)90120-0.

[144] L. Mathelin, M. Y. Hussaini, and T. A. Zang. Stochastic approaches to uncertainty quantification in CFD simulations. *Numerical Algorithms*, 38(1–3):209–236, 2005. doi:10.1007/BF02810624.

[145] H. Matthies and A. Keese. Galerkin methods for linear and nonlinear elliptic stochastic partial differential equations. Technical Report 2003-08, TU Braunschweig, 2003. Available from: http://www.digibib.tu-bs.de/?docid=00001489.

[146] H. Matthies and G. Strang. The solution of nonlinear finite element equations. *International Journal for Numerical Methods in Engineering*, 14(11):1613–1626, 1979. doi:10.1002/nme.1620141104.

[147] H. G. Matthies. Existence theorems in thermo-plasticity. *Journal de Mécanique*, 18:695–712, 1979.

[148] H. G. Matthies. Finite element approximation in thermo-plasticity. *Numerical Functional Analysis and Optimization*, 1(2):145–160, 1979. doi:10.1080/01630567908816008.

[149] H. G. Matthies. Quantifying uncertainty: modern computational representation of probability and applications. In *Proceedings of the NATO Advanced Research Workshop on Extreme Man-Made and Natural Hazards in Dynamics of Structures*. Opatija, Croatia, 1998. doi:10.1007/978-1-4020-5656-7_4.

[150] H. G. Matthies. Computational aspects of probability in non-linear mechanics. In *NATO-ARW, Multi-physics and Multi-scale Computer Models in Non-Linear Analysis and Optimal Design of Engineering Structures under Extreme Conditions*. Bled, Slovenia, 2004. Available from: http://www.wire.tu-bs.de/forschung/talks/stoch-mech.pdf.

[151] H. G. Matthies. Uncertainty quantification with stochastic finite elements. In *Encyclopedia of Computational Mechanics*. John Wiley & Sons, Ltd, 2004. doi:10.1002/0470091355.ecm071.

[152] H. G. Matthies. Stochastic finite elements: computational approaches to stochastic partial differential equations. *Zeitschrift für Angewandte Mathematik und Mechanik (ZAMM)*, 88(11):849–873, 2008. doi:10.1002/zamm.200800095.

[153] H. G. Matthies, C. E. Brenner, C. G. Bucher, and C. G. Soares. Uncertanties in probabilistic numerical analysis of structures and solids- stochastic finite elements. *Structural Safety*, 19(3):283–336, 1997. doi:10.1016/S0167-4730(97)00013-1.

[154] H. G. Matthies, A. Litvinenko, O. Pajonk, B. Rosić, and E. Zander. Parametric and uncertainty computations with tensor product representations. Technical Report 2011-09, Institut für Wissenschaftliches Rechnen, TU Braunschweig, 2011. Available from: http://www.digibib.tu-bs.de/?docid=00043415.

[155] H. G. Matthies and B. V. Rosić. Inelastic media under uncertainty: Stochastic models and computational approaches. In B. Daya Reddy, editor, *IUTAM Symposium on Theoretical, Computational and Modelling Aspects of Inelastic Media*, volume 11 of *IUTAM BookSeries*, chapter 17, pages 185–194. Springer Netherlands, Dordrecht, 2008. doi:10.1007/978-1-4020-9090-5_17.

[156] H. G. Matthies and E. Zander. Solving stochastic systems with low-rank tensor compression. *Linear Algebra and its Applications*, 436(10):3819–3838, 2011. doi:10.1016/j.laa.2011.04.017.

[157] H. G. Matthies and E. Zander. Sparse representations in stochastic mechanics. In Manolis Papadrakakis, George Stefanou, and Vissarion Papadopoulos, editors, *Computational Methods in Stochastic Dynamics*, volume 22 of *Computational Methods in Applied Sciences*, pages 247–265. Springer, Berlin, 2011.

[158] M. H. Meuwissen. Yield criteria for anisotropic elasto-plastic metals. Technical Report 95.125, Faculteit der Werktuigbouwkund, Technische Universiteit Eindhoven, 1995. Available from: http://alexandria.tue.nl/repository/books/653055.pdf.

[159] D. Michael and M. Meisel. Some remarks to large deformation elastoplasticity (continuum formulation). Technical Report 28, TU Chemnitz, 1998. Available from: http://citeseerx.ist.psu.edu/viewdoc/summary?doi=10.1.1.41.1546.

[160] M. Mićunović. *Thermomechanics of viscoplasticity. Fundamentals and Applications*. Springer Verlag, Berlin, 2009.

[161] A. Mielke and S. Müller. Lower semi-continuity and existence of minimizers in incremental finite-strain elastoplasticity. *Journal of Applied Mathematics and Mechanics*, 86(3):233–250, 2006. doi:10.1002/zamm.200510245.

[162] J. J. Moreau. Numerical aspects of the sweeping process. *Computer Methods in Applied Mechanics and Engineering*, 177(3-4):329–349, 1999. doi:10.1016/S0045-7825(98)00387-9.

[163] J. J. Moreau. On unilateral constraints, friction and plasticity. In Gianfranco Capriz and Guido Stampacchia, editors, *New Variational Techniques in Mathematical Physics*, volume 63 of *C.I.M.E. Summer Schools*, pages 171–322. Springer Berlin Heidelberg, 2011. doi:10.1007/978-3-642-10960-7_7.

[164] T. Moselhy and L. Daniel. Variation-aware interconnect extraction using statistical moment preserving model order reduction. In *Proceedings of Conference on Design Automation and Test in Europe (DATE)*, pages 453–458, 2010. doi:10.1109/DATE.2010.5457161.

[165] T. Moselhy and L. Daniel. Variation-aware stochastic extraction with large parameter dimensionality:review and comparison of state of the art intrusive and non-intrusive techniques. In *The International Symposium on Quality Electronic Design (ISQED)*, pages 508–517, 2011. doi:10.1109/ISQED.2011.5770775.

[166] G. Naldi, P. Venini, and K. Urban. Wavelet based methods in elastoplasticity and damage analysis. In *Proceedings of the Fifth World Congress on Computational Mechanics (WCCM V)*. Vienna University of Technology, Austria, 2002. Available from: http://www.uni-ulm.de/fileadmin/website_uni_ulm/mawi.inst.070/urban/papers/nuv2.pdf.

[167] S. Nemat-Nasser and M. Hori. *Micromechanics: overall properties of heterogeneous materials*. North-Holland: London, 1968.

[168] Q. S. Nguyen. On elastic plastic initial-boundary value problem and its numerical implementation. *International Journal for Numerical Methods in Engineering*, 11(5):817–832, 1977. doi:10.1002/nme.1620110505.

[169] Q. S. Nguyen. *Stability and Nonlinear Solid Mechanics*. John Wiley & Sons, Chichester, 2000.

[170] L. Ning, T. Wilson, and Z. Jiashou. Reliability of elasto-plastic structure using finite element method. *Acta Mechanica Sinica*, 18(1):66–81, 2002. doi:10.1007/BF02487525.

[171] F. Nobile, R. Tempone, and C. G. Webster. An anisotropic sparse grid stochastic collocation method for partial differential equations with random input data. *SIAM Journal on Numerical Analysis*, 46(5):2411–2442, 2008. doi:10.1137/070680540.

[172] F. Nobile, R. Tempone, and C. G. Webster. A sparse grid stochastic collocation method for partial differential equations with random input data. *SIAM Journal on Numerical Analysis*, 46(5):2309–2345, 2008. doi:10.1137/060663660.

[173] A. Nouy. A generalized spectral decomposition technique to solve a class of linear stochastic partial differential equations. *Computer Methods in Applied Mechanics and Engineering*, 196(45-48):4521–4537, 2007. doi:10.1016/j.cma.2007.05.016.

[174] A. Nouy and O. P. Le Maître. Generalized spectral decomposition for stochastic nonlinear problems. *Journal of Computational Physics*, 228(1):202–235, 2009. doi:10.1016/j.jcp.2008.09.010.

[175] V. A. Ogorodnikov and S. M. Prigarin. *Numerical modeling of random processes and fields: algorithms and applications*. VSP, Utrecht, Netherlands, 1996.

[176] B. Øksendal. *Stochastic differential equations: an introduction with applications*. Springer Heidelberg Dordrecht London New York, 6th edition, 2003.

[177] M. Ortiz and E. P. Popov. Accuracy and stability of integration algorithms for elastoplastic constitutive relations. *International Journal of Numerical Methods in Engineering*, 21(9):1561–76, 1985. doi:10.1002/nme.1620210902.

[178] M. Ortiz and J. C. Simo. An analysis of a new class of integration algorithms for elastoplastic constitutive relations. *International Journal of Numerical Methods in Engineering*, 23(3):353–66, 1986. doi:10.1002/nme.1620230303.

[179] M. Ostoja-Starzewski. Random field models of heterogeneous materials. *International Journal of Solids and Structures*, 35(19):2429–2455, 1998. doi:10.1016/S0020-7683(97)00144-3.

[180] O. Pajonk, B. Rosić, A. Litvinenko, and H. G. Matthies. A deterministic filter for non-Gaussian Bayesian estimation. *Physica D: Nonlinear Phenomena*, 241(7):775–788, 2012. doi:10.1016/j.physd.2012.01.001.

[181] P. Papadopoulos and R. L. Taylor. On the application of multi-step integration methods to infinitesimal elastoplasticity. *International Journal for Numerical Methods in Engineering*, 37(18):3169–3184, 1994. doi:710.1002/nme.1620371810.

[182] A. Papoulis. *Probability, random variables and stochastic processes*. McGrawHill, Singapore, 1991.

[183] M. F. Pellissetti and R. G. Ghanem. Iterative solution of systems of linear equations arising in the context of stochastic finite elements. *Advances in Engineering Software*, 31(8–9):607–616, 2000. doi:10.1016/S0965-9978(00)00034-X.

[184] Dj. Perić and D. R. J. Owen. A model for finite strain elastoplasticity based on logarithmic strains: computational issues. *Computer Methods in Applied Mechanics and Engineering*, 94(1):35–61, 1992. doi:10.1016/0045-7825(92)90156-E.

[185] T. Rahman and J. Valdman. Fast MATLAB assembly of fem stiffness- and mass matrices in 2D and 3D: nodal elements. Technical Report 11, Max-Planck-Institut für Mathematik in der Naturwissenschaften, Leipzig, 2011. Available from: http://www.mis.mpg.de/preprints/tr/report-1111.pdf.

[186] P. Rendahl. Projection methods and Smolyak's algorithm, working paper. Technical report, European University Institute, 2005.

[187] S. G. Revesz and Y. Sarantopoulos. The generalized Minkowski functional with applications in approximation theory. *Journal of Convex Analysis*, 11(2):303–334, 2004. Available from: http://arxiv.org/abs/math/0703388.

[188] R. T. Rockafellar. *Convex Analysis*. Princeton University Press, Princeton, New Jersy, 1970.

[189] B. Rosić. Implicit integration of constitutive hyperelastic relations. Master's thesis, Faculty of Mechanical Engineering, University of Kragujevac, Serbia, 2006.

[190] B. Rosić. A review of computational stochastic elastoplasticity. Technical Report 2008-08, Institute of Scientific Computing, TU Braunschweig, 2008. Available from: http://www.digibib.tu-bs.de/?docid=00024317.

[191] B. Rosić, A. Kučerová, J. Sýkora, O. Pajonk, A. Litvinenko, and H. G. Matthies. Parameter identification in a probabilistic setting. *Engineering Structures, availible online*, 50:179–196, 2013. doi:10.1016/j.engstruct.2012.12.029.

[192] B. Rosić, A. Litvinenko, O. Pajonk, and H. G. Matthies. Sampling-free linear bayesian update of polynomial chaos representations. *Journal of Computational Physics*, 231(17):5761 – 5787, 2012. doi:10.1016/j.jcp.2012.04.044.

[193] B. Rosić and H. G. Matthies. Computational approaches to inelastic media with uncertain parameters. *Journal of Serbian Society for Computational Mechanics*, 2:28–43, 2008. Available from: http://www.sscm.kg.ac.rs/jsscm/downloads/Computational_Approaches_to_Inelastic_Media_with_Uncertain_Parameters.pdf.

[194] B. Rosić, H. G. Matthies, and M. Živković. Uncertainty quantification of inifinitesimal elastoplasticity. *Scientific Technical Review*, 61(2):3–9, 2011. Available from: http://www.vti.mod.gov.rs/ntp/rad2011/2-11/1/1.pdf.

[195] B. V. Rosić and H. G. Matthies. Stochastic variational principles in elastoplasticity: The linear case. Technical Report 2012-02, Institut für Wissenschaftliches Rechnen, TU Braunschweig, 2011. Available from: http://www.digibib.tu-bs.de/?docid=00044320.

[196] B. V. Rosić and H. G. Matthies. Identification of properties of stochastic elastoplastic systems. In Manolis Papadrakakis, George Stefanou, and Vissarion Papadopoulos, editors, *Computational Methods in Stochastic Dynamics*, volume 26 of *Computational Methods in Applied Sciences*, pages 237–253. Springer Netherlands, 2013. doi:10.1007/978-94-007-5134-7_14.

[197] C. W. Rowley and J. E. Marsden. Reconstruction equations and the Karhunen-Loève expansion for systems with symmetry. *Physica D*, 142(1–2):1–19, 2000. doi:10.1016/S0167-2789(00)00042-7.

[198] Y. A. Rozanov. *Random fields and stochastic partial differential equations*. Kluwer, Dordrecht, 1998.

[199] M. Ruijter. *Numerical treatment of stochastic control problems by Fourier-cosine expansions*. PhD thesis, Delft University of Technology, Netherlands, 2010. Available from: http://ta.twi.tudelft.nl/users/vuik/numanal/ruijter_afst.pdf.

[200] Y. Saad. Overview of Krylov subspace methods with applications to control problems. Technical Report MTNS89, NASA Ames Research center, Moffett Field, CA, 1989. Available from: http://www-users.cs.umn.edu/~saad/PDF/MTNS89.pdf.

[201] S. K. Sachdeva, P. B. Nair, and A. J. Keane. Hybridization of stochastic reduced basis methods with polynomial chaos expansions. *Probabilistic Engineering Mechanics*, 21(2):182–192, 2006. doi:10.1016/j.probengmech.2005.09.003.

[202] M. Sauter. *Numerical analysis of algorithms for infinitesimal associated and non-associated elasto-plasticity*. PhD thesis, Karlsruher Institut für Technologie, 2010. Available from: http://digbib.ubka.uni-karlsruhe.de/volltexte/1000019551.

[203] M. Schather. Introduction to positive definite functions and to unconditional simulation of random fields. Technical report, Department of Mathematics and Statistics, Lancaster University, UK, 1999. Available from: http://www.stochastik.math.uni-goettingen.de/~schlather/.

[204] G. Schueller and P. Spanos. *Monte Carlo simulation*. Balkema, Rotterdam, 2001.

[205] R. Schurer. A comparison between (quasi-) Monte Carlo and cubature rule based methods for solving high-dimensional inteschatherration problems. *Mathematics and Computers in Simulation*, 62(3–6):509–517, 2003. doi:10.1016/S0378-4754(02)00250-1.

[206] A. Schwarz, J. Schröder, and G. Starke. Least-squares mixed finite elements for small strain elasto-viscoplasticity. *International Journal for Numerical Methods in Engineering*, 77(10):1351–1370, 2009. doi:10.1002/nme.2456.

[207] I. E. Segal and R. A. Kunze. *Integrals and Operators*. Springer Verlag, Berlin, 1978.

[208] K. Sett, B. Jeremić, and M. L. Kavvas. Probabilistic elasto-plasticity: solution and verification in 1D. *Acta Geotechnica*, 2(3):211–220, 2007. doi:10.1007/s11440-007-0037-9.

[209] K. Sett, B. Jeremić, and M. L. Kavvas. The role of nonlinear hardening/softening in probabilistic elasto-plasticity. *International Journal for Numerical and Analytical Methdos in Geomechanics*, 31(7):953–975, 2007. doi:10.1002/nag.571.

[210] C. Shannon, N. Petigara, and S. Seshasai. A mathematical theory of communication. *The Bell System Technical Journal*, 27:379–423, 1948. Available from: http://cm.bell-labs.com/cm/ms/what/shannonday/shannon1948.pdf.

[211] H. Shtrikman. On some variational principles in anisotropic and nonhomogeneous elasticity. *Journal of Mechanical Physics of Solids*, 10:335–342, 1962. doi:10.1016/0022-5096(62)90004-2.

[212] J. C. Simo. On the computational significance of the intermediate configuration and hyperelastic stress relations in finite deformation elastoplasticity. *Mechanics of Materials*, 4(3–4):439–451, 1985. doi:10.1016/0167-6636(85)90039-0.

[213] J. C. Simo. Algorithms for static and dynamic multiplicative plasticity that preserve the classical return mapping schemes of the infinitesimal theory. *Computer Methods in Applied Mechanics and Engineering*, 99(1):61–112, 1992. doi:10.1016/0045-7825(92)90123-2.

[214] J. C. Simo and S. Govindjee. Non-linear B-stability and symmetry preserving return mapping algorithms for plasticity and visco-plasticity. *International Journal of Numerical Methods in Engineering*, 31(1):151–76, 1991. doi:10.1002/nme.1620310109.

[215] J. C. Simo and T. J. R. Hughes. *Computational inelasticity*. Springer Verlag, New York, 1998.

[216] J. C. Simo and C. Miehe. Associative coupled thermoplasticity at finite strains: Formulation, numerical analysis and implementation. *Computer Methods in Applied Mechanics and Engineering*, 98(1):41–104, 1992. doi:10.1016/0045-7825(92)90170-O.

[217] J. C. Simo and M. Ortiz. A unified approach to finite deformation elastoplastic analysis based on the use of hyperelastic constitutive equations. *Computer Methods in Applied Mechanics and Engineering*, 49(2):221–245, 1985. doi:10.1016/0045-7825(85)90061-1.

[218] J. C. Simo and K. S. Pister. Remarks on rate constitutive equations for finite deformation problems: computational implications. *Computer Methods in*

Applied Mechanics and Engineering, 46(2):201–215, 1984. doi:10.1016/0045-7825(84)90062-8.

[219] S. Smolyak. Quadrature and interpolation formulas for tensor products of certain classes of functions. *Soviet Mathematics, Doklady*, 4:240–243, 1963.

[220] C. Soize. Maximum entropy approach for modeling random uncertainties in transient elastodynamics. *Journal of the Acoustical Society of America*, 109(5):1979–1996, 2001. doi:10.1121/1.1360716.

[221] C. Soize. Non-Gaussian positive-definite matrix-valued random fields for elliptic stochastic partial differential operators. *Computer Methods in Applied Mechanics and Engineering*, 195(1–3):26–64, 2006. doi:10.1016/j.cma.2004.12.014.

[222] C. Soize. Construction of probability distributions in high dimensions using the maximum entropy principle. Applications to stochastic processes, random fields and random matrices. *International Journal for Numerical Methods in Engineering*, 76(10):1583–1611, 2008. doi:10.1002/nme.2385.

[223] G. Starke. Adaptive least squares finite element methods in elasto-plasticity. In *Springer Lecture Notes in Computer Science 5910*, pages 671–678. Springer Science+Business media, Luxemburg, 2010.

[224] U. Stefanelli. A variational principle for hardening elastoplasticity. *SIAM Journal on Mathematical Analysis*, 40(2):623–652, 2008. Available from: http://arxiv.org/abs/0710.2425.

[225] G. Strang and G. J. Fix. *An analysis of the finite element method*. Wellesley-Cambridge Press, Cambridge MA, 1988.

[226] W. Subber and A. Sarkar. Primal and dual-primal iterative substructuring methods of stochastic PDEs. *Journal of Physics: Conference Series*, 256(1):1–27, 2010. Available from: http://stacks.iop.org/1742-6596/256/i=1/a=012001.

[227] B. Sudret and A. der Kiureghian. *Stochastic finite element methods and reliability- a state-of-the-art report*. University of California, Berkeley, 2000.

[228] R. L. Taylor. Finite element analysis program FEAP. Structural Engineering, Mechanics and Materials Department of Civil and Environmental Engineering University of California, Berkeley. Available from: http://www.ce.berkeley.edu/projects/feap/.

[229] R. Temam. *Mathematical problems in plasticity*. Wiley, Bordas, Paris, 1983.

[230] R. A. Todor and C. Schwab. Convergence rates for sparse chaos approximations of elliptic problems with stochastic coefficients. *IMA Journal of Numerical Analysis*, 27(2):232–261, 2007. doi:10.1093/imanum/drl025.

[231] E. Ullmann. *Solution strategies for stochastic finite element discretizations*. PhD thesis, Fakultät für Mathematik und Informatik, TU Bergakademie Freiberg, 2008. Available from: http://tubaf.qucosa.de/recherche/frontdoor/cache.off?tx_slubopus4frontend[id]=2251.

[232] E. Ullmann, H. C. Elman, and O. G. Ernst. Efficient iterative solvers for stochastic Galerkin discretizations of log-transformed random diffusion problems. *SIAM Journal on Scientific Computing*, 34(2):659–682, 2012. doi:10.1137/110836675.

[233] T. Ullrich. *Smolyak's algorithm, sparse grid approximation and periodic function spaces with dominating mixed smoothness*. PhD thesis, Fakultät für Mathematik und Informatik, der Friedrich-Schiller-Universität Jena, 2007. Available from: http://www.db-thueringen.de/servlets/DerivateServlet/Derivate-11554/Disserta.pdf.

[234] N. Valoroso. *Theory and implementation of plasticity and viscoplasticity*. Class Notes, Rome, Italy, 2002.

[235] E. Vanmarcke. *Random fields: analysis and synthesis*. The MIT Press, Cambridge, MA, 1988.

[236] M. N. Viladkar, J. Noorzaei, and P. N. Godbole. Convenient forms of yield criteria in elasto-plastic analysis of geological materials. *Computers & Structures*, 54(2):327–337, 1995. doi:10.1016/0045-7949(94)E0199-C.

[237] M. Živković. Finite element program PAK. Faculty of Mechanical Engineering, University of Kragujevac. Available from: http://fempak.fink.rs/en/.

[238] N. Wiener. The homogeneous chaos. *The American Journal of Mathematics*, 60(4):1936–1938, 1938. Available from: http://www.jstor.org/stable/2371268.

[239] C. Wieners. Orthogonal projections onto convex sets and the application to problems in plasticity. Technical report, Fakultät für Mathematik, Karlsruhe Institute of Technology, 1999. Available from: http://citeseerx.ist.psu.edu/viewdoc/summary?doi=10.1.1.25.700.

[240] C. Wieners. Nonlinear solution methods for infinitesimal perfect plasticity. *ZAMM - Journal of Applied Mathematics and Mechanics / Zeitschrift für Angewandte Mathematik und Mechanik*, 87(8-9):643–660, 2007. doi:10.1002/zamm.200610339.

[241] M. L. Wilkins. Calculation of elastic-plastic flow. *Methods of Computational Physics*, 3:1–20, 1964. Available from: http://www.dtic.mil/cgi-bin/GetTRDoc?Location=U2&doc=GetTRDoc.pdf&AD=ADA395185.

[242] F. Xiong, W. Chen, Y. Xiong, and S. Yang. Weighted stochastic response surface method considering sample weights. *Struct. Multidiscip. Optim.*, 43(6):837–849, 2011. doi:10.1007/s00158-011-0621-3.

[243] D. Xiu. Fast numerical methods for stochastic computations: A review. *Computer Physics Communications*, 4(2–4):242–272, 2009. Available from: http://www.ece.uvic.ca/~bctill/papers/numacoust/Xiu_2008.pdf.

[244] D. Xiu. *Numerical methods for stochastic computations: a spectral method approach*. Princeton University Press, 2010.

[245] D. Xiu and J. S. Hesthaven. Higher order collocation methods for differential equations with random inputs. *SIAM Journal of Scientific Computing*, 27(3):1118–1139, 2005. doi:10.1137/040615201.

[246] D. Xiu and G. Karniadakis. The Wiener–Askey polynomial chaos for stochastic differential equations. *SIAM Journal of Scientific Computing*, 24(2):619–644, February 2002. doi:10.1137/S1064827501387826.

[247] D. Xiu and G. E. Karniadakis. Modeling uncertainty in steady state diffusion problems via generalized polynomial chaos. *Computer Methods in Applied Mechanics and Engineering*, 191(43):4927–4948, 2002. doi:10.1016/S0045-7825(02)00421-8.

[248] D. Xiu and G. E. Karniadakis. Modeling uncertainty in flow simulations via generalized polynomial chaos. *Journal of Computational Physics*, 187(1):137–167, 2003. doi:10.1016/S0021-9991(03)00092-5.

[249] Q. Yang, L. Stainier, and M. Ortiz. A variational formulation of the coupled thermo-mechanical boundary-value problem for general dissipative solids. *Journal of Mechanics Physics of Solids*, 54(2):401–424, 2006. doi:10.1016/j.jmps.2005.08.010.

[250] O. C. Zienkiewicz and R. L. Taylor. *The finite element method*. Butterworth-Heinemann, 2000.

Curriculum Vitae

Personal Data

- **Name:** Bojana Vukašin Rosić
- **Date of birth:** 16.08.1982
- **Place of birth:** Kragujevac, Serbia

Education

- **2007-2012 Dual degree PhD Studies between Carl-Friedrich-Gauß-Fakultät, Technische Universität Braunschweig, Germany and Faculty of Mechanical Engineering, University of Kragujevac, Serbia**
  - Dissertation defended: 16.11.2012
  - Dissertation final mark: summa cum laude
  - Subject: uncertainty quantification, applied mechanics
  - Thema: *Variational Formulations and Functional Approximation Algorithms in Stochastic Plasticity of Materials*
  - Supervised by: Prof. Hermann G. Matthies, Ph.D., and Prof. Dr. Miroslav Živković
- **2001-2006 Faculty of Mechanical Engineering, University of Kragujevac**
  - Academic degree: Dipl.-Ing.
  - Average mark: 10 (excellent)
  - Subject: applied mechanics and automatic control

  - Diploma thesis: *Implicit Integration of Constitutive Relations for Hyperelastic Material Models*

- **1997-2001 I Gymnasium Kragujevac**
  - Subject: natural sciences and mathematics
  - Average mark: excellent
- **1989-1997 Primary School Rada Šubakić, Gruža**

Career

- 2010-today Research assistant, Institut für Wissenschaftliches Rechnen, Technische Universität Braunschweig

Projects

- Solving Multiphysics Problems with the help of Software PAK (SOMUPAK), DAAD PPP-Serbien, 2012-today
- Quantification of Uncertainty and Updating in the Description of Heat and Moisture Transport in Heterogeneous Materials (BeWuF), DAAD PPP-Tschechien, 2011-2012
- Grundlagen des Hochauftriebs künftiger Verkehrsflugzeuge (SFB880), DFG Project, 2010-today
- Quantification of Uncertainty in the Description of Heat and Moisture Transport in Heterogeneous Materials, DFG Project, 2010-today

Scholarships and Prizes

- Jan.-May 2010 DAAD Scholarship
- 2007-2010 Institut für Wissenschaftliches Rechnen, Technische Universität Braunschweig Scholarship
- 2005 Student of generation, University Kragujevac
- 2005 The best student in engineering science of Republic of Serbia
- 2005 Mihailo Pupin Scholarship

- 2004-2005 Studenica Scholarship
- 2004-2006 Serbian Republic Foundation for Young Talents Scholarship
- 2001 Diploma Vuk Karadzić, Prva Kragujevacka gimnazija

Additional Activities

- WS 2012 Teaching Assistant, Introduction to Scientific Computing, Institut für Wissenschaftliches Rechnen, TU Braunschweig
- WS 2011 Teaching Assistant, Introduction to Scientific Computing, Institut für Wissenschaftliches Rechnen, TU Braunschweig
- SS 2011 Teaching Assistant, Advanced Methods for ODEs and DAEs, Institut für Wissenschaftliches Rechnen, TU Braunschweig
- SS 2004 Teaching Assistant, Continuum Mechanics, Faculty of Mechanical Engineering, University of Kragujevac
- Universität Erlangen-Nürnberg Sommer Schule 2004, Petrovac, Montenegro
- Aug. 2006 Praxis (PLC kontrolers), Firma MV Engineering, Krefeld, Germany
- 2003-2005 Mašinijada competitions

Publications

Journal Papers

[1] **B. Rosić** and H. G. Matthies. *Stochastic Plasticity - A Variational Inequality Formulation and Functional Approximation Approach I: The Linear Case*. Submitted to Computer Methods in Applied Mechanics and Engineering, 2013

[2] **B. Rosić**, A. Kučerová, J. Sýkora, O. Pajonk, A. Litvinenko and H. G. Matthies. *Parameter Identification in a Probabilistic Setting*. Engineering Structures, Available online, 2013, doi: 10.1016/j.engstruct.2012.12.029

[3] **B. Rosić**, A. Litvinenko, O. Pajonk and H. G. Matthies. *Sampling Free Bayesian Update of Polynomial Chaos Representations*. Journal of Computational Physics, 231 (17): 5761-5787, 2012, doi: 10.1016/j.jcp.2012.04.044

[4] O. Pajonk, **B. Rosić**, A. Litvinenko and H. G. Matthies. *A Deterministic Filter for Non-Gaussian Bayesian Estimation — Applications to Dynamical System Estimation with Noisy Measurements*. Physica D: Nonlinear Phenomena, 241(7): 775–788, 2012, doi: 10.1016/j.physd.2012.01.001

[5] O. Pajonk, **B. Rosić**, and H. G. Matthies. *Sampling-free Linear Bayesian Updating of Model State and Parameters Using a Square Root Approach*. Computers and Geosciences, 2012, Available online, doi: 10.1016/j.cageo.2012.05.017

[6] A. Kučerová, J. Sýkora, **B. Rosić** and H. G. Matthies. *Acceleration of Uncertainty Updating in the Description of Transport Processes in Heterogeneous Materials*. Journal of Computational and Applied Mathematics, 236(18): 4862-4872, 2012, doi: 10.1016/j.cam.2012.02.003

[7] **B. Rosić** and H. G. Matthies and M. Živković. *Uncertainty Quantification of Infinitesimal Elastoplasticity*. Scientific Technical Review, 61(2): 3-9, 2011, `http://www.vti.mod.gov.rs/ntp/rad2011/2-11/1/1.pdf`

[8] **B. Rosić** and H. G. Matthies. *Computational Approaches to Inelastic Media with Uncertain Parameters*. Journal of Serbian Society for Computational

Mechanics, 2(1): 28-43, 2008, http://www.sscm.kg.ac.rs/jsscm/downloads/

Proceedings and Collections

[9] **B. Rosić**, H. G. Matthies and M. Živković and A. Ibrahimbegović. *Formulation of Heterogeneous Stochastic Elastoplastic Material*. In Computational Plasticity IX: Fundamentals and Applications, E. Oñate, D. R. J. Owen and B. Suárez (Eds.), IX International Conference on Computational Plasticity, COMPLAS IX, Barcelona, Spain, September 2007.

[10] H. G. Matthies and **B. Rosić**. *Inelastic Media under Uncertainty: Stochastic Models and Computational Approaches*. In IUTAM Symposium on Theoretical, Computational and Modelling Aspects of Inelastic Media, B. Daya Reddy (Ed.), 11:185-194, January 2008, http://www.springerlink.com/content/q1w8642101632425/

[11] **B. Rosić**, H. G. Matthies, M. Živković and A. Ibrahimbegović. *Uncertainty and Plasticity: Stochastic Formulation and Computations*. In Proceedings of 2nd South-East Europpean Conference on Computational Mechanics, SEECCM 2009, Rhodos, Greece, June 2009, ftp://ftp.ensieta.fr/pub/12_CSMA_Dossiers/12_CSMA_ROZIC/1-paper1-rosic.pdf

[12] **B. Rosić** and H. G. Matthies. *Formulation and Computational Application of Inelastic Media with Uncertain Parameters*. In Computational Plasticity X: Fundamentals and Applications, E. Oñate, D. R. J. Owen and B. Suárez (Eds.), p344, X International Conference on Computational Plasticity (COMPLAS X), Barcelona, Spain, September 2009, http://congress.cimne.com/complas09/proceedings/pdfs/p344.pdf

[13] **B. Rosić**, H. G. Matthies and M. Živković. *Mathematical Formulation and Numerical Simulation of Stochastic Elastoplastic Behaviour*. In Proceedings of IVth European Conference on Computational Mechanics, p489, Paris, France, May 2010, http://www.eccm2010.org/complet/fullpaper_489.pdf

[14] **B. Rosić** and H. G. Matthies. *Stochastic Galerkin Method for the Elastoplasticity problem with Uncertain Parameters*. In Recent Developments and Innovative Applications in Computational Mechanics, D. Mueller-Hoeppe, S. Loehnert, S. Reese (Eds.), 303–310, Springer, Berlin, Heidelberg, 2011, http://www.springer.com/materials/mechanics/book/978-3-642-17483-4

[15] **B. Rosić**, A. Kučerová, J. Sýkora, O. Pajonk, A. Litvinenko and H. G. Matthies. *Bayesian Updating of Uncertanties in the Description of Heat and Moisture Transport in Heterogenous Materials*. In Adaptive Modelling and Simulation, D. Aubry, P. Díez, B. Tie and N. Parés (Eds.), 415–423, V International Conference on Adaptive Modeling and Simulation (ADMOS), Paris, France, June 2011, http://congress.cimne.upc.es/admos2011/frontal/doc/ADMOS2011.pdf.

[16] **B. Rosić** and H. G. Matthies. *Plasticity Described by Uncertain Parameters — A Variational Inequality Approach*. In Computational Plasticity XI: Fundamentals and Applications, E. Oñate, D. R. J. Owen, D. Perić and B. Suárez (Eds.), 385–397, XI International Conference on Computational Plasticity (COMPLAS XI), Barcelona, Spain, September 2011, http://congress.cimne.com/complas2011/frontal/doc/Complas_11_ebook.pdf

[17] H. G. Matthies and **B. Rosić**. *A Deterministic Filter for Estimation of Parameters Describing Inelastic Heterogenous Media*, In Computational Plasticity XI: Fundamentals and Applications, E. Oñate, D. R. J. Owen, D. Perić and B. Suárez (Eds.), 410–422, XI International Conference on Computational Plasticity (COMPLAS XI), Barcelona, Spain, September 2011, http://congress.cimne.com/complas2011/proceedings/full/p71.pdf

[18] O. Pajonk, **B. Rosić**, A. Litvinenko and H. G. Matthies. *A Deterministic Filter for non-Gaussian State Estimation*. PAMM Proc. Appl. Math. Mech., 11: 703 -704, 2011, doi: 10.1002/pamm.201110341

[19] H. G. Matthies, A. Litvinenko, O. Pajonk, **B. Rosić** and E. Zander, *Parametric and Uncertainty Computations with Tensor Product Representations*. In IFIP Advances in Information and Communication Technology: Uncertainty Quantification in Scientific Computing, A. Dienstfrey and R. Boisvert (Eds.), 137: 139–150, Springer-Verlag, Heidelberg, 2012, doi: 10.1007/978-3-642-32677-6

[20] **B. Rosić** and H. G. Matthies. *Identification of Properties of Stochastic Elastoplastic Systems*. In Computational Methods in Applied Sciences: Computational Methods in Stochastic Dynamics, M. Papadrakakis, G. Stefanou, and V. Papadopoulos (Eds.), 26: 237–253, Springer, Dordrecht, 2013, http://www.springer.com/materials/mechanics/book/978-90-481-9986-0

Theses

[21] **B. Rosić**. *Variational Formulations and Functional Approximation Algorithms in Stochastic Plasticity of Materials*. Dual degree PhD thesis, Technische Universität Braunschweig and University of Kragujevac, 2012.

[22] **B. Rosić**. *A State of the Art Report: Stochastic Elastoplasticity*. PhD access thesis, Faculty of Mechanical Engineering, University of Kragujevac, 2010.

[23] **B. Rosić**. *Implicit Integration of Constitutive Relations for Hyperelastic Material Models*. Diploma thesis, Faculty of Mechanical Engineering, University of Kragujevac, 2006.

Technical Reports

[24] **B. Rosić**, *A Review of Stochastic Elastoplasticity*. Informatikbericht 2008-08, TU Braunschweig, http://www.digibib.tu-bs.de/?docid=00024317

[25] **B. Rosić**, A. Litvinenko, O. Pajonk and H. G. Matthies. *Direct Bayesian Update of Polynomial Chaos Representations*. Informatikbericht 2011-02, TU Braunschweig, http://www.digibib.tu-bs.de/?docid=00039000

[26] O. Pajonk, **B. Rosić**, A. Litvinenko and H. G. Matthies. *A Deterministic Filter for Non-Gaussian Bayesian Estimation*. Informatikbericht 2011-04, TU Braunschweig, http://www.digibib.tu-bs.de/?docid=00038994

[27] H. G. Matthies, A. Litvinenko, O. Pajonk, **B. Rosić** and E. Zander. *Parametric and Uncertainty Computations with Tensor Product Representations*. Informatikbericht 2011-09, TU Braunschweig, http://www.digibib.tu-bs.de/?docid=00043415

[28] **B. Rosić**, A. Kučerová, J. Sýkora, O. Pajonk, A. Litvinenko and H. G. Matthies. *Parameter Identification in a Probabilistic Setting*. Informatikbericht 2011-10, TU Braunschweig, http://www.digibib.tu-bs.de/?docid=00042261

[29] O. Pajonk, **B. Rosić** and H. G. Matthies. *Deterministic Linear Bayesian Updating of State and Model Parameters for Chaotic Model*. Informatikberict 2012-01, TU Braunschweig, http://www.digibib.tu-bs.de/?docid=00042266

[30] **B. Rosić** and H. G. Matthies. *Stochastic Plasticity - A Variational Inequality Formulation and Functional Approximation Approach I: The Linear Case*, Informatikbericht 2012-02, TU Braunschweig, http://www.digibib.tu-bs.de/?docid=00044320

[31] A. Kučerová, J. Sýkora, **B. Rosić** and H. G. Matthies: *Acceleration of Uncertainty Updating in the Description of Transport Processes in Heterogeneous Materials*, CoRR, 2011, http://arxiv.org/abs/1110.2049

[32] **B. Rosić**, *Non-intrusive Methods for the Uncertainty Quantification of Basic Aircraft Model (BACM)*. In SFB 880 – Fundamentals of High-Lift for Future Commercial Aircraft, Biennial report, 2013

Invited Talks

[33] **B. Rosić**. *Mathematical Formulation and Numerical Simulation of Elastoplastic Material with Uncertain Parameters*, 5 August 2010, Institut für Technische Mechanik, TU Clausthal

Conferences

[34] **B. Rosić** and M. Živković. *Hyperelastic Material Models*. First Serbian (26th YU) Congress on Theoretical and Applied Mechanics, Kopaonik, Serbia, April 2007

[35] H. G. Matthies and **B. Rosić**. *Inelastic Media under Uncertainty: Stochastic Models and Computational Approaches*. IUTAM Symposium on Theoretical, Modelling and Computational Aspects of Inelastic Media, Cape Town, South Africa, January 2008

[36] **B. Rosić** and H. G. Matthies. *Computational Approaches for Inelastic Media with Uncertain Parameters*. 8th World Congress on Computational Mechanics WCCM8 and 5th European Congress on Computational Methods in Applied Sciences and Engineering ECCOMAS 2008, Venice, Italy, July 2008.

[37] **B. Rosić**, H. G. Matthies, M. Živković and A. Ibrahimbegović. *Stochastic Plasticity*. 6th International Congress of Croatian Society of Mechanics, 6th ICCSM, Dubrovnik, Croatia, October 2009

[38] **B. Rosić**. *Stochastic Elastoplasticity, Mathematical Modelling and Numerical Simulation*, Institutskolloquium: Dünne Tensor Produkte, Institut für Wissenschaftliches Rechnen, TU Braunschweig, November 2009

[39] A. Kučerová, J. Sýkora, **B. Rosić** and H. G. Matthies. *Uncertainty Updating in Description of Heterogeneous Materials with Nonlinear Constitutive Law*. In IV European Conference on Computational Mechanics, Paris, France, May 2010

[40] H. G. Matthies, A. Litvinenko, M. Espig, E. Zander, **B. Rosić** and D. Liu. *Low Rank-Representation Numerical Methods for Uncertainty Quantification Equations*. Workshop on Uncertainty Quantification, Edinburgh, UK, May 2010

[41] O. Pajonk, **B. Rosić**, A. Litvinenko and H. Matthies. *A Deterministic Filter for non-Gaussian State Estimation*, 2nd Annual Scientific Conference (GAMM2011), Graz, Austria, April 2011

[42] **B. Rosić**, T. El-Moselhy, A. Litvinenko, O. Pajonk, H. G. Matthies. *Bayesian Identification for non-Gaussian Parameters*. 1st International Symposium on Uncertainty Modelling in Engineering, Prague, May 2011

[43] **B. Rosić**, H. G. Matthies, O. Pajonk, A. Kučerová and J. Sýkora. *Efficient Bayesian Updating of Parameters for Heat and Moisture Transport in Heterogenous Materials*. SIAM conference on Optimisation (OP11), Darmstadt, Germany, May 2011

[44] A. Kučerová, J. Sýkora, H. G. Matthies and **B. Rosić**. *Uncertainty Updating in Description of Coupled Transport Processes in Heterogeneous Materials*. 1st International Symposium on Uncertainty Modelling in Engineering, Prague, Czech Republic, May 2011

[45] A. Kučerová, J. Sýkora, H. G. Matthies and **B. Rosić**. *Acceleration of Uncertainty Updating in Description of Transport Processes in Heterogeneous Materials*. FEMTEC, Reno, USA, May 2011

[46] H. G. Matthies and **B. Rosić**. *Identification of Properties of Stochastic Dynamic Elasto-Plastic Systems*. 3rd ECCOMAS Thematic Conference on Computational Methods in Structural Dynamics and Earthquake Engineering (COMPDYN), Corfu, Greece, May 2011

[47] **B. Rosić**, H. G. Matthies and M. Živković. *A Variational Inequality Formulation of Stochastic Elastoplasticity*. Third Serbian Congress on Theoretical and Applied Mechanics, Vlasina lake, July 2011

[48] H G. Matthies, **B. Rosić**, A. Litvinenko, O. Pajonk and A. Kučerova, Jan Sýkora. *Information Updating As a Stochastic Optimisation Procedure*. 7th International Congress on Industrial and Applied Mathematics (ICIAM), Vancouver, Canada, July 2011

[49] **B. Rosić**. *Bayesian Identification for non-Gaussian Parameters*. 17th Conference of the International Linear Algebra Society, Braunschweig, Germany, August 2011

[50] H. G. Matthies, A. Litvinenko, O. Pajonk, **B. Rosić** and E. Zander. *Parametric and Uncertainty Computations with Tensor Product Representations*. IFIP Working Conference on Uncertainty Quantification in Scientific Computing, Boulder, Colorado, USA, August 2011

[51] A. Litvinenko, H. G. Matthies, **B. Rosić**, O. Pajonk. *Bayesian Update in Low-Rank Tensor Format*. Deutsch-französische Sommerschule "Quantifizierung von Ungewissheiten in Mechanik und Werkstoffwissenschaften", Pforzheim, August 2011

[52] **B. Rosić** and H. G. Matthies.*Stochastic Galerkin method for the Elastoplasticity Problem with Uncertain Parameters*. Trends & Challenges in Computational Mechanics (TCCM). A Conference in honor of Peter Wriggers' 60th birthday, Padua, Italy, September 2011

[53] **B. Rosić**, A. Litvinenko and H. G. Matthies.*Low-Rank Response Surface for Uncertainty Quantification in Numerical Aerodynamics*, 4 Dresdner-Probabilistik-Workshop, Dresden, Germany, October 2011

[54] **B. Rosić**, O. Pajonk, A. Litvinenko, A. Kučerová and J. Sýkora. *Inverse Problems for Nonlinear Systems via Bayesian Parameter Identification*. SIAM Conference on Uncertainty Quantification, Raleigh, USA, April 2012

[55] A. Kučerová, J. Sýkora, **B. Rosić** and H. G. Matthies. *Comparison of Stochastic Methods for Bayesian Updating of Uncertainty in Parameters of Nonlinear Models*. SIAM Conference on Uncertainty Quantification, Raleigh, USA, April 2012

[56] J. Sýkora, A. Kučerová, **B. Rosić** and H. G. Matthies. *Bayesian Updating of Uncertainty in the Description of Transport Processes in Heterogeneous Materials*. SIAM Conference on Uncertainty Quantification, Raleigh, USA, April 2012

[57] **B. Rosić**, O. Pajonk, A. Kučerová, J. Sýkora and H. G. Matthies. *Bayesian Parameter Identification for Nonlinear Systems*. ESCO 2012: 3rd European Seminar on Computing, Pilsen, Czech Republic, June 2012

[58] H. G. Matthies,**B. Rosić**, O. Pajonk, A. Kučerová and J. Sýkora.*Bayesian Identification of Parameters Describing Nonlinear Models of Heterogeneous Media*. IUTAM Symposium on Multiscale Problems in Stochastic Mechanics, Karlsruhe, Germany, June 2012

[59] H. G. Matthies, A. Litvinenko,**B. Rosić** and O. Pajonk. *Tensor Approximation Methods for Parameter Identification*. SIAM Conference on Applied Linear Algebra, Valencia, Spain, June 2012

[60] **B. Rosić**, O. Pajonk, A. Litvinenko, and H. G. Matthies. *Inverse Problems for Nonlinear Elastoplastic Models via Bayesian Parameter Identification*. European Congress on Computational Methods in Applied Sciences and Engineering (ECCOMAS), Vienna, Austria, September 2012

[61] H. G. Matthies and **B. Rosić**. *Tensor Approximation for Parameter Identification*. European Congress on Computational Methods in Applied Sciences and Engineering (ECCOMAS), Vienna, Austria, September 2012

The focus of this study is set on the rate-independent evolutionary problem with general hardening whose material characteristics are assumed to be uncertain. In this regard, within the framework of infinitesimal and large displacement elastoplasticity theory, a class of abstract stochastic variational inequalities of the second kind is considered, both theoretically and numerically. By exhibiting the structure of the stochastic evolutionary equations in a convex setting, the mathematical description of an abstract primal variational formulation is carried over to the computationally more suitable mixed variational description for which the existence and uniqueness of the solution is studied. Time discretised as usual with backward Euler, the inequality is reduced to a minimisation problem for a convex functional on discrete tensor product subspaces whose unique minimiser is obtained via a stochastic closest point projection algorithm based on “white noise analysis”.

Institut für Wissenschaftliches Rechnen
Hans-Sommer Straße 65
Braunschweig, Germany

Fakultet inženjerskih nauka
Ul. Sestre Janjić br. 6
Kragujevac, Serbia